Geologic and Isotopic Investigations of the Early Cretaceous Sierra Nevada Batholith, Tulare Co., CA, and the Ivrea Zone, NW Italian Alps: Examples of Interaction Between Mantle-Derived Magma and Continental Crust

Thesis by
Diane Clemens Knott

In Partial Fulfillment of the Requirements
for the Degree of
Doctor of Philosophy

California Institute of Technology
Pasadena, California
1992

(Defended April 6, 1992)

...no vestige of a beginning, no prospect of an end...

James Hutton

I also became the river by knowing how it was made.

Norman Maclean

Acknowledgements

I have waited a long time to write this and, as a result, am indebted to many more individuals than there is room to thank ... but I shall try anyway. This thesis is complete due to the inspiration and support of my research advisors. For this and much more I owe them my thanks: Hugh P. Taylor, Jr., who waited for me to discover my research interests and then supported my choice of a thesis; Jason B. Saleeby, who introduced me to Stokes Mountain and encouraged creative, scientific thought; Leon T. Silver, who shared with unlimited eagerness the excitement of igneous petrology, regional geology, and modeling in the third dimension. In addition, thanks to other members of the Caltech faculty for their input and advice: Peter J. Wyllie, Edward M. Stolper, Samuel Epstein, George Rossman, Arden Albee and Robert Sharp. I also want to acknowledge former UCLA faculty members, Donald J. DePaolo and Clemens A. Nelson, for encouraging a commitment to geologic generalism as well as specialism.

This thesis has evolved on two continents. In Europe, I benefitted from the help of many. Special thanks go to my friend and colleague, Silvano Sinigoi, for his introduction to the Ivrea Zone as well as to the fine points of Italian culture. *Gracie* to many members of the Universities of Trieste and Milano, particularly Gabriella DeMarchi, Luigi Burlini, Alba Zappone and Attilio Boriani, for their introductions to the Ivrea-Strona-Ceneri section, overwhelming hospitality, and hours spent attempting to teach me Italian. And, lastly, thanks to an unofficial thesis advisor, David M. Fountain, for opening many doors, both in Europe and to the lower continental crust.

Closer to home, in my beloved Sierra Nevada, my appreciation goes to the ranchers and farmers of the Stokes Mountain region for permission to access their properties; in particular, I want to mention the Chrismans, Collins, Edminstons and Travolis who were generous both with their hospitality and with sharing their love of the land. Others have helped greatly with this research project: Bruce W. Chappell provided the geochemical

analyses and advice on the analysis; David Pickett taught me "everything I know" about the techniques of Sr and Nd isotopic analysis; Michael Baker supplied his fractionation program and insight on geochemical modeling. In addition, my research has benefitted immeasurably from the training and expertise provided by the excellent technical, postdoctoral and secretarial staff. Those who invested generously of their time and patience include Joop Goris, who cheerfully performed the mass spectrometric analyses on the majority of oxygen analyses contained in this study, Eleanor Dent, who solved and soothed many lab panics, Paul Carpenter, who shared his SEM and Macintosh wisdom, as well as library wizards, Jim O'Donnell and Pat Kelly.

I feel lucky to have traversed the graduate obstacle course with a cadre of extremely talented and interesting individuals. More than thanks go to my office mates, Mike Wolf and Yigal Erel, and their delightful wives, Susan and Osnat, for their patience and humor over four plus years of close confinement; to classmates David Bell, Joel Blum, Jackie Eaby Dixon, Sally McGill, Charlie Rubin, Jack Sheng and Phil Shaller; and to "pitmates" Mark Fahnestock, Andy Gaynor, Phil Ihinger, Cathy Smither and Frank Webb who showed me the ropes upon my early arrival. I have learned more from these individuals, and the many other Caltech students with whom I have overlapped during the last seven years, than from any other ingredient of my education.

Thanks to long-time friend and soccer coach, Karen Rothblatt, for continuing to believe in a 9-year-old's pronouncement of her desire to become a professor. Thanks to the C.S.U. Fullerton geology faculty, particularly chair Jerry Brem, who helped make that dream a reality.

My family has provided unquestioning support and encouragement during my education. My thanks and love to them all: my Los Angeles family, for their understanding during all of the family gatherings that I have missed because of lab and field work; my siblings, Cath, Lis and Will, who have kept me honest and aware of life outside of the physical sciences; my mother, who, in her own way, made it clear that the choices

in life were mine to make and supported those that I made; my father, whose tutelage and advice I have usually listened to while he suffered through my 10-alarm chili and caribou stew; and to the newest member, Zuma Jay, whose tiny presence has filled what could have been a very stressful spring with excitement and anticipation.

Finally, thanks and much more to my husband, Jeff, who has ridden the Caltech roller coaster with me from Day #1, providing the perspective and humor that I needed to survive and thrive. He has suffered much, having busted more peridotites, tasted more Italian wine, and drafted more figures than should be requested of any partner. Having found the perfect revenge for seven years of such treatment, he'll soon have me measuring ground cracks and collecting dirt samples. That seems a fair trade.

* * * *

This thesis is dedicated to my grandparents, Estella and Clem, who introduced my father to bones and, with him, encouraged my interest in rocks and flowers.

Abstract

Two igneous suites containing layered ultramafic-mafic cumulates were investigated with the intent to characterize the parental magma and to identify processes significant to the petrogenesis of these rocks. In both study areas, the early Cretaceous Sierra Nevada batholith and the Ivrea Zone, isotopic systematics of the cumulates were found to preserve the characteristics of the mantle-derived parental magma and to record the effects of fractional crystallization and assimilation. Modeling the relative importance of these processes and characterization of the material derived from the mantle are necessary to understanding the growth of the continental crust.

Geologic mapping of 110 mi^2 of the 125 to 110 Ma Stokes Mountain region reveals the presence of layered cumulate megaxenoliths and two coeval ring dike complexes. Petrographic analysis and geochemical modeling of 125 dominantly mafic and intermediate samples demonstrate the comagmatic nature of this suite. Combined oxygen, strontium and neodymium analysis of 22 samples indicates, however, that each ring complex was fed by an isotopically distinct parental magma ($\varepsilon_{Nd(115)} = +6.1$, $Sr_i = 0.70338$, $\delta^{18}O = 6.6‰$; $\varepsilon_{Nd(115)} = +5.7$, $Sr_i = 0.70372$, $\delta^{18}O = 6.7‰$) both of which were derived from a variably contaminated, depleted mantle source. Minor assimilation of continentally-derived metasediments and mafic-ultramafic material of the Kings-Kaweah ophiolite further affected the isotopic evolution of the two subsuites. Hydrothermal alteration in the subvolcanic environment is recorded only by rare stoped xenoliths of 120 Ma hypabyssal intrusives.

Late Hercynian ($\approx$ 300 - 270 Ma) magmatism produced the 10 km thick Mafic Complex lying at the base of the Ivrea-Strona-Ceneri crustal cross section. $\delta^{18}O$ analysis of 237 whole rock samples and 26 mineral separates reveals that presumably early intrusions into the cool crust preserve the depleted mantle signature of the modeled parental magma ($\varepsilon_{Nd(115)} = +7$, $Sr_i = 0.703$, $\delta^{18}O = 6.5‰$) while later intrusions assimilated significant amounts of the 10 - 12‰ metapelite. Subsequent intrusion of voluminous

basaltic magma formed a large, convecting magma chamber in which assimilation was concentrated within boundary layers. Such lower crustal production of high-^{18}O ($\delta^{18}O = 8$ - 10‰) mafic magmas is suggested as contributing to the petrogenesis of upper crustal Permian granites.

Table of Contents

Title Page i

Statement ii

Acknowledgements iii

Abstract vi

Table of Contents viii

List of Figures, Tables and Plates xv

Chapter 1. Introduction 1

1.1. The Case Studies 3

Chapter 1 Bibliography 5

Chapter 2. Petrography and Field Relations of the Stokes Mountain Region 7

2.1. Petrographic Description of the Stokes Mountain Suite 8

2.1.1. Khtr = Ultramafic-Mafic Cumulates 10

2.1.1.1. Hornblende-Poor Layered Adcumulates 11

2.1.1.2. Hornblende-Rich Layered Cumulates 13

2.1.1.3. Massive, Hornblende-Rich Orthocumulates 14

2.1.1.4. Orbicular Gabbros 14

2.1.1.5. Ocellar Gabbros 16

2.1.2. Kpg = Two Pyroxene Leucogabbro 16

2.1.3. Khpg = Biotite Hornblende Two Pyroxene Gabbro to Quartz Gabbro 17

2.1.4. Khg = Hornblende Gabbro 17

2.1.5. Kx1 = Mingled Norite, Khg, Kpg and Khpg 19

2.1.6. Kpht = Two Pyroxene Biotite Hornblende Quartz Diorite to Tonalite 21

2.1.7. Khbt = Hornblende Biotite Tonalite to Granodiorite With Lesser Biotite Leucotonalite 22

2.1.8. Kx2 = mingled Kpg, Khg, Khpg, Kx1 (Norite Facies), Kpht, Khbt, Minor Massive Ktr 23

2.1.9. Kgd = Hornblende Biotite Granodiorite With Lesser Muscovite Biotite Granite 24

2.1.10. Kx3 = Mingled Khg, Khbt and Kgd 26

2.1.11. Kp = Silicified, Porphyritic, Hypabyssal Xenoliths 27

2.1.12. m = Metamorphic Wallrocks 28

2.1.13. Qa = Quaternary Alluvium 30

2.2. Discussion of Petrographic Elements 31

2.2.1. Formation of Layered Cumulates 31

2.2.2. Formation of Orbicular and Ocellar Gabbros 34

2.2.3. Origin and Significance of Symplectites 37

2.2.4. Predominance of Orthopyroxene Over Clinopyroxene 38

2.2.5. Magma Mingling vs. Magma Mixing 40

2.2.6. Related Plutonic Suites 43

2.2.6.1. South America 43

2.2.6.2. Peninsular Ranges 44

2.2.6.3. Sierra Nevada 44

2.3. Geochronology of the Stokes Mountain Plutonic Suite 46

2.4. Discussion of Textural and Structural Elements in the Stokes Mountain Region 48

2.4.1. The Ultramafic-Mafic Cumulate Megaxenoliths 49

2.4.2. Supersolidus Structures and Post-Magmatic Deformation 50

2.4.3. Igneous Foliations and Intrusion-Related Mylonitization 52

2.4.4. The Stone Corral Shear Zone: Super- and Subsolidus Deformation 53

2.4.5. The Ring Complexes 55

2.4.6. Relationship of the Stone Corral Shear Zone (SCSZ) to the Ring Complexes 60

2.5. Discussion of Crustal Structure and Uplift History 63

2.5.1. Geophysical Anomalies 63

2.5.2. Implications for Crustal Structure and Uplift 67

2.6. Geologic History of the Stokes Mountain Region 71

Chapter 2 Figures 73

Chapter 2 Tables 79

Chapter 3. Geochemistry and Isotope Systematics of the Stokes Mountain Region 86

3.1. Geochemistry of the Early Cretaceous Batholith 87

3.1.1. Analytical Techniques 87

3.1.2. Analysis of Geochemical Data 88

3.2. Crystal Fractionation Model 91

3.2.1. The Fractionation Model 91

3.2.2. Discussion of Model Results 93

3.3. Isotope Systematics of the Stokes Mountain Region 96

3.3.1. Analytical Techniques for $\delta^{18}O$ Analysis 96

3.3.2. Analytical Techniques for Rb-Sr and Sm-Nd Analysis 98

3.3.3. Stokes Mountain Region: The Complete Data Set 99

3.3.3.1. Oxygen Isotope Systematics 100

3.3.3.1.1. Mineral Separates 100

3.3.3.1.2. Whole Rock Samples 101
3.3.3.2. Strontium and Neodymium Isotope Systematics of the Stokes Mountain Suite 103
3.3.3.3. Summary of Isotopic Systematics for Complete WKB Suite 104
3.3.4. Contrasting Isotopic Systematics of the WRC and ERC 104
3.3.4.1. Strontium and Neodymium Isotopic Systematics 105
3.3.4.2. Combined Stable and Radiogenic Isotopic Systematics 108
3.3.4.3. Isotopic Summary 114
3.4. Summary 116
Sierra Nevada Bibliography 119
Chapter 3 Figures 133
Chapter 3 Tables 153

Chapter 4. Introduction to the Ivrea and Strona-Ceneri Zones 171
4.1. The Ivrea Zone as a Lower Crustal Cross Section 171
4.1.1. Geophysical Characteristics 172
4.1.2. Metamorphic Facies and Thermobarometry 173
4.1.3. Structural Relationship to the Strona-Ceneri Zone 175
4.2. Petrologic Overview of the Ivrea Zone 176
4.2.1. Metamorphic Petrology 176
4.2.1.1. Metapelites 178
4.2.1.2. Migmatites 178
4.2.1.3. Metacarbonates 179
4.2.1.4. Amphibolites 179
4.2.2. Petrology of the Noncumulate Peridotites 181
4.2.2.1. The Balmuccia Peridotite 182

4.2.2.2. The Finero Peridotite 186

4.2.2.3. The Premosello Area 188

4.2.3. Petrology of the Mafic Complex 188

4.2.3.1. The Layered Series 189

4.2.3.1.1. The Basal Zone (BZ) 191

4.2.3.1.2. The Intermediate Zone (IZ) 192

4.2.3.1.3. The Upper Zone (UZ) 193

4.2.3.1.4. The Monte Capio Sill 194

4.2.3.2. The Main Gabbro (MG) 195

4.2.3.3. Diorites 196

4.2.3.4. Charnockites 197

4.3. Stuctural Characteristics of the Mafic Complex 198

4.3.1. Syn-Magmatic Structures 198

4.3.2. Syn- to Post-Magmatic Shear Zones 199

4.3.3. Post-Magmatic Faulting and Folding 201

4.4. Petrologic Overview of the Strona-Ceneri Zone 201

4.4.1. Metamorphic Serie dei Laghi 201

4.4.2. Igneous Graniti dei Laghi and Appinites 202

4.5. Evaluation of the Proposed Compound Igneous Suite 204

4.5.1. Geochemical Affinity of Compound Igneous Suite 205

4.5.2. Isotopic Models of Magmagenesis 205

4.6. Geologic History of the Ivrea Zone 207

4.6.1. Tectonic Environment of Magmagenesis 207

4.6.2. Tectonic Reconstructions 208

4.6.2.1. Convergent Margin 208

4.6.2.2. Extensional Regime 209

4.6.3. Geologic History of the Ivrea-Strona-Ceneri Crustal Section 210

4.7. Identification of Petrologic Significance 212

Chapter 4 Figures 214

Chapter 5. Oxygen Isotopic Investigation of the Mafic Complex and Associated Lithologies (Ivrea and Strona-Ceneri Zones, Southern Alps) 222

5.1. Review of Previous Oxygen Isotopic Work in the Ivrea Zone 222

5.2. The Present Study 224

5.2.1. Mineral Separates 225

5.2.1.1. Isotopic Reversals 226

5.2.1.2. Geothermometry 227

5.2.2. Stratigraphic Variations of Isotopic Systematics 228

5.2.3. Fractional Crystallization Modeling 232

5.2.4. Assimilation-Fractional Crystallization Modeling 233

5.2.4.1. Extension of the Voshage et al. (1990) Model to Oxygen Isotopes 233

5.2.4.2. Evaluation of Model Parameters 234

5.2.4.3. Test of Mixing Models and Identification of Discrepancies of the Model 237

5.2.4.4. Possibility of Isotopically Distinct Parental Magmas 240

5.2.4.5. Nature of the Crustal Contaminant(s) 241

5.2.4.6. Summary of Variations in $Sr_{(270)}$- $\varepsilon_{Nd(270)}$-$\delta^{18}O$ Space 243

5.2.5. Variations of $\delta^{18}O$ with SiO_2 Content 244

5.2.5.1. The Layered Series 244

5.2.5.2. The Main Gabbro 245

5.2.5.3. The Diorites 246

5.2.5.4. The Finero and Premosello Peridotites 248

5.2.5.5. The Monte Capio Sill 250

5.2.5.6. The Southern Ivrea Zone 251

5.2.6. Variations of $\delta^{18}O$ with Sr_i in the Graniti dei Laghi, Strona-Ceneri Zone 254

5.3. Summary and Interpretation of $\delta^{18}O$ Variations 257

5.4. Discussion of Other Hercynian Localities 260

Ivrea Zone Bibliography 266

Chapter 5 Figures 288

Chapter 5 Tables 320

List of Figures, Tables and Plates

Chapter 2 Figures

2.1: Approximate location of the Stokes Mountain region, California 73

2.2: Generalized stratigraphic column of the Stokes Mountain region, Tulare County, California 74

2.3: Reproduction of Figure 1 from Lesher and Walker, 1988 75

2.4: Generalized geologic map and geochronologic data 76

2.5: Structural overlay of the Stokes Mountain region illustrating the formation of the synmagmatic left-lateral Stone Corral Shear Zone between two, impinging, radially-extending ring complexes 77

2.6: Location of Stokes Mountain ring complexes relative to geophysical anomalies 78

Chapter 2 Tables

2.1: Mineral compositions of samples from the greater Stokes Mountain region including those used for the fractional crystallization model 79

2.2: Zircon isotopic age data 85

Chapter 3 Figures

3.1: Peacock variation diagram for WKB suite 133

3.2: SiO_2 vs. Al_2O_3 for WKB plutonic suite 134

3.3: SiO_2 vs. FeO* (total iron) for WKB plutonic suite 135

3.4: SiO_2 vs. MgO for WKB plutonic suite 136

3.5: SiO_2 vs. CaO for WKB plutonic suite 137

3.6: SiO_2 vs. Na_2O for WKB plutonic suite 138

3.7: SiO_2 vs. K_20 for WKB plutonic suite 139

3.8: SiO_2 vs. TiO_2 for WKB plutonic suite 140

3.9 SiO_2 vs. MnO for WKB plutonic suite 141

3.10 SiO_2 vs. whole rock $\delta^{18}O$ for samples from the Stokes Mountain region and the surrounding early Cretaceous batholith 142

3.11 SiO_2 vs. whole rock $\delta^{18}O$ for unaltered igneous samples from the Stokes Mountain region and the surrounding early Cretaceous batholith 143

3.12 Initial $^{87}Sr/^{86}Sr$ vs. εNd for samples from the Stokes Mountain region plus sample WKB65 144

3.13 1/Sr vs. initial $^{87}Sr/^{86}Sr$ for samples from the Stokes Mountain region plus sample WKB65 145

3.14 1/Sr vs. $^{87}Sr/^{86}Sr$ (115) 146

3.15 $^{147}Sm/^{144}Nd$ vs. εNd 147

3.16 $^{87}Sr/^{86}Sr$ vs. εNd (115) 148

3.17 $\delta^{18}O$ vs. $^{87}Sr/^{86}Sr$ (115) with metapelite sample 149

3.18 $\delta^{18}O$ vs. $^{87}Sr/^{86}Sr$ (115) without metapelite sample 150

3.19 Sr contours for the Stokes Mountain plutonic suite on generalized geologic map 151

3.20 εNd (115) contours for Stokes Mountain plutonic suite on generalized geologic map 152

Chapter 3 Tables

3.1: Whole rock geochemical analyses of WKB (Western Cretaceous Batholith) samples 153

3.2: Parameters for fractional crystallization model 162

3.3: Oxygen isotope data and calculated mineral pair temperatures from the Stokes Mountain region 163

3.4: $\delta^{18}O$ and SiO_2 analyses for selected WKB samples 165

3.5: Rb-Sr isotopic data for WKB samples 166

3.6 Sm-Nd isotopic data for WKB samples 167

3.7 Summary of $Sr_{(115)}$ and $\varepsilon Nd_{(115)}$ with SiO_2 and $\delta^{18}O$ for WKB samples 168

3.8 Approximate latitude and longitude of WKB samples locations for those samples collected prior to this study 169

Chapter 4 Figures

4.1: Location map showing the Ivrea Zone of NW Italy & S Switzerland with respect to major political and geomorphic boundaries 214

4.2: Map showing major geologic provinces, river valleys and lakes of the Ivrea and Strona-Ceneri Zones 215

4.3: Schematic cross section through the northwestern Italian Alps in the vicinity of the Ivrea Zone, the Strona-Ceneri Zone and the M. Nudo basin (after Zingg et al., 1990) 216

4.4: Map showing generalized geology, prominent igneous bodies and locations 217

4.5: Sample location and generalized geology of the Finero Peridotite Complex after A. Steck & J.-C. Tieche (1976) 218

4.6: Generalized geologic map of the central Mafic Complex 219

4.7: Map showing sample locations and generalized geology of the Monte Capio Region, Ivrea Zone 220

4.8: Generalized geology of Monte Barone area, southern Ivrea Zone 221

Chapter 5 Figures

5.1: $\delta^{18}O$ for coexisting plagioclase and pyroxene 288

5.2: $\delta^{18}O$ for coexisting plagioclase and amphibole 288

5.3: Variation of oxygen isotopic composition of mineral and whole rock samples with stratigraphic height within the Mafic Complex 289

5.4: Variation of mineral pair temperature with stratigraphic position within the Mafic Complex 290

5.5: Whole rock $\delta^{18}O$ vs. calculated mineral pair temperature 291

5.6: Stratigraphic variation of εNd (270) and Sr (270) within the Mafic Complex of the Ivrea Zone (after Voshage et al., 1990) 292

5.7: Generalized geologic map and oxygen isotopic analyses of the central Mafic Complex 293

5.8: Whole rock $\delta^{18}O$ values of samples from the central Mafic Complex, Ivrea Zone 294

5.9 SiO_2 vs. $\delta^{18}O$ for the Mafic Complex, Ivrea Zone 295

5.10 Reproduction of Figure 4 from Voshage et al., 1990 296

5.11 Sr_i (270) vs. εNd (270) for subset of Voshage et al. (1990) samples analyzed for $\delta^{18}O$ 297

5.12 εNd vs. $\delta^{18}O$ with simple mix and AFC curves between mantle and crustal components 298

5.13 Sr_i (270) vs. $\delta^{18}O$ with simple mix and AFC curves drawn between mantle and crustal components 299

5.14 Whole rock $\delta^{18}O$ values of wall rock and septa divided by lithology and field occurrence 300

5.15 Sr_i vs. 1/Sr showing AFC and simple mixing curves 301

5.16 Nd vs. 1/Nd with mixing curve between mantle and crustal components 302

5.17 Sr_i vs. $\delta^{18}O$ for the central Mafic Complex, Ivrea Zone 303

5.18 εNd vs. $\delta^{18}O$ for the central Mafic Complex, Ivrea Zone 304

5.19 SiO_2 vs. $\delta^{18}O$ for the Layered Series 305

5.20 SiO_2 vs. $\delta^{18}O$ for the BZ, IZ, UZ and MG 306

5.21 SiO_2 vs. $\delta^{18}O$ for the UZ, MG and diorite samples with arrow showing maximum increase in $\delta^{18}O$ attributable to fractional crystallization 307

5.22 SiO_2 vs. $\delta^{18}O$ contrasting normal diorites to roof diorites 308

5.23 SiO_2 vs. $\delta^{18}O$ for samples from mingling horizons in the diorite unit 309

5.24 SiO_2 vs. $\delta^{18}O$ for the MG compared to aphanitic dikes and enclaves found within the diorite unit 310

5.25 SiO_2 vs. $\delta^{18}O$ for samples from the Finero Complex, Ivrea Zone 311

5.26 Stratigraphic comparison of $\delta^{18}O$ from the Finero and Premosello peridotite complexes 312

5.27 SiO_2 vs. $\delta^{18}O$ for samples from the Monte Capio Sill 313

5.28 SiO_2 vs. $\delta^{18}O$ for gabbros, diorites and charnockites from the southern Ivrea Zone 314

5.29 SiO_2 vs. $\delta^{18}O$ for charnockites and wall rocks in the southern Ivrea Zone (Valle Sessera and Valle Strona di Postua) 315

5.30 Sr_i vs. $\delta^{18}O$ comparing the Graniti dei Laghi to the Mafic Complex 316

5.31 Sr_i vs. $\delta^{18}O$ comparing appinites from the Strona-Ceneri Zone to the Mafic Complex 317

5.32 Sr_i vs. $\delta^{18}O$ comparing appinites and granites of the Strona-Ceneri Zone to charnockites of the southern Ivrea Zone 318

5.30 SiO_2 vs. $\delta^{18}O$ for Massif Central xenoliths and Hercynian plutonics compared to the Mafic Complex, Ivrea Zone 319

Chapter 5 Tables

5.1: Major element chemistry, location and oxygen isotope analysis of samples from the central Mafic Complex, Ivrea Zone, Italy 320

5.2: Major element chemistry and oxygen isotopes of samples from Finero (F), Monte Capio Sill (MC), Rocca d'Argimonia (RA) and Strona di Postua (SP), Ivrea Zone 329

5.3: Major element and isotopic data from the Ivrea Zone 338

5.4: Major element and radiogenic isotope data from the Mafic Complex, Ivrea Zone 344

5.5: $\delta^{18}O$ and Sr_i data from the Strona-Ceneri Zone 346

5.6: Major element chemistry for samples in Table 5.5 347

5.7: Oxygen isotope values of samples from the Ivrea and Strona-Ceneri Zones which lack other isotopic or chemical data 348

5.8: Oxygen isotope data and calculated mineral pair temperatures from the Mafic Complex, Ivrea Zone 349

Plates (located in affixed envelope)

1: Geologic map of the Stokes Mountain region, Tulare County, California

2: Geologic and sample location map of the Stokes Mountain region, Tulare County, California

Chapter 1: Introduction

With the advent of deep continental drilling and improved geophysical techniques earth scientists theoretically have the tools necessary to study the structure and composition of the continental crust in three dimensions. The nature of the lower crust remains elusive, however, due to the technical difficulties of deep drilling and to the model-dependent nature of geophysical interpretations. Geologists have two lines of recourse: (1) study lower crustal xenoliths brought to the surface by volcanic eruptions; (2) study exposures of the lower continental crust. Drawbacks are inherent to both schemes: xenoliths represent random and possibly altered samples while exposed lower crustal terranes are rare and may not be representative of the lower continental crust. Xenoliths do provide a valuable view of the heterogeneity of the in situ lower crust, but the absence of spatial relationships between samples makes the study of exposed terranes the more viable technique for studying the compositional structure of the lower crust.

Identification and analysis of exposed lower crustal terranes has been the subject of recent interest in the earth science community (Boriani and Fountain, 1988; Salisbury and Fountain, 1990). Three of the recognized lower crustal terranes stand out as possible cross sections through lower crust: the Ivrea Zone of the western Italian Alps, the Kohistan complex of Pakistan, and the Wawa - Kapuskasing terrane in southeastern Canada. Of these the Ivrea Zone is most representative of Phanerozoic continental crust; the Kohistan complex is a cross section through an island arc (Jan and Howie, 1981; Dietrich et al., 1983) while the Kapuskasing terrane is a section through Proterozoic crust (Percival, 1988).

One similarity that the proposed cross sections share with many of the other exposures of high pressure crustal rocks, such as those found in the Musgrave range of central Australia, the Lewisian granulite terrane of Scotland, and the Kasila Group of western Africa, is the presence of layered ultramafic-mafic cumulates (Davies, 1974; Williams and Williams, 1976; Moore and Goode, 1978; Sills et al., 1982). Such rocks

have independently been proposed as being significant constituents of the lower crust based on their abundance in xenolith suites (Kay and Kay, 1981) and on the interpretations of geophysical studies (Smithson and Brown, 1977). The apparently common occurrence of layered cumulates in the lower crust suggests that the analysis of these rocks might reveal general characteristics of lower crustal magmatism or processes of crustal evolution. It is this hypothesis which formed the initial motivation for this thesis.

Two case studies were investigated with the aim of testing the suitability of cumulate studies to exploring the genesis of the lower continental crust: the layered Mafic Complex of the Ivrea Zone and cumulate megaxenoliths of the early Cretaceous Sierra Nevada batholith. The 10 km thick Mafic Complex is the best available example of a layered intrusion exposed at the base of a crustal cross section; this body records the chemical evolution of underplated magmas in an extending continental environment. The cumulates of the Sierra Nevada batholith provide information concerning the mafic endmembers involved in the generation of a thick crustal column at a convergent margin.

The significance of layered cumulates provided by these case studies is summarized as follows. Layered ultramafic-mafic cumulates found in lower crustal environments may represent the first products formed upon the intrusion of mantle-derived mafic melts into the crust. The presence of layering is inconsequential beyond the fact that the textures are indicative of the cumulate process and are suggestive of a dynamic state within the magma chamber stable enough to allow the preservation of such layers within the semi-crystalline pile. What is significant is the composition of such cumulates: the ultramafic nature indicates that they are the crystallization products of a chemically unevolved magma. Whereas bulk chemistry will be controlled by the elemental partition coefficients for the crystallizing phases, the isotope systematics of these cumulates have the potential to record both the character of the material added to the crust and the effects of processes operative during the earliest stages of evolution of the mantle-derived magma. The study of the

isotope systematics of lower crustal layered ultramafic-mafic cumulates, therefore, addresses both the nature and the evolution of the lower crust.

This type of analysis not only provides insight into the lower continental crust, but also demonstrates the range of modifications that a melt can experience in the lower crustal environment. Such knowledge is necessary to interpret the geochemical characteristics of middle and upper crustal igneous rocks which contain components generated in the lower continental crust.

1.1 The Case Studies

Analysis of the oxygen isotope systematics of the Mafic Complex is presented in Chapter 5. This study was part of a collaborative effort in which the field relationships, petrography, bulk geochemistry, and radiogenic isotope systematics were studied by other researchers. These data have been combined to model the effects of the emplacement of a large volume of melt into the base of a hot, thick crust and to speculate on the significance of this magmatism in the generation of middle and upper crustal Hercynian igneous rocks. The Sierra Nevada study consists of the field investigation, petrographic and isotopic analyses of the Stokes Mountain region; geochemical analyses were provided by a collaborator. The field and geochemical data are modeled as recording the effects of the intrusion of a large volume of mantle-derived melt(s) into a relatively thin, cold crust of a transitional composition between oceanic and continental affinity.

The products of this study are as follows: (1) the most extensive oxygen isotope data base to date for lower crustal igneous rocks in which field, geochemical and, in many cases, radioisotopic (Sr, Nd) control is also available; (2) a geologic map of approximately 110 mi^2 of the western foothills of the Sierra Nevada (Plate 1; scale 1:64,000 reduced from complete coverage at 1:24,000); (3) one of the most detailed petrologic, geochemical and isotopic studies of a single suite of ultramafic to intermediate igneous rocks from the North American Cordillera. Beyond the discussions included in this thesis, the geochemical analyses produced by Dr. B. W. Chappell and Dr. S. Sinigoi for the western

Cretaceous batholith and Ivrea Zone suites, respectively, will be analyzed further elsewhere. The complete analyses are published here in order to provide the maximum possible cohesiveness between the geochemical and isotopic data bases.

The presentation order of these two case studies has been reversed in the following chapters. This order was chosen because the Sierran study involves the description and analysis of many types of geologic data while the Ivrean study is an in depth analysis of a single type of isotopic data: many topics discussed in the Sierra Nevada study are thus referred to in the Ivrea Zone discussions. The petrographic, geochronologic and field relations of the Stokes Mountain region are described in Chapter 2; in Chapter 3 the geochemical and isotopic data are analyzed in light of the previously developed geologic history. In Chapter 4 all pertinent literature and observations are reviewed which are relevant to the interpretation of the isotopic evolution of the Mafic Complex which is detailed in Chapter 5.

Chapter 1 Bibliography

Boriani, A. C. and D. M. Fountain, 1988, Programme, abstracts, field trip guide. Italy - U.S. Workshop on the Nature of the Lower Continental Crust, Verbania, Italy, Universita di Milano: Ricerca Scientifica ed Educazione Permanente.

Davies, F. B., 1974, A layered basic complex in the Lewisian, south of Loch Laxford, Sutherland: Journal of the Geological Society of London, v. 130, p. 279-284.

Dietrich, V. J., W. Frank and K. Honnegger, 1983, A Jurassic-Cretaceous island arc in the Ladakh-Himalayas: Journal of Volcanology and Geothermal Research, v. 18, p. 405-433.

Jan, M. Q. and R. A. Howie, 1981, The mineralogy and geochemistry of the metamorphosed basic and ultrabasic rocks of the Jijal Complex, Kohistan, NW Pakistan: Journal of Petrology, v. 22, n. 1, p. 85-126.

Kay, R. W. and S. M. Kay, 1981, The nature of the lower continental crust: Inferences from geophysics, surface geology, and crustal xenoliths: Reviews of Geophysics and Space Physics, v. 19, n. 2, p. 271-297.

Moore, A. C. and A. D. T. Goode, 1978, Petrography and origin of granulite-facies rocks in the western Musgrave Block, Central Australia: Journal of the Geological Society of Australia, v. 25, n. 6, p. 341-358.

Percival, J. A., 1988, A field guide to the Kapuskasing Uplift, a cross section through the Archean Superior province in Salisbury, M. H. and D. M. Fountain, ed., Exposed Cross-Sections of the Continental Crust: Dordrecht, Holland, Kluwer Academic Publishers, ed. p. 227-284.

Salisbury, M. H. and D. M. Fountain, Ed., 1990, Exposed cross-sections of the continental crust. NATO Advanced Science Institutes Series C: Mathematical and Physical Sciences. Netherlands, Kluwer Academic Publishers.

Sills, J. D., D. Savage, J. V. Watson and B. F. Windley, 1982, Layered ultramafic-gabbro bodies in the Lewisian of northwest Scotland: geochemistry and petrogenesis: Earth and Planetary Science Letters, v. 58, p. 345-360.

Smithson, S. B. and S. K. Brown, 1977, A model for lower continental crust: Earth and Planetary Science Letters, v. 35, p. 134-144.

Williams, H. R. and R. A. Williams, 1976, The Kasila Group, Sierra Leone, an interpretation of new data: Precambrian Research, v. 3, p. 505-508.

Chapter 2. Petrography and Field Relations of the Stokes Mountain Region

The Stokes Mountain region is located in the westernmost foothills of the Sierra Nevada mountain range, approximately 16 miles miles northeast of Visalia and 40 miles southeast of Fresno, CA (Figure 1). Approximately 110 mi^2 of citrus groves and cattle pastures was mapped at a scale of 1:24,000 during the period of fall of 1988 to spring of 1990. The map region occupies the totality of the Stokes Mountain, CA 7.5' quadrangle (SM) and portions of the adjoining Auckland (A), Ivanhoe (I), Orange Cove South (OCS), Tucker Mountain (TM) and Woodlake (W) quadrangles. Due to the large number of field sheets and the large aerial extent of many of the mapped units, the geology of the Stokes Mountain region has been reduced to a scale of 1:62,500 on Plate 1. WKB (Western Cretaceous batholith) sample locations as well as locations of samples I2A, SM3, SM199, SM204, and W170 are plotted on Plate 2. Approximate locations for samples WKB 1-68, which were collected prior to this study, are listed in Table 3.8.

The original intent of this study was to investigate the geochemistry of the km-scale blocks, or megaxenoliths, of layered ultramafic-mafic cumulates which form the prominent mountains known as Colvin, Stokes and Tucker. Such lithologies are rarely exposed in the Cordilleran batholith chain yet have been proposed as forming a large component of the sub-batholithic crust. By studying the cumulates we hoped to learn something of the growth of the lower regions of the Sierran batholith. While this goal was approached, the project was soon enlarged to include an investigation of the petrogenesis and structure of the surrounding noncumulate lithologies which appear to be consanguineous with the megaxenoliths. Subsequent mapping revealed one, and possibly two, large ring complexes, and the study of the associated textures and structures in light of the geochronological systematics of the suite has constrained much about the upper crustal emplacement history of the exposed lithologies. Finally the recognition of a spatial relationship between the ring complexes and recognized geophysical anomalies mandated an interpretation of these anomalies in terms of the details of the Stokes Mountain suite.

In this chapter, the petrology of the mapped units is described and discussed with reference to pertinent magmatic processes and complementary case studies. Following this, the geochronological and structural relationships are described and interpreted. After considering what is understood concerning the geophysical structure of the batholith, the geologic history of the Stokes Mountain region is reconstructed. In the following chapter, the interpretation of the geochemical and isotopic systematics will be demonstrated as being highly dependent upon the geologic framework described in the present chapter.

2.1 Petrographic Description of the Stokes Mountain Suite

The Stokes Mountain plutonic suite is dominated by gabbros and tonalites in contrast to the granodioritic average composition of the exposed Sierra Nevada batholith. Between 130 and 110 Ma (section 2.3) the early Cretaceous suite was emplaced into metamorphic lithologies of the Kings-Kaweah ophiolite, fragments of which are exposed in the study area. The mineralogy of the plutonic suite varies regularly from olivine- to pyroxene- to hornblende- to biotite- dominated lithologies, and whole rock chemical variations are smooth for all elements over a range of SiO_2 from 40% in the cumulates to 78% in the rare granites. As discussed in Chapter 3, fractional crystallization accounts for the range in igneous lithologies although evidence exists for limited magma mingling and possible mixing.

While this study presents the first detailed mapping and geochemical analysis of the Stokes Mountain region, other researchers have previously described the geology in partially overlapping and neighboring areas. Those parts of the Woodlake and Auckland quadrangles included in this study comprised the western edge of study of the metamorphic lithologies of the Three Rivers area (Durrell, 1940). More detailed understanding of the petrogenesis of the metamorphic lithologies as well as the first detailed description of the ultramafic-mafic lithologies of the early Cretaceous batholith was provided in Saleeby's study of the Kings-Kaweah ophiolite belt (Saleeby, 1975). In addition to Saleeby's work, the igneous lithologies which comprise the early Cretaceous batholith in the area in question

have been described elsewhere: the Academy zoned complex and associated gabbroids to the northwest (Macdonald, 1941; Mack et al., 1979; Mack et al., 1986), the Rocky Hill stock to the southeast (Putman and Alfors, 1965), and the range of lithologies in the Stokes Mountain and neighboring areas (Durrell, 1940; Saleeby and Sharp, 1980). Strong similarities are evident between the studied suites and those described below; the lithologic variations and structural relations specific to the Stokes Mountain region, however, merit a detailed characterization prior to interpreting the details of the isotope systematics.

Although Plate 1 represents the smallest scale map available of the igneous lithologies of the Stokes Mountain region, it should be noted that the intent of this project is the identification and characterization of the lithologies of the early Cretaceous batholith. As such, locations of contacts may not be always as precise as possible. This is especially true of gradational contacts separating units Kphg and Kpht and Khbt, the pyroxene-, hornblende- and biotite-bearing quartz diorites, tonalites and granodiorites. Such contacts may, in fact, be very simplified contours of mafic mineral abundances, but more intense scrutiny of the exact location of these contacts was not deemed significant at this time.

The petrologic descriptions are organized in the following order: plutonic units are described in approximate order of increasing silica content; associated lithologies are described in order of decreasing age from the preplutonic metamorphic lithologies to the postplutonic sediments. Rock names are based on the Streckheisen classification (Streckheisen, 1973). A copy of the explanation for Plate 1 is included in the text for reference to the geologic symbols (Fig. 2.2). A limited number of mineral compositions are included in the following descriptions. Most were analyzed in this study using a scanning electron microscope; these compositions are compiled with older compositional data (J. B. Saleeby, personal communication) in Table 2.1 and discussed further in Chapter 3. Additional estimates of plagioclase composition were determined optically by the Michel-Levy technique and are included only in the following discussion. The following abbreviations of mineral names will be employed in Chapters 2 and 3: ol (olivine), opx

(orthopyroxene), cpx (clinopyroxene), plag (plagioclase), hb (hornblende), sp (spinel). The cumulate terminology employed follows the definitions found in Irvine (1987).

2.1.1. Khtr = Ultramafic-Mafic Cumulates

This unit is comprised of troctolites of variable hypersthene and hornblende contents. The most striking characteristic of the cumulates is the common occurrence of well developed layering in the hornblende-poor varieties. Layering in the hornblende-rich lithologies, formed by aligned hornblende oikocrysts, is equally distinctive but not as planar. Associated with, as well as found separately from, the layered cumulates is a very distinctive, massive, hornblende-rich mesocumulate of comparable mineralogy. These three common textural types, along with two rare textural types, orbicular and ocellar gabbros, will be described in some detail below. Each of the five textural types is designated with an individual map overlay pattern on Plate 1 at outcrops where the texture is well developed.

It should be emphasized that a number of intermediate and relatively unimpressive textural varieties are associated with the above types. These types are not individually designated on the map and will not be described in detail. It is presumed that the mineralogical and chemical variations discussed in this and following sections apply equally to these textural types. These types include irregularly layered to massive, very fine- to medium-grained, hornblende-poor troctolites, pods of olivine-poor anorthosites often with isolated hornblende oikocrysts, and olivine norites. Commonly there is a chaotic spatial relationship between these types on outcrop scale; dikes of hornblende gabbro, unit Khg, of highly variable grain size, is often associated in these cases. Examples of such relationships are found on central and southern Colvin Mountain, on the ridge south of Tucker Mountain, and on the northwest corner of Stokes Mountain. It is notable that the best developed orbicular gabbros are found in the latter case at the intrusive contact between such a texturally chaotic area and a distinct igneous unit, Kpg. A similar association has been recognized in the Peruvian Coastal batholith (Bussell, 1988)

2.1.1.1. Hornblende-poor Layered Adcumulates

Rhythmic layering is defined predominantly by modal variations of the cumulate phases plagioclase, olivine and orthopyroxene as well as the intercumulate phase, amphibole. The ratio of olivine to orthopyroxene within the melacratic layers varies greatly; with the exception of western Stokes Mountain, however, olivine is significantly more abundant than orthopyroxene. In other words, orthopyroxene-free layered cumulates are common, whereas olivine-free layered cumulates have not yet been recognized. The hornblende content is highly variable resulting in adcumulate and mesocumulate textures.

The plagioclase is unzoned and highly calcic, ranging from anorthite to labradorite (An92- 60). It is tabular, with crystal faces best developed in contact with amphibole. Albite twinning is dominant, with lesser Carlsbad and pericline twinning. In thin section, the plagioclase c-axes may be crudely oriented parallel to the plane of layering. Olivine is moderately fosteritic (Fo78 - Fo70) and is sub- to euhedral, with a grain size ranging from 0.5 - 5 mm. The orthopyroxene is bronzite to hypersthene having an Mg number of 0.78 to 0.65, rarely singly twinned, and pleochroic tan to pink. Occasionally it contains exsolved clinopyroxene lamelli or exsolved spinel rhombs forming a schiller texture. Where cumulate, it is of a comparable grain size to olivine. Where noncumulate it either rims the cumulate olivine or is involved in a symplectic intergrowth with spinel. The primary amphibole is hornblende which is pleochroic tan to brown. The hornblende varies in texture from rimming to poikilitic with respect to the mafic cumulate phases as the abundance of amphibole increases. Rarely, there are trace amounts of acicular, red-brown biotite which do not appear texturally to be secondary. Small amounts of fine-grained, sub- to euhedral, optically opaque phases (Fe-Ti oxides) are also present.

The secondary amphibole replacing the hornblende is optically classified as uralite (pale green to colorless, low birefringence) and may be cummingtonite. The uralite is fibrous and is commonly oriented radially to any enclosed cumulate phase. Orthopyroxene (both that rimming the olivine and the cumulate grains) may be similarly replaced.

A variety of minerals are secondary after olivine. Most commonly a mixture of deep golden yellow iddingsite and fine-grain opaques forms along the cracks and as fibrous masses at the margins of the olivine grains. Apparently lower temperature, serpentine alteration attacks remnant olivine forming a fine-grained mixture of serpentine, talc, magnesite, magnetite, clinozoisite and quartz. In these instances, the coexisting plagioclase is moderately saussuritized and marginally recrystallized, but at the stage when only uralite has formed the coexisting plagioclase appears unaltered. The earlier formed uralite is usually preserved during the serpentinization, but has also been found altered to medium-grained, fibrous serpentine and iron oxides. In the latter instance, any remaining hornblende is subject to chloritization.

The layering is dominantly cm to dm (0.5 - 30 cm) thick, although surprisingly continuous monograin layers of olivine occur. Layer thickness may vary considerably within a single outcrop. Total thickness of layered packages is impossible to estimate due to incomplete outcrop, but may be many hundreds of meters thick on Colvin, Stokes and south Tucker mountains. For similar reasons the laterally continuity of individual layers is limited by outcrop length which is generally less than 10^1 m, occasionally increasing 10^2 m on places such as the western end of Stokes Mountain.

The best defined layering is formed by duplets of olivine- and plagioclase-rich layers which are separated from adjacent duplets by sharp boundaries; the boundary within the doublet is gradational, spread over many grain widths. Occasionally, multiple duplets of varying thicknesses will occur between a pair of sharp boundaries. The layers are modally graded and are classified as rhythmic. If the dunitic layer is presumed to form at the base of the doublet then the modal grading is usually normal, but examples of reverse modal grading, particularly within the anorthositic layers, also occur. Whereas olivine mode decreases towards the anorthositic layer its grain size may increase in this direction such that the poorly developed grain size grading opposes the modal grading. In general, all phases in the anorthositic layers are coarser than the corresponding phases in the dunitic

layers. Sometimes there are associated mesocratic troctolite layers (ol = 20%) in addition to the anorthositic (90% or greater modal plagioclase) and dunitic (approximately 90% modal olivine) layers.

Variations between layers and localities include the development or absence of symplectite, the grain size of a given phase, the degree of secondary alteration, and the degree of plagioclase polygonalization. The latter feature is attributable to recrystallization and is also manifest as a bimodal distribution of plagioclase grain sizes. In these cases the large plagioclase grains preserve crenulate margins and are surrounded by small, equant neoblasts with dominantly 120° crystal face intersections. The extent of all of these features may be controlled by a combination of deformation-related recrystallization and layer parallel fluid flow. Such flow was either near-solidus fluid flow in the case of symplectite development or hydrothermal fluid flow in the development of alteration mineralogies.

2.1.1.2. Hornblende-rich Layered Cumulates

Less common layering is formed in the hornblende-rich troctolites to olivine gabbros by the modal variation of hornblende. Olivine, pyroxene and plagioclase are present as inclusions within the hornblende. The layering within these hornblende-rich cumulates is less well defined than in the hornblende-poor cumulates because the layers are formed by planar concentrations of very coarse-grained (3 - 7 cm) hornblende oikocrysts. The layers are generally one oikocryst thick, resulting in scalloped boundaries between the hornblende- and plagioclase-rich layers. The horizontal continuity of the layers is not great; textures and grain sizes vary widely. Rarely pegmatitic layers display comb layering (Saleeby, 1975) which may indicate the presence of a free aqueous fluid phase (Moore and Lockwood, 1973).

The hornblende-rich layered cumulates are not found interspersed with the hornblende-poor layered cumulates, but instead form isolated packages. Abundant Khg dikes are associated with the hornblende-rich Khtr. The mineralogic affinity of this textural subtype with Khg should be noted; however, the moderate abundance of olivine and

pyroxene as well as the layered texture prompted the assignment of the hornblende-rich layered cumulates to unit Khtr.

2.1.1.3. Massive, Hornblende-Rich Orthocumulates

Associated with the layered cumulates are bodies of massive, medium- to very coarse-grained hornblende troctolite. Intrusion of this material appears to be directly correlated with deformation of the layered cumulates as discussed below. Where the margins of the massive bodies are observable, the bodies are irregular to pod shaped. These rocks also occur as dike-like masses either enclosing large xenoliths of layered material or without any associated layered troctolites.

The color index varies with the modal abundance of interstitial hornblende which is generally greater than 20% and may reach 70%. Such rocks may contain up to equal amounts of orthopyroxene and olivine (hypersthene troctolite); occasionally they contain clots of fine-grained orthopyroxene and opaques. Plagioclase grains frequently reach 4 cm in length and often are strikingly inclusion-free; small plagioclase neoblasts may rim the coarser grains. In some relatively hornblende-poor mesocumulates, the interstitial amphibole has been altered resulting in a uralite rim surrounding a pyroxene rim which surrounds the remnant olivine.

2.1.1.4. Orbicular Gabbros

Orbicular gabbros are characterized by the presence of closely packed, spherical to ellipsoidal orbicules. They are dominantly 2 - 25 cm in diameter although exceptions occur, including one possible orbicule approximately 2 m long. The orbicules shells are composed of very fine-grained layers of granular orthopyroxene and plagioclase with highly variable amounts of olivine. The orthopyroxene tends to be coarser than the olivine, but rarely there are medium-grained olivines at the boundary between olivine- and orthopyroxene-rich layers. Rarely the olivine is moderately elongate in a radial fashion. The individual layers are composed of opx + plag, opx + ol + plag, ol + plag and plag-only. In some orbs there is a slight concentration of opaque phases at the boundaries

between ol- and opx-dominant layers which highlights the layers, but otherwise the opaques are randomly distributed. The types and arrangement of layers varies between orbs, but may be similar within a given outcrop, and the variability is most strongly related to the relative proportions of olivine and orthopyroxene. There are also layers defined by the presence of subhedral hornblende oikocrysts; otherwise hornblende in the layered region is minor and found enclosing or associated with the orthopyroxene-rich layers.

The groundmass and centers of the orbs are mineralogically similar to non-orbicular, olivine-bearing to olivine-free, hornblende norites with the possible exception being the more frequent occurrence of coarse-grained poikilitic hornblende and medium-grained poikilitic orthopyroxene within the orb centers. For example, in one orb there are two large glomerocrysts of orthopyroxene and hornblende in the core. In the groundmass olivine, when present, occupies cores of orthopyroxene.

In places, the layered shells are truncated by reentrants of medium-grained plagioclase, orthopyroxene and olivine (as cores in opx) and poikilitic hornblende. The layers end abruptly and are not pinched, so they were either replaced or were never formed in the reentrant. In one case, a reentrant connects with a rare medium-grained shell; this relationship may suggest the recrystallization of this shell and the reentrant to a coarser-grain size.

The orbicules occur in closely packed swarms and are often touching. In one instance, the nuclei of two orbicules appear to have joined with the enclosing layers encircling both nuclei. This orb is unique in that it contains trace amounts of acicular biotite oriented randomly near the core. Commonly the orbs are deformed, with the orientation of the long axis of the resulting ovoid being roughly constant within an outcrop. They are generally surrounded by a 1- to 2-grain thick plagioclase zone, although rarely a single hornblende oikocryst spans this mafic-depleted zone. Occasionally, coarse orthopyroxene appears to have nucleated around the outside of the orb, and may be marginally intergrown with the outer fine-grain layer of the orb.

2.1.1.5. Ocellar Gabbros

The ocellar gabbros are small bodies without discernable margins, found associated with layered and massive cumulates. Ocellar troctolites differ from orbicular gabbros in many respects. Most noticeably, the structures are not composed of fine-grained spherical layers of equant phases, but instead are composed of highly elongate, radially oriented grains of olivine that form a single shell. The olivine appears to have nucleated on a large-grained plagioclase crystal or glomerocryst or on a coarse hornblende crystal. The ocelli are 2 to 5 cm in diameter and are more commonly spherical than ovoid. Any olivine within the core appears to be smaller than olivine external to the structures; generally only minor amounts of hornblende is found in the core. Minor anhedral or poikiolitic orthopyroxene is found in association with the olivine; there is also some highly corroded medium-grained orthopyroxene surrounded by hornblende in the ocellar groundmass. Amphibole, dominantly a pale, fibrous uralite, rims the olivine.

2.1.2. Kpg = Two Pyroxene Leucogabbro

This unit is comprised of fine- to medium-grained, leucocratic, two pyroxene gabbro to quartz gabbro. The orthopyroxene is pink to tan pleochroic hypersthene (En62) and is subequal to greater in abundance than the pale green augite. The plagioclase is andesine (An48) which forms subhedral laths displaying albite twinning. Generally the plagioclase crystals are larger than the pyroxene; some unusually large plagioclase crystals contain abundant pyroxene inclusions. The unit contains minor olive hornblende which occurs either as thin rims around the pyroxenes or as isolated oikocrysts. Dark reddish brown biotite is rare. Quartz, found in low amounts, is interstitial and is associated with myrmekite. The total content of hydrous phases increases with the quartz mode.

The dominant texture is massive. Exceptions include igneous foliation defined by aligned pyroxene glomerocrysts and lineation defined by aligned plagioclase laths. Small pods of massive Khtr orthocumulate are associated with these varieties (Stokes and Colvin Mountains). Planar distributions of elongate hornblende oikocrysts are rare; the possible

origin of this fabric is discussed in section 2.4.2. Polygonal, apparently recrystallized, plagioclase is not common, but may indicate the presence of internal contacts: for example, the central area of Curtis Mountain may be formed by a 100-300 m wide dike of foliated, recrystallized Kpg surrounded by unfoliated Kpg. Protogranular texture is found on Stokes Mountain and may be related to the Stone Corral Shear Zone which is discussed in section 2.4.4.

2.1.3. Khpg = Biotite Hornblende Two Pyroxene Gabbro to Quartz Gabbro

This unit is similar to Kpg except that it is dominantly medium-grained and has an overall greater abundance of quartz and hydrous phases. The hydrous phases are less to subequal in abundance with total pyroxene, and the unit grades into Kpht (section 2.1.6) as the pyroxene mode becomes less than that of the hydrous phases. Olive-brown hornblende is the dominant, hydrous phase, but some varieties are dominated by dark reddish-brown biotite. The minor amount of secondary amphibole is blue-green. Plagioclase laths are andesine (An46) in composition. Salitic clinopyroxene is less abundant than hypersthene, and some varieties are actually hornblende norites and quartz norites. In the latter, the quartz forms medium-grained, subhedral phenocrysts. Fine-grain glomerocrysts of equant hypersthene and spinel are rarely present. These are believed to represent recrystallized symplectites after olivine. All phases are subhedral, equant with hornblende oikocrysts; on Tucker Mountain, however, this lithology is found as an isolated dike bearing acicular hornblende.

The dominant texture is massive, however lesser amounts of other units are intermingled producing relationships similar to those described for unit Kx1. The overall steep topography results in poor outcrops of this unit.

2.1.4. Khg = Hornblende Gabbro

The dominant phases are olive hornblende and plagioclase, with variable brown biotite and spinel contents. Hornblende is variably replaced by blue-green amphibole and the plagioclase is commonly sericitized. Olivine and pyroxene crystals may occur as

resorbed cores within the hornblende. As the abundance of such cores increases the rock grades into orthopyroxene-bearing unit Khtr described above, with the exception that the olivine and pyroxene cores found in Khg are commonly ragged in appearance. Fine-grain glomerocrysts of equant hypersthene and spinel are rarely present but suggest the previous presence of olivine. Some bodies contain trace amounts of euhedral epidote and sphene. The plagioclase (An82) is commonly euhedral, particularly when surrounded by poikilitic hornblende.

This unit is texturally extremely variable. The grain sizes range from very fine-grained to plagioclase-porphyritic to hornblende porphyritic (tabular to acicular) to medium-grained to very coarse-grained. Fabrics include comb layering with acicular hornblende in the coarse-grained varieties and weak layering defined by sieve textured hornblende oikocrysts similar to that found in hornblende-rich Khtr. Generally, the unit is unlineated except in dikes where plagioclase crystals or acicular hornblende may be well aligned. Often there is a bimodal distribution of plagioclase grain size, with the smaller grains being of a comparable size to the groundmass hornblende. In many of the dikes, the coarse plagioclase crystals have a single, outer mantle of different composition which may have formed subsequent to quenching and during the rapid crystallization of the fine-grained groundmass.

This lithology is found as dikes cutting the layered cumulates, small to large bodies composed of 100% cross cutting dikes and pods of a spectrum of textural varieties and as large bodies of homogenous, plagioclase porphyritic gabbro. Diking was an important mode of emplacement for this unit. Even the large, texturally homogenous body which forms Red Mountain displays roughly concentric air photo lineaments which may be controlled by the emplacement of discrete dikes or inwardly dipping cone sheets. The presence of this rock as dikes as well as the intimate coexistence of an extreme range of grain sizes suggests that this lithology was extremely mobile and may have been characterized by a wide range of fluid activities. Cross cutting relationships, as well as the

zircon geochronology, argue for multiple generations of this unit spanning the complete age range for the Stokes Mountain plutonic suite.

Khg also occurs as variably deformed enclaves within mingling zones (see units Kx1, Kx2, Kx3). The enclaves are composed of both the fine-grained and the plagioclase porphyritic varieties and rarely are quartz-bearing. The enclaves range from spherical to strongly ovoid where generally the longest dimension (width to height ratios of 1:8 to 1:20) is near vertical; the shortest dimension is always perpendicular to any foliation within the surrounding unit. As might be expected from its composition, this unit appears to have been emplaced at a higher temperature than the intermediate units with which it comingled; the enclaves are quenched relative to the surrounding matrix although there is some mineralogic suggestion of limited mixing producing quartz in Khg at the enclave margins. Occasionally enclaves and dikes of Khg are fractured and filled with felsic material emanating from Khbt.

A minor facies of Khg occurs as 2-5 meter wide dikes which cut northwest across the foliations and contacts of the southern edge of the Eastern Ring Complex (section 2.4.5). This facies contains sub- to euhedral, blue-green hornblende which forms well defined subhedral clots. The texture suggests replacement, possibly after pyroxene. Rare clots of orthopyroxene and spinel suggest complete replacement of olivine. The zircon date of sample W116 is slightly discordant suggesting minor local assimilation of Jurassic (?) material (section 2.3) which the dike cuts across.

2.1.5. Kx1 = Mingled Norite, Khg, Kpg and Khpg

This unit contains chaotically mingled Khg, Khpg and lesser Kpg in which the contact relations between lithologies do not display any recognizable, systematic pattern and many texturally intermediate varieties are present.

In addition to those units previously described, unit Kx1 contains abundant norite and hornblende norite which is not mapped as a separate unit elsewhere. The norite is composed of fine- to medium-grained, equigranular to pyroxene-porphyritic varieties and

may contain minor quartz. In the equigranular varieties the hornblende, when present, rims the pyroxene. The orthopyroxene porphyritic variety contains minor clinopyroxene and olivine; the latter is associated with symplectites and only occurs as highly replaced cores in masses of fine-grained hypersthene. One pod contains abundant (2%) poikilitic opaques which interfinger with hornblende oikocrysts. Overall, it appears that this unit is transitional between orthocumulate Khtr and Kpg, with the medium-grained variety more closely resembling Khtr and the fine-grained variety resembling Kpg. Fine- and medium-grained varieties of quartz norite are found intermingled with Khg; such mingling may produce hornblende quartz norites.

The fine-grained norite includes a highly distinctive textural variety. This variety has a spotted appearance in which strongly aligned, ovoid volumes of hornblende-absent norite of 1 to 3 cm in length are surrounded by orthopyroxene-free, fine-grained Khg. The olive hornblende is medium-grained directly adjacent to the norite blebs; this coarser grain size may be due to expulsion of water from the hornblende-free norite during crystallization. Eu- to subhedral opaque phases are evenly distributed. All phases are roughly aligned with the elongation direction of the blebs and defining a fair igneous foliation.

This facies is interpreted to represent mingled hornblende-free norite and biotite-bearing Khg. Justification for this interpretation is derived form two sources. First, in the Stone Corral Shear Zone this "blebby" facies is associated with meter-wide dikes of what clearly is interdiked norite and Khg in which the individual veins of each lithology are approximately 5 mm wide (see section 2.1.8). It is not difficult to envision the individual veins "breaking up" into ovoid structures of similar dimensions thus forming the spotted facies. Second, in thin section it is clear that the spotting is not simply the result of hornblende oikocrysts as there is no way to explain the exclusion of orthopyroxene crystals from the hornblende-rich areas or, conversely, the exclusion of hornblende crystals from the orthopyroxene-rich areas. It should be noted that all three phases -- orthopyroxene,

hornblende and plagioclase -- are sub- to euhedral, are of equivalent size, and apparently crystallized relatively simultaneously. It is not possible that the ovoids are the result of subsolidus deformation of interdiked norite and Khg as none of the crystals display internal deformation or are recrystallized.

From these relationships the blebby norite facies of Kx1 is interpreted as forming during small scale mingling during simultaneous emplacement of Khg and norite within dikes. There are also samples in which mixing is approached. In such rocks, remnant pods of medium-grained, hornblende-free norite are found in fine-grained biotite hypersthene hornblende gabbro. Additional evidence for mixing and disequilibrium is the very coarse, moderately resorbed xenocrysts of plagioclase which contain many fine-grained biotite and hornblende inclusions.

2.1.6. Kpht = Two Pyroxene Biotite Hornblende Quartz Diorite to Tonalite

This unit contains lithologies mineralogically gradational between Khpg and Khbt and Kpg and Khbt; as a result it is somewhat variable in appearance and may have a relatively wide range of geochemical characteristics. The unit is defined as having hornblende plus biotite contents greater than the pyroxene content. Pyroxene crystals are dominantly found inside the core of hornblende crystals and are variably replaced by masses of fine-grain, blue-green amphibole and quartz blebs. The replaced pyroxenes are easy recognizable in hand sample as rusty cores. Replacement of primary olive-brown hornblende and pyroxene by blue-green amphibole is near complete in the eastern section of the map (specifically in the Eastern Ring Complex or ERC discussed in section 2.4.5) while in the west (the Western Ring Complex or WRC) most pyroxene in this unit is relatively unaltered. Hypersthene is more abundant than augite although to the north the two pyroxenes are modally subequal. The abundance of golden yellow to brown pleochroic biotite is quite variable, and the grains range from fine-grained euhedral crystals to coarse, isolated oikocrysts. The small amount of potassium feldspar in the more evolved

lithologies is interstitial and commonly involved in a myremekitic intergrowth with the interstitial quartz. Minor oxides and sphene are present.

Outcrops of Kpht weather a distinctive purplish-brown to blue-grey color. Generally the lithology is massive and medium-grained, but small masses of fine-grained equivalents can also be found. It contains unmapped, irregular lenses of Khbt, lesser pods of Kpg and Khpg, and scattered to abundant, elongate Khg enclaves often forming swarms (similar to unit Kx3). The enclave elongation defines the only recognizable foliation within this unit. In some outcrops there is evidence for multiple generations of Khg enclaves, and dikes of Khg are commonly located at mapped contacts between Kpht and Khbt. Finally, a single, small xenolith of layered Khtr was found in unit Kpht east of Curtis Mountain mimicking the larger scale relationship between units Kpht and Khtr found on Colvin Mountain.

2.1.7. Khbt = Hornblende Biotite Tonalite to Granodiorite With Lesser Biotite Leucotonalite

This unit is much more homogenous in appearance than Kpht. Pyroxene is uncommon to absent and is limited in occurrence to the altered cores of hornblende crystals. More commonly the past presence of pyroxene is identifiable by cores within the hornblende of fine-grained, pale blue-green hornblende and quartz. The hornblende to biotite ratio is highly variable. Hornblende is pleochroic tan to blue-green while biotite is pleochroic tan to dark brown. Increased quartz and potassium feldspar contents are correlated with the disappearance of pyroxene cores. The potassium feldspar is interstitial and associated with myremekite while the plagioclase (An40-25) forms subhedral laths. Minor amounts of spinel and sphene, commonly associated with clots of biotite and hornblende, are present along with subhedral, secondary epidote in the mildly altered samples. Apatite is present in the volumetrically minor biotite leucotonalite.

Outcrops of unit Khbt are medium grey to white. This unit generally displays a nonpervasive, weak to moderate igneous foliation often highlighted by the presence of

meter-wide swarms of elongate Khg, Khpg and biotite hornblende quartz diorite enclaves. Within the topographic moat outside of Blue Mountain but within the Eastern Ring Complex, this unit contains lesser amounts of undivided Kpht, Khg and Kgd.

The unit is strongly foliated near some intrusive contacts and along discreet shear zones. In addition a pervasively protomylonitic facies of Khbt exists in the southwestern section of the ERC. Deformation is recorded by oscillatory to recrystallized quartz ribbons, bent albite twins, and biotite flakes smeared around the marginally recrystallized, plagioclase porphyroclasts. This facies forms screens within unfoliated Khbt and Kpht. As the main facies of Khbt can display foliation along intrusive margins, the contacts between the protomylonitic and undeformed facies are not easily identified.

2.1.8. Kx2 = mingled Kpg, Khg, Khpg, Kx1 (Norite Facies), Kpht, Khbt; Minor Massive Ktr

This unit is comprised of mingled and interdiked bodies of the units listed in the definition. Individual dikes range from cm to m in thickness; mingling occurs on a similar scale. The details of the structural relationships between the encompassed lithologies will be discussed in section 2.4.4 concerning the Stone Corral Shear Zone (SCSZ). Furthermore, all lithologic components are described elsewhere in this section with one exception being a volumetrically minor facies of norite. This facies forms veinlets which cross cut the strong fabric of the SCSZ. These veinlets are distinctive in that euhedral, 0.5-3 mm hypersthene crystals are concentrated either within the center or along the margins of the vein.

The intermingled norite and Khg (section 2.1.5) displays additional peculiarities in this unit. First, the norite forms thin dikes and tubules in addition to isolated blebs. The hypersthene still appears fine-grained in thin section (0.5-1 mm), but is often optically continuous with many, but not all, of the other orthopyroxene grains. Moreover, the 2 mm long oikocrysts, containing plagioclase inclusions, are vertically elongate parallel to the dike margins suggesting growth during upward emplacement. Another distinctive feature

is the presence of 2 mm plates of brown biotite within the 0.1 - 0.5 mm hornblende gabbro which are oriented parallel to the igneous foliation and are fragmented but not disrupted in both the vertical and horizontal directions. No other phases display any internal deformation. This, and the coarser grain size, suggests that the biotite was an early crystallizing phase which experienced differential stress during emplacement and prior to complete solidification. This lithology is interpreted as intermingled norite and hornblende gabbro, as discussed in section 2.1.5, with an overprint of synmagmatic shear (section 2.4.4).

Despite the apparent similarity between Kx1 and Kx2 in terms of the great overlap in which units are involved in the mingling, this unit differs significantly from Kx1. Unit Kx2 appears to represent mingling between mapped units along an intrusive contact with subordinate contributions from other units. For example, in Kx2 the abundance of a lithology defining one side of the contact decreases regularly with distance from the mapped body of that particular lithology across the mingled zone. Furthermore, all fabrics, both igneous and deformational, within the zone are parallel to the enclosing contacts. Neither is the case in Kx1 with the exception of the body at the western edge of Red Mountain in which internal contacts may parallel the enclosing mapped contacts. Kx1 appears to represent mingling at deeper levels than currently exposed while in Kx2 mingling appears to have been frozen in at the current level of exposure.

2.1.9. Kgd = Hornblende Biotite Granodiorite With Lesser Muscovite Biotite Granite

The most abundant facies is a medium- to coarse-grained, pink to white weathering, seriate biotite granodiorite. It is leucocratic, having a color index of less than or equal to 10. Blue-green hornblende and/or muscovite occur in lesser amounts with brown biotite. Pyroxene cores within hornblendes are exceptionally rare. Quartz is interstitial to anhedral; potassium feldspar, with recognizable microcline twinning and mild perthitic texture, is both interstitial and forms anhedral equant grains. A minority of the sub- to anhedral plagioclase (An35) crystals are coarse-grained and inclusion-rich suggestive of a complex

crystallization history. Minor subhedral sphene, often concentrated along biotite cleavages where it may be secondary, and lesser apatite are present.

Kgd contains lesser elongate schlieren and mafic enclaves of Khbt and Khg, but the unit is otherwise unfoliated, except where as emplaced as thin dikes in which case the margins may be protomylonitic. In these instances the quartz forms ribbons which grade in texture from displaying oscillatory extinction to polygonal recrystallization. The feldspars are marginally recrystallized, and the micas are smeared around the porphyroclast boundaries. The interfingering outcrop pattern suggests that this unit was intruded as thin sheets, generally concordant with the foliation in the adjacent units. Slightly crosscutting relationships also occur suggesting that the Kgd was the last unit to be emplaced. Kgd often contains unmapped, discreet dikes of Kpht, and dikes of Khg are found intruded along margins of the Kgd pods.

This unit is rarely involved in mingling relations with other units. Minor mingling, and possible mixing, with other units forming unusually textured granitoids appears to occur only at the tapered tails of well defined Kgd pods.

Included in this unit are a number of volumetrically minor lithologies which have been emplaced as thin, crosscutting dikes. These are predominantly quartzofeldspathic bodies bearing lesser muscovite and include pegmatitic quartz veins and perthitic potassium feldspar veins with minor quartz and muscovite. Graphic intergrowths are common. The most distinctive lithology included in this unit is a leucocratic dike containing zoned, schorl tourmaline and plagioclase rosettes which are distributed along the dike's central plane surrounded by a granular quartz matrix. Along this plane the rosettes can be seen to be evenly spaced in two dimensions. This lithology is volumetrically minor but is widespread, being found on Tucker, Curtis and Stokes Mountains.

The third lithology to be included in this unit is a cordierite garnet muscovite leucogranite. It represents a minor volume of rock found only in the northwestern corner of the mapped area. It is medium-grained to aplitic in texture, and is characterized by the

presence of euhedral, 1-4 mm red garnet crystals. The garnet is found either disseminated or concentrated in leucocratic veins. A single, subhedral xenocryst of andalusite mantled by muscovite has been identified. At the margin of the garnet muscovite leucogranite is another unusual texture which is localized at the contact with the unit Khbt. It is characterized by leucocratic, hollow spheres having a 2-4 cm diameter. These bleached spheres are composed of twinned cordierite and quartz and do not appear to have an unusual phase present in the nucleus. The origin of these structures is presently unclear.

2.1.10. Kx3 = Mingled Khg, Khbt and Kgd

This unit is dominated by Khbt containing up to 35% by area of ellipsoidal enclaves of aphanitic and plagioclase porphyritic Khg with a lesser amount of Kgd forming discrete lenses. Less commonly Khbt forms poorly defined lenses within Khg. Kx3 is located between mapped bodies of Khg, Khbt and Kgd within the ERC (section 2.4.5) and represents mingling between these lithologies at the present level of exposure. Both groundmass and enclaves may be unfoliated, foliated or protomylonitic.

Involved in the mingling is a very coarse-grained, quartz diorite facies of Khbt which is uncharacteristic for this unit in two respects: this facies lacks pyroxene cores and is generally devoid of sphene. The Khg enclaves also differ somewhat from the mapped unit : in general, the enclaves are more biotite- and quartz-rich, and the hornblende is not brown but blue-green. The Khg enclaves rarely contain inclusion-rich, plagioclase xenocrysts. These plagioclase display a thin, sericitized (white mica and epidote) mantle which is surrounded by an inclusion-free outermost zone which is interpreted as an overgrowth. These observations suggest that the lithologies present in Kx3 are somewhat compositionally modified from the "normal" composition of the units found removed from the mingled zones. Such modification may be due to limited mixing or diffusional exchange with enhanced low temperature alteration. Finally, there are smaller bodies within unit Kx3 which appear to be related to the common plagioclase-porphyritic Khg by

the removal of much of the fine-grained groundmass. Such removal might be an example of flow segregation.

The enclave groundmass is in places highly texturally variable containing diffuse schlierin, chaotic grain size variations, and faintly defined enclaves having a color index intermediate to Khg and Khbt. There are small amounts of texturally nonequilibrium rocks containing rimmed plagioclase xenocrysts. While these relationships suggest that the formation of thoroughly mingled, or mixed, lithologies is possible in this environment, mixing does not appear to have been an efficient mechanism for producing large volumes of magma having intermediate compositions at this level of exposure.

2.1.11. Kp = Silicified, Porphyritic, Hypabyssal Xenoliths

This unit forms four, 100 m^2 perched outcrops within Khbt in the Western Ring (?) Complex (section 2.4.5) and five, similar sized outcrops within the Eastern Ring Complex. The lithology is orangish-white to grey weathering with 1-3 mm pits where the plagioclase and pyroxene phenocrysts have been preferentially weathered. The unit is extremely resistant and breaks under protest into sharp slivers.

In thin section it can be seen that this resistance results from the presence of a fine-grained silica matrix interpreted as resulting from hydrothermal deposition. Oxygen isotope systematics, discussed in Chapter 3, agree with this interpretation for all blocks within the WRC. No isotopic analyses were performed on the outcrops in the ERC.

The pyroxenes are strongly resorbed as evidenced by the corroded margins and mottled birefringence as well as possibly by the unusual abundance of opaque inclusions. The hornblende and biotite are less resorbed. The feldspar population is unusual in that the plagioclase are commonly zoned; this texture is otherwise found only in dikes of Khg but is a common feature of shallow and extrusive igneous rocks. The zoning, in addition to the porphyritic texture, supports the interpretation of an hypabyssal environment of emplacement. Potassium feldspar, displaying microcline twinning, forms discrete, anhedral grains.

Unit Kp contains small (2-10 cm) xenoliths which appear to be olivine and pyroxene-bearing, but they are also highly silicified making protolith identification difficult. The presence of a clot of fine-grained, euhedral orthopyroxene and oxides similar to clots found in intermediate lithologies (such as units Kpg and Khg) which were interpreted as recrystallized symplectites after olivine suggests a genetic link or at least a common mineralogic evolution between unit Kp and the surrounding Stokes Mountain plutonic suite.

2.1.12. m = Metamorphic Wallrocks

This unit is comprised of a variety of dominantly metasedimentary lithologies which are exposed along the eastern edge of the map area. These lithologies have been previously divided into the Lemon Cove schist, the Homer quartzite, and the Yokohl amphibolite (Durrell, 1940), but this division was not applied in this study.

Metamorphic rocks in the field area are exposed predominantly on the eastern half of the mapped area. In the northeast the major lithologies are banded quartzite, pelitic-psammitic schist and a highly distinctive and continuous, stretched quartzite pebble conglomerate. In the southeast the small area of unit m exposed is composed of finely laminated chert and carbonate. Whether a significant difference in protolith exists between the southern and northern ends cannot be addressed with the small number of metamorphic samples studied. It should be noted that in Drumm Valley (one mile east of the northeast corner of the mapped area) there is a body of blue calcite which has in the past been mined for tungsten (contact metamorphism related scheelite) and decorative building stone,

The metamorphic mineralogy does differ between the northeast and southeast. In the northeast, partial melting occurred near the igneous contact form leucocratic veins which in places bear hornblende and euhedral almandine garnet . Melting and limited magmatic assimilation possibly occurred along contacts where abundant, strongly veined, metasedimentary xenoliths are found in the igneous unit. In addition to partial melting, the presence of high temperatures within the contact aureole is documented by the common

occurrence of fibrous sillimanite and some samples are highly recrystallized. Sillimanite is a common contact mineral associated with the early Cretaceous batholith (Dodge, 1971). These rocks contain abundant cordierite attesting to the aluminous and magnesian composition of the protoliths and the low pressure of contact metamorphism.

In the southeast garnet is the dominant metamorphic mineral: garnet forms both fine-grained, granular aggregates and coarse-grained, anhedral oikocrysts. The light green carbonate has been metamorphosed at the albite-epidote hornfels facies. The chert contains abundant clinozoisite instead of epidote reflecting the relatively iron-poor bulk chert composition. Whereas the garnet-bearing leucosomes are not found in the south, minor cordierite-bearing quartz veins cross cut one chert sample.

The presence of sillimanite with garnet and cordierite indicates that conditions of contact metamorphism reached the hornblende hornfels and possibly the pyroxene hornfels facies. Estimates of the average conditions of contact metamorphism in the Sierra Nevada range from 550 to 679°C assuming a water pressure of 1-2 kbar (Kerrick, 1960). The general lack of retrograde metamorphic effects in Sierran contact aureoles has been attributed to the batholithic magmas being undersaturated with respect to volatiles until the latest stages of crystallization (Putman and Alfors, 1965).

Most foliations are near vertical and parallel the igneous contact. The stretching lineation in the pebble conglomerate is also near vertical, and aspect ratios are approximately 1:10 in vertical cross section. The intrusion contact can be straight or highly convolute, but tends to parallel foliation. Meter scale folds document limited intrusion-related deformation; quartz in all lithologies, however, is commonly undulatory.

There are a few outcrop-sized xenoliths enclosed by the Stokes Mountain igneous suite which are possibly metaigneous. These samples contain minor amounts of sphene, elongate to acicular blue-green amphibole as well as biotite with lesser muscovite. These phases bear resemblance to the igneous suite, but in addition contain cordierite making a definite protolith assignment problematic.

While few metamorphic rocks are exposed along the western edge of the mapped area, there is reason to believe that the protoliths of the wall rocks of the WRC differed from those of the ERC. This hypothesis is suggested by the northwestward extension of a contact mapped in the Lemon Cove area approximately 15 miles to the southeast (J.B. Saleeby, unpublished mapping) which projects into the mapped area coincident with the ERC-WRC boundary, This contact separates metabasalts and serpentinites to the southwest from continentally-derived clastics on the northeast. The clastic lithologies are believed to have been either deposited upon or thrust into the Kings-Kaweah ophiolitic basement. In a gross sense, this contact is reflected by outcrop pattern in the Stokes Mountain region as correlatives of the clastics are exposed along the eastern edge of the field area, while metabasalts and serpentinites are exposed 5 km beyond the western edge of the mapped area on Smith Mountain near Dinuba. From outcrop, however, it is not apparent that the contact conforms with the ERC-WRC boundary, but isotope systematics discussed in Chapter 3 indicates this to be the case.

2.1.13. Qa = Quaternary Alluvium

This unit is comprised of poorly consolidated fluvial deposits composed of cobble- to silt-sized particles. Boulder-sized particles are included in the incised fanglomerates which are poorly developed along the western side of the ridge between Tucker and Curtis Mountains identified as the Pleistocene, nonmarine, Riverbank Formation (Oliver and Robbins, 1982). Most of the particulate matter presently being deposited, with the exception of material carried by Sand and Cottonwood Creeks, is derived from outcrop within the mapped area.

The age of the deposits can be constrained to the late Pleistocene by the presence of a fossil mammoth tusk found in the deposits of Cottonwood Creek east of Colvin Mountain (W. A. Clemens, personal communication).

Quaternary mass movement may have affected the outcrop pattern of many of the units discussed above. Although landslide-related features are not the subject of this study,

two possible examples will be noted. The first is located in section 1 of the Tucker Mountain quadrangle NNW of Tucker Mountain. Here the mapped outcrops of Ktr and Khg are unusual: Khg forms two lobate protrusions projecting downslope and Ktr forms isolated masses unusual in that they are not ridge forming (one mass is low-lying and the other is composed of blocks on the side of a very steep slope). Outcrops of both units are limited to meter-sized blocks lacking any interblock relationships. The poorly developed dendritic drainage pattern around these units may indicate the presence of an ancient (>10,000 yr), deep-seated landslide which emanated northward from Tucker Mountain. The second example is located on the NE side of Colvin Mountain between 1300 and 600 feet in section 10. Here the jagged topography and downslope scars possibly result from recent, wedge-type failure controlled by jointing. Large blocks of Ktr are located at the base of the slope beneath these rock fall scars. The formation of such scars may be a common characteristic of the oversteepened slopes surrounding the outcrops of this particularly resistant lithology.

2.2. Discussion of Petrographic Elements

The Stokes Mountain suite contains features of general petrologic interest as well as elements which provide insight into processes involved in generation of this specific suite. In this section the formation of layered cumulates, orbicular and occellar gabbros and orthopyroxene-spinel symplectites is discussed. Subsequently the significance of orthopyroxene and mafic enclaves is explored and the suite is evaluated in comparison to similar suites in the Cordillera.

2.2.1. Formation of Layered Cumulates

The best developed layered cumulates in the study area are the rhythmically layered hornblende-poor troctolite adcumulates composed of cm to dm-scale duplets which grade from olivine-rich at one margin to plagioclase-rich at the other. While this study does not provide any new insight into the formation of layered cumulates, three subjects need to be

reviewed in order to understand the range of possible formation processes for these rocks: adcumulate growth, rhythmic layers and modal layering.

The major difficulties with the origin of adcumulates is identifying the chemical renewal and physical removal mechanisms of the residual intercumulus liquid, the prior presence of which is required for the growth of unzoned crystals. Chemical communication between the intercumulus liquid and the magma chamber by chemical diffusion is limited by diffusion lengths to the uppermost levels of the cumulate pile. Convective circulation of the intercumulus liquid through the cumulate pile might extend the formation of adcumulates to deeper levels of the cumulate pile but is limited by permeability to a connected porosity of approximately 11% (Kerr and Tait, 1985) which is above the 0 to 7% intercumulus material strictly considered appropriate for adcumulates (Irvine, 1987). Compaction of the intercumulate pile and upward expulsion of the fractionating intercumulus liquid might promote infiltration metasomatism and aid adcumulus growth (Irvine, 1980), but compaction requires either an exceptional thickness or deformation of the cumulate pile (Stolper et al., 1981).

The formation of rhythmic layers has been attributed to the multiple intrusion of discrete magma batches as well as the interplay of chemical and thermal diffusion rates with nucleation and crystallization (McBirney and Noyes, 1979). In this model, crystallization of a phase produces a local zone of depletion of the requisite chemical components for that phase. Due to small chemical diffusion rates relative to thermal diffusion rates, the depleted zone may not be replenished of the depleted component prior to solidification, so crystallization of that phase will be chemically suppressed in the depleted zone. It is difficult to envision this process as forming cumulates at the base of a magma chamber as the temperature gradient should increase upwards, but may be important in the nucleation dominated, outward growth of the Stokes Mountain orbicular gabbros (section 2.2.2).

The role of crystal settling in forming modally graded layers has recently come under scrutiny as the settling time scales have been estimated and relationships suggesting

growth in situ have been identified. Lesher and Walker (Lesher and Walker, 1988) have experimentally tested a process called thermal migration which may be particularly appropriate for the modally layered troctolite adcumulates of the Stokes Mountain suite. The model relies upon the existence of a thermal gradient across the individual layer without addressing how that layer is formed, and evaluates the combined effect of that gradient with the temperature dependence of the composition of the liquidus phase in a simple binary system. Initially nuclei of the liquidus phase will be evenly distributed through the layer but will be preferentially dissolved at one end of the thermal gradient as the chemical constituents migrate down their respective concentration gradients (Fig. 2.3).

Next Lesher and Walker consider the effect of the differing diffusivities of the chemical constituents within the melt. This effect is called the Soret effect and basically means that matrix builders preferentially diffuse towards the hot end of the gradient. When these two processes are combined in an olivine-saturated magmas for a plagioclase-olivine binary the two effects reinforce each other leading to adcumulus growth of olivine at the cold end of the thermal gradient. Experiments with the thermal gradient decreasing upward demonstrated that thermal migration counteracts crystal settling. The authors estimate that thermal migration may operate on a dm scale for a 1 km thick cumulate pile which is appropriate for the Stokes Mountain cumulates.

The processes discussed above are possibly involved in cumulate formation, but no claim is made as to the exact origin of the Stokes Mountain cumulates. The layered cumulates of the Stokes Mountain suite do provide a good view of the processes presumed to be significant in forming the dominantly granitoid batholith, but as these rocks are only exposed as internally deformed xenoliths, the origin of rhythmic modal layering is probably best explored by the theoretical consideration of more complete exposures of fossil magma chambers. In terms of understanding the petrogenesis of the Stokes Mountain suite, the important point is that olivine and plagioclase were efficiently fractionated, although the specific processes involved in the fractionation are unconstrained.

Two less common types of layering are present in the study area. In two localities hornblende-plagioclase cumulates contain layers which are defined by coarse hornblende oikocrysts. This type of layering has been attributed to diffusion rate controlled oscillations in the availability of the hornblende component in the intercumulus liquid (Saleeby, 1975). Rare, coarse grained comb layers appear to represent the inward growth of hornblende in a volatile-rich magma or fluid phase (Moore and Lockwood, 1973). The presence of such layers separating cumulate from noncumulate intervals as previously described (Saleeby, 1975; Walawender, 1976) was not recognized in this field area.

2.2.2. Formation of Orbicular and Ocellar Gabbros

As Leveson stated in his 1966 review of orbicular rocks, there are many varieties of orbicular rocks and there is no reason for a single model to explain all types, except that it seems that the development of all types may be somehow controlled by the rate of chemical diffusion (Leveson, 1966). He proposed a division of orbicules into two types: those in which the core and the surrounding matrix were compositionally similar and those in which there was substantial chemical contrast. The orbicules described in this study are of the former class.

Orbicules are found at other localities in the Sierra Nevada and Peninsular Ranges batholiths (Lawson, 1904; Moore and Lockwood, 1973). In some cases the orb cores are identified as being previously crystallized material such as fragments of orbs or layered cumulates and xenoliths (Emerson, 1963). The formation of Sierran diorite-hosted orbicules have been interpreted in terms of a model for the formation of comb, or Willow Lake-type layering (Moore and Lockwood, 1973). Both orbicules and the associated comb layering are believed to crystallize from an upward moving, low viscosity aqueous fluid, the orbicules being carried by this rapidly streaming fluid. Rapid changes in fluid composition responsible for formation of the layering are ascribed to new magma pulses in the underlying, devolatilizing magma chamber or to structural movements allowing new fluids in the underlying chamber to be tapped. This model requires that the spaces between

the orbicules be subsequently filled with magma or by crystallization from the aqueous fluid. Perhaps the model is appropriate for the Graveyard Lakes locality where the diorite orbicules are surrounded by a granitic to granodioritic matrix, but this model cannot be easily extended to the Stokes Mountain area where the core and matrix of the orbicules are compositionally and texturally identical.

There are suggestions for both orbicules and ocelli of the Stokes Mountain gabbros that the core was frequently dominated by a preexisting phenocryst or glomerocryst. This is clear in the ocelli where the radially arranged, acicular olivine presumably nucleated from the center and grew rapidly outwards. It is less apparent in the orbicules where central glomerocrysts or oikocrysts are only occasionally identifiable; in general the grain size of orthopyroxene and plagioclase is identical in the cores and the groundmass of the orbicules in contrast to the exceptionally coarse-grained cores of the ocelli. Perhaps the phenocryst size equivalence inside and outside of the orbicules is an indication of the spatial distribution of crystals within the magma prior to orbicule formation. If the crystal mush was composed of glomerocrysts and scattered crystals, then the glomerocrysts may have acted as orbicule nuclei while similar yet isolated crystals were trapped between the orbicules. The rare occurrence of medium-grained olivine within the shell layers suggests that the coarser crystals were occasionally trapped within the outward growing layers of the orbicules. Crystallization continued within the groundmass after orbicule formation as is demonstrated by the poikilitic intergrowth of groundmass orthopyroxene with the fine-grained outer layers of some orbicules.

Close packing of the orbicules suggests the possible removal of some of the groundmass after orbicule formation (Moore and Lockwood, 1973). Despite the present close packing of the orbicules only one example of two fused orbicules has been recognized. This suggests that during orbicule growth, the orbicules generally were not closely spaced.

In the Stokes Mountain region as well as other localities (Moore and Lockwood, 1973; Walawender and Smith, 1980), orbicules are found along vertically oriented intrusive contacts. The significance of this observation is unclear but may indicate that a thermal disturbance prompted the rapid crystallization of the orbicules. Juxtaposition next to a cooler wall rock during intrusion may have prompted rapid undercooling of the host magma along the contact. The importance of formation near an intrusive contact is further suggested by the common deformation of the orbicule swarms which indicates that the orbicule host continued to flow and experience shearing during or shortly after orbicule formation. Flow is also supported by the infrequent occurrence of truncated layers within the shells suggestive of physical abrasion during shell formation. Reports of broken orbicules forming cores of orbs in other localities indicates that deformation occurred during orbicule formation (Moore and Lockwood, 1973).

The difference between orbicule and ocellus formation may be partially related to the host lithology. The ocelli are present in troctolites in which olivine was the crystallizing mafic phase. Quenching, or undercooling, would have promoted rapid nucleation and radial growth of olivine on preexisting phenocrysts. In contrast, the orbicular gabbro host and core lithology is a hornblende norite in which olivine is present only as cores within the orthopyroxene yet fine-grained olivine is abundant in the orbicule shells. This indicates that at the onset of orbicule formation, olivine was not present on the liquidus. Somehow intrusion of the host magma changed the conditions of crystallization and brought olivine back onto the liquidus during orbicule crystallization.

The observations noted above implicate rapid growth resulting from local supercooling during emplacement as a probable process involved in orbicule formation. Oscillation between orthopyroxene- and olivine-rich layers may have been caused by a diffusion controlled, localized depletion of the orthopyroxene component similar to the formation of Liesegang rings (Leveson, 1966). In other words, rapid nucleation and crystallization of orthopyroxene depleted the immediately surrounding magma in silica and

promoted the renewed crystallization of olivine. Leveson states that this possibility requires that the liquid composition be near a eutectoid, so that minor local depletion of a given component would drive the liquid into another mineral's stability field. This is reasonable given that olivine is found in the cores of the larger orthopyroxene crystals indicating that olivine had been on the liquidus previously. Rapid, acicular growth of the olivine crystals as formed the ocelli did not occur in the orbicules because the surrounding magma was not saturated in olivine.

In light of the above observations, the following scenario for orbicule formation appears appropriate. Upwards intrusion adjacent to a cooler wallrock supercooled the border zone of the upwardly moving magma. Rapid nucleation of the liquidus phases, orthopyroxene and plagioclase, occurred on glomerocrysts or possibly on brecciated pieces of a partially crystallized mush. Undercooling promoted rapid growth of the nucleated phases which outpaced the inward diffusion of silica. Olivine was thus compositionally stabilized in the local silica-depleted environment; nucleation and growth of this phase counteracted the dearth of silica, and orthopyroxene was once again stabilized. Continued movement of the host magma adjacent to the wall rock produced the ellipsoidal geometry of the orbicules and the close packing through removal of some fraction of the surrounding matrix magma. During the latest stages, intercumulus phases crystallized between the orbicules and the groundmass.

2.2.3. Origin and Significance of Symplectites

As mentioned above, noncumulate orthopyroxene often occurs in small amounts in a symplectite intergrowth with spinel as a partial to complete replacement of the cumulate olivine. Such growths are interpreted as resulting from near solidus disequilibrium between the early crystallized olivine and the most evolved melt fraction. These intergrowths form wart-like patches primarily along the margins of the olivine grains, and their development appears to be enhanced in the vicinity of primary oxide crystals. This

orthopyroxene is optically discontinuous within the intergrowth allowing identification of this paragenesis even when replacement of the olivine has proceeded to completion.

Apparently the symplectites are subject to recrystallization when entrained and preserved in more siliceous, olivine-free lithologies. Recrystallization results in clots of euhedral, fine-grained orthopyroxene and spinel; the clots are of a size comparable to the original olivine grains and symplectites and occasionally surround relict olivine cores. Similar textures have been observed in other gabbros of the Sierra Nevada and Peninsular Ranges (Walawender, 1976; Russell, 1982). Preservation of such recrystallized symplectites documents an earlier history of olivine crystallization and suggests a mineralogic continuity between the olivine-bearing cumulate and olivine-free noncumulate lithologies.

2.2.4. Predominance of Orthopyroxene over Clinopyroxene

Many Cordilleran plutonic rocks contain greater clinopyroxene than orthopyroxene. This is particularly true of the ultramafic Alaskan-type intrusions which are composed dominantly of olivine and clinopyroxene. Orthopyroxene enters with plagioclase at more evolved magmatic stages, but clinopyroxene remains the dominant pyroxene throughout the magmatic evolution. The Stokes Mountain region differs form this general case in that orthopyroxene enters before clinopyroxene and is modally dominant in all lithologies. The reason for this exception will not be positively identified by this study, but the possible controlling parameters will be discussed.

Considering the extreme case, it is possible that the composition of the parental magma of the Stokes Mountain plutonics was slightly unusual relative to the bulk of the Cordillera. For example, the primary magma composition might have been unusual, but this special pleading does not seem warranted as the isotopic and geochemical compositions of the intermediate lithologies are not unusual for the Sierran batholith. Alternatively, the parental melt may have been somewhat unusual due to an earlier history of fractionation. The relatively Fe-rich olivine and orthopyroxene compositions suggest some earlier

fractionation of Fo-rich olivine from a mantle-derived melt, and removal of significant calcium and alumina may have occurred by previous fractionation of plagioclase. Lower calcium contents may have stabilized orthopyroxene over clinopyroxene, but as the Stokes Mountain suite is calcic (Chapter 3) this seems to be an unlikely cause. Assimilation of silica-rich material may have altered an otherwise normal primary magma composition. This would serve to bring orthopyroxene on to the liquidus at an earlier stage of fractionation (Grove et al., 1982). This latter possibility is unlikely due to the abundant field and isotopic evidence against any significant amount of crustal assimilation in the Stokes Mountain suite (see Chapter 3). In summary, neither an unusual primary magma nor an unusual previous fractionation history appears to explain the predominance of orthopyroxene over clinopyroxene.

The highly anorthitic plagioclase found in the Stokes Mountain cumulates might have been caused by a relatively high water activity as crystallizing plagioclase may have 5 to 10 wt. % higher anorthite content than in an anhydrous environment. The high hornblende content of the cumulates further attests to the hydrous character of the parental magma. A high water content may have lowered the temperature of the pyroxene solvus preventing the early crystallization of clinopyroxene. A high water content has been implicated as the cause of unusual orthopyroxene abundances by other investigators of Cordilleran orthopyroxene rich gabbros (Russell, 1982) and seems appropriate in this suite as well.

A final possibility is that orthopyroxene may have an increased stability if magma differentiation occurred in the presence of olivine-bearing rocks. This possibility arises from experimental work on tonalitic magmas in which orthopyroxene was determined to be the liquidus phase in tonalite which had assimilated limited amounts peridotite at 15 and 30 kbar (Carroll and Wyllie, 1989; Johnston and Wyllie, 1989). Similar results are hypothesized as being possible at lower pressures as well (Carroll and Wyllie, 1989). As will be discussed in section 2.5.1, there is ample evidence supporting the presence of a

great abundance of olivine-rich cumulates at shallow depths beneath the Stokes Mountain region suggesting a possible cause for the enhanced stability of orthopyroxene over clinopyroxene. Alternatively, assimilation of ultramafic and mafic ophiolitic material of the Kings-Kaweah ophiolite belt may have stabilized orthopyroxene; such assimilation may be recorded by the stable and radiogenic isotope systematics of the WKB suite (section 3.3.4.2).

Whereas not definitively demonstrated here, it appears that the efficient fractionation of significant amounts of fosteritic olivine and possibly magnetite from an otherwise normal hydrous primary basaltic magma may have formed a relatively hydrous, slightly iron-rich Stokes Mountain parental magma in which orthopyroxene arrived on the liquidus prior to clinopyroxene. This model will be used in the fractional crystallization model presented in the next chapter.

2.2.5. Magma Mingling vs. Magma Mixing

There is abundant field evidence documenting magma mingling between various units in the Stokes Mountain area. Most striking are the ring dikes composed of roughly 10-30% rounded, melacratic enclaves in a tonalitic to granodioritic matrix; similar elongate enclaves form swarms within the foliated intermediate units. In addition, there are chaotic relationships suggestive of mingling and possible mixing between the mafic lithologies, one of the better developed examples being the fine-grained, intermingled Khg and norite described in unit Kx1 (section 2.1.5). Relations demonstrating that the host was not fully crystalline during diking include rare mafic dikes with cuspate margins and common mafic dikes disrupted by movement of the host lithology after emplacement. Beyond the textural evidence for mingling, however, it is difficult to evaluate the significance of mixing on the development of the final lithologic diversity as geochemical and isotopic results are often equivocal unless large isotopic variations exist between the two magmas prior to mixing. It is therefore necessary to review what is currently understood about the origin of enclaves in

calcalkaline batholiths. The rare xenoliths of obvious wallrock affinity are omitted from this discussion.

Pabst (Pabst, 1927) presented the first detailed description of "autoliths" in the Sierra Nevada, and carefully concluded that these features were igneous rocks that had not been fully crystalline when the host magma was emplaced; moreover, while they were mineralogically similar to the enclosing rocks, the "autoliths" did not represent early fractionates from the host's parental magma. Since then, a number of possible origins for enclaves have been proposed, each of which is probably correct on some instance yet none is universally applicable. Of current favor is the hypothesis that the enclaves represent chilled pillows of mafic magma that was injected into a cooler, more siliceous crystal mush (Blake et al., 1965; Vernon, 1983). The term magma mingling describes this process wherein the final product is not a hybrid, or well mixed, body of intermediate composition.

Mixing is believed to occur only when both magmas have relatively low viscosities after reaching thermal equilibrium (Sparks and Marshall, 1986) which is modeled in high Sierran, late Cretaceous plutonics as occurring if there is a less than 10% SiO_2 variation between the magmas or when there is a greater than 50% mass fraction of mafic magma (Frost and Mahood, 1987). The relationship of the mafic magma to the siliceous magma is not specified by this model, and the possibility that the mafic magma represents a previously formed hybrid has been applied in a limited fashion to enclaves in the Sierra Nevada (Frost and Mahood, 1987) as well as to enclaves in middle to upper crustal Hercynian granites of Europe (Cantagrel et al., 1984; Holden et al., 1987; Pin et al., 1990). In the first case, minor mixing is presumed to have occurred at near emplacement levels while in the latter extensive mixing between mantle and crustal melts is hypothesized as having occurred in the lower crust. This point will be returned to in Chapter 5.

Finally, one conclusion of Frost and Mahood is that simple mixing will rarely produce hybrids having greater than 63% SiO_2, leaving fractional crystallization as the process controlling the lithologic diversity in intermediate and siliceous rocks. Reid

(1983), however, hypothesizes that most chemical variation is the result of mixing between variably fractionated, partially crystalline mafic magmas and crystal-free, felsic crustal melts in which the mafic minerals in the mixed lithologies actually are disaggregated remnants of the mingled mafic magma. A minority view is that shallow level mixing between high-silica and primitive mafic magmas is capable of producing a full spectrum of compositions (Vogel, 1982) but this model does not successfully address the rheological problems of mixing.

One alternate view which has been applied to enclaves in the Sierra Nevada (Dodge and Kistler, 1990) is that many enclaves are "autoliths" composed of disrupted cumulates enclosed by more evolved but cogenetic magmas. This view is based on the lack of significant Sr isotopic variation between enclave and host, and inherently questions the textural evidence for the presence of two liquid phases. It should be noted that there is substantial Nd isotopic variation (0.4 - 2.1 ε_{Nd} units) between the enclave and host magma and that the Sr isotopes could have equilibrated through a diffusing fluid phase during plagioclase recrystallization (Holden et al., 1987; Pin et al., 1990). This isotopic data could equally well be interpreted in terms of deeper mixing producing isotopically evolved gabbros (Chapter 5) prior to mingling.

A final contrasting hypothesis is that the enclaves are restitic, originating in the metaigneous or metasedimentary source region (White and Chappell, 1977). While the restite unmixing model may apply in hotter and deeper levels of batholiths developed on relatively thick crust (Chen et al., 1990), the magma mingling hypothesis has gained more favor for the Sierra Nevada batholith (Reid, 1983; Frost and Mahood, 1987), as well as for deeper levels (25-30 km) of the Cordillera exposed in the Idaho batholith (Hyndman and Foster, 1988; Foster and Hyndman, 1990).

Given the above considerations, the enclave-rich swarms and ring dikes of the Stokes Mountain region can be confidently interpreted as mingled magmas. The same interpretation applies to the small scale mingling between mafic magmas (hornblende

gabbro and norite) in unit Kx1. In both instances mingling appears to have resulted from the energetic coinjection of both magmas into the same ring fracture or shear zone. Recognizing that this suite was emplaced in a shallow, subvolcanic environment, mingling probably occurred near surface during eruption. Possible mixing is limited to localized features such as swarms of poorly defined enclaves of intermediate composition having gradual margins and limited, texturally heterogeneous zones separating granodioritic and tonalitic dikes. As such, mixing was probably not responsible for the production of volumetrically significant hybrid units in the exposed suite and therefore is discarded as a possible process involved in the differentiation of the Stokes Mountain suite. It should be recognized, however, that mixing could have occurred at deeper levels in the crust.

2.2.6. Related Plutonic Suites

The Stokes Mountain suite is of particular petrographic interest because of the abundance of ultramafic and mafic lithologies as well as the well exposed features including the megaxenoliths of layered cumulates and the ring complexes. While this suite may be one of the most lithologically complete, it is not unique. Below are brief descriptions and pertinent interpretations of other Cordilleran batholithic suites described in the literature. These are discussed in geographic order from south to north.

2.2.6.1. South America

Rocks of the Coastal batholith of Peru bear many strong lithologic and structural similarities to the Stokes Mountain suite (Mullan and Bussell, 1977). For example, in the Huaura complex, hornblende-bearing plagioclase and pyroxene layered cumulates with orbicular structures are found associated in well formed ring complexes with pyroxene-bearing hornblende biotite quartz diorites to biotite hornblende tonalites (Pitcher, 1978). Basaltic dikes intruded throughout the history of the complex. Unlike the Stokes Mountain region, substantial vertical relief exposes the transition between the near vertical ring dikes and the the underlying bell jar plutons which fed them. Cauldron subsidence can be demonstrated as providing space for the upward movement of crystal-rich magmas, while

coeval deformation produced crystalloblastic textures and synmagmatic deformation (Bussell, 1988). Based on regional analysis, similar gabbros are estimated as forming 7-16% of the Peruvian Coastal Batholith.

Another similar example is the Jurassic to early Cretaceous Antofagasta ring complex (Pichowiak et al., 1990). The ring complex is dominated by clinopyroxene-, hornblende-, biotite-bearing quartz diorites, tonalites and granodiorites and is associated with contemporaneous basaltic to andesitic volcanics and slightly older olivine- and hornblende-bearing two pyroxene gabbros. The layered gabbros are composed of modally layered anorthosites and gabbronorites which display synmagmatic deformation features.

2.2.6.2. Peninsular Ranges

Mafic to intermediate suites which are mineralogically similar though less lithologically diverse than the Stokes Mountain suite comprise the San Marcos Gabbro and assorted tonalites of the Peninsular Ranges batholith (Larsen, 1949; Walawender, 1976; Walawender and Smith, 1980; Hill, 1988). These rocks share many of the characteristics described in this chapter, such as emplacement as a ring or centered complex, the presence of comb layering, orbicular gabbros with modally layered cumulates, often as xenoliths, texturally variable hornblende gabbro, and the predominance of orthopyroxene over clinopyroxene, the former often in symplectic intergrowths after olivine. The Peninsular Ranges rocks have been interpreted as fractionation products of a high alumina basalt crystallizing at shallow depths with an elevated water pressure as evidenced by calcic plagioclase, abundant amphibole and the abundance of hypersthene. With the exception of the early role of clinopyroxene in the fractionation series proposed by Walawender and Smith (1980), the petrogenesis of these gabbros appears similar to that proposed for the Stokes Mountain suite (section 3.2).

2.2.6.3. Sierra Nevada

The Emigrant Gap mafic complex contains some of the best known ultramafic lithologies of the Sierra Nevada batholith (James, 1971). Lithologically and structurally

there are great similarities to the Stokes Mountain region: in both areas the central ultramafic rocks are in sharp contact with the surrounding two pyroxene gabbros which grade outwards into undifferentiated, but concentrically arranged, biotite two pyroxene diorite, tonalite and granodiorite. These lithologies are interpreted as the differentiation products of a single gabbroic magma. Symplectites of orthopyroxene and magnetite are present as olivine coronas in the ultramafic rocks and as olivine-absent clots in the two pyroxene rocks indicating that olivine was an early phase in the two pyroxene rocks. Xenoliths of the ultramafic lithologies are found in all surrounding units, and some are surrounded by orbicular overgrowths. The ultramafic rocks in the two areas are, however, substantially different, those in the Emigrant Gap complex being composed of olivine and clinopyroxene in contrast to the olivine-plagioclase-orthopyroxene cumulates of the Stokes Mountain region. The dominance of clinopyroxene over orthopyroxene makes the Emigrant Gap suite more similar to the Alaskan-type zoned complexes than the orthopyroxene-rich Stokes Mountain suite and San Marcos Gabbro of the Peninsular Ranges batholith.

An orthopyroxene-rich suite is located in the northeastern Sierra Nevada batholith southwest of Lake Tahoe. In this small area, orthopyroxene-rich diorites, hornblende quartz diorites and hornblende biotite quartz diorite to granodiorite are found associated with modally and Willow Lake layered cumulates (Loomis, 1963). The latter type of layering is found only along contacts and surrounding inclusions and is distinct from the cm scale layering found in anorthositic to noritic xenoliths enclosed by norites. The mineral compositions of the layered xenoliths are less evolved than the surrounding norite, and compositional trends are roughly consistent with an earlier fractionation of the plagioclase and orthopyroxene cumulates from a magma similar to that which produced the surrounding norite.

The reversely zoned Academy pluton (36°30'N, 119°30'W) and the associated outcrops of amphibole-rich gabbros are undoubtedly related to the Stokes Mountain suite.

Plutonism in the two areas was roughly contemporaneous, being dated at 121 to 114 Ma for the Academy pluton and associated tonalites and at 125 to 116 Ma for the main pulse of cumulate formation and intrusion in Stokes Mountain region (see section 2.3). The Academy area gabbros are plagioclase- and amphibole-rich and contain variable amounts of olivine, orthopyroxene and clinopyroxene (Saleeby and Sharp, 1980; Russell, 1982; Mack et al., 1986). Layering defined by hornblende oikocrysts is similar to that found in Khtr, but modally layered troctolites are rare outside of the study area. Detailed petrographic descriptions of the intergradational quartz norite, hypersthene quartz diorite, biotite hornblende quartz diorite and tonalite units of the Academy pluton (Mack et al., 1979) reveal strong similarities with units from the Stokes Mountain region.

2.3. Geochronology of the Stokes Mountain Plutonic Suite

The first geochronological data for the Stokes Mountain region presented in Saleeby and Sharp (1980) included a single K/Ar date from the hornblende-rich cumulates of Colvin Mountain (sample KRO22) and six zircon U-Pb dates (KB samples) from the surrounding lithologies. In conjunction with the present study Dr. Saleeby analyzed three new zircon samples (WKB samples). These data are presented in Table 2.2 in addition to being displayed with triangular symbols on Figure 2.4; the six preexisting zircon analyses are displayed in this figure with square symbols. All zircon dates are concordant; analytical details are described in (Saleeby and Sharp, 1980) and in the footnote of Table 2.2.

The early Cretaceous batholith was emplaced into the Foothills metamorphic belt between 130 and 110 Ma with the majority of zircon dates clustering between 125 and 115 Ma (Saleeby and Sharp, 1980). The ten dates for the Stokes Mountain suite span the period between 125 and 110 Ma. This magmatic pulse precedes the more voluminous middle Cretaceous intrusions which began at roughly 102 Ma in which the majority of the exposed Sierra Nevada batholith was emplaced.

Two samples from the Western Ring (?) Complex yield dates of 120 (KB3) and 116 Ma (KB7); a xenolith of Kp enclosed by Kpht of the WRC was also dated at 120 Ma (WBK129). This latter date is of particular significance. As discussed in section 2.1.11, the fine-grained porphyritic texture of this xenolith suggests it was emplaced in a hypabyssal environment (section 2.5.1). That these xenoliths have been hydrothermally altered and their host lithologies have not indicates that hydrothermal alteration occurred after zircon crystallization at 120 Ma but prior to stoping and incorporation estimated as occurring between 120 and 116 Ma during emplacement of the WRC. Development of a hydrothermal system and isotopic exchange must have occurred soon after the 120 Ma intrusion of the hypabyssal material. The implication of the geochronologic and isotopic data is that the exposed section of the WRC was emplaced near surface and cannibalized part of its own volcanic carapace.

Zircon from a Khbt sample from the main trough of the Eastern Ring Complex crystallized at 123 Ma (WBK131); another sample of this unit from the southwest edge of the complex yielded a date of 120 Ma (KB4). A minimum emplacement date for the ERC is well constrained at 117 Ma (W170) by one of a continuous series of hornblende gabbro dikes which intrude the southern margin of the ring complex. Sample WBK79 was collected at the same outcrop as W170 so should be chemically representative of W170. These petrologically unique dikes cut perpendicularly across the ring dikes and clearly postdate emplacement of the ring complex As structural evidence for the Stone Corral Shear Zone indicates that the western margin of the ERC was emplaced simultaneously with the WRC which was active between 120-116 Ma, it is quite possible that the ERC was active for some time after 120 and before 117 Ma.

There is some indication that the ERC may have been active for the complete period between 123 and 117 Ma. A sample of two pyroxene gabbro from the southern tip of Colvin Mountain was dated at 117 Ma (KB6). Apparently this is the date at which the previously crystallized Colvin Mountain megaxenolith was disrupted and emplaced into the

upper crust. Due to the alluvial cover, the relationship of the 117 Ma sample to the ring complexes is unclear, but extension of the ERC outcrop pattern suggests that this sample was emplaced into the ERC. This assignment is tentative, however, as the date overlaps the emplacement periods of both ring complexes.

Based on the zircon data, the ring complexes of the Stokes Mountain suite have minimum emplacement duration of 4 and 6 Ma. These minimum estimates agree well with estimates of the emplacement times of other ring complexes. For example, the Peruvian Fortaleza (Bussell et al., 1976) and Huaura ring dike complexes are believed to have had life spans of approximately 2 to 5 Ma (Pitcher, 1978; Bussell, 1988). It is argued that these short thermal durations are consistent with the relatively small contact metamorphic aureoles that surround the ring complexes.

The youngest date is from a dike from a chaotic suite of cross cutting Khg (KB9). Field relationships provide no constraint concerning the significance of this date, but as Khg appears to have been intruded throughout the emplacement history of the Stokes Mountain suite, the 110 Ma date is interpreted as representing the last gasp of magmatism in this region.

The single K/Ar analysis dates the Colvin Mountain megaxenolith at 123 $\pm$ 3 Ma (KRO22) while an associated two pyroxene gabbro produced a zircon date of 125 Ma (KB1). These dates indicate that the ultramafic and mafic lithologies of the Stokes Mountain suite are equal to slightly older in age compared to the mafic and intermediate lithologies of the neighboring ring complexes. The data are consistent with the petrographic interpretation that the cumulates formed early in the same magmatic system that produced the more evolved lithologies of the ring complexes. This hypothesis will be investigated chemically and isotopically in Chapter 3.

2.4. Discussion of Textural and Structural Elements in the Stokes Mountain Region

The Stokes Mountain region preserves some spectacular structures related to emplacement of the early Cretaceous Sierra Nevada batholith. In this section the cumulate

megaxenoliths, the Stone Corral Shear Zone, the Eastern and Western (?) Ring Complexes and the possible relationship between these features are discussed. Additional evidence supporting a shallow emplacement for the Stokes Mountain suite is also presented.

2.4.1. The Ultramafic-Mafic Cumulate Megaxenoliths

The resistant masses of troctolitic cumulates form the highest exposures in the mapped area. While the outer contact is never exposed, the xenolith origin is based on the observation that masses are surrounded and underlain by noncumulate intermediate lithologies with no gradational lithologies separating the cumulate and noncumulate rocks. The well preserved cumulate textures indicate that the blocks reached their final position in the near or completely crystalline state.

The megaxenoliths are interpreted as cumulates formed in the same magmatic plumbing system as the host magmas. Both the overlapping ages and suggestion of mineralogic continuity support this hypothesis; as discussed in Chapter 3, isotopic and geochemical data are consistent with a genetic relationship between cumulate and noncumulate lithologies.

Such large blocks could not have been transported vertically in the crust for any great distance, and therefore the cumulates probably formed at crustal depths only slightly greater than those presently exposed (section 2.5.2). Energetic magma pulses are required to dislodge these large blocks; this energy presumably was provided by rapid volatile exsolution accompanying upward magma movement during volcanic eruption. Recrystallization of the cumulates producing a polygonal texture may have formed as a response by the layered cumulates to inclusion as megaxenoliths in the surrounding, hotter magmas.

The abundance of synmagmatic deformation features in the megaxenoliths indicates that the crystallization environment was dynamic even during the early stages of cumulate formation. As evidenced by the 130 Ma pervasively foliated Khbt, plutonism and, by analogy to the younger suite, volcanism, may have occurred prior to and possibly during

formation of the layered cumulates at 123 ± 3 Ma. Response to movements of magma in the surrounding crust may have promoted the widespread synmagmatic deformation recognized in the cumulates and discussed in section 2.4.2.

Synmagmatic Structures and Post-Magmatic Deformation

2.4.2. Supersolidus Structures and Textures in the Layered Cumulates

Though the layers are dominantly planar and laterally extensive, there exists a wide range of layer deformation within the Stokes Mountain region. Deformation increases from monoclinal warping and interlayer isoclinal folding (cm to m amplitudes) to chaotic swirling. Such deformation often appears spatially related to the presence of irregular pods of very coarse-grained massive hornblende troctolite. The effect of the intrusion of such pods ranges from gentle folding of the surrounding layers, layer attenuation and formation of load and cast-type structures, to intense folding and near obliteration of the original layering. Structures such as chevron folding, layer truncation or possible cross bedding and layer branching are rarely observed.

There are some textures that formed after a point when the crystal mush could sustain brittle deformation; this point is believed to be reached above sixty per cent crystallization. Such supersolidus fracturing may account for the formation of a texture best described as elongate hornblende striping. This generally forms in hornblende poor gabbros and is characterized by a generally planar arrangement of elongate hornblende oikocrysts that define a magmatic lineation. The oikocrysts do not record any internal strain, and the inclusions are not aligned. These relationships suggest that the oikocrysts crystallized in an elongate form in strong contrast to the circular hornblende oikocrysts found in all other lithologies.

Possibly the elongate oikocrysts formed along fractures within a crystal mush. Hornblende-rich interstitial melt might have migrated down the resultant pressure gradient into the opened fracture resulting in the localization and concentration of the latest crystallizing phase, hornblende. A similar argument is presented for banded gabbros in the

Peruvian Coastal batholith (Mullan and Bussell, 1977) with the difference being that the bands are comprised of plagioclase. An alternate scenario is that foreign hornblende components may have been introduced along the fractures. In fact, such fractures may have facilitated the emplacement of dikes of unit Khg in the chaotic regions of Khtr, but whether this occurred before complete solidification is generally unclear.

It is fairly common to find autoliths and breccias of layered cumulates within the cumulate pile. In these instances, the formation of layering often resumed after inclusion of the autolith as subsequent layering is draped unconformably over layered autoliths. In one breccia, the margins of the inclusions were apparently recrystallized to a finer-grain size suggesting a thermal or chemical disequilibrium between layered autolith and layered host.

Finally, in one locality south of Tucker Mountain (TM104) a few meter thick, plastically deformed section of layered cumulates is present within an otherwise undeformed outcrop near the edge of a megaxenolith. Foliation and lineation are steeply vertical and cannot be attributed to a known regional deformation; this suggests localized deformation perhaps related to uplift of the megaxenolith. The lineation is defined by elongate olivine crystals which record a variety of textures ranging from oscillatory extinction to kink bands to complete recrystallization forming discreet domains. The enclosing amphibole has recrystallized into fine-grained, equant neoblasts and exsolved a wormy, leaf green spinel. The plagioclase matrix is dominantly polygonally recrystallized, but also demonstrates a recrystallized and reduced grain size in the pressure shadows of the deformed olivines.

In summary, these features indicate that the magma chamber in which the layered cumulates formed was repeatedly subject to deformation during which the near solidus cumulates responded in both ductile and brittle manners. The massive hornblende troctolite, which presumably formed within the same chamber as the cumulates, appears to have been easily mobilized in this dynamic environment such that it intruded and deformed the layered crystal mush.

2.4.3. Igneous Foliations and Intrusion-Related Mylonitization

Igneous foliations are developed in all lithologies. The foliation found in the layered cumulates is defined by modal variations. Foliation in the more evolved lithologies is defined by the preferential alignment of mafic phases. Weak foliations may be found in the pyroxene-rich gabbros, but in general the foliations are more distinctive in the hornblende- and biotite-bearing lithologies. Such foliations are generally oriented parallel to contacts between units and are interpreted as having formed by magmatic flow during emplacement. These mineralogic foliations parallel foliations defined by the long axes of mafic enclaves and by the trends of enclave swarms.

Protomylonitic foliations are formed along and parallel to intrusion contacts; these deformation fabrics grade into magmatic foliations with distance away from the contact. Protomylonitic fabrics are characterized by elongate ribbons of oscillatory to dynamically recrystallized quartz within a fine-grained, granoblastic mortar. Plagioclase grains may be slightly marginally recrystallized, but usually they have acted as rigid clasts around which the biotite grains are bent. Less commonly quartz-free rocks are protomylonitic. In these instances, hornblende, biotite and plagioclase are strongly aligned and internally deformed. These fabrics are particularly well developed within the Eastern Ring Complex and are attributed to shearing along contacts during intrusion of dikes of variably crystallized magmas (Bateman et al., 1983) (section 2.4.5).

The development of pervasive cataclastic foliations within similar rocks of the early Cretaceous batholith has been described by (Bateman et al., 1983). Although their "Blackhawk deformation" was possibly tectonic in origin, they conclude that the deformation of the approximately 114 Ma tonalite of Blue Canyon and its metamorphic wallrocks was related to the emplacement of a 113 Ma leucotonalitic body which contained greater than 30% crystals at the time of emplacement. A similar origin is proposed for the NNW-trending, penetrative deformation of the screens of protomylonitic Khbt. In analogy to the Blackhawk area, this deformation probably occurred soon after emplacement and

was related to the intrusion of surrounding ring dikes. Crosscutting relationships support the claim that the cataclastic foliation formed dominantly before emplacement of the undeformed Khbt. A similar argument for intrusion-related formation of penetrative deformation of roof pendants is made by Saleeby (Saleeby et al., 1990) while similar deformation of plutonic lithologies is found in the Peruvian ring complexes (Pitcher, 1978).

2.4.4. The Stone Corral Shear Zone: Super- and Subsolidus Deformation

The Stone Corral Shear Zone (SCSZ) is a north-northeast trending structure which truncates all contact and foliation trends of the Eastern Ring Complex (ERC) at its western margin and coincides with the eastern border of the Western Ring (?) Complex. The SCSZ is composed of highly variable lithologies displaying an unusual range of syn- and post-magmatic deformation fabrics and structures. The SCSZ is interpreted as a zone of magmatic and structural interaction between the Western and Eastern ring complexes. Detailed microstructural analysis is warranted but has not been attempted in this study.

The dominant igneous process relating the lithologies is magma mingling at many scales (see unit Kx1, section 2.1.5, for full descriptions). On a meter scale, dikes and highly elongate pods of units Kpg, Khpg, Khg and Khbt are juxtaposed. On a centimeter scale, individual dikes and enclaves may represent the mingled product of two lithologies thus documenting multiple mingling episodes (see the "blebby rock" description in section 2.1.5). Although strongly aligned, the minerals preserve igneous textures and steeply southeast dipping to near vertical igneous foliations usually without any record of internal deformation. For example, a sample of Khbt displays a strong igneous foliation defined by the alignment of individual phases and by concentrations of hydrous phases, and the only record of internal deformation are weakly oscillatory quartz grains.

Syn-magmatic shear strain is unequally distributed within zone. Shear stress is recorded by the presence of isoclinally folded, mafic and felsic dikes and infilled tension gashes of a cm- to m-scale. The fold axes are roughly parallel to the trend of the shear

zone, but in other cases the relations are more complex suggesting the possibility of deformed vein networks. The tension gashes are filled with hornblende gabbro or mingled hornblende gabbro and norite. These structures are composed of thin limbs which parallel the shear zone trend and are joined by a thick section which cuts obliquely across the shear zone. The orientation of these features indicates a left lateral sense of shear during magmatism.

Limited post-crystallization magmatism within the SCSZ is documented by the minor abundance of cross cutting veinlets in which fine- to medium-grained hypersthene occupies the centers of the quartzofeldspathic veinlets.

The effects of post-magmatic shearing are exposed at the northern end of the SCSZ at a 0.4 km higher elevation than the outcrops described previously. At this point, where the SCSZ intersects Boyd's Grade, evidence for magma mingling is minimal; here the shear zone is marked by a 10 m wide zone of strongly foliated to mylonitic Khbt in which the foliation is near vertical. Quartz, both oscillatory and microcrystalline, forms elongate ribbons, plagioclase clasts are rounded and display marginal recrystallization, and biotite and hornblende porphyroclasts display brittle behavior. Shearing along the vertical plane appears to have been predominantly horizontal as indicated by the horizontal continuity of biotite stringers and the horizontal elongation of plagioclase clasts. Moreover a single mafic enclave is elongate horizontally within the plane of the shear zone in contrast to the typical vertical orientation of enclaves found in mingling zones. The presence of blue-green instead of olive hornblende, abundant, oriented epidote and a single fragmented crystal of blue tourmaline suggest metasomatism, possibly by a vapor-rich phase, during shearing. The igneous foliations in unit Khbt 3 km to the east of the SCSZ are oriented approximately perpendicular to the SCSZ; they gradually rotate into parallelism with increased proximity to the SCSZ indicating a syn-magmatic component to the shear deformation which was subsequently overprinted within the shear zone.

Post-magmatic shearing may also occur at the southern end of the SCSZ, but exposure there is poor due to the steep terrain. Isolated protomylonitic lithologies are located within 1 km on either side of the southern projection of the shear zone: blocks of protomylonitic, hornblende-rich cumulates are located near the top of Stokes Mountain; epidotized, protomylonitic Kpg pods can be found at lower elevations on the southeastern slope of Stokes Mountain. These pods roughly parallel a set of east-northeast trending air photo lineaments. The nature of these lineaments is unclear and additional work is necessary to constrain the pertinent relationships, but the locations of these outcrops suggest a westward bend of the shear zone around the southern side of Stokes Mountain. Such a relationship might be expected if the shear zone were intimately related to the emplacement of the Western Ring Complex, of which Stokes Mountain is the southernmost exposure. The field context of the SCSZ will be discussed in a following section.

2.4.5. The Ring Complexes

The Stokes Mountain area contains one particularly well developed ring dike complex, the Eastern Ring Complex (ERC; Figure 2.5), located north of the town of Elderwood. It is dominated by a central plug of hornblende gabbro on Red Mountain which is surrounded by a resistant, 1 km thick ring dike of biotite granite. The topographically low moat between these two structures is occupied by tonalite which has been crudely divided into pyroxene-rich and -poor rings (units Kpht and Khbt). An outer moat separating the granite dike from the metamorphic wall rocks is composed of undivided tonalite and granodiorite. Smaller, arcuate dikes of gabbro and granite, both mapped and unmapped, are concentrically dispersed throughout the 8 km in diameter structure. Due to the remote location, the eastern edge of the complex was not mapped; the contact with the wall rocks can be traced on air photos southward, with minor complications, into the southeast corner of the field area joining the mapped contact in Antelope Valley. The structure is generally circular with two recognized dike-like apophyses intruding the metasediments at the northern and eastern edges.

One of the more remarkable features of the ERC are the arcuate zones in the south composed of mingled gabbro, tonalites and granodiorites. The mafic enclaves in these dikes are commonly 10 to 100 cm in diameter and range in shape from crude spheres to highly attenuated ellipsoids; the degree of elongation is correlated with the intensity of the igneous foliation in the host lithology. The direction of maximum elongation is near vertical while the intermediate elongation direction is roughly horizontal and parallel to the dike margins. While enclave swarms and mingled zones along dike contacts are found throughout the complex, these mappable comingled dikes do not continue northward into the tonalite moat. This difference may be partially due to a different structural level of exposure of approximately 1600' in the south compared to less than 3200' in the central moat.

Detailed analysis of the orientations of igneous foliations and maximum elongation directions of enclaves was not performed, but these appear to be oriented within 15° of vertical within the ring complexes. Outcrop pattern of the more continuous granitic dikes suggests a dominantly vertical orientation with slight outward dips for the thick Kgd dike on the north side of the inner gabbro plug as well as for smaller Kgd and Khg dikes in the southwest sector. This latter example may not be representative, however, due to possible deformational complications associated with the Stone Corral Shear Zone.

There are remarkably few xenoliths or stoped blocks within the ERC. Two small bodies of quartzite are mapped in the northern section. In addition, directly southeast of the Red Mountain gabbro plug are five small pods tentatively assigned to unit Kp which is believed to have formed part of the volcanic carapace of the ring dike complex. Oxygen isotopic analysis of similar Kp xenoliths from the WRC yield ^{18}O-depleted values indicative of hydrothermal alteration; the significance of this is discussed in Chapter 3. The remnant mafic mineralogy of Kp (two pyroxenes, hornblende and biotite possibly with remnant olivine) and the enclosed mafic xenoliths is consistent with a broadly cogenetic relationship between unit Kp and the Stokes Mountain plutonic suite. Zircon

geochronology indicates that Kp is identical in age, within the resolution of the chronometer, to the surrounding 120 Ma Kpht which is not hydrothermally altered. This relationship indicates that hydrothermal alteration followed by the stoping of Kp by Kpht occurred soon after Kp crystallization. Combined with the mineralogical similarities, the chronology suggests that Kpht cannibalized its own volcanic and hypabyssal carapace through stoping.

The lack of a significant volume of included wall rock material revives a space problem encountered in other subvolcanic complexes. If cauldron subsidence provided the space now occupied by the early Cretaceous lithologies then the caldera floor must have subsided as a piston beneath the current level of exposure. Alternatively, it is possible that transtension provided some of the requisite space for the intrusive complex. This possibility has been proposed for some of the large batholiths in the high Sierras (Tobisch et al., 1986; Saleeby, 1990), and may be particularly appropriate for the second, northwest elongate, ellipsoidal ring complex in the field area.

The Stokes Mountain region contains a second centered complex which has been labeled the Western Ring (?) Complex (WRC). The query reflects the fact that while the mapped bodies are elongate, arcuate,and near vertical, the dike form of the individual units is well expressed only at the mapped scale and not on an outcrop scale as in the ERC. If this is in fact a closed ellipsoidal feature then the entire western half of the complex is buried under alluvium. Based on the outcrop pattern and the lithologic composition, the cumulate and gabbro pod on and around Tucker Mountain has been considered as the center of the complex, but this assignment is not definitive. Only the southeast quadrant of the complex is located in the study area; continuation of the ring dikes to the north and west is suggested by arcuate lineaments on air photos. Additional support for the dike genesis beyond the mapped form comes from the following observations: arcuate air photo lineaments occur in the mapped Kpht suggest that this large intrusive mass may be composed of individual dikes; textural evidence suggests that the core of Curtis Mountain

may be composed of a thick, well foliated dike of Kpg surrounded by unfoliated Kpg perhaps representing two distinct magma pulses. Some of the difference between the two complexes may result from the more mafic average composition of the WRC compared to the ERC and the slightly lower elevation of exposure of the WRC.

Present mapping indicates that the WRC is strongly ellipsoidal with the maximum elongation axis oriented NNW. This geometry suggests of emplacement in a structural trough, possibly created by transtension parallel to the subduction zone. Such an emplacement might lessen the space problem discussed above, but more work would need to be done to constrain this hypothesis.

Previously the early Cretaceous mafic suite was interpreted as having formed the roots of basaltic to basaltic-andesite volcanos (Saleeby, 1986). The presence of two ring complexes in the Stokes Mountain region supports this interpretation. In general, ring complexes are recognized as volcano-plutonic in origin, being the structural, textural and genetic intermediaries between volcanos and the underlying magma chambers in calcalkaline batholiths (Ustiyev, 1963; Pitcher, 1978; Walker, 1984; Bussell, 1988). The presence of ring dikes, therefore, indicates a high crustal level of emplacement for the Stokes Mountain suite.

There exists additional evidence for a shallow depth of emplacement for the Stokes Mountain suite. First, the close match between K/Ar ages on hornblende and biotite and the range of zircon ages recorded by the early Cretaceous plutonic suite indicates that the rocks must have cooled rapidly (Saleeby and Sharp, 1980). This observation is consistent with a shallow depth of emplacement. Second, unit Kp is interpreted as representing blocks of hydrothermally altered, hypabyssal material. This suggests that the level of exposure of Kpht is within a few km of the original emplacement depth. The maximum depth of exhumation of the Stokes Mountain region is thus limited to the distance that a 1000 m^3 block of Kp could sink from near-surface levels within a semi-crystallized tonalitic magma.

On air photos, shallow arcuate lineaments on the southern side of the central gabbro plug of the ERC (Red Mountain) suggest the presence of shallow, inward-dipping cone sheets. If this interpretation is correct, then the ERC is composed of vertical to outwardly-dipping ring dikes, a central plug which is possibly composed of relatively shallow, inwardly-dipping cone sheets and rare, cross cutting radial dikes such as those dated at 117 Ma (sample W170) in the southern margin of the ERC. There is currently some debate concerning the specific relationships between magma pressure and intrusive style (Robson and Barr, 1964; Phillips, 1974; Koide and Bhattacharji, 1975; Park, 1989), but it is agreed that all three features - vertical ring dikes, inward dipping cone sheets and radial dikes - can form over a shallow magma body. Cone sheets and ring dikes are emplaced along conjugate sets of conical of shear fractures during relatively high magma pressure while radial dikes form during lower pressure stages.

Features exposed in other Cordilleran ring complexes shed additional light on the relation between ring complexes and the overlying volcanos. In the Peruvian complexes, the ring dikes intrude their volcanic roofs; the association of hypabyssal rocks, intrusive breccias and ring dikes leads to the hypothesis that ring fractures may vent at the surface (Bussell et al., 1976; Pitcher, 1978). The flat roof of the central bell-jar pluton in the Peruvian examples is believed to indicate subsidence of the overlying caldera (Bussell et al., 1976); subsidence would have facilitated emplacement of ring dikes along the surrounding ring fractures. Some authors suggest that the subsided central block is overlain by a horizontal magma sheet (Marshall and Sparks, 1984).

Dikes of mingled magmas occur in many of the ring complexes of the British Tertiary Igneous Province; these dikes are hypothesized as forming during caldera formation over compositionally zoned magma chambers (Marshall and Sparks, 1984). The formation of banded pumice has been hypothesized as a result of eruption of such mingled dikes (Sparks and Marshall, 1986); this relationship is suggested by the Loch Ba ring dike which is composed of banded, rhyolitic, welded tuff (Sparks, 1988). Other features

linking ring dikes to volcanic eruptions include the presence of brecciation and miarolitic cavities which are believed to be products of the rapid exsolution of gases accompanying eruption.

Considering the above discussion, the best interpretation of the ERC and WRC is that these complexes formed at shallow crustal levels beneath two volcanic edifices. The dimensions of the ERC - approximately 8 km in diameter - is similar to other ring complexes (Walker, 1984; Yoshida, 1984). The presence of stoped blocks of hydrothermally altered, silicified hypabyssal rock (unit Kp) indicates that at least part of the intrusion roof was composed of material appropriate for the volcanic carapace. In the WRC similar material has been demonstrated as being essentially identical in age (120 Ma; sample WBK 129) to the surrounding plutonic material as would be predicted if the carapace and ring complex formed in the same magmatic episode. As mentioned in section 2.1.11, the presence of a clot of fine-grained, euhedral orthopyroxene and oxides similar to clots found in intermediate lithologies which were interpreted as recrystallized symplectites after olivine suggests a genetic link or at least a common mineralogic evolution between unit Kp and the surrounding Stokes Mountain plutonic suite.

Although similar to the concentrically zoned igneous complexes such as the Tuolemne intrusion, ring dike complexes have not been previously described in the Sierra Nevada batholith; they have, however, been reported in other Cordilleran batholiths. For example, tonalite-dominated ring complexes have been described in the Peninsular Range batholith (Merriam, 1941; DePaolo et al., 1975), and a number of compositionally diverse ring complexes are located in the Peruvian Coastal batholith (Bussell et al., 1976) (see section 2.2.6.1).

2.4.6. Relationship of the Stone Corral Shear Zone (SCSZ) to the Ring Complexes

The Stone Corral Shear Zone bounds the WRC on its eastern margin and truncates the ERC along its western edge (Fig. 2.5 described below). The intimate association of the shear zone and the ring complexes merits examination. Determining the exact nature of this

structure requires detailed field and microstructural analysis which is beyond the scope of this study, but at present two endmember scenarios can be evaluated. First, the SCSZ may have been an expression of a regional tectonic regime unrelated to the position of the ring complexes; for example, the SCSZ could have accommodated some amount of the arc-parallel extension which has been hypothesized as a possible mechanism for providing the space required for emplacement of the Stokes Mountain suite. Both left- and right-lateral shear events have been recognized in the history of the batholith margin (J.B. Saleeby, personal communication), but as there is no direct correlation of the SCSZ to outside events during 123 to 116 Ma this possibly cannot be demonstrated. Alternatively, this structure may have only local significance and result from the unusually close spacing of the ring complexes. This latter possibility is consistent with the sense of synmagmatic shear along the SCSZ and will be explored below.

The ERC and WRC are located in unusually close proximity for contemporaneous centers. The mean spacing for volcanic centers in the central Andes of 6 Ma or younger is estimated as 10 km, while only 10% of all volcanos were emplaced at 5 km or less from each other (Baker, 1974; Vogt, 1974). As spacing is interpreted as reflecting the thickness of the overlying roof of the batholith exceptionally shallow magma emplacement depths might permit an even closer spacing of volcanic centers as seen in the Stokes Mountain area. As will be demonstrated in Chapter 3, the ERC and WRC are not satellites cones of a single magmatic plumbing system as they tapped isotopically distinct magma reservoirs. Therefore, the complexes may be close together because they sampled separate plumbing systems that did not communicate at depth.

Figure 2.5 is a structural overlay of the Stokes Mountain region shown in Figure 2.4. Lithologic contacts separating adjacent ring dikes, trends of igneous foliations and air photo lineaments are shown in dashed lines. The geometries and positions of the two ring complexes as well as their relation to the SCSZ are well displayed; for example, the truncation of the western margin of the ERC by the SCSZ is readily apparent. Evidence for

synmagmatic left-lateral shear along the SCSZ, including infilled tension gashes and the orientations of folded dikes, was described in section 2.4.4. Geochronologic relationships supporting the contemporaneous emplacement of the two ring complexes was discussed in section 2.3.

In map view, the gabbro plug of Red Mountain is readily considered the center of the circular ERC. As the WRC is incompletely exposed and mapped, the center of this complex is less evident. For the purposes of this discussion, the Khg and Khtr association on and south of Tucker Mountain are considered to form the center of the elliptical WRC. This assignment is based predominantly on the appropriate location of these rocks, but also on the abundance of gabbro similar to the central plug of the ERC. Possibly the Tucker Mountain cumulate megaxenoliths clogged the volcanic neck of the WRC. Arrows have been drawn around each of the purported volcanic centers in Figure 2.5 to indicate the direction of radial extension expected during ring dike emplacement and tumescence of the crust. As displayed in Figure 2.5, when these vectors are resolved along the trace of the SCSZ, a left-lateral sense of shear is produced for the segment of the SCSZ between the two volcanic centers.

The Stone Corral Shear Zone is believed to have resulted from the interference of the closely spaced and simultaneously active volcanic centers which tapped separate magmatic plumbing systems. The SCSZ accommodated left-lateral shear during radial extension around these two volcanic centers; in addition this structure served as a conduit for magma emplacement and mingling, involving magmatic components from both plumbing systems (section 2.1.8). If this model is appropriate, then the SCSZ would not be predicted to extend southwestward beneath the alluvium as the components of extension around both centers would point in the same direction resulting in little or no shear along this projection.

There is some evidence that magmas from the WRC magmatic system intruded across the SCSZ into the northwestern ERC. The small, suspect intrusions are composed

of Kpg and Khpg and contain a xenolith of layered Khtr, lithologies which are rare in the ERC but common in the WRC. While this observation alone is equivocal, the radioisotopic signature of a single sample from the suspect intrusions is characteristic of the WRC and not the ERC. The trend of the suspect intrusions mimics the trends of the northern ERC indicating that, regardless of the source of these intrusions, they were emplaced into the stress regime characterizing the ERC.

2.5. Discussion of Crustal Structure and Uplift History

One of the original goals of this study was to evaluate the layered cumulates as possible components of the lower batholithic crust. In order to do so, the Stokes Mountain suite must be interpreted in terms of the geophysical investigations of the Great Valley and the Sierra Nevada batholith which have been directed towards identifying the structure and composition of the central Californian crust. Geophysical problems which are of particular interest to the present study are the origin of magnetic and gravity anomalies located in the Great Valley and the thickness of crust beneath the batholith. Due to the absence of appropriate geobarometers in the Stokes Mountain suite, the degree of uplift of the area must be evaluated in order to constrain the formation depth of these rocks. This subject will be addressed in section 2.5.2.

2.5.1. Geophysical Anomalies

Two linear gravity and magnetic anomalies parallel the batholith's margin within the Great Valley. The western anomaly, named the Great Valley anomaly (Cady, 1975), is modeled as a 10 km thick, west dipping slab of ophiolitic material (Saleeby, 1986) which forms the basement of the Great Valley.

The eastern anomaly, named the Dinuba magnetic and gravity high or lineament (Oliver and Robbins, 1982), coincides with the trend of the Kings-Kaweah ophiolite belt as well as with outcrops of ultramafic-mafic intrusives of the early Cretaceous batholith including those of the Stokes Mountain region (Fig. 2.6). The gravity anomaly trends N40W and is defined by local highs of 10 to 30 mgal imposed upon a 20 km wide, 20

mgal high known as the Dinuba pedestal (Oliver and Robbins, 1982). The magnetic anomaly coincides with the gravity high and is defined as the axis of a set of closed, ellipsoidal field contours between 1000-1600 gammas (Cady, 1975). The Dinuba anomaly has been modeled as an eastward dipping slab of cumulate sheets extending from the surface to a depth of 9 km which surrounds a smaller wedge of ophiolitic metagabbro (Saleeby, 1975). While the ophiolite belt is believed to contribute to the anomaly, only the early Cretaceous intrusives have both high density and magnetism to account for the anomaly; serpentinites are strongly magnetic but are not very dense while nonmagnetic peridotites and ophiolitic metabasites are relatively dense. One other possibility is that the Dinuba anomaly is the result of late Jurassic intrusion of a sheeted dike complex which was intruded in the early Cretaceous by the batholith suite.

The location of the Western Ring (?) Complex (WRC) coincides with the eastern margin of the Dinuba gravity anomaly and the axis of the Dinuba magnetic anomaly while the Eastern Ring Complex (ERC) is not associated with any anomalous signature. This contrast is the result of two factors. First, the average exposed lithology of the gabbro-dominated WRC is more magnetic and dense than that of the tonalite-dominated ERC. Second, the wallrocks of the WRC, which are exposed on Smith Mountain to the west of the mapped area, are much more magnetic and/or dense than those of the ERC. The ERC wallrocks, comprised of psammitic and pelitic material (section 2.1.12), are neither relatively dense nor magnetic. In fact, the boundary between the two ring complexes approximately coincides with the northwestward projection of a regional contact within the ophiolite belt which separates a sharp infold or thrust stack of continentally-derived metasediments to the east from metabasalts and serpentinites to the west (J. Saleeby, personal communication). This contact relationship is reflected by the isotope systematics of the ERC and WRC samples and will be discussed further in Chapter 3.

Within the Dinuba anomaly are a number of local gravity highs. While many of the sources are buried within the valley fill, some of the anomalies are located over outcrops of

ophiolitic, presumably peridotitic, material often without any associated intrusive gabbros. As a result of the mapping in this study, a small positive anomaly located at the westernmost tip of Stokes Mountain can be assigned to a previously unrecognized, partially exposed body of layered ultramafic-mafic cumulates which extends to, and presumably underneath, the alluvium. The relatively small cumulate megaxenolith capping Stokes Mountain may be responsible for the slight wiggles in the gravity contours, but this is not a dramatic effect especially considering the possible errors (Oliver and Robbins, 1982).

The lack of positive anomalies associated with the cumulate megaxenoliths on Colvin and Tucker Mountains seems unusual with respect to the large dimensions of these bodies This absence may be due to the fact that these bodies do not extend beneath the valley floor and are completely surrounded, and possibly underlain, by less dense lithologies (Kpht, Kpg, etc.). As a result, the majority of their signature may be removed by the terrane correction applied to the data. Furthermore, no readings were made over the megaxenoliths, possibly because they are incorrectly identified on the California State map as metamorphic and granitic material. The lack of anomalies over Campbell and Jesse Morrow mountains to the northwest may be the result of being dominated by hornblende-rich and relatively olivine-poor lithologies (Russell, 1982; Mack et al., 1986). A final note should be made regarding the Stone Corral Shear Zone (SCSZ) which does not have any signature on the gravity and magnetic maps. This structure, which is oriented at approximately 30° to the regional contact and anomaly trends, is believed to be a relatively near surface phenomena related to the growth of the volcanic edifices overlying the WRC and ERC, so its lack of geophysical signature does not present a problem.

One implication of the Dinuba gravity high is that the parental magma of the WRC apparently was emplaced at a relatively shallow crustal level before it underwent substantial chemical evolution through crystal fractionation. This conclusion results from a number of considerations. Basically, the parental magma of the ultramafic-mafic cumulate megaxenoliths could not have been very chemically evolved and still crystallize olivine of a

composition Fo78. Moreover, the large size of the dense megaxenoliths precludes their transport any great vertical distance by the enclosing magmas. Therefore the magma from which the cumulates, and presumably the more evolved WRC lithologies, formed must have been emplaced into magma chambers at close to the current level of exposure. Moreover, it is this same material which is believed to be the dominant cause of the Dinuba anomalies which is modeled as extending to roughly 7.5 km present depth.

In contrast, the lack of any anomalies over the ERC argues against the presence of much mafic material at upper crustal depths, so fractional crystallization within that complex must have occurred deeper in the crust. It will be argued in Chapter 3 that the parental magmas of the WRC and ERC were compositionally similar and that they followed grossly similar crystallization paths resulting in similar lithologies in both complexes. Therefore, while assimilation-fractional crystallization within the ERC must have occurred at greater depths than in the WRC, the pressure must not have been great enough to substantially affect the liquidus relationships.

The reason for the relatively shallow emplacement of the WRC parental magma needs to be evaluated. There are structural possibilities: (1) the serpentinite wallrock may have offered a relatively easy path to the surface due to its strong foliation and lesser thickness than the neighboring continentally-derived clastics; (2) a regional tectonic discontinuity projecting southeastward along the trend of the Dinuba anomaly which has been proposed based upon trends of late Jurassic sheeted dike complexes may have facilitated magma emplacement. Alternatively the WRC parental magma may have been more hydrous and thus more buoyant than that of the ERC: certainly there is a great abundance of hornblende in the WRC and the associated complexes to the northwest, but the small amount of mafic material exposed in the ERC is equally amphibole-rich so this seems unlikely to have caused the shallow emplacement of the WRC parental magma.

The coincidence of the Dinuba gravity anomaly and the eastern margin of the WRC indicates that the material responsible for the anomaly is indeed the mafic batholithic rocks

as modeled by Saleeby (1975). Furthermore, recognition that the cumulate megaxenoliths and the related mafic lithologies must have fractionated at shallow crustal levels indicates that the plumbing systems of the two ring complexes differed spatially as well as chemically. Specifically the mafic WRC parental magma must have been emplaced at a shallow depth within the crust.

2.5.2. Implications for Crustal Structure and Uplift

Currently there is great debate (Kerr, 1988) concerning the thickness of crust beneath the batholith as well as the driving force for the rapid, late Cenozoic uplift of the range which is estimated at 2 - 2.5 km over the last 9 - 10 Ma (Christensen, 1966). One school of thought is that the range is buoyed up by a seismically modeled, 50+ km thick, low density crustal root. This root presumably formed during the Mesozoic batholith emplacement, and was probably responsible for the uplift of the late Mesozoic - early Cenozoic mountain range. Isostatic equilibrium, however, should have been reached long before the last 9 Ma, so the relationship between the recent uplift and the old root is unclear. One model invokes the Miocene rupture of a 50 km thick, elastic plate along the eastern Sierran escarpment which released the previously restrained, buoyant Mesozoic root allowing the range to rise and seek isostatic equilibrium (Chase and Wallace, 1986). Another school of thought based upon seismic tomography invokes a young, low density anomaly within the upper mantle to account for the recent uplift. Whether thinning of the mantle lithosphere and emplacement of the hot asthenosphere beneath the Sierran crest has been accomplished by the cessation of subduction coupled with an unusually high asthenospheric heat flux (Crough and Thompson, 1977), formation of a mantle lithospheric drip (Humphreys, 1987) or a low angle lithospheric fault (Jones, 1987) is presently unclear. These models also implicitly question our ability to estimate the thickness of the Mesozoic root by seismic methods as hot asthenosphere might be the dominant cause of the low density anomaly that has been previously ascribed to the thick batholith root. The apparent contradiction between the measured surface heat flow, which at 0.4 - 1.5 HFU

(Henyey and Lee, 1976) is the lowest in the United States, and the proposed shallow heat anomaly is resolved by calculations which demonstrate that thermal equilibrium by conduction has not been obtained during the 10 Ma life of the anomaly (Henyey and Lee, 1976; Crough and Thompson, 1977).

If the batholith root has been stripped away during the last 10 Ma how can we presently determine the nature of the original lower crust? One way is to examine crust and mantle xenoliths which have been carried through the batholith by late Cenozoic volcanic eruptions (Dodge and Bateman, 1988). Based on xenolith and field studies Dodge and coauthors propose a middle crust composed of a 10 km thick lense of hornblende-rich, meta-igneous amphibolites and granulites similar to rocks exposed in the southernmost Sierra Nevada (Ross, 1985; Pickett, 1991) underlying the uppermost granitic and metamorphic rocks. These authors envision the lower crust as being composed of deformed, mafic-ultramafic intrusions extending to 40 km depth with the lowermost crust composed of feldspar-poor granulites. Of particular relevance to this study, xenoliths from the Chinese Peak locality are interpreted as originating at 17 - 30 km depth in an orthopyroxene-rich, intrusive complex and associated quartz-poor granulites in which the associated cumulate (?) peridotites are relatively iron-rich (Dodge et al., 1986). These rocks bear a striking resemblance to the mafic and ultramafic rocks of the Stokes Mountain region and are part of the justification for studying the Stokes Mountain suite in the context of the lower crust. The isotopic composition of the Chinese Peak xenoliths is the focus of a study in progress.

Evidence suggestive of a shallow emplacement depth for the Stokes Mountain region has been discussed above and include the formation of ring complexes, the positive gravity anomaly indicating mafic material at less than 9 km depth, and the stoped blocks of hypabyssal material which could not have sunk far from their near-surface formation environment. This evidence must be evaluated in light of the uplift history of the western Sierra Nevada. Although estimates south of the San Joaquin River are problematic, the

Neogene uplift apparently has not affected the Stokes Mountain Region as it located along the zero uplift contour or hingeline ascribed to by most rigid block rotation and uplift models for the Sierra Nevada range. The placement of this contour is pinned by the points where the present river profiles intersect the Tertiary river profiles, which locally occurs at the Friant Dam on the San Joaquin River (Christensen, 1966). A comparable estimated location of the zero uplift contour is 3 km west of the Friant Dam at Little Table Mountain (Huber, 1981) where the gradient of the approximately 10 Ma base-level of the San Joaquin river intersects the bedding gradient of the upper Ione Formation. Westward rotation of a rigid, Sierra Nevada block may not be an appropriate model south of the San Joaquin River as faults and possible rotation may complicate the western range margin (Christensen, 1966; Huber, 1981); furthermore, the southern Sierra may have been uplifted 2 km at about 36° latitude in the upper Kern River drainage and tilted southward during this period (Jones, 1987). In light of these possible complications, an estimate for the study area of substantially less than 1 km uplift during the last 10 Ma is based upon the proximity along batholith strike to the Friant Dam site (0 km uplift) and distance along latitude to the southern range crest (2 km uplift).

Uplift of the Stokes Mountain region from approximately 55 Ma to 10 Ma is also estimated as being negligible based upon the paleotopography and paleodrainage of the San Joaquin River (Christensen, 1966; Huber, 1981) which, until approximately 3.2 Ma when it was beheaded by a combination of faulting and volcanic activity, drained the eastern side of the Sierra Nevada range. Substantial uplift resulting in exposure and erosion of the crystalline rocks prior to deposition of the Eocene Ione Formation (50 Ma) is evidenced by these clay- and quartz-rich deposits which lack immature, granitic pebbles (Wahrhaftig, 1962; Huber, 1981). The early Tertiary landscape in the present location of the western foothills had a maximum relief of only a few hundred feet (Christensen, 1966). The dip of the Ione Formation does indicate substantial uplift of the crest during this period, but as the

position of the hinge is unknown and is taken as being at Little Table Mountain, uplift estimates for the Stokes Mountain regions are again minimal.

All estimates point to a minimal amount (1 km?) of uplift having occurred in the Stokes Mountain region since approximately 55 Ma. The amount of pre-55 Ma uplift in this region might be estimated from the estimated depth of emplacement of the early Cretaceous batholith. Unfortunately, the lack of geobarometers in the cumulate megaxenoliths precludes a direct depth estimate of the magma chambers, so indirect means must be sought. An emplacement depth of 5.5 km was estimated for the early Cretaceous Rocky Hill stock which is located 23 km SSW of the Stokes Mountain area (Putman and Alfors, 1965). This estimation was based on an estimation of P_{H2O} for aplitic dikes interpreted as forming during rupture of the roof rock. In the study area, the presence of sillimanite and cordierite in the contact metamorphic zone suggests an emplacement pressure less than 2 kbar. Estimates based on mineral chemistries have resulted in igneous pressure contours of 3 to 4 kbar being drawn through the Stokes Mountain region (Ague and Brimhall, 1988), but they were not tied to any data points in the area or nearby surroundings and so are probably locally meaningless.

Consideration of all available data indicates that the Stokes Mountain suite was emplaced at shallow crustal levels, perhaps at maximum depths of 5 to 6 km. Subsequent uplift of the study area resulted in erosion of the volcanic carapace and exposure of the ring complexes; the amount of uplift may have been as little as 1 km since 55 Ma. One ramification of this conclusion is that the layered cumulates, both those exposed as megaxenoliths and those responsible for the Dinuba gravity anomaly, must have crystallized at shallow depths of approximately 5 to 15 km. As such these cumulates did not form in a typical lower crustal environment, but may have instead formed near the base of a thin crust transitional between oceanic and continental thicknesses.

2.6. Geologic History of the Stokes Mountain Region

Based upon the data and deductions presented in this chapter, the following reconstruction of the geologic history of the Stokes Mountain region is proposed:

a) parental melt(s) of hydrous basalt composition were produced by partial melting of the mantle wedge in a continental margin arc environment;

b) the Stokes Mountain parental magma was emplaced at 5 - 15 km depth underneath the Western Ring (?) Complex in a thin crust composed of accreted Paleozoic and Mesozoic ophiolitic material; the lack of geophysical anomalies underlying the Eastern Ring Complex indicate that the parental magma must have been emplaced and fractionated at greater depths underneath the Eastern Ring Complex ;

c) the shallow crustal fractionation of olivine, plagioclase and spinel followed by pyroxene and hornblende produced the smooth geochemical variations in this orthopyroxene-dominated suite; the crystallization and emplacement history can be subdivided as follows:

(i) 125 - 123 Ma: formation and deformation of layered troctolite cumulates in a dynamic environment; this process may have continued during intrusion of the ring complexes;

(ii) 123 - 116 Ma: emplacement of two ring complexes accompanied by hypabyssal intrusion, hydrothermal alteration and presumably volcanic eruption; simultaneous generation of Stone Corral Shear Zone due to interaction of the overlapping magmatic centers; disruption of cumulates and formation of megaxenoliths;

(iii) 110 Ma: final magmatism in the Stokes Mountain region;

d) since 110 Ma the Stokes Mountain region has experienced a maximum of 5 km of uplift, with perhaps as little as 1 km occurring since 55 Ma; erosion of the volcanic carapace and exposure of the underlying ring complexes occurred simultaneously with uplift.

Due to its shallow level emplacement and fractionation in a thin crust, the Stokes Mountain suite provides an uncommon view of the mafic endmembers and intermediate fractionates generated in the Sierra Nevada batholith. In the following chapter, the geochemical and isotopic systematics of the Stokes Mountain will be interpreted in light of the geologic history developed above. It will be demonstrated that contamination of this shallow level suite was minimal, and that the Stokes Mountain suite may in fact provide useful isotopic information concerning the nature and generation of the mafic endmembers of the Sierra Nevada batholith.

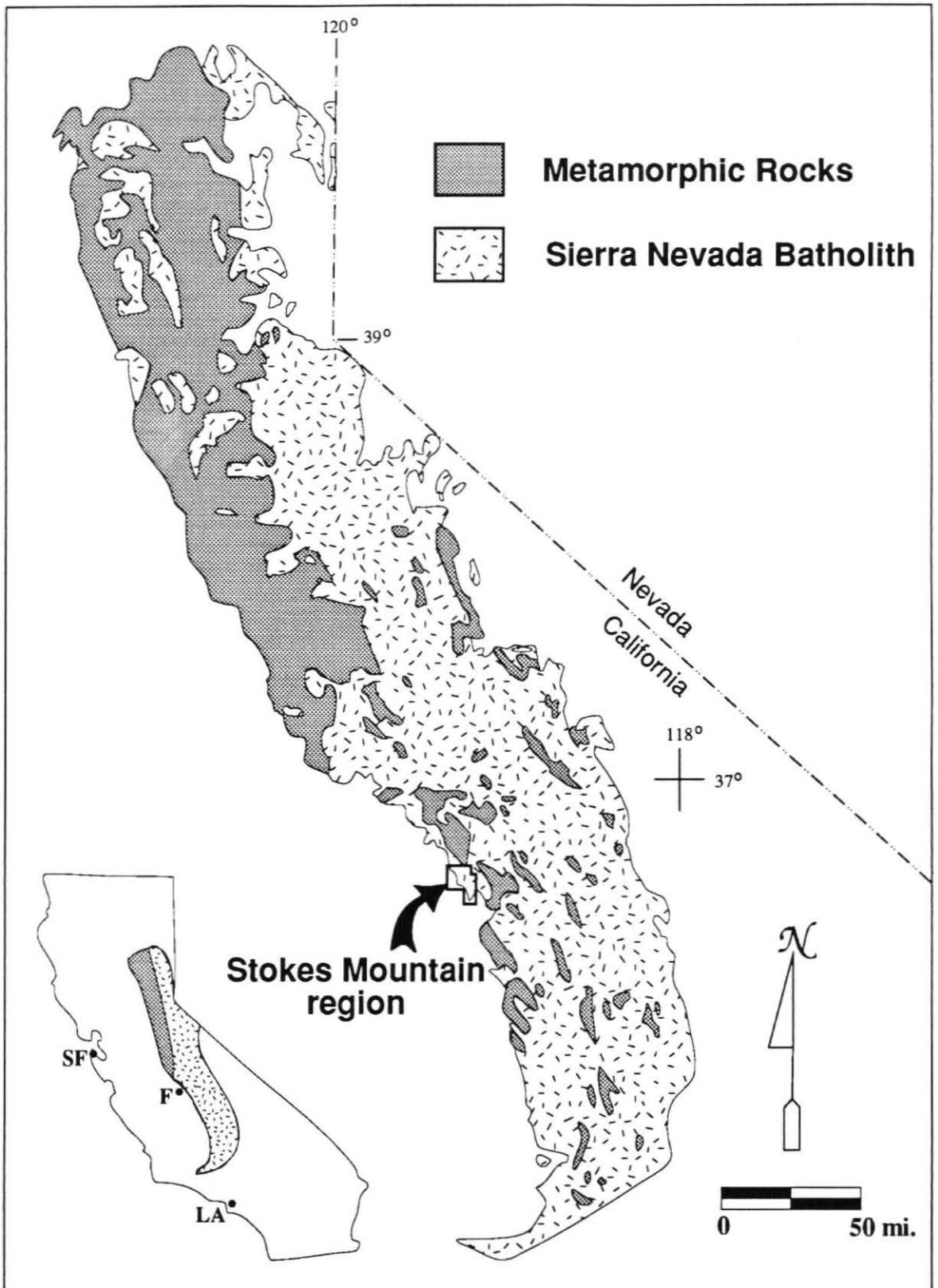

Figure 2.1: Approximate location of the Stokes Mountain region, California. Center of Stokes Mountain region is 36°30'N, 119°10'W. Generalized geology of the Sierra Nevada Batholith after Bateman (1981); SF = San Francisco; F = Fresno; LA = Los Angeles.

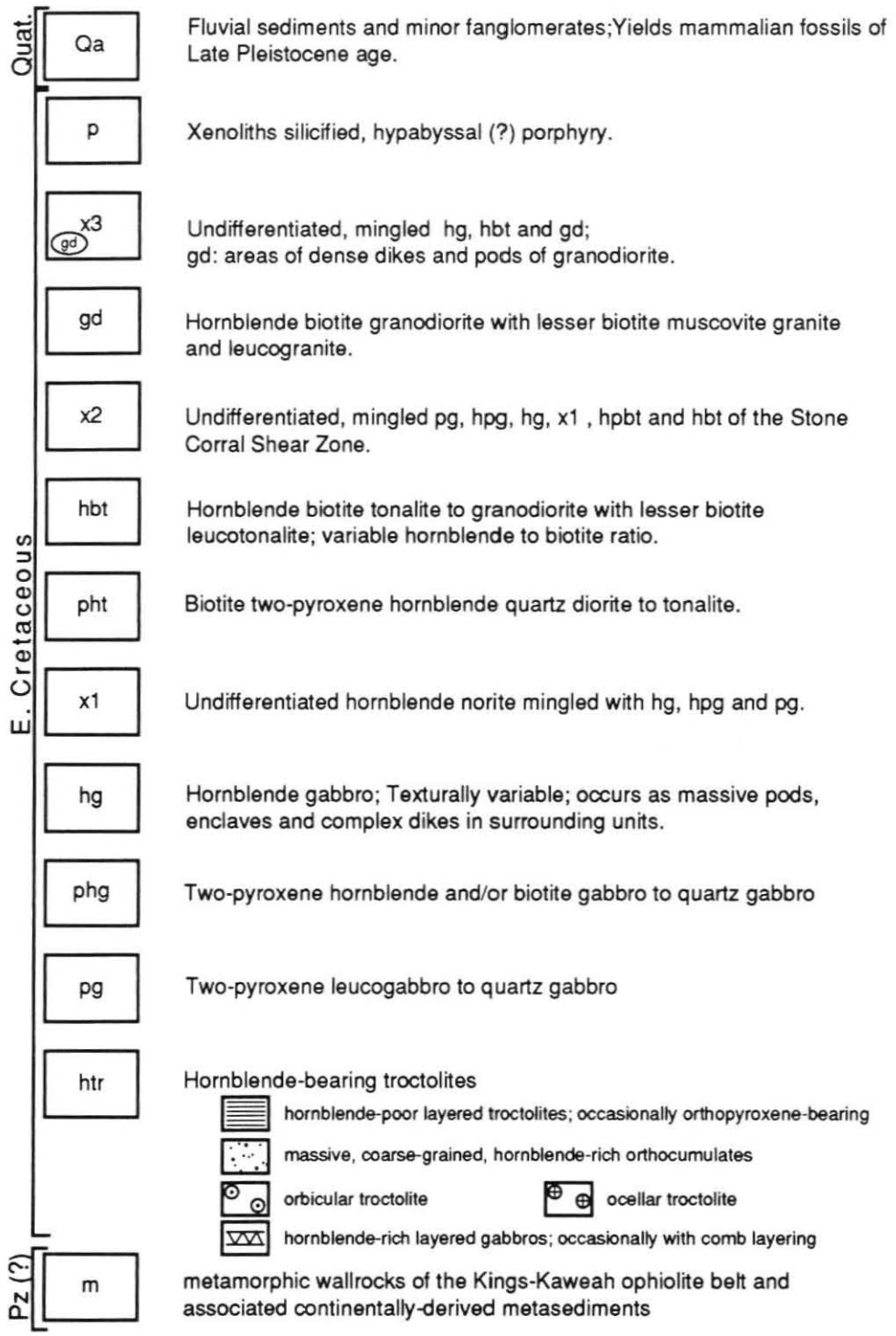

Figure 2.2: Generalized stratigraphic column of the Stokes Mountain region, Tulare County, California.

Figure 2.3: Reproduction of Figure 1 from Lesher and Walker, 1988. "Schematic illustration of saturation gradient chemical diffusion in the simple binary system A-B. The Soret effect is not considered. Phase A dissolves at the hot end and reprecipitates at the cold end as a consequence of diffusion of components A and B down their concentration gradients. The sequence of Figures 1*a*-1*c* shows the evolution from the initial to the steady state."

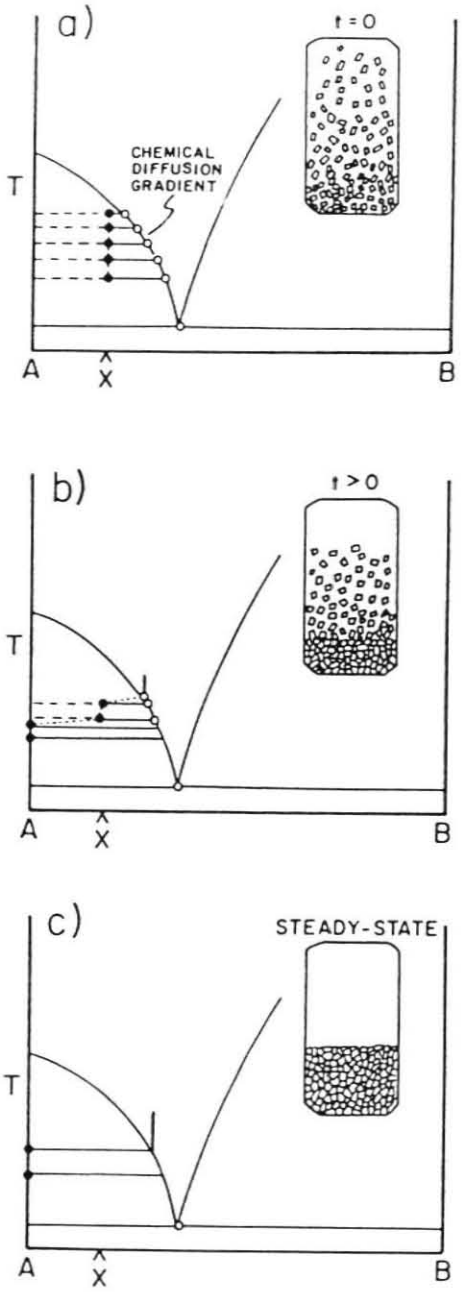

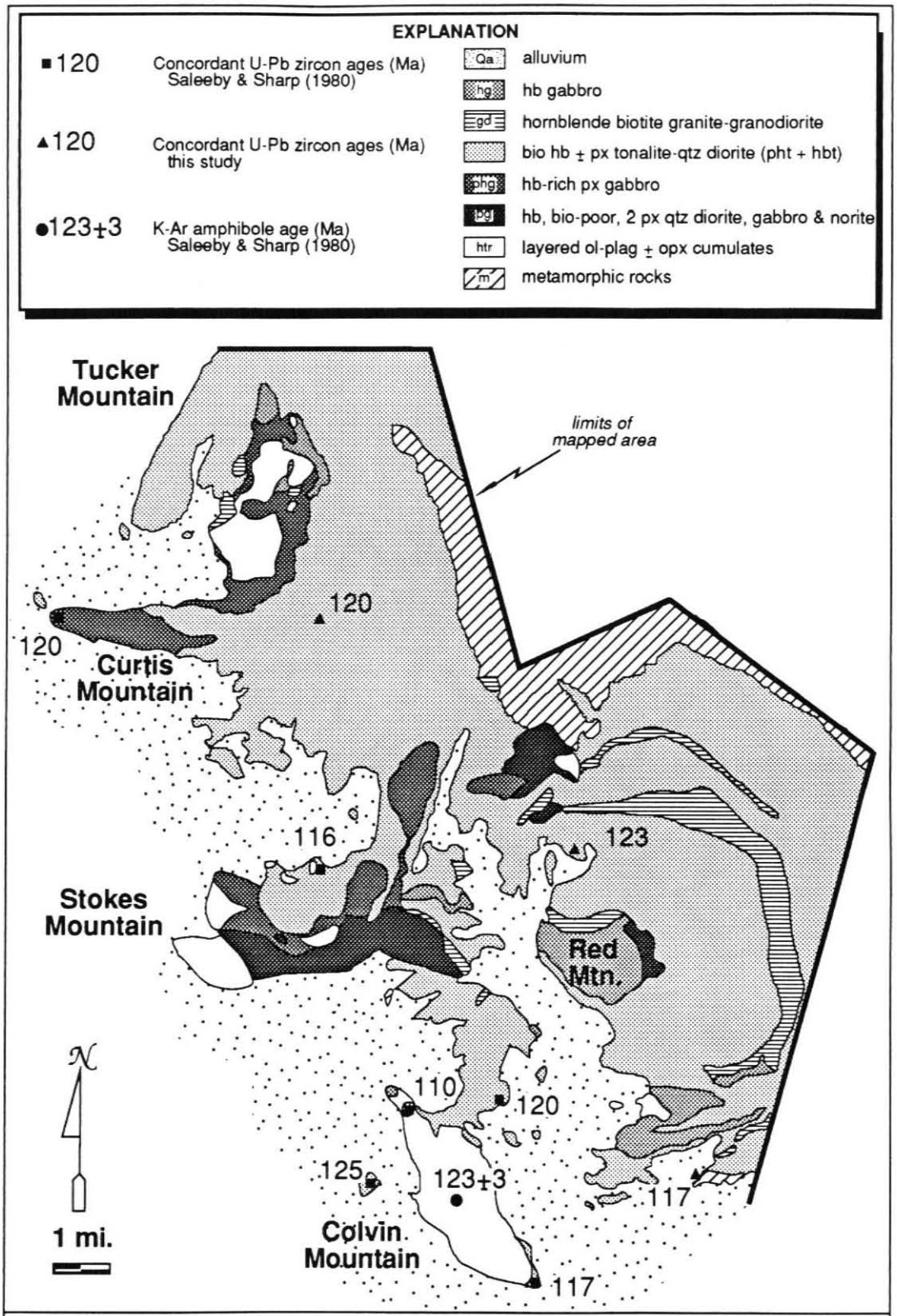

Figure 2.4: Generalized geologic map and geochronologic data.

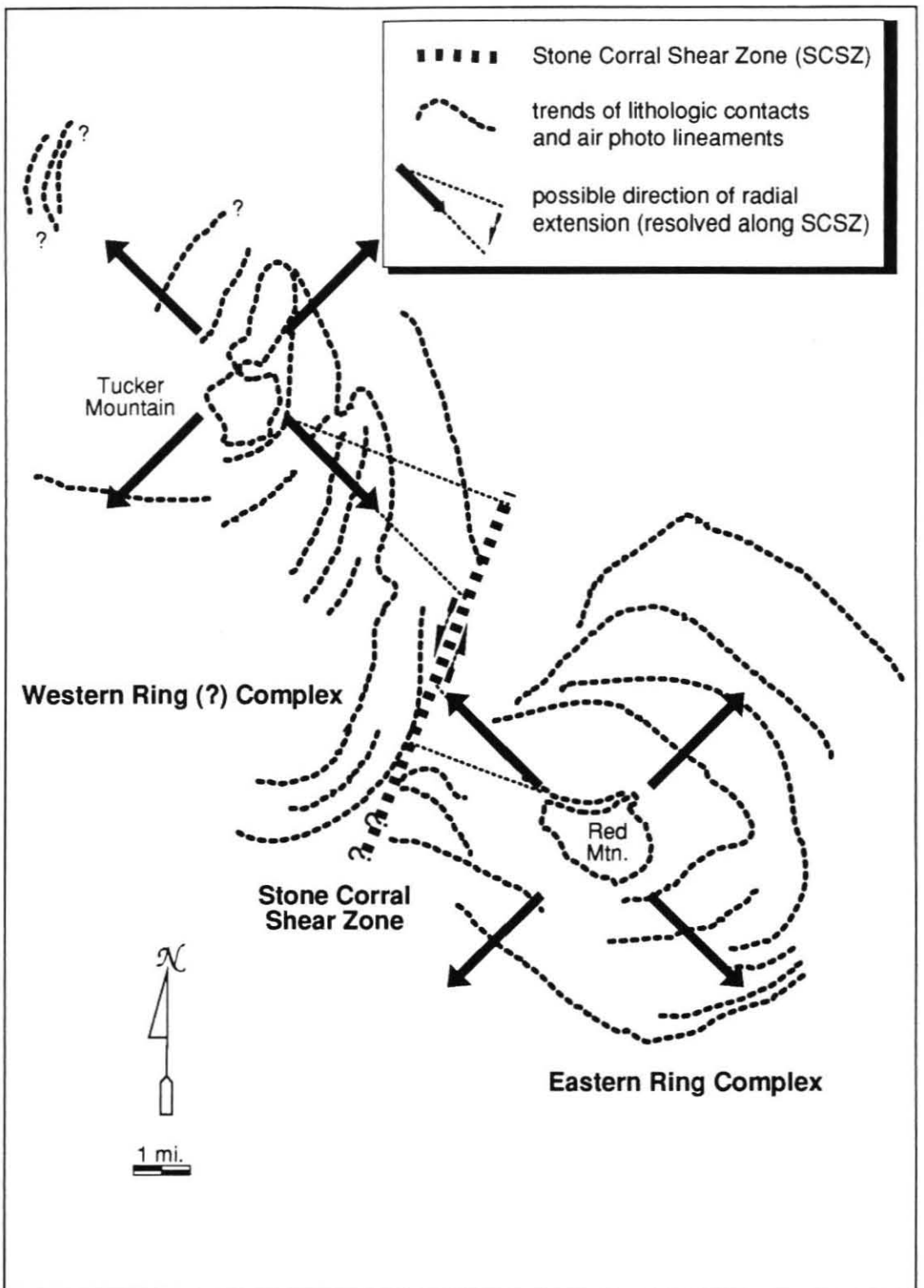

Figure 2.5: Structural overlay of the Stokes Mountain region illustrating the formation of the synmagmatic left-lateral Stone Corral Shear Zone between two, impinging, radially-extending ring complexes.

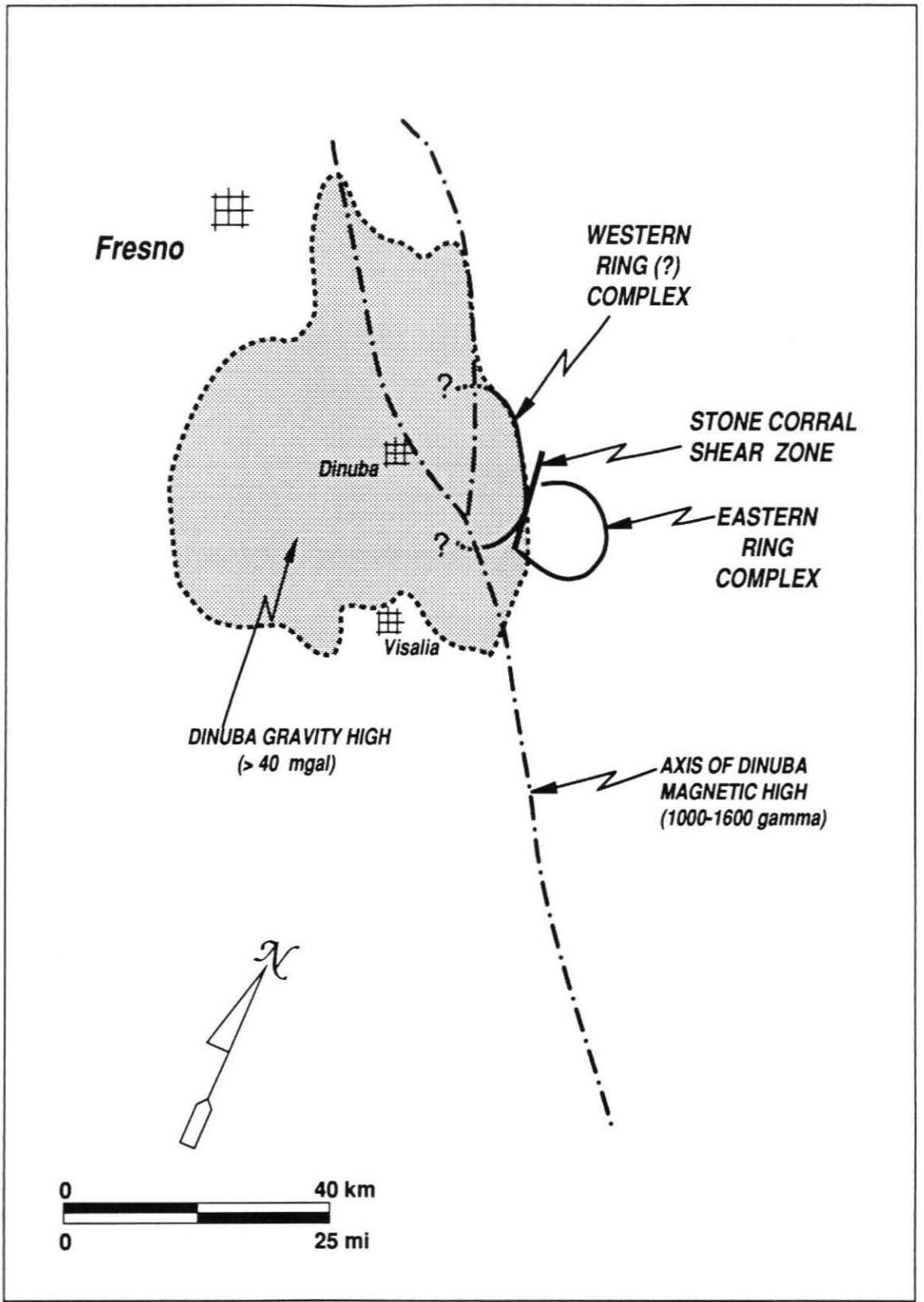

Figure 2.6: Location of Stokes Mountain ring complexes relative to geophysical anomalies. Gravity and magnetic anomalies from Cady (1975).

Mineral Phase	olivine(b)	olivine(b)	olivine(a)-1	olivine(a)-2
Sample Number	WKB53	cum gb	WKB122	WKB122
Unit	Khtr	Khtr	Khtr	Khtr
SiO2	38.42	38.85	36.18	33.60
TiO2	0.01	0.00	0.01	0.01
Al2O3	0.00	0.00	0.01	1.27
FeO	24.19	24.79	25.73	26.19
MnO	0.38	0.35	0.18	0.17
MgO	37.04	36.78	37.74	34.60
CaO	0.02	0.07	0.01	0.08
Na2O	0.00	0.00	0.37	0.01
K2O			0.01	0.01
NiO			0.01	0.01
Cr2O3				
total	100.24	100.83	100.18	95.88
Mg#	73.00	73.00	72.00	70.00
composition	Fo73	Fo73	Fo72	Fo70

Mineral Phase	olivine(a)-3	olivine(a)-1	olivine(a)-2	opx(b)
Sample Number	WKB122	WKB109	WKB109	I2A
Unit	Khtr	Khtr	Khtr	?
SiO2	35.30	35.97	36.20	36.60
TiO2	0.01	0.01	0.01	0.00
Al2O3	0.22	0.01	0.01	0.00
FeO	23.70	23.70	20.79	24.57
MnO	0.12	0.41	0.30	
MgO	37.38	39.39	41.62	38.77
CaO	0.07	0.09	0.08	0.02
Na2O	0.01	0.58	0.01	0.01
K2O	0.01	0.01	0.01	
NiO	0.01	0.01	0.01	
Cr2O3				
total	96.77	100.12	98.97	99.97
Mg#	74.00	75.00	78.00	0.74
composition	Fo74	Fo75	Fo78	bronzite

Table 2.1: Mineral compositions of samples from the greater Stokes Mountain region including those used for the fractional crystallization model. Annotations: "(a)" = scanning electron microscope (this study); "(b)" = electron microprobe (Saleeby et al., unpublished analyses); "-#" identifies multiple analyses on different mineral grains from a single sample.

Mineral Phase	opx(b)	opx(b)	opx(a)	opx(a)-1	opx(a)-2
Sample Number	WKB6	SM3	WKB109	WKB77	WKB77
Unit	?	?	Khtr	Khpg	Khpg
SiO2	52.19	51.23	52.79	50.99	50.28
TiO2	0.15	0.17	0.32	0.01	0.01
Al2O3	0.67	0.78	1.20	0.53	0.46
FeO	22.95	27.39	14.92	27.69	27.28
MnO			0.34	0.58	0.66
MgO	23.49	19.02	29.74	20.18	20.35
CaO	0.82	0.79	0.60	0.80	0.85
Na2O	0.01	0.03	0.37	0.90	1.02
K2O	0.00	0.00	0.01	0.01	0.01
NiO			0.01	0.01	0.01
Cr2O3					
total	100.28	99.41	100.24	101.64	100.86
Mg#	0.65	0.55	0.78	0.56	0.56
composition	hypersthene	hypersthene	bronzite	hypersthene	hypersthene

Mineral Phase	opx(a)-1	opx(a)-2	opx(a)-1	opx(a)-2	opx(a)-1
Sample Number	WKB75	WKB75	WKB91	WKB91	SM204
Unit	Kpg	Kpg	Kpg	Kpg	Kx2
SiO2	49.78	51.91	51.54	50.80	49.56
TiO2	0.01	0.32	0.01	0.01	0.23
Al2O3	0.47	0.86	0.40	0.92	0.88
FeO	27.77	25.09	24.47	23.49	26.24
MnO	0.77	0.60	0.53	0.59	0.88
MgO	20.51	18.00	22.73	22.48	20.21
CaO	0.86	0.91	0.76	1.73	0.62
Na2O	0.51	0.47	0.01	0.01	0.37
K2O	0.01	0.08	0.01	0.01	0.01
NiO	0.01	0.01	0.01	0.01	0.01
Cr2O3			0.01	0.17	0.12
total	100.64	98.22	100.41	100.15	99.08
Mg#	0.56	0.56	0.62	0.62	0.57
composition	hypersthene	hypersthene	hypersthene	hypersthene	hypersthene

Table 2.1: Mineral compositions of samples from the greater Stokes Mountain region including those used for the fractional crystallization model. Annotations: "(a)" = scanning electron microscope (this study); "(b)" = electron microprobe (Saleeby et al., unpublished analyses); "-#" identifies multiple analyses on different mineral grains from a single sample.

Mineral Phase	opx(a)-2	cpx(a)	cpx(a)	cpx(a)-1	cpx(a)-2
Sample Number	SM204	WKB94	WKB77	WKB91	WKB91
Unit	Kx2	Khg	Khpg	Kpg	Kpg
SiO2	49.17	52.96	50.68	51.81	51.14
TiO2	0.01	0.17	0.01	0.57	0.34
Al2O3	0.50	0.78	1.17	1.66	1.59
FeO	26.26	6.77	11.30	9.57	12.45
MnO	0.78	0.18	0.26	0.32	0.20
MgO	19.54	15.95	13.39	14.21	15.44
CaO	0.56	24.17	22.26	22.35	19.22
Na2O	0.41	0.45	0.95	0.77	0.64
K2O	0.01	0.01	0.08	0.01	0.01
NiO	0.01	0.01	0.40	0.28	0.01
Cr2O3	0.21			0.18	0.01
total	97.38	101.38	100.47	101.67	100.89
Mg#	0.56				
composition	hypersthene	salite	salite	calcic augite	augite

Mineral Phase	amph(b)	amph(b)	amph(b)	amph(b)	amph(b)
Sample Number	WKB53	cum gb	I2A	WKB6	SM3
Unit	Khtr	Khtr	?	?	?
SiO2	42.25	42.07	44.62	46.18	44.45
TiO2	2.60	2.87	0.27	1.60	1.50
Al2O3	13.11	12.47	12.67	7.83	8.73
FeO	10.06	10.12	8.94	13.62	16.47
MnO	0.17	0.12			
MgO	14.49	14.38	16.26	14.80	11.84
CaO	11.66	11.72	12.00	11.56	11.25
Na2O	2.49	2.50	2.08	1.03	1.26
K2O	0.37	0.36	0.16	0.69	0.98
NiO					
Cr2O3					
total	97.21	96.60	97.00	97.30	96.49
Mg#	0.59	0.58	0.76	0.66	0.56
composition	pargasitic hb	pargasitic hb	hornblende	hornblende	hornblende

Table 2.1: Mineral compositions of samples from the greater Stokes Mountain region including those used for the fractional crystallization model. Annotations: "(a)" = scanning electron microscope (this study); "(b)" = electron microprobe (Saleeby et al., unpublished analyses); "-#" identifies multiple analyses on different mineral grains from a single sample.

Mineral Phase	amph(a)	amph(a)-1	amph(a)-2	amph(a)
Sample Number	WKB94	WKB109	WKB109	WKB75
Unit	Khg	Khtr	Khtr	Kpg
SiO2	47.41	45.45	43.32	44.47
TiO2	1.33	1.10	1.59	1.44
Al2O3	8.51	11.38	13.34	9.22
FeO	11.40	9.23	9.28	16.39
MnO	0.19	0.01	0.01	0.33
MgO	15.08	17.20	15.81	12.75
CaO	12.44	11.81	11.62	11.72
Na2O	1.50	2.53	2.97	1.77
K2O	0.73	0.38	0.31	0.74
NiO	0.27	0.01	0.01	0.01
Cr2O3				
total	98.82	99.04	98.20	98.81
Mg#	0.56	0.65	0.63	0.43
composition	hornblende	pargasitic hb	pargasite	hornblende

Mineral Phase	amph(a)-1	amph(a)-2	amph(a)-3	amph(a)
Sample Number	WKB105	WKB105	WKB105	WKB86
Unit	Khbt	Khbt	Khbt	Khbt
SiO2	45.42	45.03	44.78	47.31
TiO2	2.12	1.95	1.28	1.13
Al2O3	8.56	8.63	8.47	6.77
FeO	18.26	18.36	17.99	16.21
MnO	0.28	0.22	0.17	0.22
MgO	11.77	11.17	11.33	13.11
CaO	11.55	11.26	11.83	12.33
Na2O	1.89	1.87	1.94	1.55
K2O	0.79	0.90	0.67	0.60
NiO	0.01	0.01	0.01	0.01
Cr2O3				0.21
total	100.59	99.37	98.43	99.41
Mg#	0.39	0.38	0.38	0.44
composition	pargasitic hb	hornblende	hornblende	hb, near trem

Table 2.1: Mineral compositions of samples from the greater Stokes Mountain region including those used for the fractional crystallization model. Annotations: "(a)" = scanning electron microscope (this study); "(b)" = electron microprobe (Saleeby et al., unpublished analyses); "-#" identifies multiple analyses on different mineral grains from a single sample.

Mineral Phase	amph(a)	plag (a)-1	plag (a)-2	plag (a)-3	plag (a)
Sample Number	SM204	WKB121	WKB121	WKB121	WKB94
Unit	Kx2	Khtr	Khtr	Khtr	Khg
SiO2	44.71	43.11	42.28	39.9	46.12
TiO2	1.53	0.01	0.01	0.01	0.01
Al2O3	9.27	35.26	35.85	34.22	34.96
FeO	15.82	0.01	0.01	0.18	0.29
MnO	0.50	0.01	0.01	0.01	0.01
MgO	12.62	0.01	0.01	0.01	0.01
CaO	11.21	19.06	17.66	19.77	17.61
Na2O	1.39	0.92	1.39	1.02	2.11
K2O	0.57	0.09	0.01	0.01	0.12
NiO	0.01	0.01	0.38	0.01	0.01
Cr2O3	0.01				
total	97.60	98.43	97.53	95.08	101.18
Mg#	0.44	An92	An88	An91	An82
composition	hornblende	anorthitite	bytownite	anorthite	bytownite

Mineral Phase	plag (a)-1	plag (a)-2	plag (a)-3	plag (a)	plag (a)
Sample Number	WKB109	WKB109	WKB109	WKB77	WKB75
Unit	Khtr	Khtr	Khtr	Khpg	Kpg
SiO2	44.8	44.06	44.6	53.92	54.72
TiO2	0.27	0.01	0.01	0.16	0.36
Al2O3	36.2	35.67	34.79	28.02	21.69
FeO	0.25	0.01	0.01	0.32	5.39
MnO	0.09	0.01	0.01	0.1	0.28
MgO	0.01	0.21	0.01	0.01	2.03
CaO	18.46	18.22	17.5	10.62	8.22
Na2O	1.49	1.49	1.62	6.64	5.33
K2O	0.11	0.01	0.01	0.33	0.3
NiO	0.01	0.26	0.01	0.01	0.22
Cr2O3					
total	101.64	99.89	99.49	100.08	98.49
Mg#	An86	An87	An87	An46	An45
composition	bytownite	bytownite	bytownite	andesine	andesine

Table 2.1: Mineral compositions of samples from the greater Stokes Mountain region including those used for the fractional crystallization model. Annotations: "(a)" = scanning electron microscope (this study); "(b)" = electron microprobe (Saleeby et al., unpublished analyses); "-#" identifies multiple analyses on different mineral grains from a single sample.

Mineral Phase	plag (a)-1	plag (a)-2	plag (a)	plag (a)
Sample Number	WKB105	WKB105	WKB122	WKB86
Unit	Khbt	Khbt	Kgd	Khbt
SiO2	58.39	56.29	58.92	60.71
TiO2	0.01	0.15	0.01	0.01
Al2O3	27.48	26.48	25.62	24.94
FeO	0.01	0.31	0.23	0.16
MnO	0.01	0.01	0.01	0.01
MgO	0.01	0.01	0.01	0.01
CaO	8.19	8.46	7.56	5.64
Na2O	7.56	6.9	7.75	9.14
K2O	0.07	0.12	0.12	0.31
NiO	0.22	0.01	0.01	0.01
Cr2O3				0.01
total	101.89	98.68	100.18	100.87
Mg#	An37	An40	An35	An25
composition	andesine	andesine	andesine	oligoclase

Mineral Phase	plag (a)	plag (a)-1	plag (a)-2
Sample Number	WKB91	SM204	SM204
Unit	Kpg	Kx2	Kx2
SiO2	52.77	53.87	55.36
TiO2	0.01	0.01	0.01
Al2O3	28.35	29.41	29.15
FeO	0.19	0.65	0.01
MnO	0.01	0.01	0.01
MgO	0.01	0.01	0.01
CaO	10.44	10.18	9.91
Na2O	5.92	7.14	7.07
K2O	0.42	0.01	0.13
NiO	0.01	0.01	0.01
Cr2O3	0.01	0.01	0.25
total	98.06	101.22	101.84
Mg#	An48	An41	An44
composition	andesine	andesine	andesine

Table 2.1: Mineral compositions of samples from the greater Stokes Mountain region including those used for the fractional crystallization model. Annotations: "(a)" = scanning electron microscope (this study); "(b)" = electron microprobe (Saleeby et al., unpublished analyses); "-#" identifies multiple analyses on different mineral grains from a single sample.

Table 2.2: ZIRCON ISOTOPIC AGE DATA

Sample #	Fraction Size§ (μm)	Amount Analyzed (mg)	Concentrations ^{238}U (ppm)	Concentrations $^{206}Pb^*$ (ppm)	Atomic Ratios $^{206}Pb/^{204}Pb$	Atomic Ratios $^{206}Pb^*/^{238}U$	Atomic Ratios $^{207}Pb^*/^{235}U$	Atomic Ratios $^{207}Pb^*/^{206}Pb^*$	Isotopic Ages (Ma)‡ $^{206}Pb^*/^{238}U$	Isotopic Ages (Ma)‡ $^{207}Pb^*/^{235}U$	Isotopic Ages (Ma)‡ $^{207}Pb^*/^{206}Pb^*$
W170	<45	0.3	131	2.1	753	0.01837(10)	0.1225	0.04842(09)	117.3	117.4	119 ± 6
WKB129	<45	1.5	446	7.2	379	0.01867(11)	0.1224	0.04836(13)	119.2	119.1	117 ± 8
	45 - 62	1.4	377	6.2	377	0.01894(12)	0.1265	0.04848(16)	120.9	120.9	122 ± 10
WKB131	<45	1.3	209	3.5	1410	0.01931(11)	0.1291	0.04853(12)	123.3	123.3	125 ± 6
	45 - 62	3.0	249	4.2	1910	0.01937(12)	0.1297	0.04858(10)	123.7	123.8	127 ± 5

§ Fractions separated by grain size and magnetic properties. Magnetic properties are given as non-magnetic split at 2° side/20° front slopes of 2/20 for 1.7 amps on a Franz Isodynamic Separator. Samples were hand-picked to 99.9% purity prior to dissolution. Dissolution and chemical extraction techniques modified from Krogh (1973).

* Denotes radiogenic Pb. Nonradiogenic correction based upon a 25 picogram Pb blank (1:18.78:15.61:38.50) and initial Pb approximations of 1: 18.645 : 15.544 : 38.230 from Chen and Tilton (1991).

‡ Decay constants used in age calculations: $\lambda^{238}U = 1.55125E\text{-}10\ yrs^{-1}$, $\lambda^{235}U = 9.8485E\text{-}10\ yrs^{-1}$ (Jaffey and others, 1971); $^{238}U/^{235}U$ atom = 137.88. Uncertainty in last two numbers of $^{206}Pb^*/^{238}U$ is given in parentheses; two-sigma uncertainty in $^{207}Pb^*/^{206}Pb^*$ is given as "±." Uncertainties calculated by quadratic sum of total derivatives of ^{238}U and ^{206}Pb concentrations and $^{207}Pb^*/^{206}Pb^*$ equations with error differntials defined as: [1] isotope ratio determinations from standard errors ($\sigma/\sqrt{n}$) of mass spectrometer runs plus uncertainties in fractionation corrections based on multiple runs of NBS 981, 982, 983, and U500 standards; [2] spike concentrations from range of deviations in multiple calibrations with normal solutions; [3] spike compositions from external precisions of multiple isotope ratio determinations; [4] uncertainty in natural $^{238}U/^{235}U$ from Chen and Wasserburg (1981); and [5] nonradiogenic Pb isotopic compositions from uncertainties in isotope ratio determinations of blank Pb and uncertainties in composition of initial Pb from estimates of regional variations based on Saleeby and Chen (1978) and consideration of rock type.

Chapter 3 Geochemistry and Isotope Systematics of the Stokes Mountain Region

Significant growth of continental crust occurs in continental margin arcs such as those which formed during the Mesozoic and Cenozoic along the western North American margin. The effectiveness of this mechanism in generating continental crust may be evaluated by estimating the proportion of the new crust which was generated by mantle magmatism. The study of multiple isotopic systems provides the best parameter with which to make this estimation because the isotopic contrast between mantle-derived melts and continental crust is typically significant. Estimation of the relative proportions of these components is possible through simple mixing or assimilation and fractional crystallization (AFC) calculations (DePaolo, 1980; Taylor, 1980). When applied on a batholithic scale such calculations are inherently simplified as the isotopic and geochemical characteristics of the end members are variable and are often not well constrained.

The Sierra Nevada batholith formed in a continental margin arc in which the amount of older crust recycled during the Mesozoic event has been estimated as approximately subequal to the amount of mantle-derived magma added (DePaolo, 1981). In earlier isotopic studies the mafic rocks of the early Cretaceous batholith, located along the western margin of the Sierra Nevada, have been identified as the least contaminated lithologies exposed in the compound batholith. The isotopic signature of these relatively uncontaminated lithologies should, therefore, most closely approach the isotopic characteristics of the mantle-derived magma.

The Stokes Mountain plutonic suite provides a rare opportunity to study the petrogenesis of the ultramafic and mafic lithologies of the Sierra Nevada batholith and to estimate the isotopic and perhaps chemical composition of the mantle-derived magma. The layered ultramafic-mafic cumulates present in the area must represent the fractionates of chemically unevolved magmas and thus may be the first products formed by fractionation of the mantle-derived magma in the crustal environment. The study of these cumulates and

the associated fractionates should help constrain the isotopic character of one of the modeled end members in the generation of the batholith: the mantle-derived magma.

In this chapter, an extensive new geochemical and isotopic data set is analyzed in terms of the petrogenesis of the early Cretaceous batholith. Due to a remarkable set of temporal, structural and chemical circumstances it is possible to deduce a significant amount of information concerning the mantle source region of the parental magmas.

3.1. Geochemistry of the Early Cretaceous Batholith

To date 126 whole rock geochemical analyses have been performed on samples from the early Cretaceous batholith. The analyses were provided by Dr. B. W. Chappell of the Australian National University; the data are listed in Table 3.1. Of these, 55 samples (WKB72 - 126) were collected in the present study; locations for the samples are shown on Plate 2. WKB samples 1 - 71 were collected prior to this study primarily along two traverses across the western foothills: one traverse to the north of the field area and one to the south (Saleeby and Chappell, personal communication). Despite the fact that these earlier samples lack detailed field control, they are useful in terms of understanding the geochemical trends displayed by the early Cretaceous batholith so have been included in the following analysis. Approximate locations for samples WKB 1-68 are listed in Table 3.8.

3.1.1. Analytical Techniques

Each sample was prepared with the intent to maximize recovery and minimize contamination in order that radioisotope and rare earth analyses could be performed if deemed appropriate. Samples containing approximately 10^6 grains were collected. Those samples prepared at Caltech were crushed in a diamond mortar and divided in an aluminum splitter. One (ANU) to three (CIT) 50 mg alloquots were crushed to powder in a tungsten carbide shatter box in which quartz sand was crushed between each sample. In addition, all equipment was cleaned between samples with two repetitions of ultrasonic cleaning and

scrubbing. The powders were then analyzed for major and twenty trace elements by X-ray spectrometry.

3.1.2. Analysis of Geochemical Data

One of the more interesting features of the early Cretaceous batholith is the calcic character which is clearly demonstrated in Figure 3.1. This calcic composition contrasts with the calcalkaline character of the majority of the younger exposed Sierra Nevada batholith (Bateman and Chappell, 1979) but is similar to the Peninsular Ranges batholith which displays a range in Peacock index varying between 65% and 62% from west to east (Silver and Chappell, 1987). The reason for this temporal distinction in the Sierra Nevada batholith is unclear but may reflect a compositional variation in the parental magma with time. One possibility is that the less voluminous early Cretaceous batholith may represent a relatively low degree of partial melt of a plagioclase-rich source. While this is only a conjecture, isotopic data presented in section 3.3 demonstrate that the calcic character of the gabbros is not the result of assimilation of the calcium-rich ophiolitic wall rocks of the western batholith margin.

Harker variation diagrams for the major elements are displayed in Figures 3.2 - 3.7; similar diagrams for TiO_2 and MnO are displayed in Figures 3.8 and 3.9 respectively. The solid symbols and arrows in these figures refer to the crystal fractionation model described in section 3.2. Ignoring these symbols, a few generalizations can be made concerning the trends in Figures 3.3 - 3.9. The most striking feature is that at SiO_2 values greater than 50% the trends display little scatter. This range corresponds to units Kpht, Khbt and Kgd which are listed in order of increasing silica content. In volcanic suites, in which rock compositions may be comparable to liquid compositions, such tight trends are generally interpreted as resulting from either fractional crystallization or magma mixing.

Plots of the alkali oxides Na_2O and K_2O do display a fair amount of scatter on the larger scale ordinates of Figures 3.6 and 3.7, but it can be seen on the smaller scale

ordinate of Figure 3.1 that the sum of these oxides forms a tight trend. Part of this scatter is therefore due to the change in ordinate scales compared to the other figures while part may be due to the complicated mineralogical control of these alkali elements by mica, amphibole and feldspar abundances. A reversal in trend for Na_2O at SiO_2 contents greater than 75% is displayed by three samples (WKB73, WKB88 and WKB102) on Figure 3.6. These samples have lower sodium and higher potassium contents than predicted by extension of the trends defined by less siliceous samples. These are plagioclase-poor leucogranites bearing abundant potassium feldspar; such rocks are not common in this suite.

Below values of 50% SiO_2, great scatter is displayed by samples from units Khtr, Kpg and Khpg. This scatter is easily explained by the efficient operation of cumulate processes for which there is ample evidence as discussed in Chapter 2. For example, in Figure 3.4, those samples with < 45% SiO_2 having high MgO contents are dunitic cumulates while those with low MgO contents are anorthositic cumulates.

Harker variation diagrams for the trace elements have not been included in this chapter, but the trends visible on such plots show similar degrees of scatter above and below 50% SiO2 as displayed by the major elements. All trends are predicted if the samples are regarded as calcalkaline liquid compositions undergoing closed system fractional crystallization (B.W. Chappell, personal communication): Ni, Cr, V, Ga, Cu, Zn, Co and Sr behave as compatible elements while large iron lithophile and high field strength elements Rb, Ba, Th, Pb, U, La, Ce and Nb behave as incompatible elements being completely excluded from the cumulates. Zr is generally incompatible, with concentrations beginning to increase at 50% SiO_2 with some samples leveling out at concentrations of approximately 150 ppm above 60% SiO_2. This trend corroborates the observation that zircon is found in all orthopyroxene-bearing rocks (> 50% SiO_2) (J.B. Saleeby, personal communication). P and Y are incompatible until 55% SiO_2 by which

point crystallization of apatite and amphibole may be responsible for the depletion of P and scatter of Y, respectively. Sc behaves compatibly until 65% SiO_2 at which point the trend reverses and concentrations of this element increase. Further analysis of this geochemical data set is pending analysis of the rare earth elements; this work is currently underway at ANU.

A Harker variation diagram for MnO is shown in Figure 3.9 because MnO displays an unusual compatible behavior at SiO_2 contents greater than 50%. There are a few possible phases which may have incorporated significant manganese during fractional crystallization. The major suspect is orthopyroxene which, as discussed in Chapter 2, is unusually abundant in the WKB suite as compared to the majority of Cordilleran suites. Eight hypersthene analyses listed in Table 2.1 span a range of MnO contents between 0.53 and 0.88%; these values compare to a clinopyroxene range of 0.18 and 0.32% MnO. The unusual predominance of orthopyroxene over clinopyroxene may, therefore, have caused manganese to behave compatibly. A bronzite from a hornblende troctolite (WKB109) contains 0.34% MnO while two WKB109 olivines have contents of 0.30 and 0.41%. The combined fractionation of olivine and bronzite during formation of the cumulates may have somewhat depleted the residual magma of manganese, although high whole rock MnO contents occur only in mafic-rich cumulates. Other phases which may have fractionated substantial manganese include ilmenite and amphibole. A single ilmenite grain containing 1.4 wt. % MnO was analyzed in this study; most opaque grains analyzed were Mn-poor magnetite. Whether the fractionation of ilmenite significantly affected the MnO evolution, however, is questionable due to the low amounts (1-2%) of ilmenite fractionation which could be accommodated by the fractionation modeling without adversely affecting the FeO* evolution (section 3.2). One analyzed hornblende (WKB204) contains 0.50 % MnO, but this phase generally contains lower amounts of manganese (0.01 - 0.33%).

In summary, smooth trends displayed on Harker variation diagrams for the samples with SiO_2 contents greater than 50% demonstrate a geochemical coherency within the suite. Unusual characteristics of the WKB suite include the calcic classification and the compatible behavior of manganese in the noncumulates. The former characteristic must be related to the parental magma while the latter may be related to the unusual abundance orthopyroxene in the suite.

3.2. Crystal Fractionation Model

Computer modeling was attempted in order to investigate the hypothesis that fractional crystallization produced the smooth geochemical variations displayed by the WKB suite within the SiO_2 range of 50 - 70%. Input model parameters (distribution coefficients, phase proportions) and calculated liquid compositions are listed in Table 3.2; mineral compositions are listed in Table 2.1. The results of the modeling are plotted as solid symbols on Figures 3.2 - 3.8.

3.2.1 The Fractionation Model

Fractional crystallization calculations are similar to those described by Grove and Baker (1984). Although complicated in detail, the calculations are simple in concept: given a starting magma composition and the compositions and abundances of minerals to be fractionated, the product magma is calculated after each 2 wt. % crystallization of the parent magma. Fe-Mg K_D-values for clinopyroxene, orthopyroxene, amphibole and biotite and and Ca-Na K_D-values for plagioclase were selected from low pressure experiments on basalts and andesites. The K_D-value for each mineral was held constant throughout the modeling.

The starting and endpoint compositions (Start A and Final, Table 3.2) were calculated from second order polynomial fits to each oxide plotted as a function of MgO. First, a curve was fit to the SiO_2 - MgO variation diagram for samples with SiO_2 contents exceeding 50% in order to exclude obvious cumulates. MgO contents corresponding to SiO_2 contents of 50 and 70% were determined from the fitted curve; these MgO contents

were 5.4% and 1.0% respectively. Next, oxide variation diagrams were plotted with MgO as the abscissa. In each fit, reasonable care was taken to exclude analyses that plotted outside of the well defined variation trends. Values of each oxide corresponding to MgO contents of 5.4% and 1.0% were then read from each curve. Finally, the total oxides (SiO_2, TiO_2, Al_2O_3, FeO*, MgO, CaO, Na_2O, K_2O) for the Start A and Final compositions were normalized to 100%.

The Start B, Start C and Start D compositions (Table 3.2) are normalized compositions of samples WKB91 (a two pyroxene quartz diorite), WKB87 (a pyroxene biotite hornblende tonalite) and WKB86 (a hornblende biotite granodiorite) respectively. These samples were chosen as representatives of the petrographically determined evolution of the suite (i.e., samples characteristic of the dominant lithologies and which document the disappearance and appearance of major mineral phases) corresponding to the geochemical range of 50 to 70% SiO_2. The analyses for each sample was normalized to 100% after excluding P_2O_5, MnO and H_2O and combining the FeO and Fe_2O_3 contents to FeO*. These normalized control compositions generally plot within the swaths defined by the unnormalized data . An alternate approach would have been to chose arbitrary values of SiO_2 and determine the most representative abundance for each oxide at each point, but constraining the model to actual rock compositions appeared most appropriate for this first attempt at modeling.

For each of the four steps, the fractionating assemblage and phase proportions were specified that closely resembled prominent lithologies in the WKB suite other than those used as the Start B, C and D compositions. Mineral compositions used in the model were chosen from rocks of similar lithologies. In Steps A and B two pyroxene hornblende gabbros are fractionated, while in Step C a hornblende gabbro and in Step D a hornblende biotite diorite is fractionated. The least satisfactory of these choices is Step B in which the abundance of fractionated clinopyroxene is greater than orthopyroxene, unlike the dominant

lithologies found in the Stokes Mountain region. Clinopyroxene-rich rocks are found, however, in neighboring areas of the early Cretaceous batholith (Saleeby and Sharp, 1980), so the possibility that significant clinopyroxene was fractionated is not wholly unreasonable for the total WKB suite.

3.2.2 Discussion of Model Results

The fractionation model closely approximates the varying abundances of Al_2O_3, FeO*, MgO in the WKB suite (Figures 3.2 - 3.8). CaO matches well except for Step D in which the absence of fractionating apatite may account for the slightly high modeled CaO abundances. The model approximates the Na_2O and K_2O trends only marginally. The inability of the model to allow Na_2O contents to increase during Step A is puzzling, but may indicate a lesser amount of fractionating amphibole or that the Na_2O content of the Start A composition is approximately 20% too low. The Step A model is also unsatisfactory in SiO_2 - TiO_2 space as a large amount of sphene was fractionated in order to decrease the CaO contents appropriately. Use of a more appropriate Ca-Na K_D-value for plagioclase (e.g., 2-4 instead of 1) would raise the anorthite content of the fractionating plagioclase and might enable the CaO trends to be matched without depleting TiO_2 by sphene fractionation during Step A. Alternatively, fractionation of more clinopyroxene relative to orthopyroxene might allow the CaO trend to be better approximated without affecting the TiO_2 trend.

The fractionation modeling generated two unpredicted observations. First, clinopyroxene may have been more important in the fractionation scheme for the WKB suite than predicted based upon observed mineral abundances in the Stokes Mountain region. This is somewhat disturbing because, as discussed in sections 2.2.4 and 2.2.6, there are other examples of orthopyroxene-dominated suites in the Cordillera; certainly not all examples are dependent upon some obscured fractionation of clinopyroxene. Clinopyroxene is common, however, in the early Cretaceous batholith outside of the

Stokes Mountain region, so perhaps the samples collected within the Stokes Mountain region are not completely representative of the WKB suite. Second, the fractionation of hornblende gabbro in Step C was not anticipated. This apparent requirement is of particular interest as this abundant lithology occupies no unique position in the lithologic spectrum of the suite: i.e., whereas other Stokes Mountain lithologies are easily positioned in order of relative degree of evolution away from the parental magma (similar to the order of units in the Explanation, Fig. 2.2), the hornblende gabbro does not appear to fit simply into this linear progression. These results bear some similarity to proposals concerning fractionation of gabbros from the Peninsular Ranges. Fractionation of plagioclase, olivine and clinopyroxene from a high alumina basalt, followed by the fractionation of plagioclase, orthopyroxene and opaques, is thought to have generated an amphibole gabbro series similar to that described in this study (Walawender and Smith, 1980).

In order to evaluate the curve fitting method used to generate the Start A composition, the process was repeated to generate a magma with 49% SiO_2 as a parental magma for the WKB suite. The composition generated is essentially a high alumina basalt. Whether or not this calculated parental magma is primary or not cannot be determined presently, but there is a great possibility that significant olivine and/or plagioclase fractionation occurred prior to generation of the exposed suite. For example, the most forsteritic WKB olivine analyzed (Fo_{78}) is substantially less Mg-rich than olivines in equilibrium with the mantle (approximately Fo_{89-91}); this suggests that the primary magma had evolved some degree by fractional crystallization prior to formation of the WKB suite.

Certainly many adjustments of the proportions of crystallizing phases are possible which might improve the fits to the observed geochemical trends. Before attempting this, however, it would be more appropriate to analyze the input variables used in the model. First, the mineral compositions used were based on a limited number of analyses; a better knowledge of the compositional variation of the crystallizing phases should be gained

before refining the model. Second, independent estimates of the conditions of fractionation (e.g., P, T, fO2, fH_2O) should be obtained. Since the fractionation program treats all iron as FeO, the Fe-Mg K_D-values should be taken from experiments at oxygen fugacities similar to those calculated for the rock suite which may, in fact, differ from the modeled QFM conditions. For example, if the crystallization environment were more oxidizing than QFM, more iron would have occurred as Fe_2O_3 which, after conversion to FeO for the purpose of modeling, would increase the calculated MgO contents. Alternatively, an increased fH_2O would increase the An-content of the fractionating plagioclase which would decrease the need to fractionate abundant sphene; this would, in turn, affect the modeled TiO_2 contents. Furthermore, the actual distribution coefficients at QFM conditions may vary up to $\pm$ 20% of the values used (M. B. Baker, personal communication), so careful consideration of the crystallization conditions might result in a more appropriate selection of the K_Ds. Third, once the above adjustments were performed, inclusion of other phases such as magnetite and apatite might improve the application of the model. Given these complex factors, it was deemed more appropriate to await the rare earth element analyses before proceeding with additional refinement of the geochemical model; such analyses are currently being performed by Dr. B. W. Chappell on 14 WKB samples.

At present, it appears safe to conclude that invoking fractional crystallization as the dominant the process responsible for the production of the smooth geochemical variation in the WKB suite is consistent with the existing data. The possibility that magma mixing may have generated some of the geochemical trends has not been quantitatively evaluated; field observations discussed in section 2.2.5, however, suggest that complete mixing was not efficient at the present level of exposure. This observation does not preclude the possibility that significant mixing occurred at deeper levels.

3.3. Isotope Systematics of the Stokes Mountain Region

Oxygen, strontium and neodymium isotopic analyses were performed in order to investigate a number of petrogenetic aspects of the early Cretaceous batholith. First we wished to investigate the appropriateness of the fractional crystallization scenario suggested by the geochemical data. In addition, given DePaolo's (1981) study of the Sierra Nevada batholith, the possibility of assimilation needed to be evaluated. It was hoped that detailed isotopic analysis could refine the characterization of the parental magma for this part of the batholith due to the unusually mafic composition of the units and the location of the Stokes Mountain region on the extreme western edge of the batholith where assimilation is estimated as being minimal [< 15%; (DePaolo et al., 1991)]. Finally, given the identification of two ring complexes, the possibility of hydrothermal alteration needed to be addressed.

The isotopic investigation revealed unexpected complexities in the Stokes Mountain region. Fractional crystallization was confirmed as being the dominant process of magmatic fractionation, while two spatially and isotopically distinct assimilants were identified. Large scale hydrothermal alteration was surprisingly absent in the ring complexes, but the oxygen isotope systematics of stoped blocks of hypabyssal material indicated that hydrothermal cells were active in the overlying carapace during emplacement of the ring complexes. Finally, the combined stable and isotopic systematics suggest the presence of two isotopically distinct parental magmas each of which fed a single ring complex. Understanding why two coeval and adjacent magmatic centers should have distinct isotopic signatures should provide insight into the evolutionary details of the western Cretaceous batholith.

3.3.1. Analytical Techniques for $\delta^{18}O$ Analysis

Whole rock sample preparation for the WKB samples is discussed in section 3.1. Mineralogically representative pieces of five additional samples which were analyzed for

$\delta^{18}O$ alone were crushed with hammer and steel plate and powdered in a tungsten carbide shatterbox. Mineral separates for $\delta^{18}O$ analysis were also prepared with hammer and steel plate; after removal of magnetite, mineral separation was performed by handpicking and separates were ground in a tungsten carbide mortar and pestle. Purity of these separates is estimated at greater than 96% based on visual inspection and calculated oxygen yields.

Typical sample size was 20 - 30 mg except for mineral separates which were occasionally as small as 15 mg. Oxygen extraction was accomplished with F_2 (g) following the method of Taylor and Epstein (1962a) which is described in detail in Solomon (1989). Standard apparatus was employed with the exception of the O_2-to-CO_2 converter: experimentation with a new design by Dr. J. R. O'Neil (U. Michigan) in which the carbon rod does not carry the electric current was found to be particularly stable.

Mass spectrometry was accomplished on a McKinney-Nier 60° sector double-collecting mass spectrometer; the majority of analyses were performed by Joop Goris of Caltech. CO_2 sample gas was analyzed relative to CO_2 liberated from a working standard of Harding Iceland Spar. The analyses generated were corrected relative to Standard Mean Ocean Water (SMOW) by use of the following equation:

$$\delta^{18}O_{SMOW} = (\delta^{18}O_{sample} - \delta^{18}O_{RQS})\{[1+(background/2520)](1.02354) + 8.45)$$

A 2σ error of $\pm 0.15‰$ was determined on the Caltech Rose Quartz standard of which one alloquot was analyzed with each set of samples. This standard has an accepted value of 9.60‰ relative to the NBS-28 standard. Over the two year period the average analyzed $\delta^{18}O_{RQS}$ for any given 3 to 4 month period varied between -13.2 and -13.5‰ relative to Harding Iceland Spar due to long term variations in the stability of the mass spectrometer which was subject to common maintenance. Variation of $\delta^{18}O_{RQS}$ between periods of maintenance was generally acceptable ($\pm 0.2‰$). Samples accompanying standards for which the yield or $\delta^{18}O$ was suspect were repeated, generally with consistent results.

3.3.2. Analytical Techniques for Rb-Sr and Sm-Nd Analysis

Details of the procedures used for the analysis of the Rb-Sr and Sm-Nd data are described in Appendix A of Dr. D. A. Pickett's 1991 Caltech doctorate thesis (cowritten by Pickett and Clemens Knott); only a brief outline of the procedure is included here. Spikes of ^{87}Rb, ^{84}Sr and mixed ^{147}Sm-^{150}Nd tracer solutions were added to the 100-300 mg powdered samples (section 3.3.1) prior to dissolution. Dissolution treatments of warm HF + HNO_3 were followed by HNO_3 and finally HCl; near complete evaporation of the mixture was attained prior to each subsequent acid treatment. Complete dissolution was checked by centrifuging the final HCl mixture; any residue was separated and treated with a similar dissolution procedure. Due to difficulties experienced when dissolving some highly siliceous samples, an alternate dissolution treatment was subsequently attempted: this treatment consisted of room temperature treatments of HF and $HClO_4$ followed by dissolution in HCl. Elution of Rb and Sr was accomplished in cation columns filled with AG50W-X8 resin; elution of the Sm and Nd was accomplished under pressure in columns filled with AG50W-X4 resin using 0.21 M 2-methyllactic acid. Maximum procedural blanks determined by Dr. Pickett were 12 pg Rb, 220 pg Sr, 7 pg Sm and 19 pg Nd.

Samples were analyzed on an automated VG Sector multicollector mass spectrometer. Rb and Sm analyses were generally measured in a static mode during collection of 100 ratios using two (masses 85 and 87) and four (masses 147, 148, 149 and 152) collectors respectively. 105 to 150 Sr isotopic ratios were measured using four collectors and a peak-switching, or multidynamic, routine. Rb interference was monitored by measuring mass 85. 105 to 150 Nd isotopic ratios were measured using five collectors in a multidynamic routine. Sm interference was monitored by measuring mass 147; correction for the ^{147}Sm spike concentration was accomplished offline. An offline program was used to correct the grand means of the significant isotopic ratios: this

program adjusts for the spike contributions to the isotopic ratios as well as the fractionation correction, and calculates the concentrations with appropriate isotope dilution equations.

The results of all standards analyzed during this and Pickett's study are tabulated in Appendix 2 of his thesis. The standards used and their measured ratios and 2σ errors are as follows (additional ratios listed in Pickett's Table 3.2): 984 Rb ($^{85}Rb/^{87}Rb = 2.6163 \pm 19$); 987 Sr ($^{87}Sr/^{86}Sr = 0.710244 \pm 5$); nSmβ ($^{148}Sm/^{147}Sm = 0.74964 \pm 19$); La Jolla Nd ($^{143}Nd/^{144}Nd = 0.511853 \pm 3$). External reproducibility for $^{87}Sr/^{86}Sr$ is estimated at ± 0.000018 (25 ppm) while that for $^{143}Nd/^{144}Nd$ is ± 0.000015 (30 ppm). The first sample analyzed, WKB94, was spiked, dissolved and eluted twice due to poor mass spectrometric behavior of Rb from the first elution. The difference between the calculated Sr_i for the first sample (0.703567) and the calculated Sr_i for the second sample (0.703545) is 0.000022; before age correction the difference in $^{87}Sr/^{86}Sr$ is 0.000015. The age corrected difference is only slightly greater than the estimated external reproducibility for the $^{87}Sr/^{86}Sr$ ratio which is reassuring as the Rb analysis produced from the first sample was marginal.

Samples not located in the mapped area but from the early Cretaceous batholith within the Greater Stokes Mountain region were analyzed for $\delta^{18}O$ by Dr. Catherine Allen Manduca of Carleton College while she was a graduate student at Caltech. Permission to include her data in this study is greatly appreciated. Dr. David Pickett of Los Alamos National Laboratory provided Sr and Nd analyses of two samples from the study area and a third early Cretaceous sample from south of the study area. The data of these researchers is identified in Tables 3.5, 3.6 and 3.7. All other isotopic analyses were performed by the author.

3.3.3. Stokes Mountain Region: The Complete Data Set

The stable and radiogenic isotope data will first be evaluated as a single suite in a manner similar to the whole rock geochemistry. In section 3.3.4. the samples are divided

geographically into those from the WRC and Colvin Mountain areas and a second group of samples collected from the ERC. Despite the regular behavior displayed by the data set as a whole, these geographic subsuites have surprisingly distinct isotopic characteristics.

3.3.3.1. Oxygen Isotope Systematics

Oxygen isotope data can lend useful insight into the formation of igneous rocks, particularly when analyzed in conjunction with radiogenic isotopes. In this particular study it was hypothesized that the stable isotopes would help identify any possible hydrothermal alteration of the suite which might potentially affect the radioisotopic systems. Alteration might be expected in shallow crustal ring complexes as volcanos commonly develop hydrothermal circulation systems. If alteration was minimal, the oxygen isotopes would also help quantify the amount of crustal material, if any, which had been assimilated by the suite.

3.3.3.1.1. Mineral Separates

Mineral separates from four representative plutonic samples were prepared and analyzed in order to evaluate the possibility post-crystallization isotopic disturbance. Such disturbance would be evidenced by non-igneous values of $\Delta_{plag\text{-}mafic}$ which are typically negative due to the fact that $\delta^{18}O_{plagioclase}$ is preferentially lowered by hydrothermal alteration. In the absence of negative or "reversed" values, the mineral pair data provides an estimate of the temperature at which sub-solidus isotopic exchange ceased; this temperature represents a minimum estimate of the temperature of crystallization.

The data are recorded in Table 3.3. All $\Delta_{plag\text{-}mafic}$ values are within the range predicted for undisturbed igneous rocks. This result validates the use of whole rock values for modeling magmatic processes. Furthermore these data provide minimum crystallization temperature estimates of 683 - 820°C (Bottinga and Javoy, 1975). The lower two temperature estimates of 683 and 716°C most likely have been slightly lowered by subsolidus exchange between the plagioclase and hornblende or pyroxene, respectively.

3.3.1.1.2. Whole Rock Samples

Whole rock $\delta^{18}O$ values of samples from the Greater Stokes Mountain region are plotted against SiO_2 in Figure 3.10. The majority of the data points form a tight, near horizontal trend ranging from 6.5 - 7‰ below 60% SiO_2. Plotted for comparison are analyses of three metamorphic rocks from the Stokes Mountain region. Assimilation of such material would produce an excursion of the plutonic data to heavier values of $\delta^{18}O$. Minimal increase of $\delta^{18}O$ occurs with increasing SiO_2 above 60% (ex. WKB106) suggestive of limited amounts of crustal assimilation in the more evolved lithologies.

Three data points do not fall in the trend in Figure 3.10, having instead distinctively lighter $\delta^{18}O$ values. These samples come from the large xenoliths of hypabyssal material (unit Kp) which crystallized at near-surface depths most likely within the volcanic carapace overlying the ring dike complex. The intense silicification of these xenoliths described in section 2.1.11 as well as the stable isotopic alteration are believed to have occurred during hydrothermal alteration of the volcanic cover. As the enclosing tonalite (sample SM198) has a normal igneous $\delta^{18}O$ value of 7.1‰, the $\delta^{18}O$ of the xenoliths must have been lowered prior to stoping. The apparent age of the xenoliths (120 Ma; section 2.3) is equivalent to the enclosing ring complex (120-116 Ma) indicating that volcanism and hydrothermal activity were near-synchronous with emplacement of the Stokes Mountain plutonic suite.

The $\delta^{18}O$ analyses of apparently unaltered igneous samples are plotted on Figure 3.11. The triangular area encloses values which could be produced by fractional crystallization alone and is defined by a maximum increase of $\delta^{18}O$ of 0.5‰ per 10% SiO_2 (Blattner et al., 1989). This rate of increase is probably much greater than is realistic in a system fractionating both plagioclase and mafic phases as such fractionation would be predicted to produce little if any increase in the $\delta^{18}O$ of the differentiated magma. Using this generous estimate, however, most of the data could be explained by simple fractional

crystallization if the parental magma(s) varied in composition from 6.5 - 7‰. One exception to this is sample WKB106 which is a garnet muscovite leucogranite. The mineralogy of the leucogranite is in itself suggestive of assimilation of aluminous material, and its heavy $\delta^{18}O$ signature corroborates this interpretation. Given the documentation of assimilation in sample WKB106 the preferred interpretation of the complete data set is that some small degree of assimilation of a high $\delta^{18}O$ material affected many of the samples with $\delta^{18}O$ greater than 7.5‰. Small degrees of assimilation will be convincingly demonstrated in section 3.3.4.2 by the combined use of oxygen and strontium isotopic data.

The isotopically heavy values of samples WKB126 and WKB98, which are quenched samples from a dike and an enclave respectively, are more difficult to interpret. These analyses could be used to propose the presence of high $\delta^{18}O$ mafic magma, but the possibility of subsequent alteration or subsolidus reequilibration of these fine-grained samples is great. This is particularly true of sample WKB98 which is an enclave located within an isotopically heavier granodiorite. Unfortunately the grain size of this sample precludes the preparation of mineral separates which might be analyzed in order to assess the possibility of high $\delta^{18}O$ magma. The possibility of disturbance of sample WKB126 is more questionable in that this cross cutting dike intruded mafic and presumably low $\delta^{18}O$ material. WKB126 is a hornblende troctolite in which the acicular hornblende is aligned parallel to the dike margins. This is an unusual sample as it is structurally late but mineralogically primitive. Its high $\delta^{18}O$ suggests that late stage mafic material may have assimilated a larger proportion of the previously heated wall rock material than the early intrusions of mafic magma which penetrated relatively cool crust. That samples WKB 126 and WKB106, the garnet muscovite leucogranite, were collected within 0.4 km of one another suggests that crustal melting and assimilation may have been highest in late stage

magmas emplaced into the NW extremity of the study area. This area corresponds to the hypothesized center of the WRC.

3.3.3.2. Strontium and Neodymium Isotope Systematics of the Stokes Mountain Suite

Radioisotopic data for the Stokes Mountain region is displayed on a plot of $Sr_{(115)}$ versus $\varepsilon_{Nd(115)}$ (Fig. 3.12). The majority of the samples cluster near the mantle array: a single sample (WKB109) plots on the mantle array while most are shifted to greater values of $Sr_{(115)}$. This relationship indicates a depleted mantle source for the parental magma(s) of the Stokes Mountain suite with an approximate end member signature of $Sr_{(115)}$ = 0.70338 and $\varepsilon_{Nd(115)}$ = 5.7. As higher values of $\varepsilon_{Nd(115)}$ were obtained for samples WKB 107 (+5.9) and WKB94 (+6.1), it is possible that a parental magma existed with a more primitive radioisotope signature. The possibility that the source(s) may have disturbed $Sr_{(115)}$ values is suggested by the spread of $Sr_{(115)}$ away from the mantle array displayed by the high $\varepsilon_{Nd(115)}$ samples. The possibility of source contamination will be further discussed in section 3.3.4.2.

The spread of $Sr_{(115)}$ parallel to the mantle array may indicate varying degrees of crustal assimilation in a manner similar to that discussed above for sample WKB106, the garnet muscovite leucogranite. On this plot mixing curves with a metapelitic contaminant form hyperbolic arrays similar to that approximated by the arrows. The shift parallel to the mantle array is best demonstrated by WKB65, a sample of a small pluton which apparently experienced moderate contamination as it was emplaced south of the study area into continental material.

The presence of a significant crustal component in sample WKB106 is confirmed in Figure 3.13. On graphs of X vs. 1/X, where X is any element or isotopic ratio, mixing hyperbolas transform to straight lines. In this figure, continental assimilation is represented by the simple mixing line between a parental magma with a strontium concentration of 500 ppm (DeBari and Sleep, 1991) and a field of metasediment analyses from DePaolo (1981)

(not shown). A mixing line could be drawn between the metapelite analyzed in this study (WKB118) and a parental magma having a strontium concentration of 830 ppm which would pass through the leucogranite, but this strontium concentration is unreasonably high for a mantle-derived melt. Also apparent on this plot is that the strontium systematics of sample WKB85, a plagioclase-rich troctolite, is dominated by plagioclase accumulation while the strontium systematics of the remainder of the suite can be explained by plagioclase fractionation with low degree of crustal assimilation (Taylor and Sheppard, 1986).

3.3.3.3. Summary of the Isotopic Systematics of the Complete WKB Suite

Considering the isotope systematics of the Stokes Mountain region a number of conclusions can be drawn. Isotopic characteristics of the parental magma(s) for the early Cretaceous batholith indicate derivation from a depleted mantle source. The best estimate for the end member is $Sr_{(115)} = 0.70338$ and $\varepsilon_{Nd(115)} = +5.7 - 6.1$, but there are some inconsistencies which suggest that some process may have shifted these values away from the mantle array. Assimilation of crustal metapelitic material is readily evident in the systematics of the garnet muscovite leucogranite. Assimilation may also account for some of the spread of the data parallel to the mantle array seen in Figure 3.12 as well as some of the increase in $\delta^{18}O$ with SiO_2 recognized in the larger data set (Fig. 3.11). Disturbance of $\delta^{18}O$ from igneous values is only recognized in the hypabyssal xenoliths (unit Kp) and is interpreted as resulting from hydrothermal alteration of the overlying volcanic carapace prior to stoping by magmas of the underlying ring complexes. In addition to the possible source contamination, variation in strontium systematics is the result of combined plagioclase fractionation and crustal assimilation.

3.3.4. Contrasting Isotopic Systematics of the WRC and ERC

During routine preparation of isotope contour maps for the study area, definite geographic patterns were recognized. Specifically, it became apparent that samples from

the two ring complexes displayed minor but systematic differences from one another. In order to explore the possibility that the two coeval magmatic centers had distinct isotopic characteristics, the Stokes Mountain data has been subdivided based on location relative to the WRC and ERC. The isotopic contour maps, shown in Figures 3.19 and 3.20, will be discussed at the end of this section.

In the following figures the data has been divided into a maximum of seven subsets. The major division is between the three samples from the WRC (WKB7, WKB75, WKB77) and six samples from the central and eastern ERC (WKB23, WKB94, WKB105, WKB107, WKB109, WKB127). During the initial stages of this analysis it was recognized that four samples (WKB86, WKB87, WKB92, WKB128) from the western edge of the ERC were isotopically akin to the WRC, so these were subdivided from both the WRC and ERC. Due to alluvial cover, four samples from and west of Colvin Mountain (WKB53, WKB85, WKB90, WKB91) display no clear cut relationship to either of the ring complexes, so have been grouped into their own set. As in section 3.3.3, the garnet muscovite leucogranite and metapelite samples have been individually identified. Finally, one sample of a hornblende gabbro enclave collected from a mingling zone in the southern ERC (WKB80) is identified with its own symbol.

3.3.4.1. Strontium and Neodymium Isotope Systematics

Perhaps the clearest distinction between the subsets exists in Sr_i vs. 1/Sr space. Comparing Figures 3.13 and 3.14 it is apparent that the Sr_i values of the majority of the ERC samples are approximately 0.00034 lower at a given Sr concentration than the Sr_i values of the WRC samples. Two trends have been identified: the eastern trend is defined by five of the six ERC samples; the western trend encompasses the WRC, western ERC and Colvin Mountain samples. Silica contents generally increase towards lower Sr concentrations along both trends. The fact that both trends are parallel indicates that plagioclase fractionation and minor assimilation of a high Sr_i material similarly controlled

the Sr evolution in both subsets. The only difference between the two trends is the Sr_i of the "parental" magmas, the eastern trend having an Sr_i of 0.70333 compared to the western Sr_i of 0.70367. For convenience, both Sr_i values have been estimated at an Sr concentration of 500 ppm similar to the best estimate for an Aleutian island arc primary magma (DeBari and Sleep, 1991); slightly higher Sr_i estimates result if larger initial Sr concentrations of the parental melts are considered appropriate.

Two samples from the ERC fall on the western trend: sample WKB127, collected from the major Kgd dike visible in Figure 2.4, and the gabbro enclave (WKB80). Based on lithologic similarities, WKB127 would have been predicted to have approximately the same signature as WKB23. Interestingly, the two samples reverse behavior on Figure 3.15 in which WKB23 falls along the western trend and WKB127 plots on the eastern trend. Evidently the Sr and Nd systematics of these lithologically and geographically similar samples have become decoupled. While further discussion is best left until all isotopic data is reviewed, it is appropriate to note that this deviant behavior only affects the most siliceous samples of which there are no equivalents in the WRC subset. The ERC enclave lies along the western trend, displaying a shift towards higher Sr_i in a manner similar to WKB127.

The $^{147}Sm/^{144}Nd$ ratio is plotted against $\varepsilon_{Nd(115)}$ on Figure 3.15. Pure fractional crystallization should produce horizontal trends moving from right to left across the figure as fractionation progresses. As in Figure 3.14, the eastern and western trends can be distinguished; at high values of $^{147}Sm/^{144}Nd$ the trends differ by approximately 1.0 epsilon unit (the difference between samples WKB94 and WKB75). Both trends would be approximately horizontal if only the high $^{147}Sm/^{144}Nd$ samples were used; the scatter towards lower values of $\varepsilon_{Nd(115)}$ is great at lower values of $^{147}Sm/^{144}Nd$ for more siliceous lithologies. This scatter may be due to limited interaction with low $\varepsilon_{Nd(115)}$ crustal

material as is evident in the garnet leucogranite. As in Figure 3.14, the ERC enclave falls along the western trend.

This analysis is extended to Sr_i - $\varepsilon_{Nd(115)}$ space in Figure 3.16. As would be predicted from the above discussion, the eastern and western groups form distinct fields, although the Kgd samples (WKB127 and WKB23) and the ERC enclave overlap the western field. In each set, shift parallel to the mantle array affects the more siliceous lithologies (WKB23 and WKB127 in the eastern group and WKB86 in the western group). As discussed in section 3.3.3.2, shift parallel to the mantle array is probably produced by limited assimilation of crustal material; appropriately the most fractionated samples display the greatest proportion of assimilant.

Perhaps the most interesting feature is the apparent shift towards higher Sr_i displayed by the mafic eastern samples with little apparent change in $\varepsilon_{Nd(115)}$. A total shift of 0.00011 occurs between samples WKB109 (unit Khtr) and WKB105 (unit Khbt) which have nearly identical $\varepsilon_{Nd(115)}$ signatures (5.7 and 5.6 respectively). Unfortunately it is impossible to determine whether the shift is purely in a horizontal direction. One possibility is that the relatively siliceous WKB105 represents a shift parallel to the mantle array from a parental magma having an even higher value of $\varepsilon_{Nd(115)}$ than WKB109. This possibility would indicate significant mantle heterogeneity within the source region of the ERC which would appear to contradict the isotopic cohesiveness of the ERC suite displayed in Figures 3.14 and 3.15. Alternatively, the shift within the ERC indicates a decoupling of the Nd and Sr systematics, such that primarily the Sr signature was affected. Due to the high partitioning of Sr into fluid phases, this shift could result from water-rock interaction with a high Sr_i fluid, such as ocean water, or heterogeneity of both Sr concentration and Sr_i in the assimilants.

A similar apparent shift is also seen if samples WKB109 and WKB85 of the eastern and western fields are compared, the western field displaying a shift to 0.00038 higher

values of Sr_i with no change in $\varepsilon_{Nd(115)}$. As has been demonstrated in Figures 3.14 and 3.15 this difference is displayed by the parental magmas of both suites and therefore is indicative of source region heterogeneity. It is unlikely that the western parental magma acquired its more radiogenic signature through crustal assimilation as it is the least evolved, ultramafic cumulates from Colvin Mountain which display these signatures. The western ERC samples define a slight shift parallel to the mantle array while the remaining western samples (those of the WRC and Colvin Mountain area) form a relatively tight grouping.

Consideration of the Sr and Nd isotope systematics of the western and eastern samples identifies the operation of a minimum of two distinct processes. First, the isotopic distinction between parental magmas and the parallel evolution of the two suites indicates heterogeneity within the source region of the ring complexes. The geochronologic and structural data which document the coeval nature of the ring complexes leads to the conclusion that the adjacent magma plumbing systems simultaneously tapped isotopically distinct sources in the depleted mantle. Second, the shift parallel to the mantle array, best demonstrated by the siliceous ERC and the western ERC samples, is attributed to assimilation of high Sr_i, low $\varepsilon_{Nd(115)}$ material. A similar shift is displayed in Figure 3.12 by the garnet muscovite leucogranite. Finally, the cause of shift towards higher Sr_i with little apparent shift in the $\varepsilon_{Nd(115)}$ values seen within the two subsets is unconstrained.

3.3.4.2. Combined Stable and Radiogenic Isotope Systematics

As will be demonstrated in Chapter 5, the combined analysis of stable and radiogenic isotopes can be a powerful tool for the elucidation of igneous processes particularly in suites for which interaction between mantle and crustal material is significant. Limited crustal assimilation has been demonstrated previously by use of either oxygen or strontium isotopes in the Stokes Mountain suite. In Figure 3.17, the combined use of these isotopes also clearly identifies the garnet muscovite leucogranite as containing a significant component of crustal metapelitic material. On this and the following figure the

arrows labeled "source contamination" and "crustal contamination" are actually segments of complementary simple mixing hyperbolas which curve around and join with the modeled high $\delta^{18}O$, high Sr_i contaminant. Crustal contamination displays a concave upward geometry while source contamination displays a concave downward geometry. Use of this figure is discussed in detail in Taylor (1986).

Simple mixing between crust and mantle melts produces a concave upward hyperbola because the Sr concentration of mantle-derived melts exceeds that of most crustal materials: a large proportion of crustal contaminant must be added before the Sr_i of the mantle melt is significantly altered. Mixing therefore, will first be evident in the oxygen isotopes as oxygen has a comparable concentration in all rocks. Source contamination refers to contamination of the mantle wedge overlying the subduction zone by melt or fluid derived from the subducted slab; potentially similar effects could be produced by melting of slab material tectonically injected into the mantle wedge prior to melting of the solid mixture. Source contamination will produce a convex downward hyperbola because the Sr concentration of the mantle wedge is much lower (ex. 25 ppm) than any slab-derived material (ex. 500 ppm) which should be enriched in incompatible elements. Source contamination will produce a modified mantle in which the Sr_i is dominated by the Sr_i of the slab-derived material. The Sr_i of the of the slab-derived material is certain to be greater than that of the depleted mantle due to inclusion of sediments and basalts that have experienced low temperature hydrothermal alteration with seawater. In contrast, as the oxygen concentrations are comparable in both mantle wedge and contaminant, the $\delta^{18}O$ of the modified mantle will not vary significantly until large proportions of contaminant have been introduced. Any melt of this modified mantle will thus have elevated Sr_i values but relatively unaltered $\delta^{18}O$ values, and such melts will define a concave downward hyperbola.

This type of plot may reveal some of the causes for the differences between the ERC and WRC subsets; in order to investigate this possibility a similar plot is shown on Figure 3.18 in which the leucogranite and metapelite samples are not included. On this figure the eastern trend defines a shift attributable to crustal contamination. This agrees with observations from both the Sr and Nd systematics (sections 3.3.4.1). The western subset, however, is offset from eastern subset in the direction of source contamination. It would be an exaggeration to claim that the western samples defined a trend parallel to the source contamination hyperbola as the isotopic variation within western group is small, particularly if the western ERC samples are excluded. But the distinction in Sr_i values between parental magmas of the western and eastern subsets which was noted previously in the plots of 1/Sr vs. Sr_i (Figs. 3.13 and 3.14) may now possibly be attributed to contamination of the mantle wedge. If source contamination is indeed the cause, then this contamination also lowered the $\varepsilon_{Nd(115)}$ of the western parental magma (Fig. 3.15). Although behavior during melting and hydrothermal alteration of the rare earth elements is less well understood compared to strontium, melts of amphibole and/or continentally-derived material should be enriched in Nd and thus dominate the $\varepsilon_{Nd(115)}$ of the modified mantle. Low $\varepsilon_{Nd(115)}$ signatures could not, however, be derived from altered ophiolitic material (McCulloch et al, 1981) suggesting the need of a continentally-derived Nd in the source contaminant.

The field defined by the western samples may reflect melting of a variously contaminated source region: samples with higher Sr_i values being produced by melting of a more extensively contaminated source. Such a variably contaminated source region might have been produced either by variable interaction with subduction-related fluids or by the tectonic interleaving of Kings-Kaweah ophiolitic material into the forearc wedge. This ophiolitic material might be expected to have a heterogeneous strontium isotope signature as a result of its complex history of seafloor hydrothermal alteration, emplacement

metamorphism and residence in the forearc wedge above the the dehydrating slab. There are a few observations, however, which suggest that this variation is not the result of source contamination. First, the coincidence of the geophysical anomalies with the WRC (section 2.5.1) suggests that a large volume of mafic magma was emplaced at shallow depths; fractionation must have occurred subsequently. The possibility of having isotopically distinct parental magmas fractionating in a parallel fashion and being emplaced into a single ring complex while preserving their isotopic heterogeneity seems improbable. Second, the increase in Sr_i and the decrease in $\varepsilon_{Nd(115)}$ displayed by the western subset in Figures 3.14 and 3.15 was positively correlated with silica content or increasing degree of fractionation. If the variation among western samples displayed in Figure 3.18 was simply due to differing proportions of contaminant then there should be no correlation with silica unless the source region variability was the result of a pre-melting, tectonically-produced chemical, as well as isotopic, heterogeneity.

The increase in Sr_i with increasing 1/Sr for the western subset was previously attributed to assimilation of a high Sr_i material, but the absence of an increase in the $\delta^{18}O$ indicates that any contaminant assimilated by the western samples was isotopically distinct from that assimilated by the eastern subset. The latter assimilant has the characteristics of typical continental crust or crustally derived sediments: high Sr_i, low $\varepsilon_{Nd(115)}$ and high $\delta^{18}O$. In order to produce the observed trends on Figures 3.14, 3.15 and 3.18, the western contaminant must have had high Sr_i, high to low $\varepsilon_{Nd(115)}$ and low (i.e., normal igneous $\approx$ 7‰) $\delta^{18}O$ signatures. One possible candidate for the western contaminant is a melt of hydrothermally altered basalt or gabbro from the Kings-Kaweah ophiolite. Melts of hydrothermally altered slab material would have $\varepsilon_{Nd(115)}$ values comparable to mantle-derived basalts or lower if any sedimentary material was incorporated. Hydrothermal alteration of sea floor basalts and ophiolitic gabbros would produce elevated values of Sr_i, and normal to low values of $\delta^{18}O$ (McCulloch et al., 1981). As described in section

2.1.12, regional geologic relationships suggest that a contact separating ophiolitic material on the west from a large wedge of continentally derived metasediments on the east projects into the study area near the boundary between the WRC and ERC. This observation helps justify invoking two isotopically distinct contaminants for each of the two coeval ring complexes.

In summary, the relationships on Figure 3.18 suggest that the distinction between the apparent radioisotopic compositions of the parental magmas for the two ring complexes may have resulted from the contamination of the mantle wedge source region of the WRC magmas. The variation of Sr_i within the western subset may result from varying degrees of partial melt of this modified source region; alternatively, the Sr_i variation within the western subset is in fact due to assimilation of a high Sr_i , low $\delta^{18}O$ material. This possibility is geologically reasonable given the distribution of metamorphic lithologies relative to the WRC and ERC boundaries.

In the above discussion it has been recognized that the western ERC samples group with the WRC samples. The cause for this overlap is presently uncertain, but may result from the combination of two factors. First, textural relations preserved in the Stone Corral Shear Zone (section 2.4.4) indicate that magmas from each of the two ring complexes mingled extensively along this boundary. It is therefore possible that magmas from the western suite were injected into the western edge of the Eastern Ring Complex. One sample in particular, WKB128, bears strong lithologic resemblance to the mafic lithologies of the WRC. Second, it is quite possible that the proposed boundary separating continental from ophiolitic material does not actually coincide with the SCSZ, but instead traverses across the western edge of the ERC. If this geometry is correct, then isotopic variation within the western ERC samples could result from interaction with the proposed western ophiolitic assimilant.

The isotopic behavior of the ERC enclave, which has a $\delta^{18}O$ signature like eastern subset and Sr_i and $\varepsilon_{Nd(115)}$ signatures like western subset, is difficult to understand. One possibility is that this very fine-grained enclave represents magma derived from the western source which equilibrated with the $\delta^{18}O$ signature of its ERC tonalite host after mingling. This enclave was collected only 3 km due east of Colvin Mountain, so the possibility that it represents magma akin to the western source region is as probable as this possibility is for the western ERC samples. Little significance is placed on this very fine-grain sample due to the possibility that the isotopic signature has been shifted by subsolidus processes.

As mentioned previously, motivation for proposing the geographic division of the Stokes Mountain samples was based upon the patterns displayed by isotopic contours. Contours of Sr_i and $\varepsilon_{Nd(115)}$ are displayed on Figures 3.19 and 3.20, respectively. The contours are based on only 18 samples: the metapelite (WKB118), the garnet muscovite leucogranite (WKB106), the crosscutting hornblende gabbro dike (WKB79) and the single sample from outside the Stokes Mountain region (WKB65) have been excluded. Due to the small number of samples in this large area, the exact location of the contours should be suspect. This is true particularly for the WRC: more extensive mapping and collecting is necessary before reasonably accurate contours can be drawn in the WRC.

Both the Sr_i and $\varepsilon_{Nd(115)}$ contours form a bulls eye pattern centered on the Red Mountain gabbro plug of the ERC. The exact centers differ slightly, but clearly the isotopic signatures of the central samples approximate the parental magma while the outer samples in the ring complex have more contaminated signatures. Part of the cause for this distinction is the fact that the outer samples tend to be more siliceous than the central samples: as AFC has been demonstrated as affecting the more evolved lithologies, the outer samples should bear more contaminated signatures. The bulls eye pattern does not appear to be, however, completely a function of lithologic distribution. It is possible that the outer samples experienced greater contamination because of their proximity to the

metamorphic rocks. Assuming that the central plug was not emplaced first, this gabbro would have been emplaced through a warmed conduit of cogenetic igneous material which would have shielded the gabbro from contamination, cooling and fractionation during ascent.

The possibility that the bulls eye pattern may be partially due to contamination during transit of the magma through the crust suggests the prediction that even with detailed sampling, no well defined bulls eye contours will be found in the WRC. The basis for this prediction is the geophysical data which has been interpreted as indicating that a large amount of mafic magma was emplaced at shallow crustal levels beneath the WRC. Fractionation and assimilation must have occurred at relatively shallow levels, and there would have been little transit distance separating the magma chamber from the ring complex. The absence of positive gravity and magnetic anomalies under the ERC indicates the absence of large amounts of mafic magma at shallow levels. Fractionation must have occurred deeper in the crust, so the variably fractionated magmas must have traveled a significant distance through the crust prior to emplacement in the ring complex.

No simple contour pattern is recognizable in the $\delta^{18}O$ data. This observation might have been predicted as there does not appear to be any significant difference in the $\delta^{18}O$ signature of the western and eastern parental magmas (Fig. 3.18).

3.3.4.3. Isotopic Summary

The variation of stable and radiogenic isotopic data from the Stokes Mountain suite is consistent with the geochemical modeling which indicates that fractional crystallization produced the majority of the lithologic heterogeneity. The detailed analysis of the isotopic data has identified the presence of two isotopically and spatially distinct parental magmas and possibly two, isotopically and spatially distinct assimilants.

The most primitive isotopic signatures recorded by the WRC and Colvin Mountain samples (the western parental magma) are $\varepsilon_{Nd(115)} = +5.7$, $Sr_i = 0.70372$ and $\delta^{18}O =$

6.7‰. A similar estimate for the eastern parental magma is $\varepsilon_{Nd(115)} = +6.1$, $Sr_i = 0.70338$ and $\delta^{18}O = 6.6$‰. If estimates are based upon extrapolation of the western and eastern trends to their most primitive ends (Figs. 3.14, 3.15, and 3.18) then the estimates vary slightly: western parental magma ($\varepsilon_{Nd(115)} = +5.1$, $Sr_i = 0.70367$ and $\delta^{18}O = 7.0$‰); eastern parental magma ($\varepsilon_{Nd(115)} = +6.1$, $Sr_i = 0.70333$ and $\delta^{18}O = 6.6$‰). Regardless of the method chosen, clearly the estimated western parental magma has isotopic signatures significantly different from the estimated eastern parental magma. The difference between these two end members is attributed to the variable contamination of the mantle wedge source region produced either by interaction with melts or fluids derived from the subducted slab or by melting of an isotopically heterogeneous source region which was produced by the tectonic interleaving of Kings-Kaweah ophiolitic material into the forearc wedge. While it is possible that source regions of both parental magmas experienced some contamination, the western source region definitely experienced a greater degree of modification by this process. As structural and geochronologic data demonstrate the coeval nature of the ring complexes (sections 2.3 and 2.4.5), the isotopic data indicates that the two isotopically distinct source regions were simultaneously tapped by adjacent magmatic plumbing systems.

The similarity of the western ERC samples to the WRC samples suggests that physical interaction between these isotopically distinct systems may have occurred during formation of the ring complexes. Other physical and/or chemical interaction between the two systems may have been limited because the depth of fractionation of the parental magmas appears to have differed: geophysical anomalies and presence of ultramafic megaxenoliths indicates that the western parental magma was emplaced at shallow crustal levels prior to undergoing substantial fractionation.

In addition to isotopically distinct parental magmas, the Sr_i and $\delta^{18}O$ indicates the presence of spatially distinct assimilants. The eastern subset displays trends explicable by

the assimilation of continental-derived sedimentary material; this material is recognized as being derived from an infold or thrust wedge of metasediments that was originally deposited on top of the Kings-Kaweah ophiolite. The limited isotopic variation within the western subset and samples from the western edge of the ERC may result from the assimilation of a high Sr_i, low $\delta^{18}O$ material; this material is believed to be melts of hydrothermally altered, ophiolitic material (sheeted dikes and high-level gabbros; McCulloch et al, 1981).

A rare sample of garnet muscovite leucogranite (WKB106) has an isotopic signature indicative of substantial mixing with aluminous, continentally-derived material. As few isotopic analyses were produced on samples from the northwestern corner of the mapped area the extent of rocks affected by high degrees of partial melting and assimilation of the metamorphic rocks is presently unclear. As this sample was collected near the approximate center of the WRC, it is possible that the ophiolitic wall rocks of the central and northern sections of the WRC contained an additional small wedge of continental material.

Hydrothermal activity associated with emplacement of the ring complexes and the hypothesized coeval volcanic activity was limited to the overlying hypabyssal-volcanic carapace of the ring complexes. Alteration is evidenced by stoped xenoliths of coeval, hypabyssal material bearing low $\delta^{18}O$ signatures. The low $\delta^{18}O$ signatures of these heavily silicified blocks indicate that the hydrothermal fluid was either meteoric or oceanic in origin.

3.4. Summary

The smooth geochemical and isotopic variations displayed by the Stokes Mountain suite were produced by the fractionation of plagioclase, two pyroxenes, hornblende, sphene, ilmenite and later biotite from a hydrous, high alumina basalt. The basalt, or its primary forbearer, was generated in the mantle wedge overlying the subduction zone.

Isotopic modification of the mantle source region by slab-derived material produced two isotopically and spatially distinct source regions which were partially melted during generation of the early Cretaceous batholith. Limited amounts of assimilation of two isotopically and spatially distinct contaminants affected these two parental magmas. Assimilation of ophiolitic material by the western parental magma possibly occurred during fractionation in the shallow crust. Assimilation of continentally-derived metasediments by the eastern magma occurred deeper in the crust and possibly during transit through the crust. Minor interaction between these isotopically distinct lineages may have occurred during the simultaneous intrusion of the two adjacent ring complexes.

Two general conclusions can be made concerning this study of the Stokes Mountain region. First, it has been demonstrated that during a limited time period (< 6 Ma) isotopically distinct parental magmas can form in the mantle, fractionate in the crust and be emplaced as adjacent plutons. This result indicates that care must be used in the interpretation of isotopic data collected on a regional scale within batholiths. Detailed mapping and sampling has the potential to reveal the presence of structures, such as the ring complexes, which fundamentally affect the interpretation of the isotopic data. Second, the layered ultramafic cumulates of Colvin Mountain preserve the least contaminated signatures of the western parental magma. This observation supports the first part of the hypothesis presented in Chapter 1: that ultramafic-mafic cumulates have the potential to record both the character of the material added to the crust and the effects of processes operative during the earliest stages of evolution of the mantle-derived magma. In this study the igneous processes of fractionation and assimilation are best studied by comparing the cumulates to the cogenetic noncumulate lithologies as the Stokes Mountain region cumulates represent only a small fractionation stage of the complete suite. In the following study of the Ivrea Zone it will be demonstrated that the cumulates of the Mafic Complex record both the initial character and the processes affecting the parental magma.

Future work in the Stokes Mountain region will focus on extending the mapping and sampling of the WRC. Better isotopic control is required on WRC and megaxenolith samples before the isotopic distinctions between the ERC and WRC can be completely understood. The isotopic identification of two parental magmas suggests the possible need to reexamine the geochemical data with regard to sample position relative to the Eastern and Western (?) Ring Complexes. The forthcoming trace element analyses should add insight into the proposed petrogenesis of the Stokes Mountain suite.

Sierra Nevada Bibliography

Ague, J. J. and G. H. Brimhall, 1988, Magmatic arc asymmetry and distribution of anomalous plutonic belts in the batholiths of California: effects of assimilation, crustal thickness, and depth of crystallization: Geological Society of America Bulletin, v. 100, p. 912-927.

Baker, M. C. W., 1974, Volcano spacing, fractures, and thickness of the lithosphere - A discussion: Earth and Planetary Science Letters, v. 23, p. 161-163.

Bateman, P. C., A. J. Busacca and W. N. Sawka, 1983, Cretaceous deformation in the western foothills of the Sierra Nevada, California: Geological Society of America Bulletin, v. 94, p. 30-42.

Bateman, P. C. and B. W. Chappell, 1979, Crystallization, fractionation and solidification of the Tuolumne Intrusive Series, Yosemite National Park, California: Geological Society of America Bulletin, v. 90, part I, p. 465-482.

Blake, D. H., R. W. D. Elwell, I. L. Gibson, R. R. Skelhorn and G. P. L. Walker, 1965, Some relationships resulting from the intimate association of acid and basic magmas: Quarterly Journal of the Geological Society of London, v. 121, p. 31-49.

Blattner, P., J. Cheng-wei and X. Yong, 1989, Oxygen Isotopes in Mantle Related and Geothermally Altered Magmatites of the Transhimalayan (Gangdese) Ranges: Contributions to Mineralogy and Petrology, v. 89, p. 438-446.

Bottinga, Y. and M. Javoy, 1975, Oxygen isotope partitioning among the minerals in igneous and metamorphic rocks: Reviews of Geophysics and Space Physics, v. 13, p. 401-418.

Bussell, M. A., 1988, Structure and petrogenesis of a mixed-magma ring dyke in the Peruvian Coastal Batholith: Eruptions from a zoned magma chamber: Transactions of the Royal Society of Edinburgh, v. 79, p. 87-104.

Bussell, M. A., W. S. Pitcher and P. A. Wilson, 1976, Ring complexes of the Peruvian Coastal Batholith: A long-standing subvolcanic regime: Canadian Journal of Earth Sciences, v. 13, p. 1020-1030.

Cady, J. W., 1975, Magnetic and gravity anomalies in the Great Valley and western Sierra Nevada Metamorphic Belt, California. Geological Society of America Special Paper no. 168.

Cantagrel, J.-M., J. Didier and A. Gourgaud, 1984, Magma mixing: Origin of intermediate rocks and "enclaves" from volcanism to plutonism: Physics of Planetary Interiors, v. 35, p. 63-76.

Carroll, M. R. and P. J. Wyllie, 1989, Experimental phase relations in the system tonalite-peridotite-H_2O at 15 kbar; Implications for assimilation and differentiation processes near the crust-mantle boundary: Journal of Petrology, v. 30, n. 6, p. 1351-1382.

Chase, C. G. and T. C. Wallace, 1986, Uplift of the Sierra Nevada of California: Geology, v. 14, p. 730-733.

Chen, Y. D., R. C. Price, A. J. R. White and B. W. Chappell, 1990, Mafic Inclusions from the Glenbog and Blue Gum Granite Suites, Southeastern Australia: Journal of Geophysical Research, v. 95, n. B11, p. 17757-17785.

Christensen, M. N., 1966, Late Cenozoic crustal movements in the Sierra Nevada of California: Geological Society of America Bulletin, v. 77, p. 163-182.

Crough, S. T. and G. A. Thompson, 1977, Upper mantle origin of Sierra Nevada uplift: Geology, v. 5, p. 396-399.

DeBari, S. M. and N. H. Sleep, 1991, High-Mg, low-Al bulk composition of the Talkeetna island arc, Alaska: Implications for primary magmas and the nature of arc crust: Geological Society of America Bulletin, v. 103, p. 37-47.

DePaolo, D. J., 1980, Trace element and isotopic effects of combined wallrock assimilation and fractional crystallization: Earth and Planetary Science Letters, v. 53, p. 189-202.

DePaolo, D. J., 1981, A neodymium and strontium isotopic study of the Mesozoic calc-alkaline granitic batholiths of the Sierra Nevada and Peninsular Ranges, California: Journal of Geophysical Research, v. 86, n. B11, p. 10470-10488.

DePaolo, D. J., P. Gromet, R. Powell and L. T. Silver, 1975, San Telmo ring complex, Peninsular Ranges Batholith, northwest Baja California, Mexico: Geological Society of America Abstracts with Programs, p. 309-310.

DePaolo, D. J., A. M. Linn and G. Schubert, 1991, The continental crust age distribution: Methods of determining mantle separation ages from Sm-Nd isotopic data and application to the southwestern United States: Journal of Geophysical Research, v. 96, n. B2, p. 2071-2088.

Dodge, F. C. W., 1971, Al_2SiO_2 minerals in rocks of the Sierra Nevada and Inyo Mountains, California: American Mineralogist, v. 56, p. 1443-1451.

Dodge, F. C. W. and P. C. Bateman, 1988, Nature and origin of the root of the Sierra Nevada: American Journal of Science, v. 288-A, p. 341-357.

Dodge, F. C. W., L. C. Calk and R. W. Kistler, 1986, Lower crustal xenoliths, Chinese Peak lava flow, central Sierra Nevada: Journal of Petrology, v. 27, n. 6, p. 1277-1304.

Dodge, F. C. W. and R. W. Kistler, 1990, Some additional observations on inclusions in the granitic rocks of the Sierra Nevada: Journal of Geophysical Research, v. 95, n. B11, p. 17841-17848.

Durrell, C., 1940, Metamorphism in the southern Sierra Nevada northeast of Visalia, California: California University Publications in the Geological Sciences, v. 25, p. 1-117.

Emerson, D. O., 1963, Orbicular and banded structures in diorite near Fisher Lake, Placer County, California: Geological Society of America Special Paper, v. 73, p. 38.

Foster, D. A. and D. W. Hyndman, 1990, Magma mixing and mingling between synplutonic mafic dikes and granite in the Idaho-Bitterroot Batholith in Anderson, J. L., ed., The Nature and Origin of Cordilleran Magmatism: Boulder, CO, Geological Society of America, p. 347-358.

Frost, T. P. and G. A. Mahood, 1987, Field, chemical, and physical constraints on mafic-felsic magma interaction in the Lamarck granodiorite, Sierra Nevada, California: Geological Society of America Bulletin, v. 99, p. 272-291.

Grove, T. L. and M. B. Baker, 1984, Phase equilibrium controls on the tholeiitic versus calc-alkaline differentiation trends: Journal of Geophysical Research, v. 89, n. B5, p. 3253-3274.

Grove, T. L., D. C. Gerlach and T. W. Sando, 1982, Origin of calc-alkaline series lavas at Medecine Lake volcano by fractionation, assimilation and mixing: Contributions to Mineralogy and Petrology, v. 80, p. 160-182.

Henyey, T. L. and T. C. Lee, 1976, Heat flow in Lake Tahoe, California-Nevada, and the Sierra Nevada-Basin and Range transition: Geological Society of America Bulletin, v. 87, p. 1179-1187.

Hill, R. I., 1988, San Jacinto intrusive complex: 1. Geology and mineral chemistry, and a model for intermittent recharge of tonalitic magma chambers: Journal of Geophysical Research, v. 93, n. B9, p. 10.325-10,348.

Holden, P., A. N. Halliday and W. E. Stephens, 1987, Neodymium and strontium isotope content of microdiorite enclaves points to mantle input to granitoid production: Nature, v. 330, p. 53-56.

Huber, N. K., 1981, Amount and timing of late Cenozoic uplift and tilt of the Central Sierra Nevada, California - Evidence from the upper San Joaquin River Basin: United States Geological Survey Professional Paper, v. 1197, p. 1-28.

Humphreys, E., 1987, Mantle dynamics of the southern Great Basin - Sierra Nevada Region: EOS, v. 68, n. 44, p. 1450.

Hyndman, D. W. and D. A. Foster, 1988, The role of tonalites and mafic dikes in the generation of the Idaho Batholith: Journal of Geology, v. 96, p. 31-46.

Irvine, T. N., 1980, Magmatic infiltration metasomatism, double-diffusive fractional crystallization, and adcumulus growth in the Muskox intrusion and other layered intrusions in Hargraves, R. B., ed., Physics of Magmatic Processes: Princeton, N J, Princeton University Press, p. 325-384.

Irvine, T. N., 1987, Appendix 1. Glossary of terms for layered intrusions in Parsons, I., ed., Origins of Igneous Layering: Dordrecht, Holland, D. Reidel Publishing Company, p. 641-647.

James, O. B., 1971, Origin and emplacement of the ultramafic rocks of the Emigrant Gap area, California: Journal of Petrology, v. 12, n. 3, p. 523-560.

Johnston, A. D. and P. J. Wyllie, 1989, The system tonalite-peridotite-H_2O at 30 kbar, with applications to hybridization in subduction zone magmatism: Contributions to Mineralogy and Petrology, v. 102, p. 257-264.

Jones, C. H., 1987, Is extension in Death Valley accommodated by thinning of the mantle lithosphere beneath the Sierra Nevada, California?: Tectonics, v. 6, n. 4, p. 449-473.

Kerr, R. A., 1988, Making mountains with lithospheric drips: Science, v. 239, p. 978-979.

Kerr, R. C. and S. R. Tait, 1985, Crystallization and compositional convection in a porous medium with application to layered intrusions: Journal of Geophysical Research, v. 91, p. 3591-3608.

Kerrick, D. M., 1960, Contact metamorphism in some areas of the Sierra Nevada, California: Geological Society of America Bulletin, v. 81, p. 2913-2938.

Koide, H. and S. Bhattacharji, 1975, Formation of fractures around magmatic intrusions and their role in ore localization: Economic Geology, v. 70, p. 781-799.

Larson, E. S., Jr., 1948, Batholith and associated rocks of Corona, Elsinore and San Luis Rey quadrangles, southern California: Geological Society of America Memoir, n. 29, p. 1-182.

Lawson, A. C., 1904, The orbicular gabbro at Dehesa, San Diego Co., California: University of California Bulletin, v. 3, n. 17, p. 383-396.

Lesher, C. E. and D. Walker, 1988, Cumulate maturation and melt migration in a temperature gradient: Journal of Geophysical Research, v. 93, n. B9, p. 10295-10311.

Leveson, D. J., 1966, Orbicular rocks: A review: Geological Society of America Bulletin, v. 77, p. 409-426.

Loomis, A. A., 1963, Noritic anorthosite bodies in the Sierra Nevada Batholith: Mineralogical Society of America, Special Paper, v. 1, p. 62-68.

Macdonald, G. A., 1941, Geology of the western Sierra Nevada between the Kings and San Joaquin Rivers, California: Bulletin of the Department of Geological Sciences, University of California Publications, v. 26, p. 215-286.

Mack, S., K. Russell, J. C. J. Bishop, D. A. Sholes and F. R. Augugliaro, 1986, Lithologic and structural variations in Cretaceous amphibole-rich gabbros in the Sierra Nevada Foothills near Fresno: California Geology, v. 1986, p. 108-113.

Mack, S., J. B. Saleeby and J. E. Farrell, 1979, Origin and emplacement of the Academy Pluton, Fresno County, California: Geological Society of America Bulletin, v. 90, p. 633-694.

Marshall, L. A. and R. S. J. Sparks, 1984, Origin of some mixed-magma and net-veined ring intrusions: Journal of the Geological Society of London, v. 141, p. 171-182.

McBirney, A. R. and R. M. Noyes, 1979, Crystallization and layering of the Skaergaard Intrusion: Journal of Petrology, v. 20, n. 3, p. 487-554.

McCulloch, M. T., R. T. Gregory, G. J. Wasserburg and H. P. Taylor, Jr., 1981, Sm-Nd, Rb-Sr, and 18O/16O isotopic systematics in an oceanic crustal section: evidence from the Samail ophiolite: Journal of Geophysical Research, v. 86, n. B4, p. 2721-2735.

Merriam, R., 1941, A southern California ring-dike: American Journal of Science, v. 239, n. 5, p. 365-371.

Moore, J. G. and J. P. Lockwood, 1973, Origin of comb layering and orbicular structure, Sierra Nevada Batholith, California: Geological Society of America Bulletin, v. 84, p. 1-20.

Mullan, H. S. and M. A. Bussell, 1977, The basic rock series in batholithic associations: Geological Magazine, v. 114, n. 4, p. 265-280.

Oliver, H. W. and S. L. Robbins, 1982, Bouger gravity map of California. Fresno sheet; 1:250,000, California Division of Mines and Geology.

Pabst, A., 1927, Observations on inclusions in the granitic rocks of the Sierra Nevada: University of California publications in the Geological Sciences, v. 17, p. 325-386.

Park, R. G., 1989, Foundations of Structural Geology: London, Blackie & Son Ltd.

Phillips, W. J., 1974, The dynamic emplacement of cone sheets: Tectonophysics, v. 24, p. 69-84.

Pichowiak, S., M. Buchelt and K. .-W. Damm, 1990, Magmatic activity and tectonic setting of the early stages of the Andean cycle in northern Chile: Geological Society of America Special Paper, v. 241, p. 127-144.

Pickett, D. A., 1991, An isotopic and petrologic study of an exposure of the deep Sierra Nevada batholith, Tehechapi Mountains, California. California Institute of Technology. Ph.D. thesis.

Pin, C., M. Binon, J. M. Belin, B. Barbarin and J. D. Clemens, 1990, Origin of microgranular enclaves in granitoids: Equivocal Sr-Nd evidence from Hercynian rocks in the Massif Central (France): Journal of Geophysical Research, v. 95, n. B11, p. 17821-17828.

Pitcher, W. S., 1978, The anatomy of a batholith: Journal of the Geological Society of London, v. 135, p. 157-182.

Putman, G. W. and J. T. Alfors, 1965, Depth of intrusion and age of the Rocky Hill Stock, Tulare County, California: Geological Society of America Bulletin, v. 76, p. 357-364.

Reid, J. B., 1983, Magma mixing in granitic rocks of the central Sierra Nevada, California: Earth and Planetary Science Letters, v. 66, p. 243-261.

Robson, G. R. and K. G. Barr, 1964, The effect of stress on faulting and minor intrusions in the vicinity of a magma body: Bulletin Volcanologique, v. 27, p. 315-330.

Ross, D. C., 1985, Mafic gneiss complex (batholithic root?) in the southernmost Sierra Nevada, California: Geology, v. 13, p. 288-291.

Russell, K., 1982, Geology of the Campbell Mountain Pluton, southern Fresno County, California. California State University, Fresno. M.S. thesis.

Saleeby, J. and W. Sharp, 1980, Chronology of the Structural and Petrologic Development of the Southwest Sierra Nevada Foothills, California: Geological Society of America Bulletin, Part II, v. 91, n. 6, p. 1416-1535.

Saleeby, J. B., 1975, Structure, Petrology and Geochronology of the Kings-Kaweah Mafic-Ultramafic Belt, Southwestern Sierra Nevada Foothills, California. University of California, Santa Barbara. Ph.D. thesis.

Saleeby, J. B., 1986, Centennial Continent/Ocean Transect #10: C-2 Central California Offshore to Colorado Plateau. The Geological Society of America.

Saleeby, J. B., 1990, Progress in tectonic and petrogenetic studies in an exposed cross-section of young (100 Ma) continental crust, southern Sierra Nevada, California in Salisbury, M. H. and D. M. Fountain, ed., Exposed cross-sections of the continental crust: Netherlands, Kluwer Academic Publishers, ed. p. 137-158.

Saleeby, J. B., R. W. Kistler, S. Longiaru, J. G. Moore and W. J. Nokelberg, 1990, Middle Cretaceous silicic metavolcanic rocks in the Kings Canyon area, central Sierra Nevada, California in Anderson, J. L., ed., The Nature and Origin of Cordilleran Magmatism: Boulder, CO, Geological Society of America, p. 251-270.

Silver, L. T. and B. W. Chappell, 1987, The Peninsular Ranges Batholith: an insight into the evolution of the Cordilleran batholiths of southwestern North America: Transactions of the Royal Society of Edinburgh: Earth Sciences, v. 79, p. 105-121.

Solomon, G. C., 1989, An 18O/16O study of Mesozoic and early Tertiary granitic batholiths of the southwestern North American Cordillera. California Institute of Technology. Ph.D. thesis.

Sparks, R. S. J., 1988, Petrology and geochemistry of the Loch Ba ring-dyke, Mull (N.W. Scotland): An example of the extreme differentiation of tholeiitic magmas: Contributions to Mineralogy and Petrology, v. 100, p. 446-461.

Sparks, R. S. J. and L. A. Marshall, 1986, Thermal and mechanical constraints on mixing between mafic and silicic magmas: Journal of Volcanology and Geothermal Research, v. 29, p. 99-124.

Stolper, E. M., D. Walker, B. H. Hager and J. F. Hays, 1981, Melt segregation from partially molten source regions: The importance of melt density and source size: Journal of Geophysical Research, v. 86, p. 6261-6271.

Streckheisen, A. L., 1973, Plutonic rocks: classification and nomenclature recommended by the IUGS Subcommission on the Systematics of Igneous Rocks: Geotimes, n. 10, p. 26-30.

Taylor, H. P., Jr., 1980, The effects of assimilation of country rocks by magmas on $^{18}O/^{16}O$ and $^{87}Sr/^{86}Sr$ systematics in igneous rocks: Earth and Planetary Science Letters, v. 47, p. 243-254.

Taylor, H. P., Jr., and S. Epstein, 1962a, Relationship between $^{18}O/^{16}O$ ratios in coexisting minerals of igneous and metamorphic rocks, Part I: Geological Society of America Bulletin, V. 73, p. 461-480.

Taylor, H. P., Jr., and S. M. F. Sheppard, 1986, Igneous rocks: I. processes of isotopic fractionation and isotope systematics in Valley, J. W., H. P. Taylor, Jr. and J. R. O'Neil, ed., Stable Isotopes in High Temperature Geological Processes: Washington, D. C., Mineralogical Society of America, p. 227-272.

Tobisch, O. T., J. B. Saleeby and R. S. Fiske , 1986, Structural history of continental volcanic arc rocks, eastern Sierra Nevada, California: A case for extensional tectonics: Tectonics, v. 5, n. 1, p. 65-94.

Ustiyev, Y. K., 1963, Problems of volcanism and plutonism. Volcano-Plutonic formations: International Geological Review, v. 7, n. 11, p. 1994-2016.

Vernon, R. H., 1983, Restite, xenoliths and microgranitoid enclaves in granites: Journal and Proceedings, Royal Society of New South Wales, v. 116, p. 77-103.

Vogel, T. A., 1982, Magma mixing in the acidic-basic complex of Ardnamurchan: Implications on the evolution of shallow magma chambers: Contributions to Mineralogy and Petrology, v. 79, p. 411-423.

Vogt, P. R., 1974, Volcano spacing, fractures, and thickness of the lithosphere: Earth and Planetary Science Letters, v. 21, p. 235-252.

Wahrhaftig, C., 1962, Geomorphology of the Yosemite Valley Region, California: California Division of Mines and Geology Bulletin, v. 182, p. 33-46.

Walawender, M. J., 1976, Petrology and emplacement of the Los Pinos pluton, southern California: Canadian Journal of Earth Science, v. 13, p. 1288-1300.

Walawender, M. J. and T. E. Smith, 1980, Geochemical and petrologic evolution of the basic plutons of the Peninsular Ranges Batholith, southern California: Journal of Geology, v. 88, p. 233-242.

Walker, G. P. L., 1984, Downsag calderas, ring faults, caldera sizes and incremental caldera growth: Journal of Geophysical Research, v. 89, n. B10, p. 8407-8416.

White, A. J. R. and B. W. Chappell, 1977, Ultrametamorphism and granitoid genesis: Tectonophysics, v. 43, p. 7-22.

Yoshida, T., 1984, Tertiary Ishizuchi Cauldron, southwestern Japan Arc: Formation by ring fracture subsidence: Journal of Geophysical Research, v. 89, n. B10, p. 8502-8510.

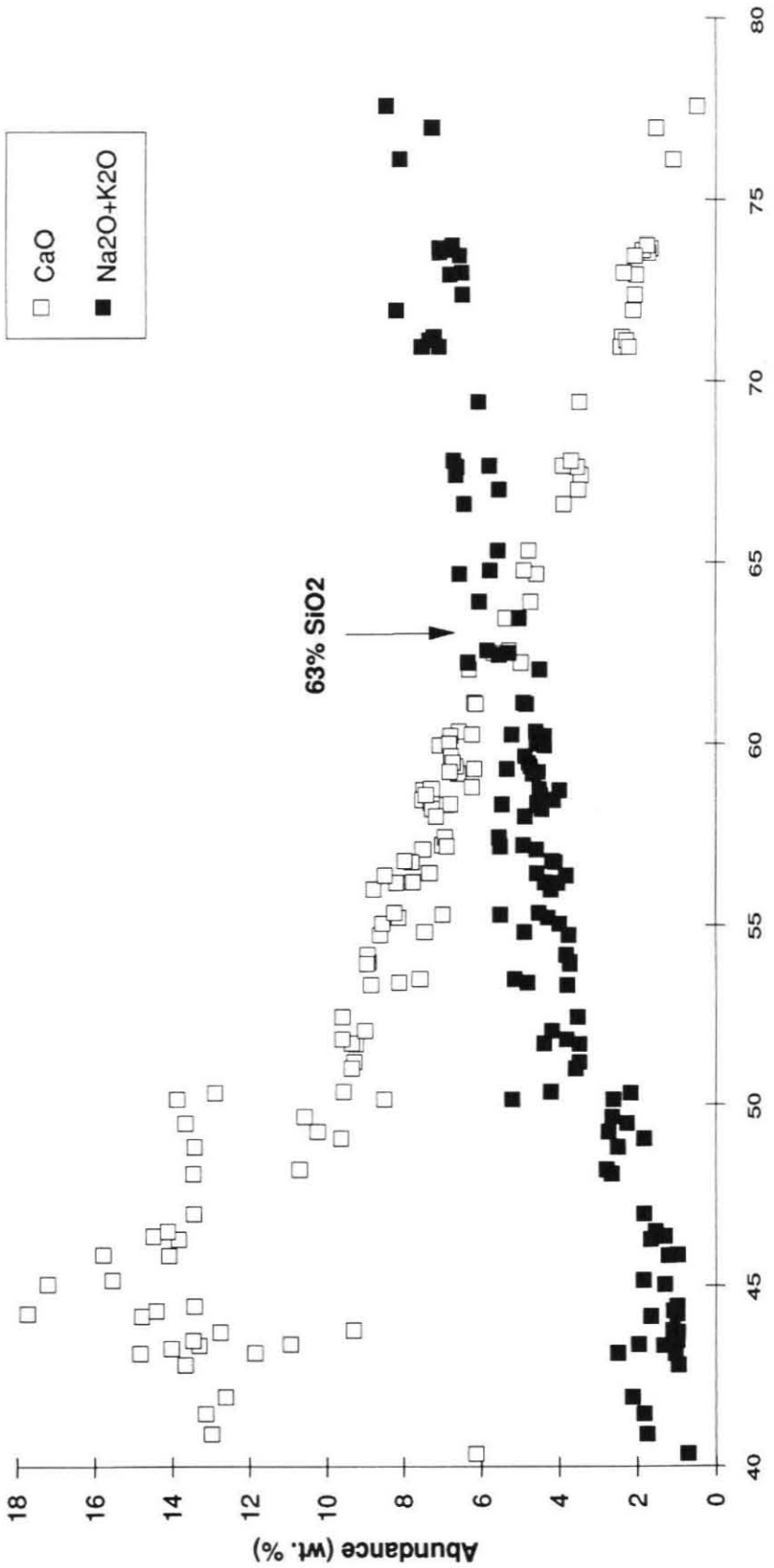

Figure 3.1: Peacock variation diagram for WKB suite. Intersection of curves at approximately 63% SiO2 defines the suite as calcic.

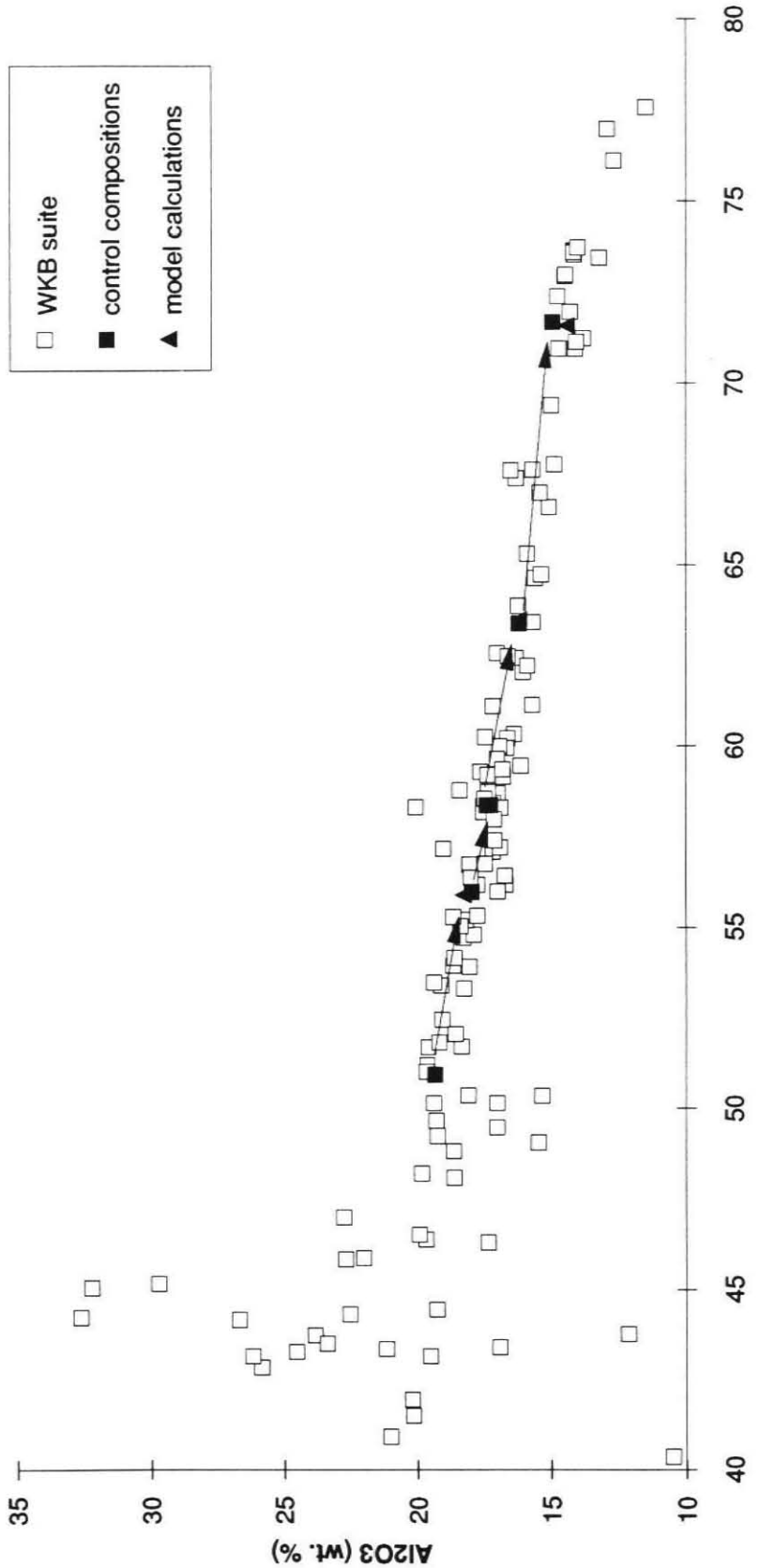

Figure 3.2: SiO2 vs. Al2O3 for WKB plutonic suite. Solid symbols are normalized WKB control compositions and calculated fractionation products; model discussed in text. Arrows connect start and end composition for each fractionation step.

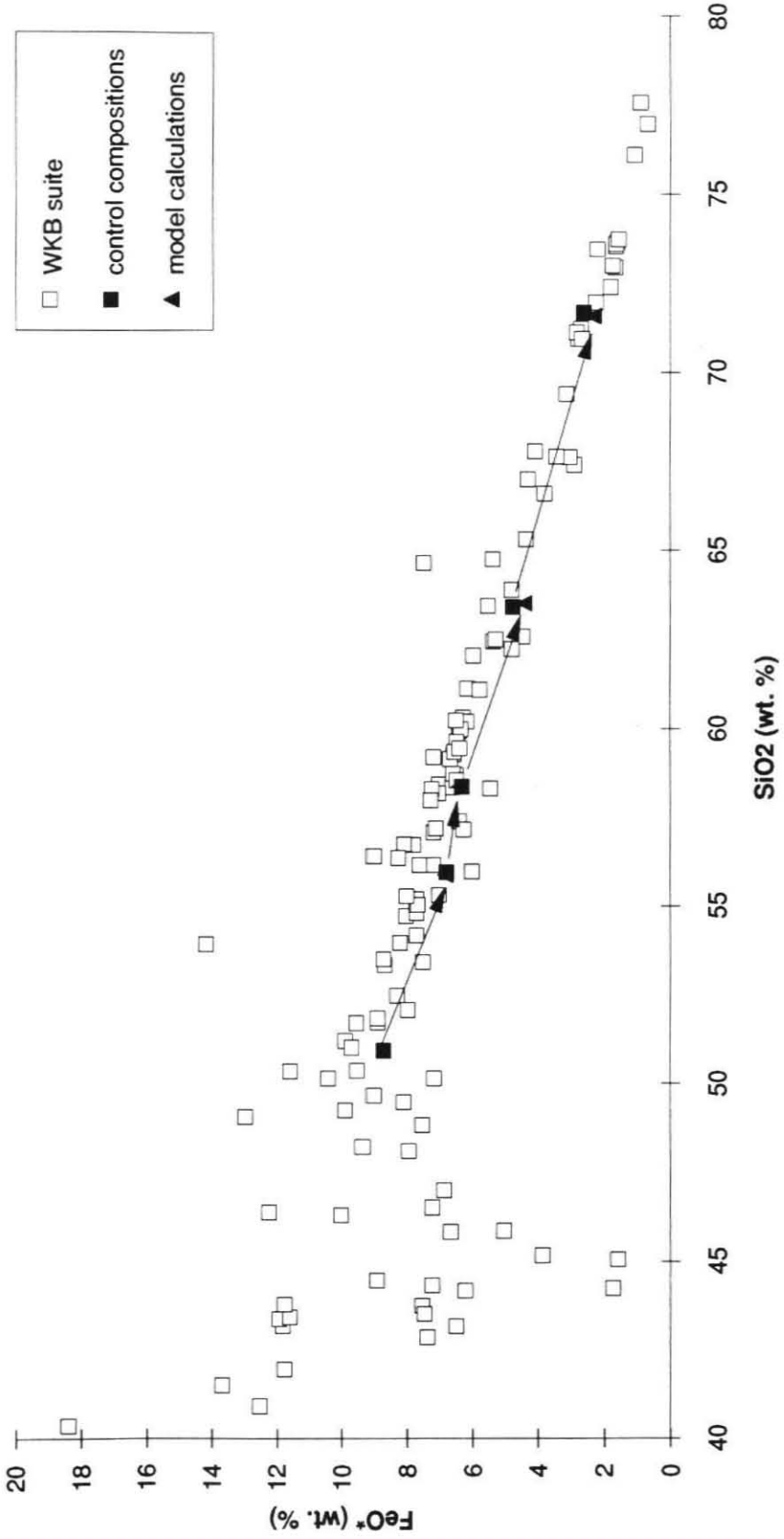

Fig 3.3: SiO2 vs. FeO* (total iron) for WKB plutonic suite. Solid symbols are normalized WKB control compositions and calculated fractionation products; model discussed in text. Arrows connect start and end composition for each fractionation step.

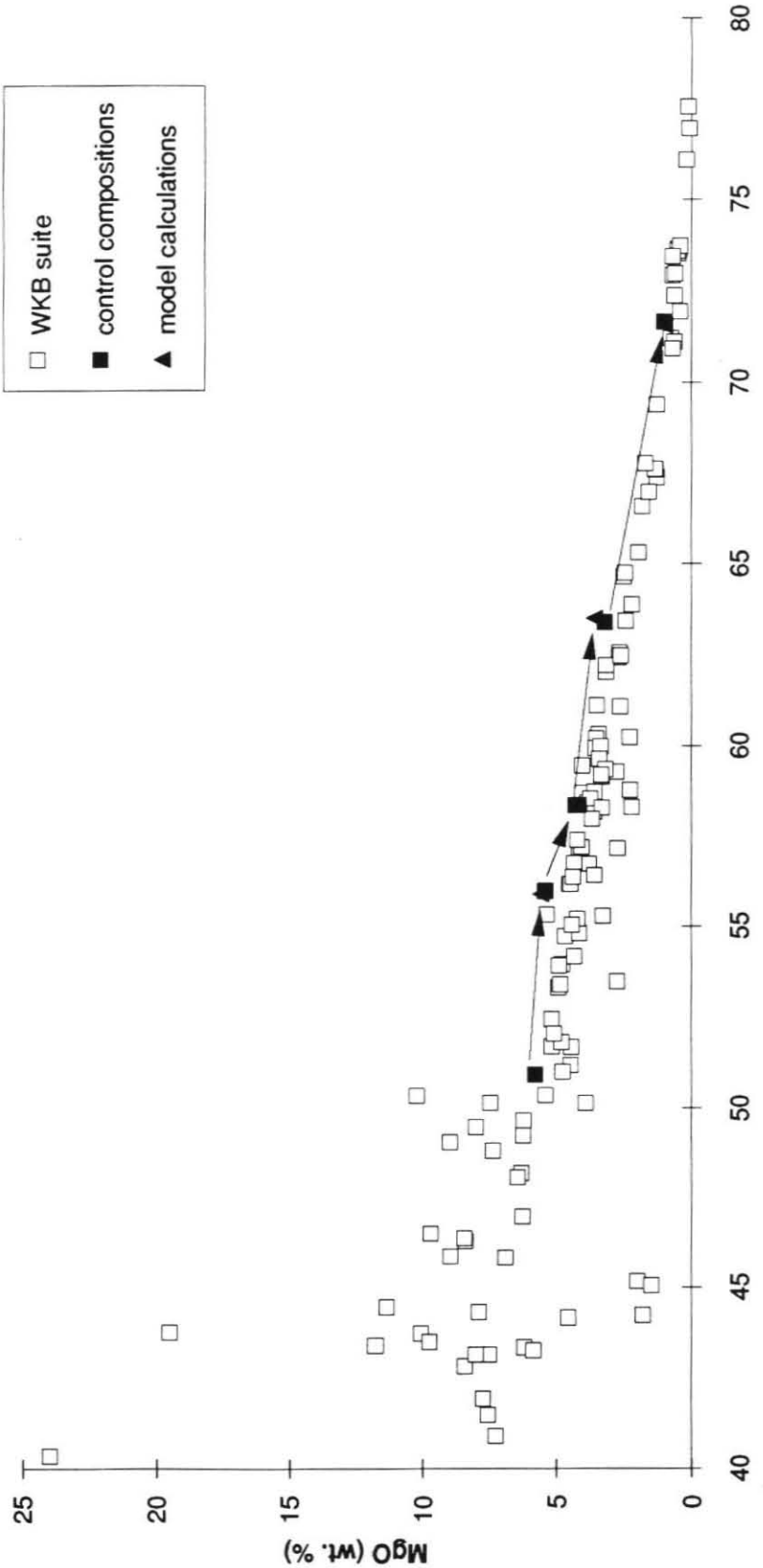

Figure 3.4: SiO2 vs. MgO for WKB plutonic suite. Solid symbols are normalized WKB control compositions and calculated fractionation products; model discussed in text. Arrows connect start and end composition for each fractionation step.

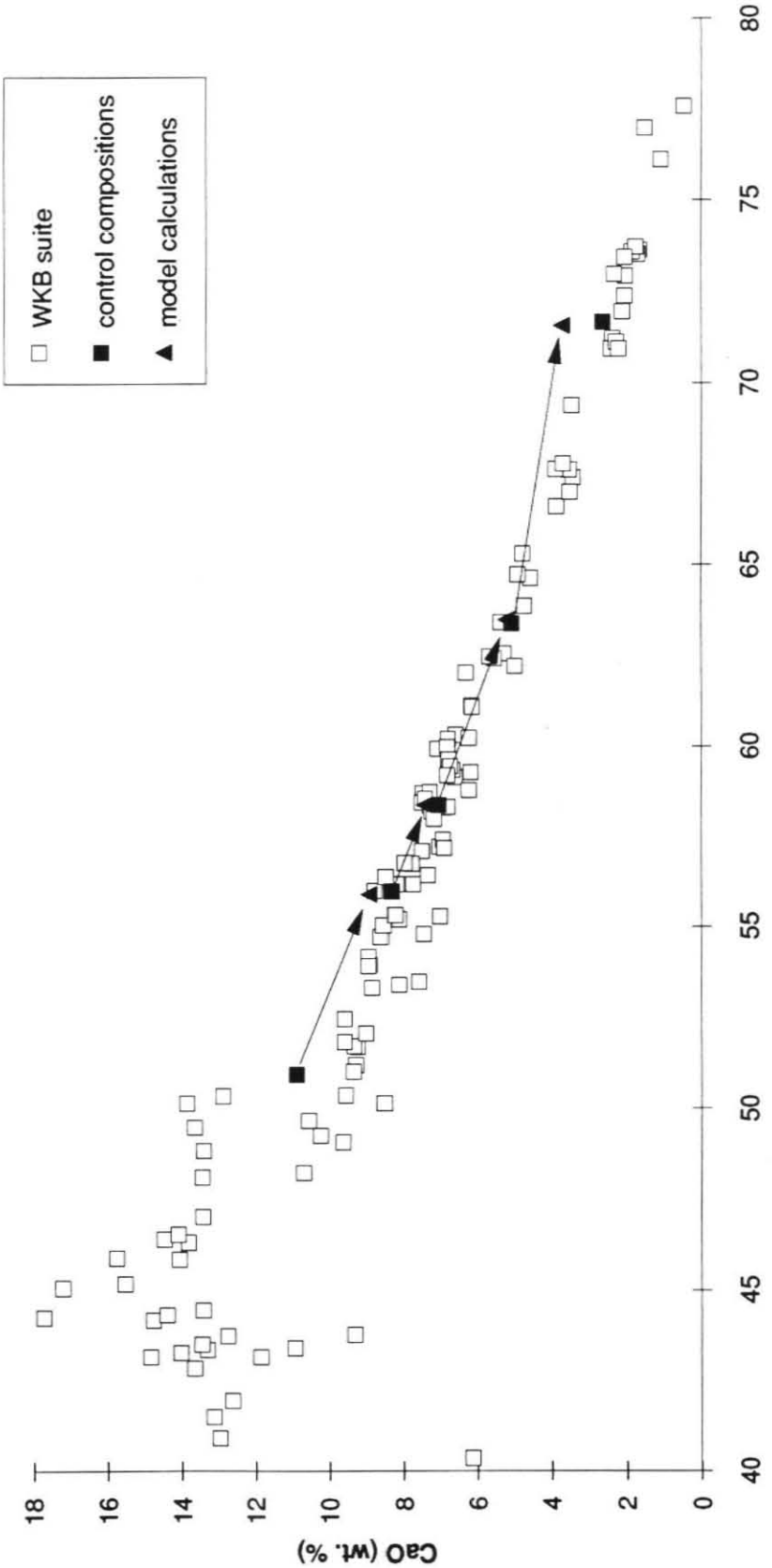

Figure 3.5: SiO2 vs. CaO for WKB plutonic suite. Solid symbols are normalized WKB control compositions and calculated fractionation products; model discussed in text. Arrows connect start and end compositions for each fractionation step.

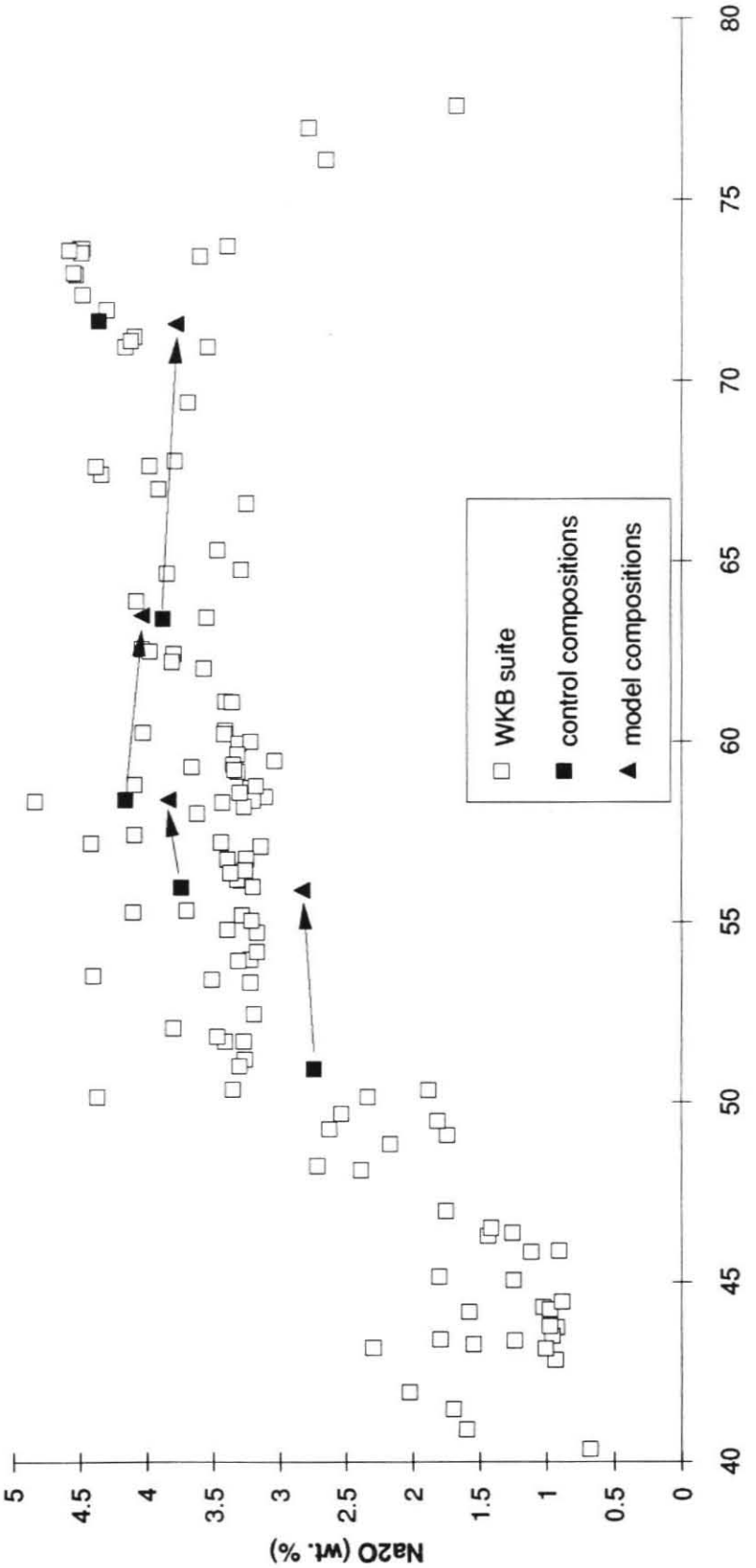

Figure 3.6: SiO2 vs. Na2O for WKB plutonic suite. Solid symbols are normalized WKB control compositions and calculated fractionation products; model discussed in text. Arrows connect start and end compostions for each fractionation step.

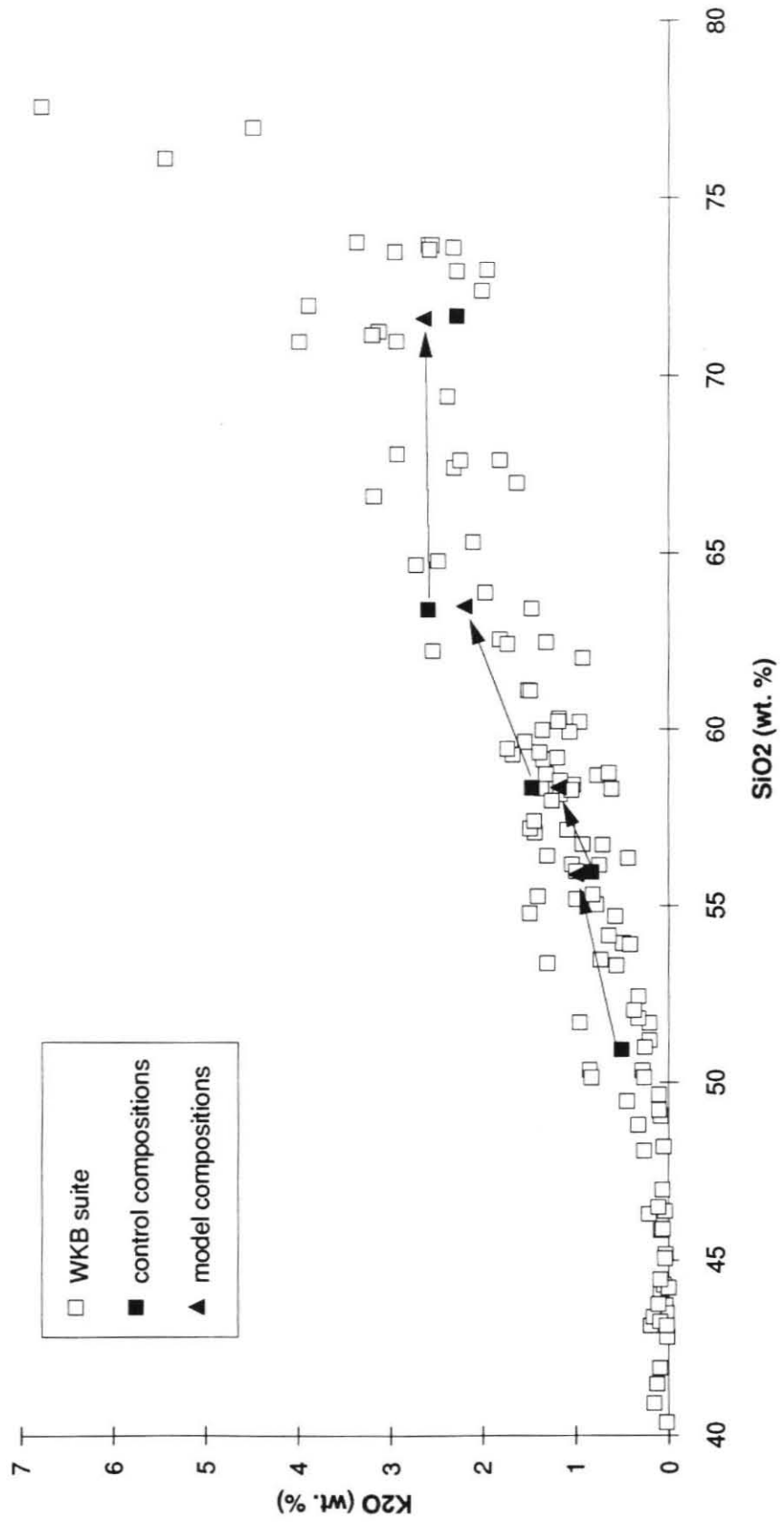

Figure 3.7: SiO2 vs. K2O for WKB plutonic suite. Solid symbols are normalized WKB control compositions and calculated fractionation products; model discussed in text. Arrows connect start and end compositions for each fractionation step.

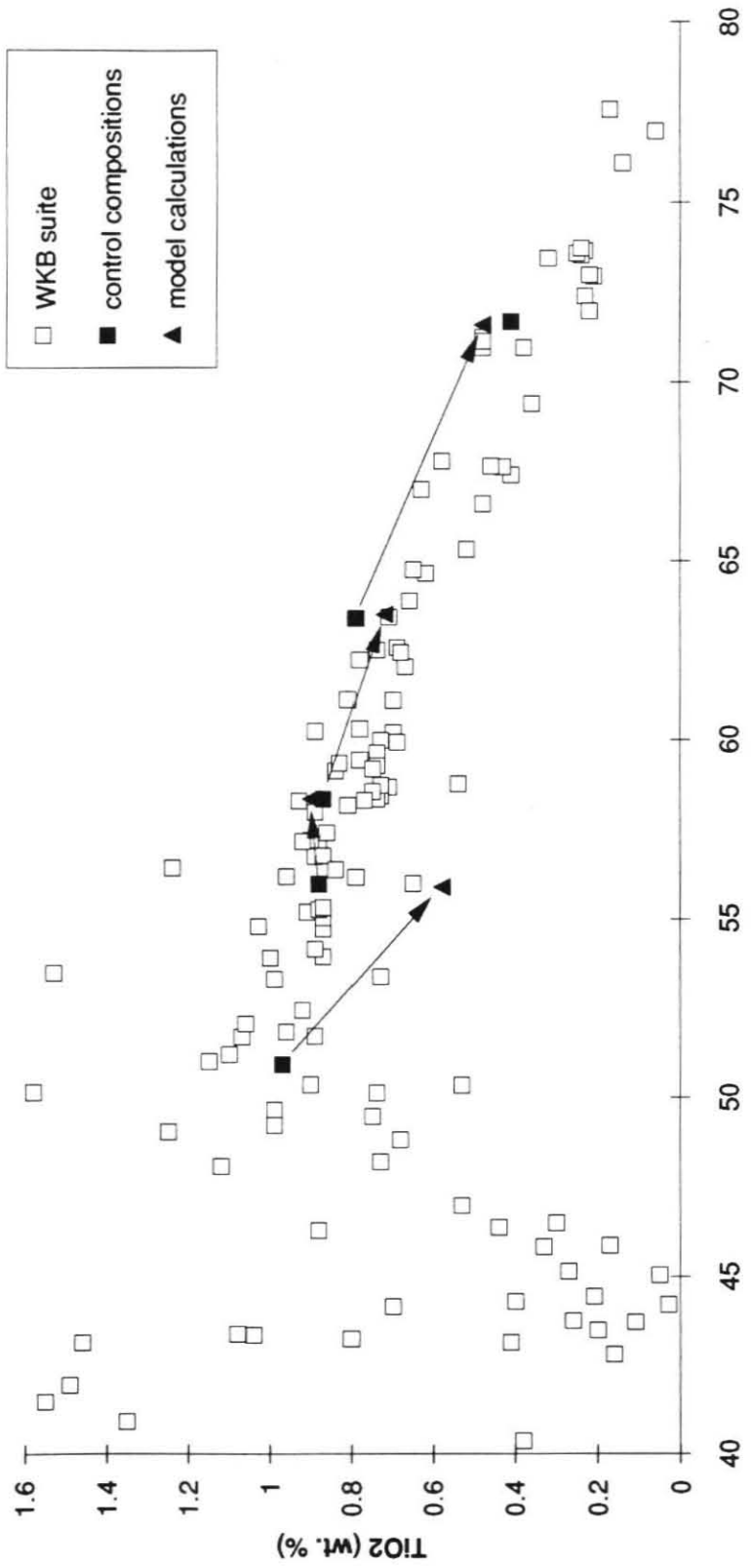

Figure 3.8: SiO2 vs. TiO2 for WKB plutonic suite. Solid symbols are normalized WKB control compositions and calculated fractionation products; model discussed in text. Arrows connect start and end composition for each fractionation step.

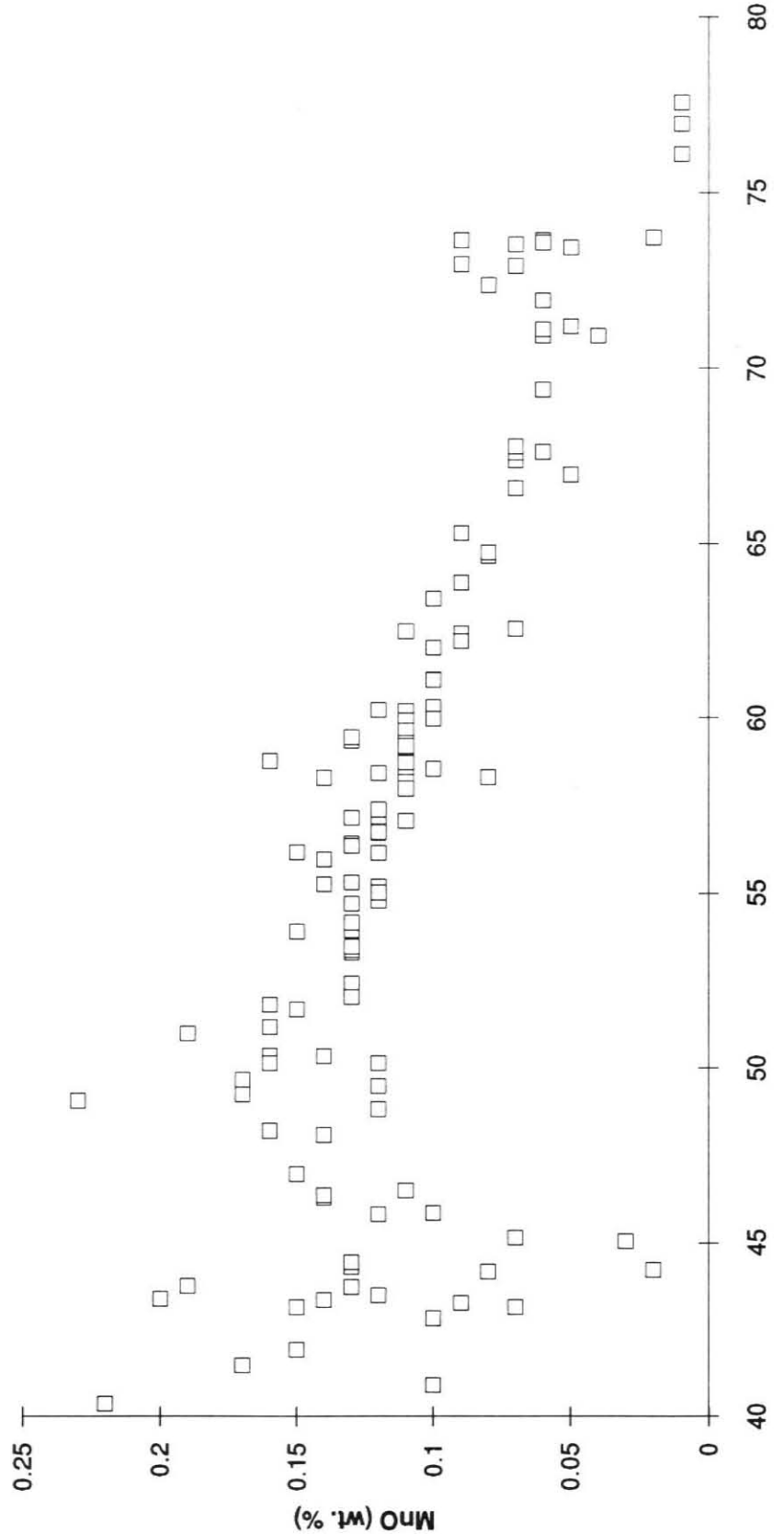

Figure 3.9: SiO2 vs. MnO for WKB plutonic suite. Somewhat unusual compatible behavior of Mn at values of SiO2 greater than 50% is possibly attributed to crystallization of Mn-bearing orthopyroxene.

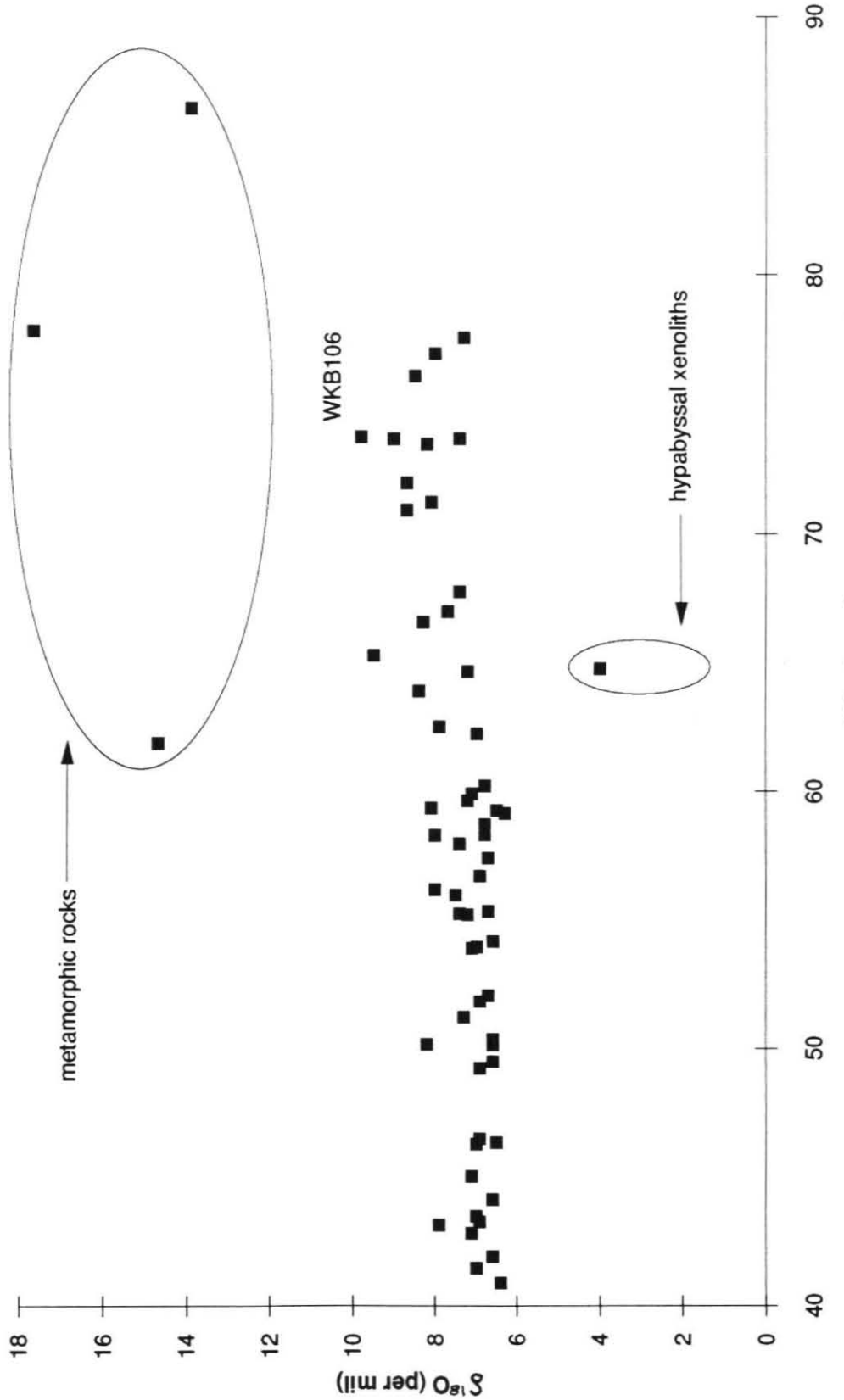

Figure 3.10: SiO2 vs. whole rock δ18O for samples from the Stokes Mountain region and the surrounding early Cretaceous batholith. Large field encloses three samples of metamorphic wall rock while small field encloses three analyses (SiO2 available for only one sample) of hydrothermally altered, hypabyssal material with δ18O ranging from 1.1 to 4.8 per mil.

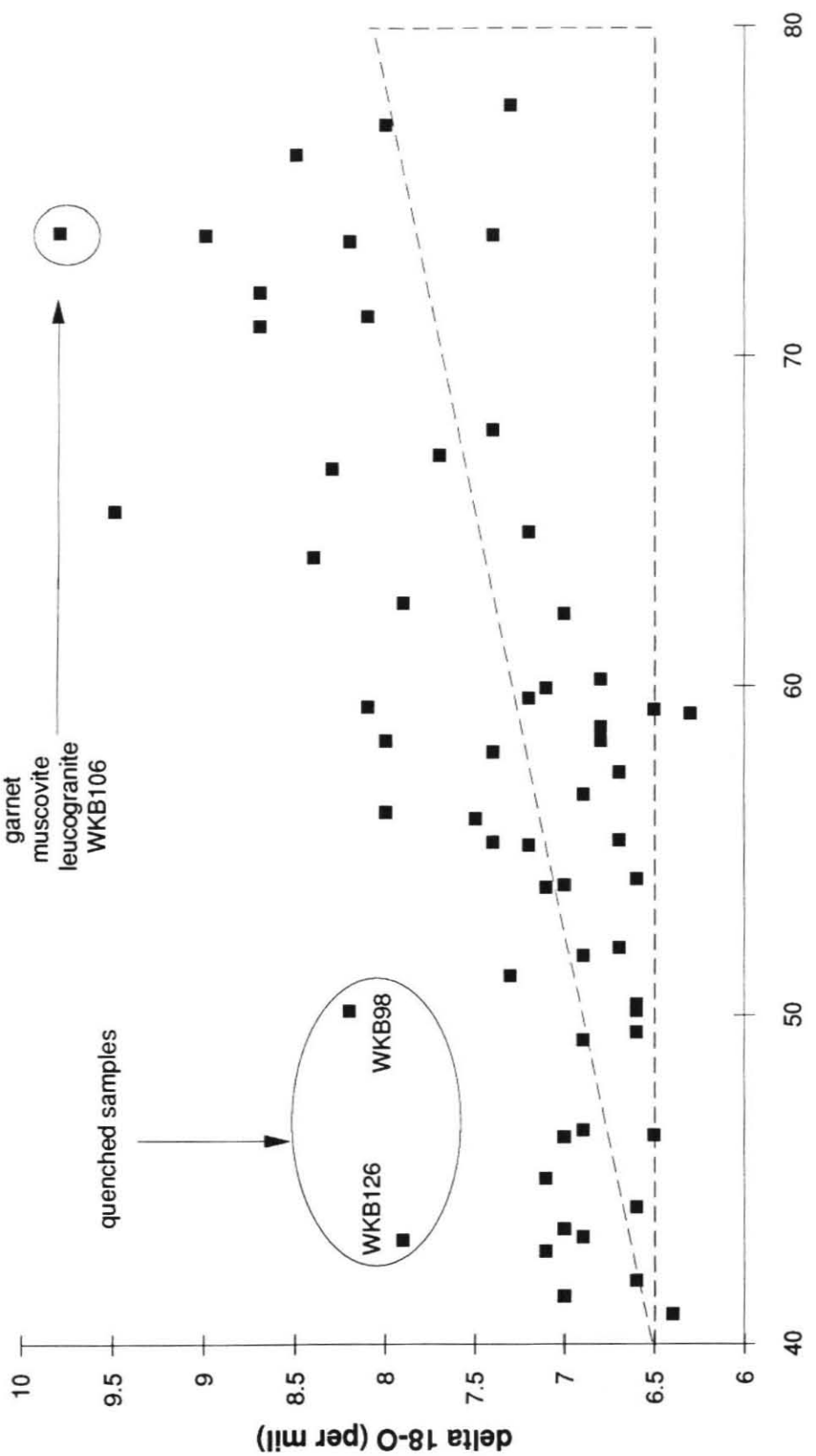

Figure 3.11: SiO2 vs. whole rock δ18O for unaltered igneous samples from the Stokes Mountain Region and the surrounding early Cretaceous batholith. WKB65 excluded. Triangular field encloses samples potentially produced by simple fractional crystallization (0.5 per mil increase per 10% SiO2 increase) without assimilation of high δ18O material. Labeled samples discussed in text.

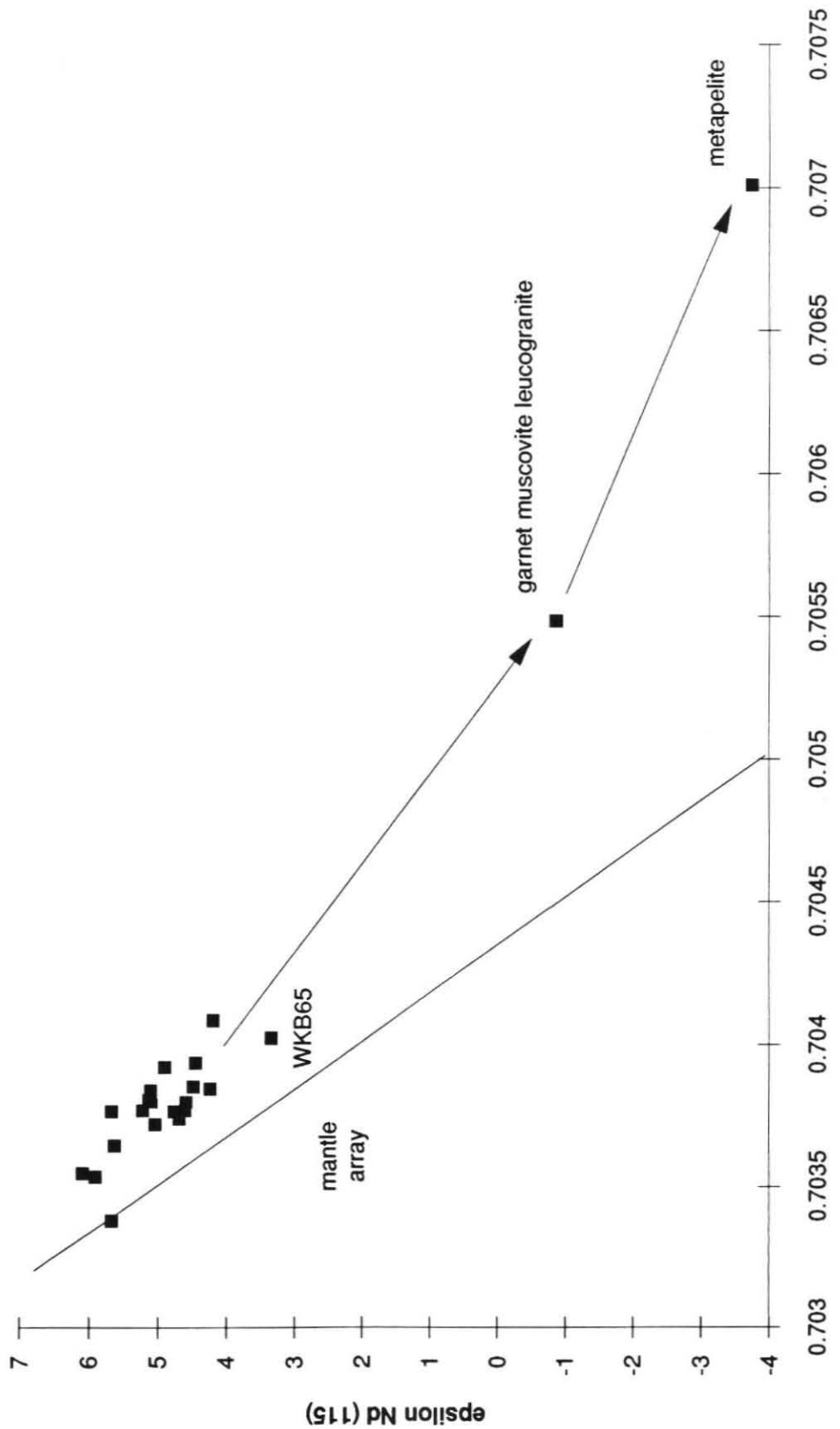

Figure 3.12: Initial 87Sr/86Sr vs. εNd for samples from the Stokes Mountain region plus sample WKB65. Samples corrected to an age of 115 Ma. Arrows point along possible hyperbolic trend generated by mixing with a crustal endmember. Mantle array shown for reference.

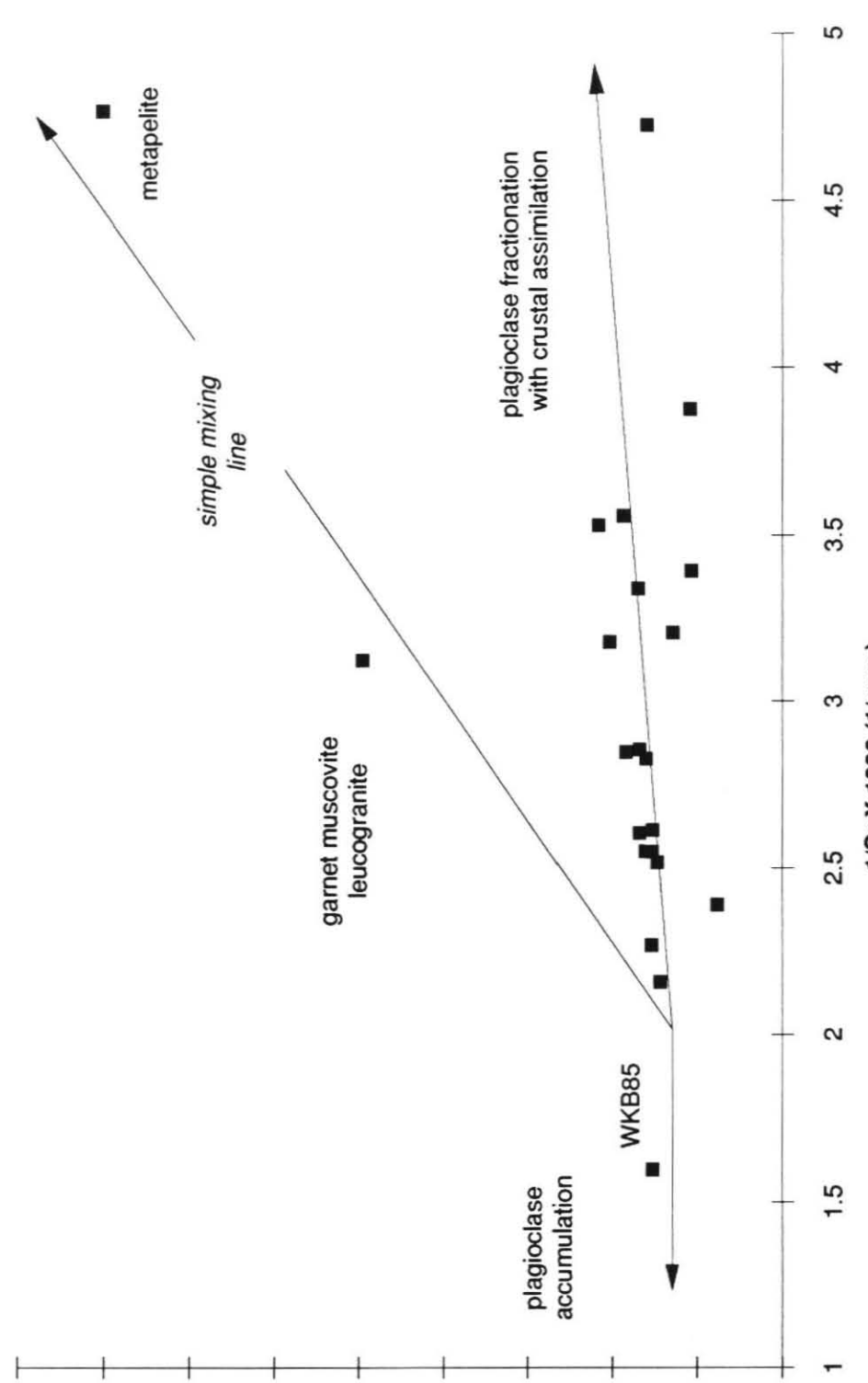

Figure 3.13: 1/Sr vs. initial 87Sr/86Sr ratio for samples from the Stokes Mountain region plus WKB65. Arrows show predicted trends for plagioclase accumulation, simple mixing with a continental endmember, and assimilation during plagioclase fractionation. Simple mixing curve projects to analyses of metasediments by DePaolo (1981).

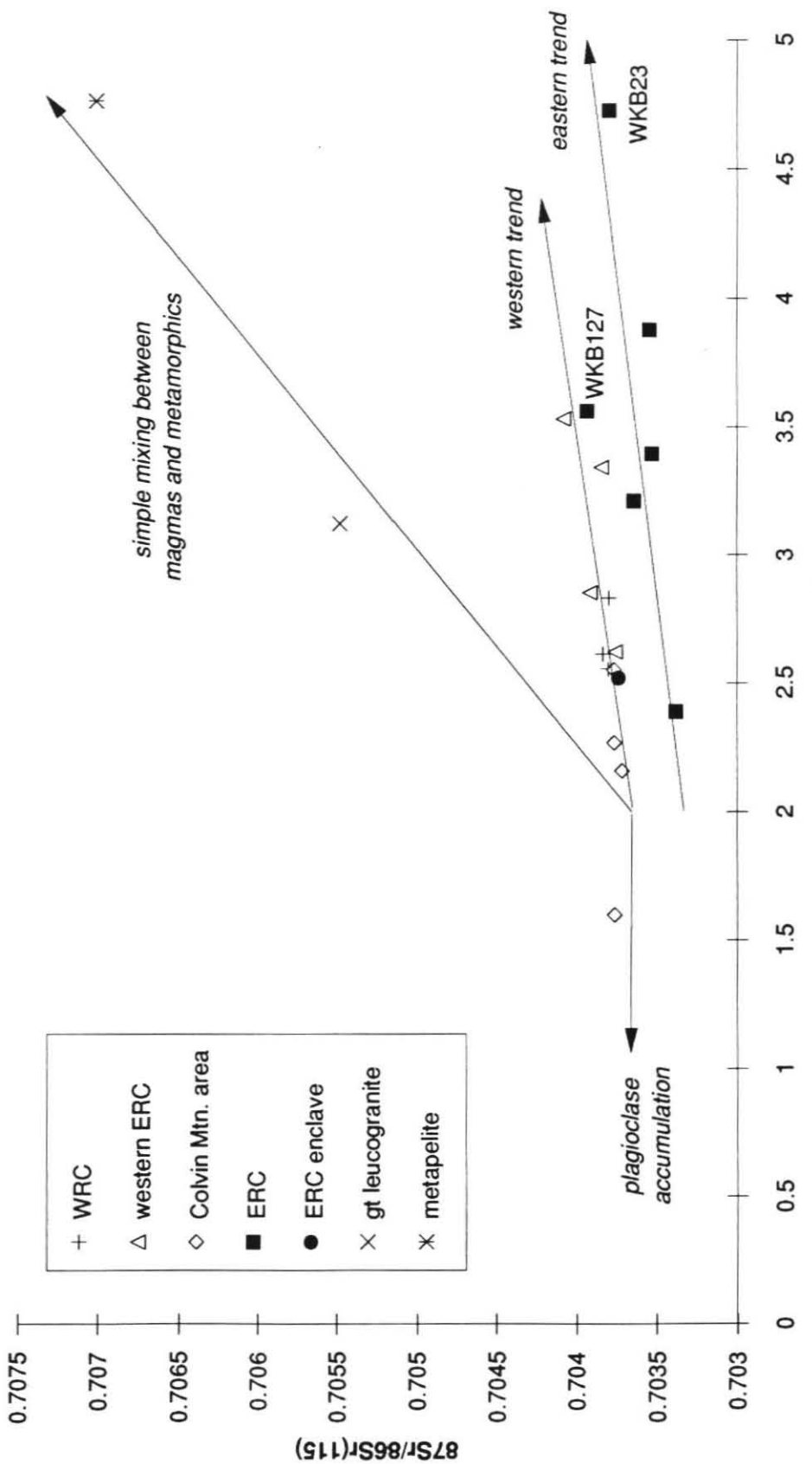

Figure 3.14: 1/Sr vs. 87Sr/86Sr(115).
Samples from the Stokes Mountain region divided by lithology and position relative to the ring complexes (WRC and ERC). Western and eastern trends are discussed in text. Data listed in Table 3.5. gt = garnet.

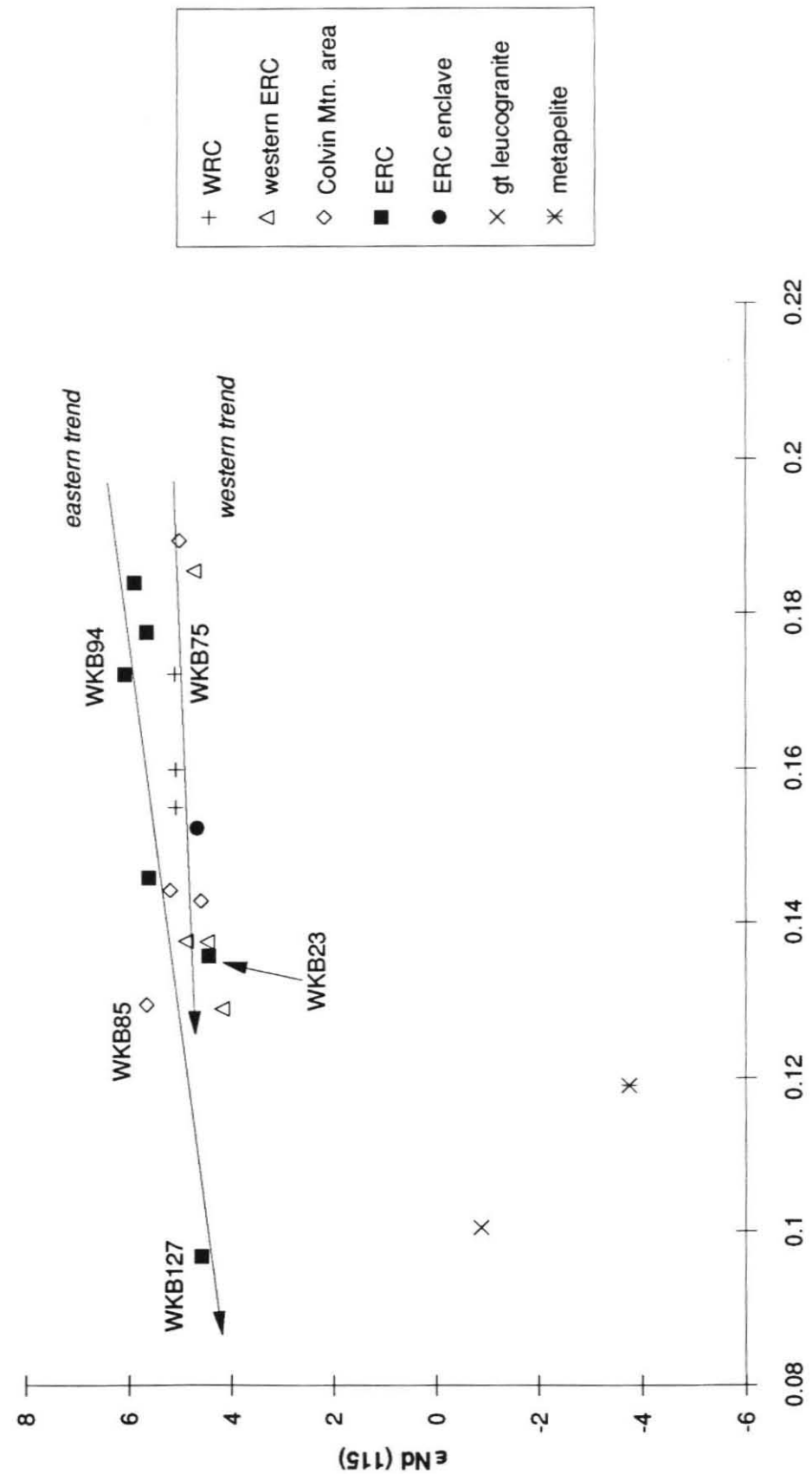

Figure 3.15: 147Sm/144Nd vs. ε Nd(115).
Samples from the Stokes Mountain region classified by lithology and position relative to the ring complexes (WRC and ERC). Western and eastern trends discussed in text. Data listed in Table 3.6. gt = garnet.

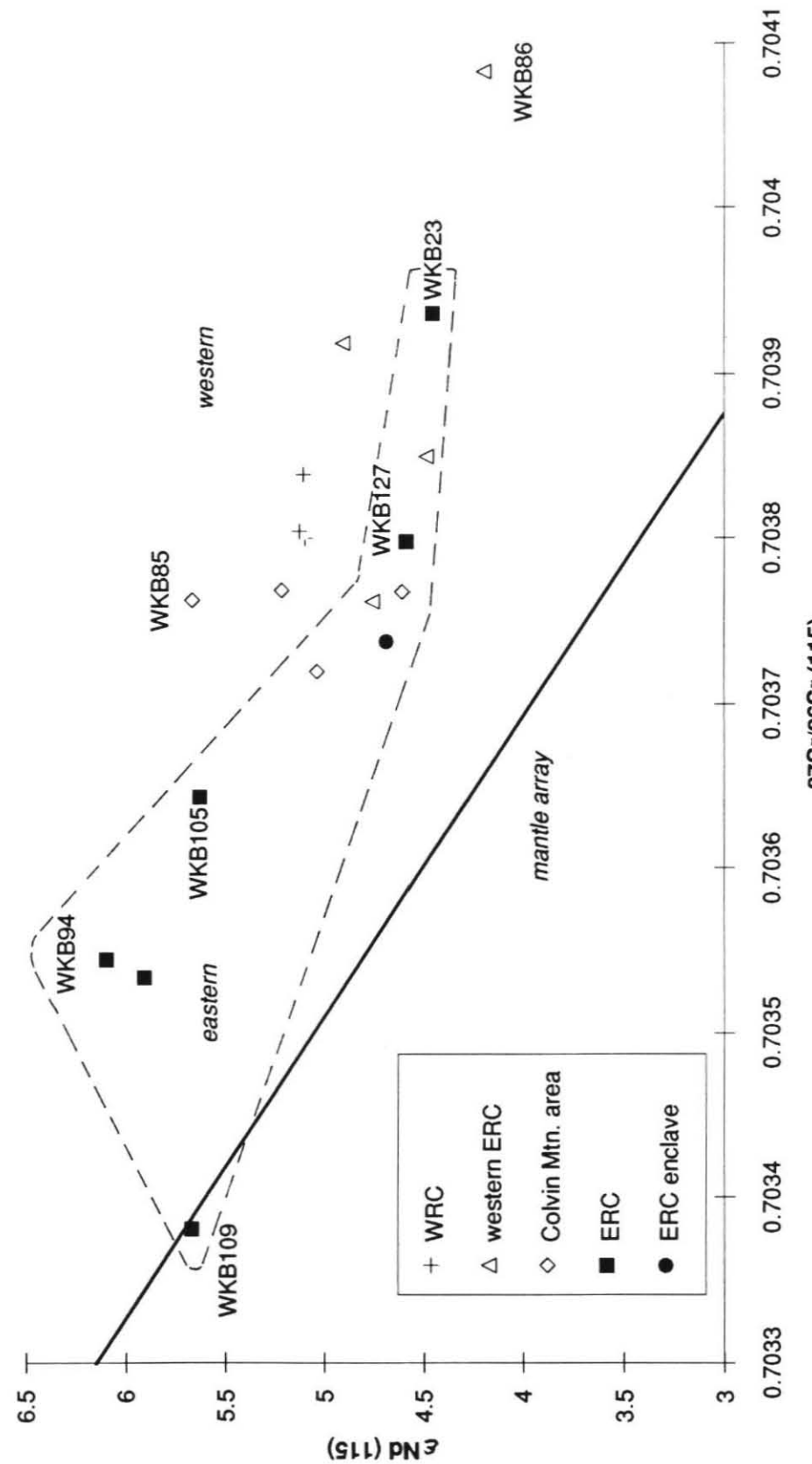

Figure 3.16: 87Sr/86Sr vs. εNd(115). Samples from the Stokes Mountain region classified by lithology and position relative to the ring complexes (WRC and ERC). Data listed in Tables 3.5 and 3.6. Mantle array shown for reference.

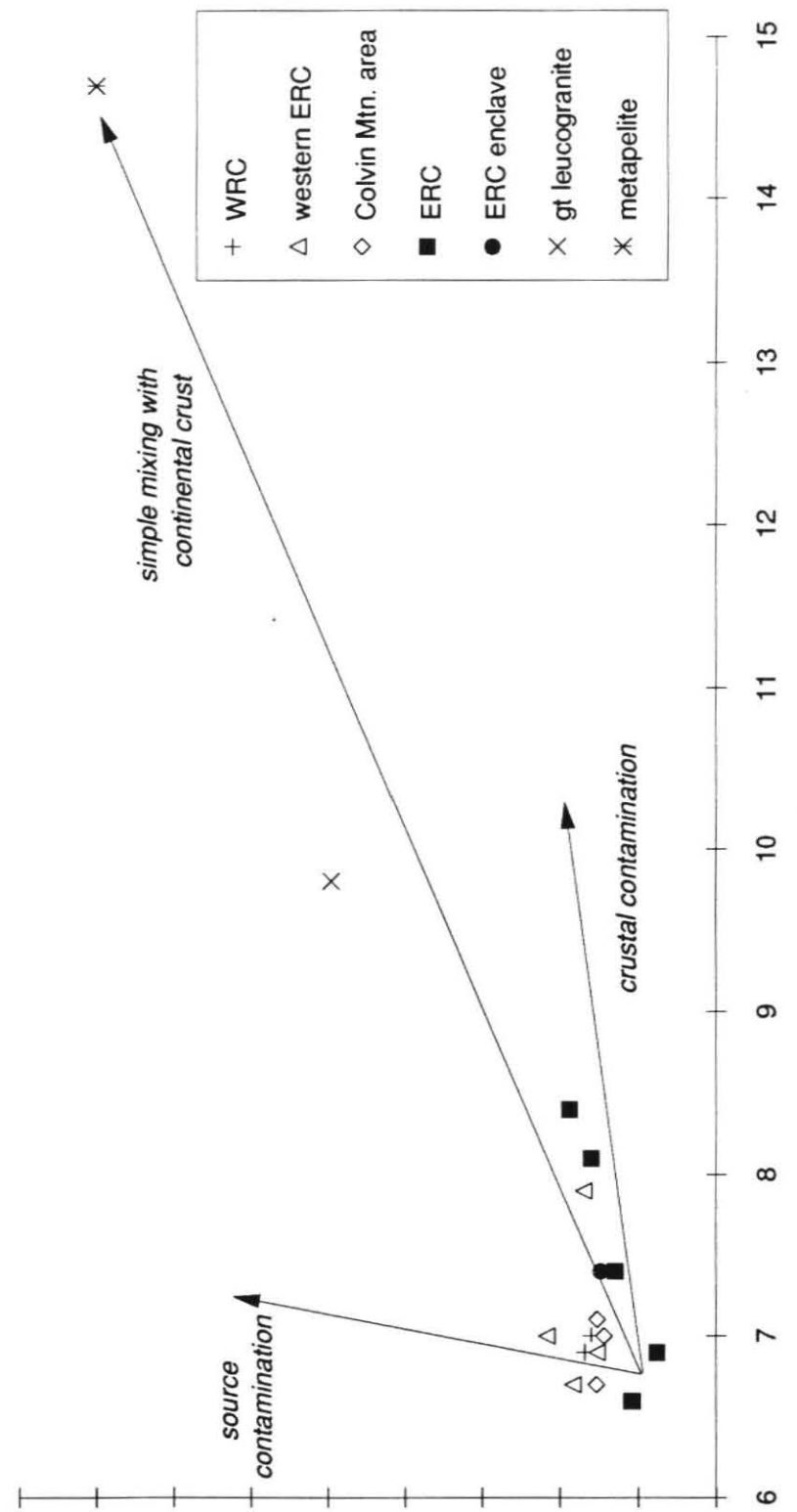

Figure 3.17: $\delta^{18}O$ (per mil) vs. 87Sr/86Sr(115) with metapelite sample. Samples divided by lithology and position relative to the Stokes Mountain ring complexes (WRC and ERC). Curves after Taylor (1986) and discussed in text. Data listed in Table 3.7.

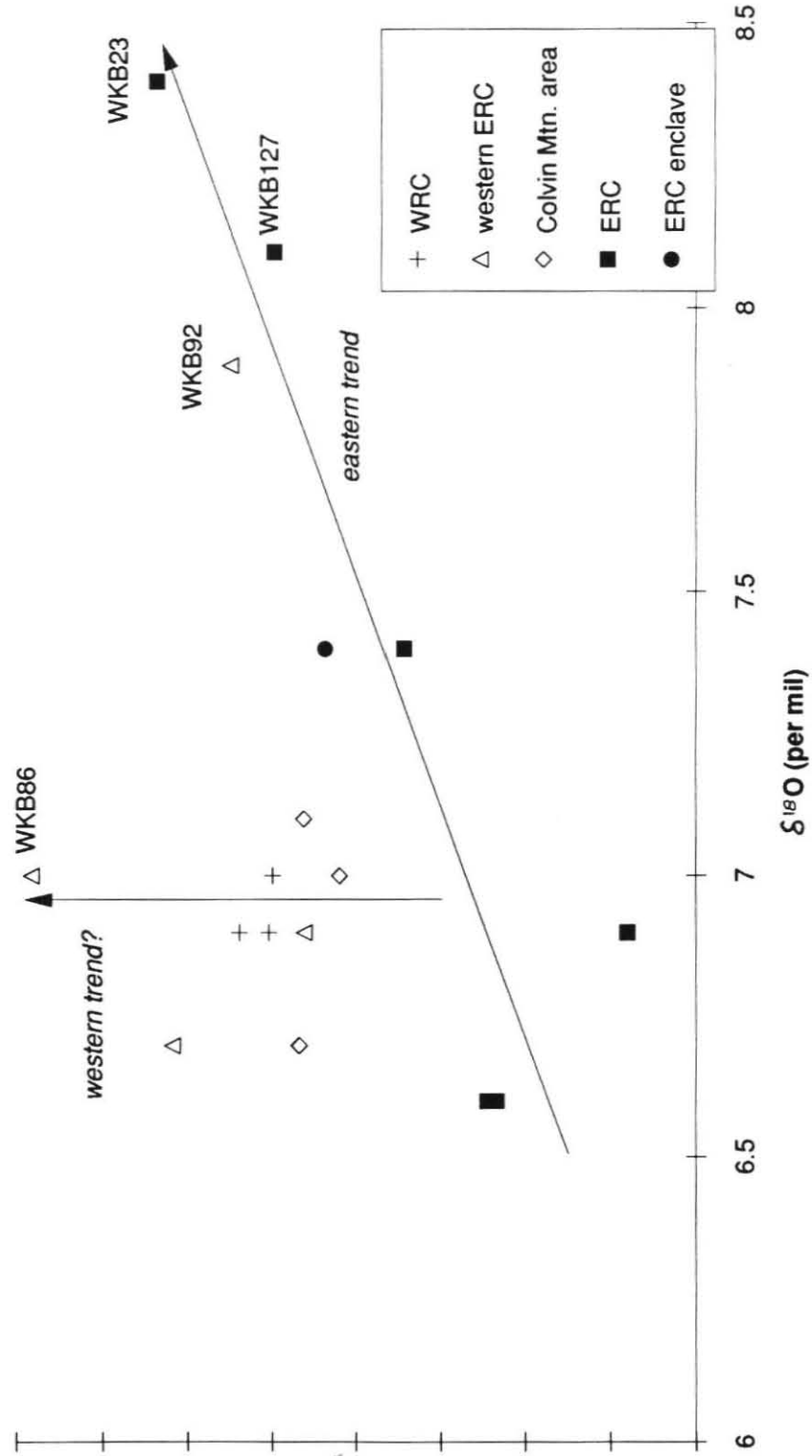

Figure 3.18: $\delta^{18}O$ (per mil) vs. 87Sr/86Sr(115) without metapelite sample. Samples divided by lithology and position relative to the Stokes Mountain ring complexes (WRC and ERC). Western and eastern trends discussed in text. Data listed in Table 3.7.

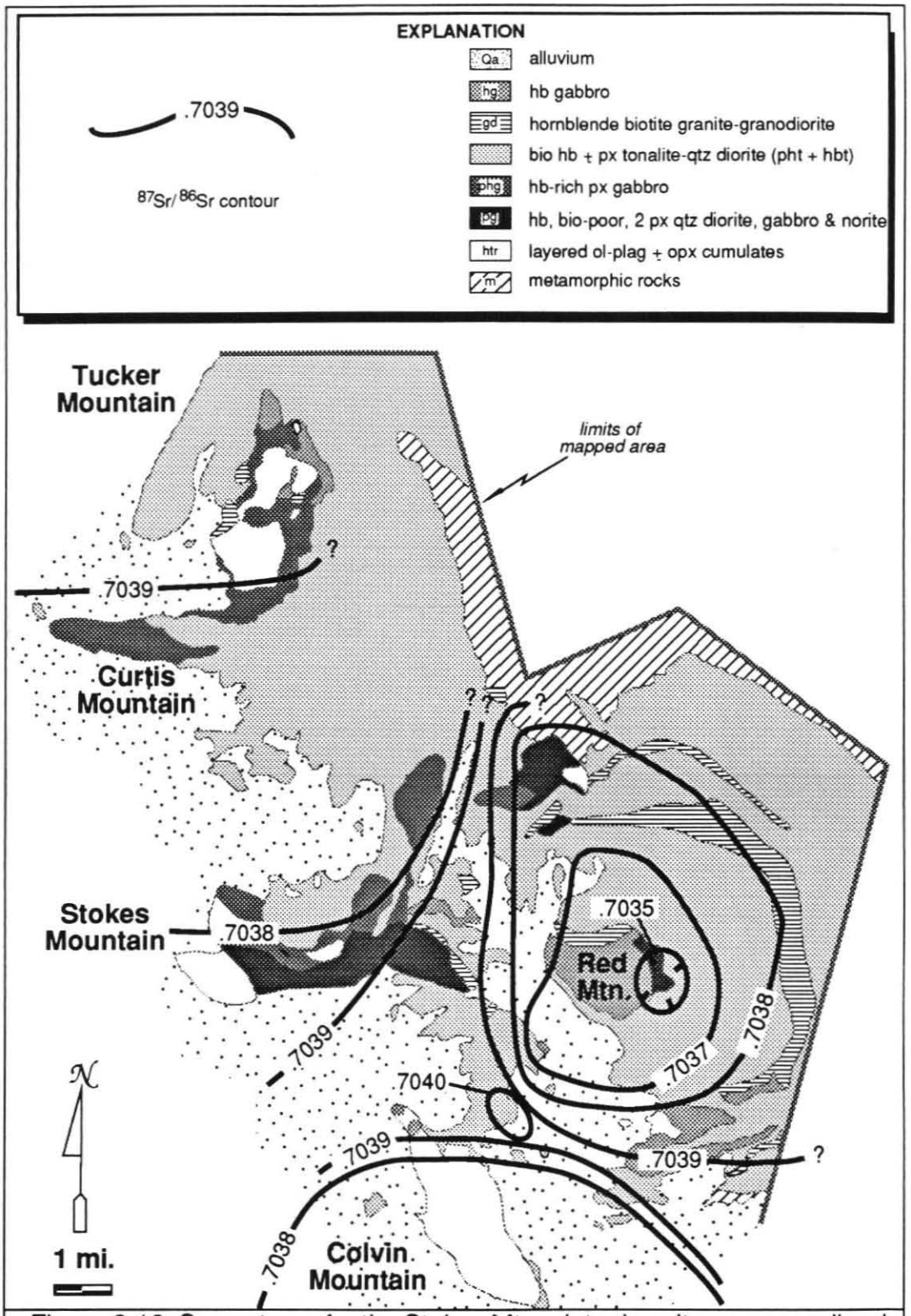

Figure 3.19: Sr_i contours for the Stokes Mtn. plutonic suite on generalized geologic map. Isotopic data listed in Table 3.4.

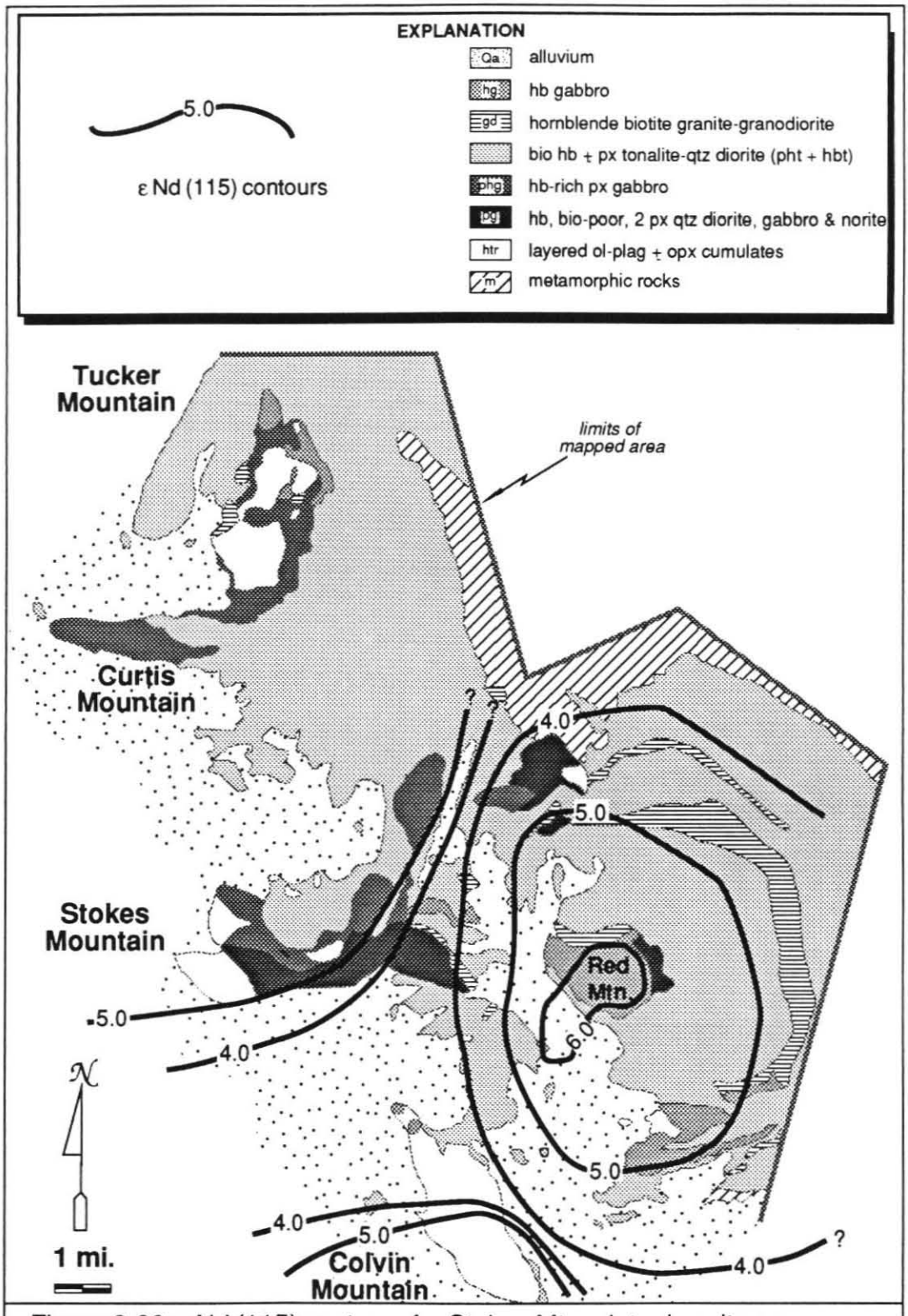

Figure 3.20: ε Nd (115) contours for Stokes Mtn. plutonic suite on generalized geologic map. Isotopic data listed in Table 3.5.

Sample #	WKB 1	WKB 2	WKB 3	WKB 4	WKB 5	WKB 6	WKB 7	WKB 8	WKB 9	WKB 10	WKB 11	WKB 12	WKB 13	WKB 14	WKB 15	WKB 16	WKB 17
SiO2	72.95	71.23	44.18	43.17	54.73	53.34	53.97	62.57	40.92	52.46	56.18	58.71	61.12	60.32	62.04	63.44	60.21
TiO2	0.21	0.48	0.7	1.46	0.87	0.99	0.87	0.69	1.35	0.92	0.79	0.71	0.81	0.78	0.67	0.71	0.7
Al2O3	14.50	13.80	26.68	19.54	18.29	18.26	18.68	17.03	21.03	19.08	17.77	17.01	15.72	16.38	16.06	15.69	16.63
Fe2O3	0.57	0.79	2.33	4.19	2.8	3.3	2.71	1.58	5.43	3.05	2.03	1.25	0.95	1.37	1.82	1.31	1.44
FeO	1.10	1.94	3.9	7.63	5.26	5.42	5.53	2.91	7.1	5.29	5.19	5.27	5.23	4.93	4.17	4.24	4.76
MnO	0.07	0.05	0.08	0.15	0.13	0.13	0.13	0.07	0.1	0.13	0.12	0.11	0.1	0.1	0.1	0.1	0.11
MgO	0.70	0.79	4.58	7.52	4.69	4.94	4.81	2.68	7.28	5.19	4.54	4.06	3.51	3.46	3.17	2.45	3.54
CaO	2.04	2.39	14.78	11.86	8.62	8.86	8.92	5.3	12.98	9.61	8.21	7.5	6.19	6.6	6.33	5.39	6.82
Na2O	4.54	4.10	1.58	2.3	3.18	3.23	3.23	4.05	1.6	3.2	3.3	3.23	3.42	3.42	3.58	3.56	3.43
K2O	2.29	3.14	0.09	0.2	0.58	0.57	0.5	1.82	0.16	0.33	0.75	0.77	1.52	1.18	0.93	1.48	0.96
P2O5	0.10	0.12	0.01	0.05	0.14	0.19	0.15	0.23	0.01	0.15	0.13	0.11	0.16	0.15	0.11	0.15	0.11
S	0.02	0.02	0.09	0.11	0.02	0.02	0.02	0.02	0.18	0.02	0.02	0.02	0.02	0.02	0.02	0.02	0.02
H2O+	0.55	0.46	0.98	1.72	0.33	0.46	0.32	0.74	1.73	0.36	0.82	0.87	0.86	1.01	0.61	0.95	0.83
H2O-	0.13	0.12	0.12	0.13	0.12	0.1	0.1	0.12	0.11	0.07	0.11	0.11	0.12	0.1	0.09	0.16	0.12
CO2	0.17	0.27	0.16	0.19	0.13	0.14	0.05	0.14	0.05	0.05	0.1	0.14	0.01	0.13	0.08	0.12	0.09
rest	0.12	0.17	0.14	0.18	0.16	0.16	0.16	0.2	0.17	0.14	0.15	0.14	0.17	0.16	0.15	0.16	0.14
O=S			0.04	0.05					0.09								
Total	100.04	99.85	100.36	100.35	100.03	100.09	100.13	100.13	100.11	100.03	100.19	99.99	99.89	100.09	99.91	99.91	99.89
Ba	530	580	45	65	225	210	205	530	40	155	235	215	340	410	330	320	260
Rb	40.5	59	0.6	1.2	9.6	11.5	6	36	1.2	4.4	17	20.5	45	30	18.5	42	24.5
Sr	209	195	520	394	364	379	353	569	363	332	287	281	231	245	236	246	247
Pb	11	10	4	4	6	6	5	8	3	4	6	7	9	7	8	7	7
Th	3.6	9	0.2	0.2	1.2	0.8	0.2	4.6	0.2	0.6	1.4	2.4	4.2	1.2	2	3.2	1.8
U	0.8	2.6	0.2	0.2	0.2	0.4	0.2	1.4	0.2	0.2	0.6	0.6	0.8	0.2	0.6	0.8	0.6
Zr	101	258	12	36	81	55	59	128	16	34	83	111	147	123	148	305	105
Nb	7	7.5	1	2	2.5	3.5	2.5	6.5	1	1.5	2.5	2	4	3	3	4	3.5
Y	13	34	7	23	17	18	17	12	14	16	21	17	30	24	26	26	23
La	13	23	2	3	8	8	7	17	1	5	8	7	12	11	10	10	9
Ce	32	54	5	9	20	22	21	41	4	15	22	20	34	28	26	28	23
Sc	3	7	28	52	27	31	32	11	49	30	31	26	24	21	23	19	24
V	12	47	179	317	186	194	194	88	418	211	175	146	144	156	128	118	133
Cr	1	4	87	80	49	53	44	29	31	46	56	55	48	34	30	11	30
Mn																	
Co	4	7	35	51	28	30	28	15	47	31	27	27	21	25	22	17	24
Ni	1	6	31	44	23	31	21	17	25	25	23	23	28	22	14	10	18
Cu	2	17	52	66	44	66	74	10	95	43	38	39	80	56	29	25	29
Zn	37	46	46	102	92	99	93	70	78	86	84	80	80	78	72	72	76
Ga	14.2	16.4	18	18.8	18.4	18.4	18.8	18.2	20	19.4	17.4	16.6	16	16.6	15.8	16	16.2

Table 3.1: Whole rock geochemical analyses of WKB (Western Cretaceous Batholith) samples. Major elements in oxide weight per cent; minor elements in ppm. Analyses provided by Dr. B. W. Chappell of the Australian National University, Canberra, Australia.

Sample #	WKB 18	WKB 19	WKB 20	WKB 21	WKB 22	WKB 23	WKB 24	WKB 25	WKB 26	WKB 27	WKB 28	WKB 29	WKB 30	WKB 31	WKB 32	WKB 33
SiO2	69.4	67.4	66.6	57.1	62.44	63.89	67.62	54.81	57.21	65.32	61.1	56.75	59.94	58.45	59.99	58.36
TiO2	0.36	0.41	0.48	0.88	0.68	0.66	0.43	1.03	0.9	0.52	0.7	0.89	0.69	0.73	0.73	0.74
Al2O3	14.99	16.29	15.09	17.19	16.32	16.23	16.51	17.9	16.92	15.9	17.18	18.06	16.68	17.16	16.93	17.54
Fe2O3	1.18	0.44	0.7	2.47	1.87	1.71	0.57	2.51	2.04	1.28	1.77	2.61	1.65	1.92	1.53	1.71
FeO	1.98	2.49	3.13	4.74	3.52	3.12	2.49	5.22	5.11	3.11	4.03	5.21	4.78	5.14	4.84	4.93
MnO	0.06	0.07	0.07	0.11	0.09	0.09	0.07	0.12	0.12	0.09	0.1	0.12	0.11	0.12	0.1	0.11
MgO	1.3	1.31	1.85	4.18	2.7	2.23	1.34	4.18	4.08	1.97	2.66	3.81	3.57	3.88	3.38	3.69
CaO	3.48	3.45	3.89	7.52	5.57	4.75	3.55	7.47	7.04	4.8	6.16	7.8	7.1	7.52	6.84	7.3
Na2O	3.7	4.35	3.26	3.15	3.81	4.09	4.39	3.4	3.45	3.48	3.37	3.4	3.32	3.12	3.23	3.21
K2O	2.39	2.32	3.19	1.44	1.74	1.98	2.25	1.5	1.49	2.11	1.49	0.71	1.07	1.03	1.36	1.37
P2O5	0.1	0.18	0.1	0.16	0.15	0.15	0.17	0.22	0.19	0.12	0.14	0.13	0.1	0.09	0.11	0.12
S	0.02	0.02	0.02	0.03	0.02	0.02	0.02	0.02	0.02	0.02	0.02	0.02	0.02	0.02	0.02	0.02
H2O+	0.7	0.73	0.78	0.69	0.97	0.86	0.65	1.37	1.28	1.05	1.07	0.56	0.79	0.72	0.76	0.8
H2O-	0.13	0.11	0.09	0.09	0.11	0.1	0.12	0.18	0.12	0.16	0.17	0.07	0.16	0.13	0.14	0.11
CO2	0.13	0.16	0.36	0.01	0.08	0.01	0.12	0.1	0.11	0.06	0.05	0.04	0.04	0.06	0.15	0.03
rest	0.14	0.17	0.18	0.19	0.17	0.18	0.17	0.17	0.18	0.17	0.2	0.14	0.16	0.15	0.16	0.16
O=S				0.01			0.01		0.01							
Total	100.04	99.88	99.77	99.94	100.22	100.05	100.46	100.18	100.25	100.14	100.19	100.3	100.16	100.22	100.25	100.18
Ba	560	570	700	470	465	545	555	365	390	655	755	220	405	290	385	320
Rb	52	53	83	44.5	48	55	46.5	49	43	55	44	15	27.5	25.5	35.5	40.5
Sr	229	387	243	371	293	281	399	330	321	312	361	319	267	264	289	301
Pb	10	10	12	9	9	8	12	8	8	12	7	8	7	7	7	8
Th	5.8	6	12.4	6	4.6	5.2	6.6	4.4	3.6	7	2.4	1.8	1.8	2.2	0.6	4
U	1.6	2.6	3.4	2	1.2	1.2	2	1	0.8	2	0.8	0.6	0.8	0.6	0.2	1.4
Zr	129	164	127	108	164	196	162	89	112	100	130	81	104	106	140	98
Nb	3.5	7	6	5.5	4.5	5.5	6	4	4	4	4	2.5	3	2.5	3.5	3
Y	13	16	21	20	23	26	15	20	23	15	18	15	18	19	23	21
La	13	20	20	15	15	17	18	12	12	12	119	7	8	7	10	9
Ce	30	49	45	36	35	42	42	30	31	21	11	18	23	20	27	25
Sc	7	6	12	22	19	15	7	26	25	13	14	29	26	29	24	27
V	49	37	72	159	116	94	39	194	167	82	4	179	150	179	148	170
Cr	9	11	21	45	25	24	12	42	53	12	19	21	37	28	29	31
Mn																
Co	8	6	10	22	19	14	7	27	27	12	14	25	23	25	23	26
Ni	6	9	8	16	13	13	9	23	23	6	4	12	16	12	13	18
Cu	2	2	6	21	20	13	3	25	29	6	19	41	36	36	43	76
Zn	45	56	55	87	69	69	57	90	88	71	86	80	76	75	74	79
Ga	14.2	16.8	14.6	17.4	16.8	17.2	17	18.2	17.2	16.2	17.6	18	16.2	16	16.2	16.8

Table 3.1: Whole rock geochemical analyses of WKB (Western Cretaceous Batholith) samples. Major elements in oxide weight per cent; minor elements in ppm. Analyses provided by Dr. B. W. Chappell of the Australian National University, Canberra, Australia.

Sample #	WKB 34	WKB 35	WKB 36	WKB 37	WKB 38	WKB 39	WKB 40	WKB 41	WKB 42	WKB 43	WKB 44	WKB 45	WKB 46	WKB 47	WKB 48	WKB 49
SiO2	59.65	55.21	51.71	51.21	59.29	58.19	55.05	58.75	58.57	54.18	59.16	67.64	60.24	50.37	51.72	43.37
TiO2	0.74	0.91	1.07	1.1	0.74	0.81	0.87	0.73	0.75	0.89	0.84	0.46	0.89	0.9	0.89	1.04
Al2O3	17.03	18.21	19.6	19.64	17.65	17.54	18.4	17.37	17.5	18.64	16.79	15.68	17.48	18.12	18.37	21.18
Fe2O3	1.79	2.11	2.8	3.3	1.91	2.14	2.52	2.14	2	2.31	1.95	1.16	2.12	3.11	2.76	5.9
FeO	4.71	5.63	6.76	6.61	4.68	4.93	5.18	4.47	4.5	5.43	4.76	2.3	4.4	6.43	6.17	6.03
MnO	0.11	0.12	0.15	0.16	0.11	0.11	0.12	0.11	0.1	0.13	0.11	0.06	0.12	0.16	0.15	0.14
MgO	3.43	4.25	4.47	4.5	2.79	3.6	4.45	3.61	3.77	4.35	3.33	1.36	2.3	5.42	5.19	6.2
CaO	6.8	8.14	9.24	9.29	6.2	7.26	8.56	7.3	7.44	8.95	6.62	3.91	6.25	9.57	9.35	13.31
Na2O	3.33	3.29	3.28	3.27	3.67	3.28	3.22	3.19	3.31	3.18	3.33	3.99	4.04	3.36	3.42	1.24
K2O	1.55	1	0.21	0.21	1.68	1.17	0.78	1.32	1.17	0.65	1.35	1.82	1.19	0.85	0.96	0.09
P2O5	0.12	0.18	0.17	0.17	0.13	0.13	0.15	0.11	0.14	0.16	0.13	0.12	0.2	0.11	0.11	0.03
S	0.02	0.02	0.02	0.02	0.02	0.02	0.02	0.02	0.02	0.02	0.02	0.02	0.02	0.02	0.02	0.02
H2O+	0.61	0.78	0.52	0.38	0.96	0.59	0.59	0.71	0.68	1.01	1.01	0.67	0.33	1.03	0.48	1.43
H2O-	0.11	0.12	0.1	0.1	0.14	0.1	0.05	0.09	0.07	0.08	0.12	0.16	0.08	0.12	0.09	0.1
CO2	0.07	0.07	0.05	0.09	0.01	0.01	0.01	0.01	0.04	0.09	0.09	0.26	0.17	0.21	0.08	0.08
rest	0.16	0.16	0.15	0.14	0.16	0.16	0.16	0.15	0.16	0.16	0.17	0.16	0.17	0.15	0.15	0.19
O=S																
Total	100.21	100.18	100.28	100.17	100.12	100.02	100.11	100.06	100.2	100.21	99.76	99.75	99.98	99.91	99.89	100.33
Ba	310	230	135	140	365	275	220	300	270	195	360	610	405	225	235	60
Rb	47	28.5	1.4	1.8	56	33	20	39.5	32.5	16	42.5	33	28.5	16.5	19	1.2
Sr	290	389	336	342	297	308	346	286	317	345	291	367	326	288	283	431
Pb	8	7	5	5	9	8	7	7	8	6	7	9	8	8	8	20
Th	4.6	2.8	0.2	0.2	3.2	3.2	2.8	4.8	3.6	1.2	5.2	3.8	2.4	1	1.8	1.6
U	1.6	1	0.2	0.2	1.2	1.2	1.2	1.6	1	0.4	1.2	0.8	0.4	0.4	0.6	0.2
Zr	121	73	41	30	134	104	79	104	106	62	143	92	165	32	35	14
Nb	3	2.5	2.5	3	4.5	3	3	2.5	3	2.5	3	4	5	2	2	0.5
Y	22	17	16	16	25	21	19	21	19	17	22	8	34	20	26	8
La	10	8	6	5	12	9	8	9	9	8	10	11	12	8	10	1
Ce	26	22	15	14	34	26	22	26	26	19	29	28	35	21	25	4
Sc	25	26	36	36	20	28	33	28	26	33	26	6	29	37	41	41
V	170	204	251	236	124	166	193	163	161	212	173	49	107	239	235	496
Cr	23	37	22	19	17	25	42	22	41	40	23	5	9	28	31	40
Mn																
Co	23	26	30	27	22	23	28	22	24	28	23	10	14	32	34	55
Ni	15	20	13	11	10	16	22	14	20	20	14	5	6	15	17	28
Cu	58	39	38	43	18	73	75	46	54	98	64	4	34	21	23	34
Zn	79	97	109	111	85	84	89	76	76	92	87	69	94	102	95	85
Ga	16.4	18.6	20.4	20.6	18	17	18	16.8	17.2	18.6	17.4	17	19.2	18	17.8	

Table 3.1: Whole rock geochemical analyses of WKB (Western Cretaceous Batholith) samples. Major elements in oxide weight per cent; minor elements in ppm. Analyses provided by Dr. B. W. Chappell of the Australian National University, Canberra, Australia.

Sample #	WKB 50	WKB 51	WKB 52	WKB 53	WKB 54	WKB 55	WKB 56	WKB 57	WKB 58	WKB 59	WKB 60	WKB 61	WKB 62	WKB 63	WKB 64	WKB 65
SiO2	44.32	43.74	47	43.51	45.17	43.41	48.23	72.4	73	73.67	73.67	73.55	73.61	58.31	59.36	49.08
TiO2	0.4	0.11	0.53	0.2	0.27	1.08	0.73	0.23	0.22	0.24	0.23	0.24	0.25	0.93	0.83	1.25
Al2O3	22.53	23.83	22.74	23.38	29.72	16.93	19.86	14.76	14.46	14.17	14.16	14.14	14.17	16.89	16.83	15.48
Fe2O3	2.91	2.3	2.36	1.84	1.63	3.74	3.56	0.57	0.7	0.56	0.86	0.88	0.61	2.29	2.04	3.9
FeO	4.34	5.25	4.53	5.65	2.25	7.87	5.83	1.25	1.06	1.06	0.76	0.77	1.05	4.97	4.54	9.09
MnO	0.13	0.13	0.15	0.12	0.07	0.2	0.16	0.08	0.09	0.09	0.06	0.07	0.06	0.14	0.13	0.23
MgO	7.91	10.08	6.27	9.77	2.03	11.78	6.33	0.64	0.61	0.46	0.53	0.51	0.54	3.34	3.19	8.99
CaO	14.41	12.76	13.45	13.47	15.55	10.94	10.71	2.06	2.34	1.67	1.67	1.72	1.86	6.91	6.68	9.63
Na2O	1.03	0.93	1.76	0.96	1.81	1.8	2.72	4.49	4.56	4.51	4.49	4.5	4.59	3.44	3.36	1.75
K2O	0.06	0.04	0.07	0.03	0.04	0.17	0.06	2.02	1.96	2.6	2.56	2.59	2.33	1.05	1.39	0.09
P2O5	0.01	0.02	0.12	0.01	0.01	0.04	0.03	0.11	0.1	0.09	0.1	0.09	0.09	0.18	0.16	0.04
S	0.02	0.02	0.02	0.03	0.02	0.07	0.02	0.02	0.02	0.02	0.02	0.02	0.02	0.02	0.06	0.09
H2O+	1.68	0.78	1.19	0.75	1.16	1.61	1.14	0.9	0.58	0.56	0.55	0.51	0.5	1.08	1.12	0.51
H2O-	0.1	0.06	0.05	0.14	0.14	0.17	0.21	0.2	0.22	0.16	0.17	0.15	0.18	0.14	0.15	0.13
CO2	0.17	0.23	0.17	0.19	0.24	0.19	0.22	0.01	0.08	0.01	0.05	0.13	0.01	0.11	0.26	0.06
rest	0.15	0.1	0.14	0.14	0.13	0.22	0.16	0.12	0.13	0.12	0.14	0.14	0.13	0.17	0.18	0.17
O=S	0.01	0.01		0.01	0.01	0.03									0.03	0.04
Total	100.16	100.37	100.53	100.17	100.23	100.19	99.95	99.84	100.11	99.97	100	99.99	99.98	99.95	100.25	100.45
Ba	45	25	55	20	30	100	65	520	525	500	615	615	510	325	440	55
Rb	0.4	0.2	0.3	0.3	0.5	0.6	0.3	38	36	40.5	55	56	49	24	40.5	0.7
Sr	478	450	498	444.1	627	360	457	221	217	222	230	228	240	333	323	309.9
Pb	16	15	15	16	14	19	17	19	19	17	19	19	19	19	20	19
Th	2.4	1.6	1.8	1.8	1.2	1.8	2	5.6	7	6.2	8.4	8.6	9.2	4.4	6	1
U	0.2	0.2	0.2	0.4	0.2	0.2	0.2	1	0.8	1.2	0.4	0.8	1.6	0.2	1.4	0.2
Zr	6	3	20	5	3	31	5	103	98	99	143	153	150	156	145	12
Nb	0.5	0.5	0.5	0.5	1	1.5	0.5	5.5	5.5	5.5	7	7	6.5	3.5	4	1
Y	5	2	11	3	3	16	8	13	15	11	13	15	13	26	27	8
La	1	1	3	1	1	3	1	14	14	14	17	17	16	12	12	1
Ce	2	3	9	2	4	7	5	32	33	33	36	41	38	31	34	2
Sc	31	10	30	19	12	38	32	4	4	4	3	2	3	24	24	42
V	136	33	84	81	99	255	308	17	17	17	14	15	14	168	157	407
Cr	183	23	186	218	108	367	55	2	2	3	1	2	2	27	28	87
Mn																
Co	56	71	42	66	15	66	46	4	3	4	2	3	4	23	23	49
Ni	52	109	42	86	19	166	32	1	1	2	1	1	1	12	14	27
Cu	53	11	5	29	14	42	22	2	4	1	1	1	1	20	49	34
Zn	51	55	71	52	34	107	89	44	79	45	37	41	39	93	87	134
Ga																

Table 3.1: Whole rock geochemical analyses of WKB (Western Cretaceous Batholith) samples. Major elements in oxide weight per cent; minor elements in ppm. Analyses provided by Dr. B. W. Chappell of the Australian National University, Canberra, Australia.

Sample #	WKB 66	WKB 67	WKB 68	WKB 69	WKB 70	WKB 71	WKB 72	WKB 73	WKB 74	WKB 75	WKB 76	WKB 77	WKB 78	WKB 79	WKB 80	WKB 81
SiO2	49.68	45.85	59.46	70.95	71.13	51.02	42.84	77.58	67	49.25	45.88	51.84	58.33	56.19	55.29	46.31
TiO2	0.99	0.33	0.78	0.48	0.48	1.15	0.16	0.17	0.63	0.99	0.17	0.96	0.77	0.96	0.88	0.88
Al2O3	19.3	22.69	16.15	14.1	14.07	19.67	25.85	11.5	15.41	19.26	22.01	19.19	20.08	16.7	18.68	17.36
Fe2O3	1.82	1.69	1.33	0.73	1.2	3.9	1.73	0.57	1.73	3.48	1.29	3.25	2.54	2.54	3.39	3.82
FeO	7.22	4.99	5.08	2.06	1.64	5.81	5.67	0.35	2.6	6.43	3.76	5.68	2.93	5.11	4.65	6.22
MnO	0.17	0.12	0.13	0.06	0.06	0.19	0.1	0.01	0.05	0.17	0.1	0.16	0.08	0.15	0.14	0.14
MgO	6.23	6.91	4.06	0.72	0.65	4.78	8.43	0.14	1.59	6.26	8.96	4.84	2.22	4.49	3.29	8.4
CaO	10.59	14.09	6.76	2.42	2.29	9.36	13.66	0.48	3.52	10.25	15.78	9.61	6.81	7.76	7.02	13.84
Na2O	2.54	1.12	3.05	4.17	4.13	3.31	0.94	1.68	3.92	2.63	0.91	3.48	4.85	3.33	4.11	1.44
K2O	0.11	0.09	1.74	2.95	3.21	0.26	0.02	6.79	1.64	0.11	0.07	0.33	0.62	1.04	1.41	0.22
P2O5	0.13	0.02	0.14	0.13	0.12	0.27	0.01	0.01	0.13	0.04	0.02	0.17	0.23	0.22	0.28	0.05
S	0.02	0.05	0.02	0.02	0.02	0.02	0.03	0.02	0.02	0.02	0.02	0.02	0.02	0.02	0.02	0.07
H2O+	0.75	1.85	1.27	0.82	0.4	0.29										
H2O-	0.12	0.19	0.14	0.18	0.19	0.1										
CO2	0.26	0.08	0.01	0.3	0.17	0.12										
rest	0.16	0.14	0.18	0.18	0.18	0.15	0.11	0.09	0.09	0.11	0.13	0.11	0.12	0.15	0.12	0.14
O=S		0.02					0.01									0.03
Total	100.07	100.19	100.28	100.25	99.92	100.38	99.53	99.36	98.31	98.98	99.08	99.62	99.58	98.64	99.26	98.86
Ba	105	35	330	620	650	165	6	600	340	76	24	160	345	400	310	58
Rb	0.6	2	62	57	69	2.6	0.5	86	50	0.5	1	1.5	6.5	22.5	36	3.5
Sr	424	468	295	216	200	461	510	95	238	389	385	382	439	345	395	325
Pb	16	16	21	19	21	18	1	11	6	2	1	4	4	5	7	1
Th	1.6	1.6	7.2	9.6	8.2	2.2	0.4	4.4	4.6	0.2	0.4	0.6	0.8	3	2.4	0.8
U	0.2	0.2	1	1.8	1.4	0.2	0.2	0.8	0.6	0.2	0.2	0.2	0.4	0.4	0.4	0.2
Zr	24	11	128	269	256	40	3	143	116	17	10	99	249	114	86	35
Nb	1.5	0.5	3.5	7	6.5	2.5	0.5	1	3.5	1.5	0.5	2.5	3	4	3.5	1
Y	14	4	23	31	29	16	1	3	5	10	4	20	20	25	18	11
La	3	1	12	21	23	6	1	5	7	2	1	7	11	10	11	3
Ce	10	2	29	55	55	16	2	9	14	5	2	19	26	25	23	8
Sc	34	27	24	7	8	26										
V	260	164	157	51	50	206	82	6	68	262	80	203	99	200	149	379
Cr	133	128	112	6	6	28	220	1	3	34	440	41	20	85	13	145
Mn							780	70	410	1310	755	1230	630	1130	1120	1100
Co	39	47	24	6	7											
Ni	36	34	36	5	5	20	65	2	5	23	104	19	9	14	9	46
Cu	5	34	23	23	15	29	22	2	23	8	4	46	3	22	50	90
Zn	103	71	79	51	48	113	47	7	61	99	35	88	61	91	98	70
Ga							15.4	9.4	16.2	19	13.6	19.4	20.6	17.4	19.2	15.6

Table 3.1: Whole rock geochemical analyses of WKB (Western Cretaceous Batholith) samples. Major elements in oxide weight per cent; minor elements in ppm. Analyses provided by Dr. B. W. Chappell of the Australian National University, Canberra, Australia.

Sample #	WKB 82	WKB 83	WKB 84	WKB 85	WKB 86	WKB 87	WKB 88	WKB 89	WKB 90	WKB 91	WKB 92	WKB 93	WKB 94	WKB 95	WKB 96
SiO2	48.11	56	43.78	45.06	62.22	57.42	76.98	41.95	52.07	55.34	62.5	53.93	50.35	64.66	46.39
TiO2	1.12	0.65	0.26	0.05	0.78	0.86	0.06	1.49	1.06	0.87	0.74	1	0.53	0.62	0.44
Al2O3	18.64	17	12.15	32.23	15.9	17.12	12.92	20.21	18.59	17.77	16.62	18.07	15.36	15.6	19.69
Fe2O3	2.53	1.78	3.36	0.46	1.28	2.04	0.42	4.64	4.33	3.15	1.97	9.07	7.17	4.58	7.96
FeO	5.44	4.26	8.42	1.14	3.55	4.4	0.28	7.13	3.68	3.9	3.35	5.13	4.44	2.94	4.3
MnO	0.14	0.14	0.19	0.03	0.09	0.12	0.01	0.15	0.13	0.13	0.11	0.15	0.14	0.08	0.14
MgO	6.45	5.43	19.52	1.5	3.17	4.24	0.11	7.74	5.1	5.38	2.63	4.92	10.24	2.53	8.45
CaO	13.46	8.79	9.31	17.22	5	6.95	1.52	12.63	9.01	8.24	5.7	8.96	12.91	4.59	14.49
Na2O	2.39	3.21	0.98	1.25	3.82	4.1	2.79	2.03	3.81	3.71	3.99	3.32	1.89	3.86	1.26
K2O	0.27	1	0.12	0.05	2.55	1.45	4.5	0.1	0.38	0.82	1.32	0.42	0.29	2.73	0.05
P2O5	0.13	0.12	0.03	0.01	0.15	0.21	0.03	0.01	0.23	0.17	0.15	0.17	0.07	0.13	0.02
S	0.04	0.02	0.09	0.02	0.02	0.02	0.02	0.16	0.02	0.02	0.02	0.02	0.02	0.02	0.09
H2O+															
H2O-															
CO2															
rest	0.14	0.11	0.16	0.1	0.15	0.18	0.15	0.16	0.15	0.16	0.2	0.12	0.21	0.17	0.14
O=S	0.02		0.04					98.4							103.42
Total	98.84	98.49	98.33	99.1	98.66	99.09	99.76	98.32	98.54	99.64	99.28	105.26	103.6	102.49	103.38
Ba	120	250	26	22	635	385	965	18	165	240	830	190	115	555	16
Rb	1.5	25	2	1	72	37	57	0.5	4	20	29.5	3.5	2.5	66	1
Sr	390	293	219	625	280	347	215	375	441	392	299	370	258	259	330
Pb	3	5	1	1	10	9	14	1	4	5	5	4	2	10	1
Th	0.4	2.4	0.8	0.2	6.8	4.4	13.2	0.2	1.2	3.2	1.6	1	0.6	3.6	0.2
U	0.4	0.6	0.2	0.2	2.2	1.2	1.8	0.2	0.2	0.6	0.6	0.6	0.2	1.4	0.2
Zr	40	78	19	6	208	171	36	19	38	72	160	100	36	169	10
Nb	2	3.5	1	1	6.5	5	1	1	3.5	4	3.5	2.5	2	4.5	1
Y	19	17	5	1	19	23	1	16	15	16	14	20	11	13	6
La	5	11	2	1	13	15	5	1	9	10	10	7	4	8	1
Ce	14	25	3	1	31	39	7	3	21	21	21	16	8	17	2
Sc															
V	246	140	93	13	109	146	9	435	193	155	114	213	162	91	170
Cr	221	93	765	66	79	84	7	67	63	112	31	55	595	51	271
Mn	1070	1070	1490	240	675	915	48	1130	1040	970	860	1160	1030	620	1060
Co															
Ni	44	41	485	16	42	47	4	35	47	62	15	22	159	27	42
Cu	67	47	36	2	37	24	7	53	50	54	10	61	71	7	79
Zn	66	65	86	14	62	79	6	86	80	76	64	92	58	52	58
Ga	17.4	16.2	9.2	17.8	16.2	18.2	11.2	18.2	19.4	18.4	16.8	18.6	12.6	16.2	14

Table 3.1: Whole rock geochemical analyses of WKB (Western Cretaceous Batholith) samples. Major elements in oxide weight per cent; minor elements in ppm. Analyses provided by Dr. B. W. Chappell of the Australian National University, Canberra, Australia.

Sample #	WKB 97	WKB 98	WKB 99	WKB 100	WKB 101	WKB 102	WKB 103	WKB 104	WKB 105	WKB 106	WKB 107	WKB 108	WKB 109	WKB 110
SiO2	43.28	50.16	53.41	53.51	57.18	76.11	70.95	67.78	58	73.75	49.49	50.15	46.52	58.79
TiO2	0.8	1.58	0.73	1.53	0.92	0.14	0.38	0.58	0.89	0.24	0.75	0.74	0.3	0.54
Al2O3	24.53	19.4	19.12	19.4	19.03	12.68	14.72	14.87	17.14	14.01	17.03	17.02	19.94	18.43
Fe2O3	8.69	10.44	7.53	8.76	6.29	1.1	2.69	4.12	7.3	1.59	8.14	7.2	7.25	7.9
FeO														
MnO	0.09	0.16	0.13	0.13	0.13	0.01	0.04	0.07	0.11	0.02	0.12	0.12	0.11	0.16
MgO	5.87	3.93	4.87	2.76	2.74	0.22	0.72	1.72	3.7	0.44	8.03	7.48	9.72	2.3
CaO	14.03	8.52	8.13	7.59	6.91	1.09	2.22	3.71	7.19	1.76	13.67	13.89	14.12	6.25
Na2O	1.55	4.38	3.52	4.41	4.43	2.66	3.55	3.8	3.63	3.4	1.82	2.34	1.42	4.1
K2O	0.1	0.83	1.31	0.74	1.09	5.45	4	2.94	1.26	3.37	0.45	0.27	0.12	0.65
P2O5	0.02	0.33	0.18	0.72	0.21	0.06	0.17	0.09	0.15	0.11	0.06	0.08	0.03	0.23
S	0.02	0	0	0	0.01	0.01	0	0	0.01	0.01	0.05	0	0.06	0
H2O+														
H2O-														
CO2														
rest														
O=S														
Total														
Ba														
Rb	1	14	32.5	15.5	25.5	82	64	95	37	90	7	3.5	1.5	7.5
Sr	447	433	337	434	408	148	163	184	304	320	291	296	417	439
Pb	1	5	4	5	5	9	7	11	6	15	2	2	1	5
Th	0.2	1	1.8	2.4	1.8	3	5.8	12.2	5.8	9.4	0.6	0.8	0.4	0.4
U	0.4	0.2	0.4	1.2	0.8	0.6	1.6	3.2	1.4	1	0.2	0.2	0.2	0.2
Zr	15	190	71	156	310	92	249	121	105	175	39	48	21	83
Nb	1	7	3.5	8.5	6	1	6	5	4	9	1	1.5	1	3
Y	8	44	18	40	41	2	22	26	22	7	13	17	7	18
La														
Ce														
Sc														
V														
Cr														
Mn														
Co														
Ni	36	3	38	5	10	2	3	7	14	2	76	53	97	1
Cu	40	16	20	13	5	2	1	29	32	2	126	53	42	6
Zn	54	117	79	93	79	12	35	48	76	56	62	58	52	114
Ga	17.4	22.2	17.4	21.8	20.2	10	15	15	17.2	17.2	14.2	14.4	13.6	19

Table 3.1: Whole rock geochemical analyses of WKB (Western Cretaceous Batholith) samples. Major elements in oxide weight per cent; minor elements in ppm. Analyses provided by Dr. B. W. Chappell of the Australian National University, Canberra, Australia.

Sample #	WKB 111	WKB 112	WKB 113	WKB 114	WKB 115	WKB 116	WKB 117	WKB 118	WKB 119	WKB 120	WKB 121	WKB 122	WKB 123	WKB 124
SiO2	73.47	48.84	56.77	59.21	71.97	77.88	86.47	61.87	64.76	56.44	44.24	40.37	44.46	56.38
TiO2	0.32	0.68	0.87	0.75	0.22	0.48	0.24	0.88	0.65	1.24	0.03	0.38	0.21	0.84
Al2O3	13.22	18.66	17.48	17.39	14.28	9.81	8.1	17.98	15.38	16.73	32.64	10.51	19.29	18.02
Fe2O3	2.21	7.56	8.12	7.21	2.27	4.91	1.2	8.05	5.41	9.05	1.75	18.39	8.95	8.29
FeO														
MnO	0.05	0.12	0.12	0.11	0.06	0.04	0.01	0.08	0.08	0.13	0.02	0.22	0.13	0.13
MgO	0.7	7.39	4.36	3.37	0.45	1.93	0.47	2.76	2.48	3.61	1.82	23.99	11.36	4.39
CaO	2.06	13.44	7.99	6.83	2.12	0.96	1.1	1.67	4.92	7.35	17.73	6.14	13.43	8.49
Na2O	3.61	2.18	3.26	3.35	4.31	1.27	0.84	1.12	3.3	3.27	0.98	0.68	0.89	3.38
K2O	2.97	0.33	0.93	1.2	3.9	1.43	0.95	2.98	2.49	1.31	0.01	0.03	0.1	0.44
P2O5	0.07	0.09	0.14	0.12	0.08	0.13	0.03	0.23	0.1	0.24	0	0.01	0.01	0.12
S	0	0.04	0	0.01	0	0.02	0	0	0	0	0	0.01	0.02	0
H2O+														
H2O-														
CO2														
rest														
O=S														
Total														
Ba														
Rb	73	2	24.5	30	70	42.5	25.5	108	88	44	0.5	0.5	2.5	2.5
Sr	167	351	339	300	248	88	146	207	236	397	720	218	294	330
Pb	8	2	5	6	15	5	5	12	14	6	1	1	1	4
Th	7	0.2	2.4	5.6	22	4.4	4.8	9	7.8	4.8	0.2	0.2	0.8	0.6
U	2	0.2	1	1.2	4.6	1	1.2	2.4	2.4	1	0.2	0.2	0.2	0.2
Zr	151	52	106	89	174	109	80	170	217	162	3	4	13	129
Nb	4.5	2.5	3	3	5	6	5	12	4.5	6.5	0.5	0.5	0.5	2.5
Y	12	15	20	19	36	14	9	24	28	31	1	3	5	21
La														
Ce														
Sc														
V														
Cr														
Mn														
Co														
Ni	3	47	26	10	1	48	16	83	11	5	5	58	36	14
Cu	6	94	64	26	16	16	1	65	43	78	1	2	8	59
Zn	29	63	85	77	34	64	24	121	67	98	10	115	61	82
Ga	12.4	16	17.6	17	13.2	11	8.6	20	15.2	19.8	19.4	7.6	13.2	18.4

Table 3.1: Whole rock geochemical analyses of WKB (Western Cretaceous Batholith) samples. Major elements in oxide weight per cent; minor elements in ppm. Analyses provided by Dr. B. W. Chappell of the Australian National University, Canberra, Australia.

Sample #	WKB 125	WKB 126
SiO2	41.49	43.16
TiO2	1.55	0.41
Al2O3	20.16	26.19
Fe2O3	13.7	6.5
FeO		
MnO	0.17	0.07
MgO	7.58	8.02
CaO	13.14	14.84
Na2O	1.7	1.01
K2O	0.13	0.03
P2O5	0.01	0
S	0.19	0.01
H2O+		
H2O-		
CO2		
rest		
O=S		
Total		
Ba		
Rb	0.5	0.5
Sr	328	535
Pb	1	1
Th	0.2	0.2
U	0.2	0.2
Zr	24	5
Nb	1	0.5
Y	29	3
La		
Ce		
Sc		
V		
Cr		
Mn		
Co		
Ni	15	21
Cu	82	6
Zn	99	35
Ga	20.2	15.8

Table 3.1: Whole rock geochemical analyses of WKB (Western Cretaceous Batholith) samples. Major elements in oxide weight per cent; minor elements in ppm. Analyses provided by Dr. B. W. Chappell of the Australian National University, Canberra, Australia.

Table 3.2: Parameters for fractional crystallization model.

Oxide (wt.%)	Start A	End A	Start B	End B	Start C	End C	Start D	End D	Final
SiO_2	50.94	55.90	55.98	58.37	58.37	63.5	63.40	71.59	71.68
TiO_2	0.97	0.58	0.88	0.90	0.87	0.72	0.79	0.48	0.41
Al_2O_3	19.36	18.3	17.97	17.29	17.4	16.20	16.20	14.42	14.95
FeO*	8.76	6.85	6.82	6.41	6.34	4.45	4.79	2.34	2.64
MgO	5.81	5.60	5.44	4.22	4.31	3.62	3.23	1.01	1.02
CaO	10.90	8.93	8.33	7.46	7.06	5.24	5.09	3.74	2.64
Na_2O	2.75	2.84	3.75	3.85	4.17	4.05	3.89	3.79	4.37
K_2O	0.51	1.00	0.83	1.19	1.47	2.21	2.60	2.65	2.29

(1) Fractional crystallization model written, explained and graciously provided by Dr. M. B. Baker (CIT).
(2) Start A and Final compositions derived by extrapolating best fit curves on the appropriate Harker variation diagrams for WKB suite to 50.0 and 70.0 weight % SiO_2 respectively. This range corresponds to a range of MgO between 5.4 and 1 weight %. Start B, C and D compositions are normalized compositions from actual WKB samples which were chosen as petrographically representative of the suite; sample B = WKB91, C = WKB87, D = WKB86. End A, B ,C and D compositions were generated by the fractional crystallization model using the preceding Start composition as the parent magma. Each large step consists of multiple steps of 2% crystallization of magma.
(3) The per cent proportions of crystallizing phases used for each step of the fraction model are as follows (plagioclase: clinopyroxene: orthopyroxene: amphibole: biotite: sphene: ilmenite)
Step A = 60: 12: 7: 13: 0: 6: 2; Step B = 61: 6: 15: 15: 0: 2: 1;
Step C = 60: 4: 0: 30: 0: 5: 1; Step D = 50: 5: 0: 20: 22: 2: 1.
Mineral compositions used in each step of the model correspond to the analyzed mineral compositions for the specific starting WKB sample (or closest available sample) used in that step (Table 2.1).
(4) Mineral K_D values (QFM conditions): clinopyroxene = 0.35; amphibole = 0.56; biotite = 0.56, where

$$K_D = \left(\frac{X_{Fe}^{xl} X_{Mg}^{liq}}{X_{Mg}^{xl} X_{Fe}^{liq}} \right), \text{ and } K_D^{plag} = \left(\frac{X_{Ca}^{pl} X_{Na}^{liq}}{X_{Na}^{pl} X_{Ca}^{liq}} \right) = 1$$

sample number	lithology	mode (plag:px:hb)	unit	$\delta^{18}O$ plagioclase (+‰)	$\delta^{18}O$ mafic (+‰)	$\delta^{18}O$ whole rock (+‰)	Δ plag-mafic (+‰)	T (°C)
WBK75	2 px leucogabbro	(70:30:0)	Kpg	7.0	6.1	6.9	0.9	820
WBK128	hb norite	(65:30:5)	Khpg	7.3	6.4	6.9	0.9	820
WBK90	2 px leucogabbro	(70:25:5)	Kpg	7.5	6.4	6.8	1.1	716
WBK94	hb gabbro	(55:0:45)	Khg	7.8	6.4	6.6	1.4	683

Table 3.3: Oxygen isotope data and calculated mineral pair temperatures from the Stokes Mountain region.

Abbreviations: plag = plagioclase; px = pyroxene; hb = hornblende; "mafic" refers to pyroxene except for sample WBK94 in which mafic refers to hornblende.
Temperatures calculated using the following equations from Bottinga and Javoy (1975):
$\Delta_{plag\text{-}px} = (1.076 \times 10^6)/T^2$ (K) and $\Delta_{plag\text{-}amph} = -0.30 + (1.554 \times 10^6)/T^2$ (K).

Sample #	Unit	SiO_2 (wt. %)	$\delta^{18}O$ (‰)
WKB2		71.23	*8.1
WKB3	Khtr	44.18	*6.6
WKB7	Kpg	53.97	7.0
WKB9		40.92	*6.4
WKB17		60.21	*6.8
WKB20		66.60	*8.3
WKB23	Kgd	63.89	8.4
WKB27		65.32	*9.5
WKB29	Kphg	56.75	*6.9
WKB30		59.94	*7.1
WKB33	Kphg	58.36	*6.8
WKB34	Kphg	59.65	7.2
WKB35	Kphg	55.21	*7.2
WKB37		51.21	*7.3
WKB38		59.29	*6.5
WKB41		58.75	*6.8
WKB43		54.18	*6.6
WKB44		59.16	*6.3
WKB53	Khtr	43.51	7.0
WKB59		73.67	*9.0
WKB60		73.67	*7.4
WKB64		59.36	*8.1
WKB65	Khbt?	49.08	7.8
WKB72	Khtr	42.84	7.1
WKB73	Kgd	77.58	7.3
WKB74	Khbt	67.00	7.7
WKB75	Kpg	49.25	6.9
WKB77	Kphg	51.84	6.9
WKB78	Kphg	58.33	8.0
WKB79	Khg	56.19	8.0
WKB80	Khg	55.29	7.4
WKB81	Khtr	46.31	7.0
WKB83	Khg	56.00	7.5
WKB85	Khtr	45.06	7.1
WKB86	Khbt	62.22	7.0
WKB87	Kpht	57.42	6.7
WKB88	Kgd	76.98	8.0
WKB89	Khg	41.95	6.6
WKB90	Kpg	52.07	6.7

Table 3.4: $\delta^{18}O$ and SiO_2 analyses for selected WKB samples.
SiO_2 analyses provided by Dr. B. W. Chappell (ANU).
Unit designated if sample is located within study area.
* 18 samples analyzed for $\delta^{18}O$ by Dr. C. A. Manduca (CIT).

Sample #	Unit	SiO_2 (wt. %)	$\delta^{18}O$ (‰)
WKB91	Kphg	55.34	6.7
WKB92	Kphg	62.50	7.9
WKB93	Kphg	53.93	7.1
WKB94	Khg	50.35	6.6
WKB95	Khbt	64.66	7.2
WKB96	Kphg	46.39	6.5
WKB97	Khtr	43.28	6.9
WKB98	Khg	50.16	8.2
WKB102	Kgd	76.11	8.5
WKB103	Kgd	70.95	8.7
WKB104	Kp	67.78	7.4
WKB105	Khbt	58.00	7.4
WKB106	Kgd	76.75	9.8
WKB107	Khg	49.49	6.6
WKB108	Khtr	50.15	6.6
WKB109	Khtr	46.52	6.9
WKB111	Kgd	73.47	8.2
WKB115	Kgd	71.97	8.7
WKB116	m	77.88	17.7
WKB117	m	86.47	13.9
WKB118	m	61.87	14.7
WKB119	Kp	64.76	4.0
WKB121	Khtr	44.24	7.4
WKB125	Khg	41.49	7.0
WKB126	Kphg	43.16	7.9
WKB127	Kgd	n/a	8.1
WKB128	Kphg	n/a	6.9
WKB129	Kp	n/a	3.6
WKB130	Kgd	n/a	8.9
WKB131	Khbt	n/a	7.0
WKB132	Khbt	n/a	7.8
A125	Khbt	n/a	8.2
A128	Kgd	n/a	8.8
SM149	Kp	n/a	4.7
SM155	Kp	n/a	1.1
SM198	Kpht	n/a	7.1

Table 3.4 (cont.): $\delta^{18}O$ and SiO_2 analyses for selected WKB samples. Table also includes $\delta^{18}O$ for isolated samples from Stokes Mountain (SM) and Auckland (A) quadrangles.
SiO_2 analyses provided by Dr. B. W. Chappell (ANU).
Unit designated if sample is located within study area.
* 18 samples analyzed for $\delta^{18}O$ by Dr. C. A. Manduca (Carleton College).

Sample #	Rb (ppm)	Sr (ppm)	$^{87}Rb/^{86}Sr$	$^{87}Sr/^{86}Sr(0)$	$^{87}Sr/^{86}Sr(115)$
WKB7*	6.31	355.1	n/a	0.70389	0.70380
WKB23	57.77	282.4	0.5880	0.704898	0.70394
WKB53*	0.330	444.1	n/a	0.70373	0.70372
WKB65*	0.719	309.9	n/a	0.70403	0.70402
WKB75	0.467	391.8	3.423×10^{-3}	0.703810	0.70380
WKB77	1.926	383.4	1.444×10^{-2}	0.703863	0.70384
WKB79	23.56	350.0	0.1935	0.704160	0.70384
WKB80	38.35	397.0	0.2777	0.704192	0.70374
WKB85	1.036	632.0	4.711×10^{-3}	0.703763	0.70376
WKB86	74.44	283.0	0.7562	0.705319	0.70408
WKB87	38.41	350.5	0.3150	0.704434	0.70392
WKB90	3.562	446.7	2.292×10^{-2}	0.703807	0.70377
WKB91	17.2	393.9	0.1259	0.703974	0.70377
WKB92	29.95	303.6	0.2836	0.704314	0.70385
WKB94	2.562	258.1	2.854×10^{-2}	0.703592	0.70354
WKB105	39.00	311.8	0.3596	0.704232	0.70364
WKB106	89.95	313.4	0.8251	0.706834	0.70548
WKB107	7.640	294.6	7.454×10^{-2}	0.703655	0.70353
WKB109	1.642	418.4	1.128×10^{-2}	0.703400	0.70338
WKB118	111.7	209.6	1.533	0.709516	0.70701
WKB127	56.61	211.6	0.7693	0.705056	0.70380
WKB128	1.665	382.0	1.253×10^{-2}	0.703783	0.70376

Table 3.5: Rb-Sr isotopic data for WKB samples.

Estimated 2σ uncertainties: $^{87}Rb/^{86}Sr$ = 2‰; $^{87}Sr/^{86}Sr$ = 0.025‰.
Estimate for initial ratio does not include age uncertainty. $\lambda_{Rb} = 1.42 \times 10^{-11} a^{-1}$.
* Analysis provided by Dr. D. A. Pickett (CIT).

Sample #	Sm (ppm)	Nd (ppm)	$^{147}Sm/^{144}Nd$	ε_{Nd} (0)	ε_{Nd} (115)
WKB7*	3.060	11.57	n/a	4.6	5.1
WKB23	4.864	21.66	0.1357	3.6	4.5
WKB53*	0.3650	1.165	n/a	4.9	5.0
WKB65*	0.933	2.818	n/a	3.4	3.3
WKB75	1.213	4.258	0.1722	4.8	5.1
WKB77	3.087	12.04	0.1550	4.5	5.1
WKB79	4.052	15.81	0.1549	3.6	4.2
WKB80	3.407	13.52	0.1524	4.0	4.7
WKB85	0.2199	1.027	0.1295	4.7	5.7
WKB86	3.978	18.64	0.1290	3.2	4.2
WKB87	4.637	20.37	0.1376	4.0	4.9
WKB90	2.969	12.44	0.1443	4.4	5.2
WKB91	3.200	13.54	0.1429	3.8	4.6
WKB92	2.543	11.18	0.1376	3.6	4.5
WKB94	1.766	6.200	0.1722	5.7	6.1
WKB105	3.895	16.14	0.1459	4.9	5.6
WKB106	3.935	23.66	0.1005	-2.3	-0.87
WKB107	1.988	6.530	0.1841	5.7	5.9
WKB109	1.024	3.486	0.1776	5.4	5.7
WKB118	5.154	26.17	0.1191	-4.9	-3.7
WKB127	1.545	9.651	9.687×10^{-2}	3.1	4.6
WKB128	0.6644	2.165	0.1855	4.6	4.8

Table 3.6: Sm-Nd isotopic data for WKB samples.

Estimated 2σ uncertainties: $^{147}Sm/^{144}Nd$ = 2‰; $^{143}Nd/^{144}Nd$ = 0.03‰ (0.3ε). For initial ratio, estimate does not include the age uncertainty. eNd (t) calculated as in DePaolo and Wasserburg (1976) with $^{143}Nd/^{144}Nd_{CHUR}(0)$ = 0.512638, $^{147}Sm/^{144}Nd_{CHUR}$ = 0.1966, $\lambda_{Sm} = 6.54 \times 10^{-12} a^{-1}$.
* Analysis provided by Dr. D. A. Pickett (CIT).

Sample #	Unit	SiO_2 (wt. %)	$\delta^{18}O$ (‰)	Sr_i (115)	ε_{Nd} (115)
WKB7	Kpg	53.97	7.0	*0.70380	*5.1
WKB23	Kgd	63.89	8.4	0.70394	4.5
WKB53	Khtr	43.51	7.0	*0.70372	*5.0
WKB65	Khbt	49.08	7.8	*0.70402	*3.3
WKB75	Kpg	49.25	6.9	0.70380	5.1
WKB77	Kphg	51.84	6.9	0.70384	5.1
WKB79	Khg	56.19	8.0	0.70384	4.2
WKB80	Khg	55.29	7.4	0.70374	4.7
WKB85	Khtr	45.06	7.1	0.70376	5.7
WKB86	Khbt	62.22	7.0	0.70408	4.2
WKB87	Kpht	57.42	6.7	0.70392	4.9
WKB90	Kpg	52.07	6.7	0.70377	5.2
WKB91	Kphg	55.34	6.7	0.70377	4.6
WKB92	Kphg	62.50	7.9	0.70385	4.5
WKB94	Khg	50.35	6.6	0.70354	6.1
WKB105	Khbt	58.00	7.4	0.70364	5.6
WKB106	Kgd	76.75	9.8	0.70548	-0.87
WKB107	Khg	49.49	6.6	0.70353	5.9
WKB109	Khtr	46.52	6.9	0.70338	5.7
WKB118	m	61.87	14.7	0.70701	-3.7
WKB127	Kgd	n/a	8.1	0.70380	4.6
WKB128	Kphg	n/a	6.9	0.70376	4.8

Table 3.7: Summary of $Sr_{(115)}$ and $\varepsilon Nd_{(115)}$ with SiO_2 and $\delta^{18}O$ for WKB samples.
* Sr and Nd isotopic analyses for 3 samples provided by Dr. D. A. Pickett (CIT).

Table 3.8: Approximate latitude and longitude of WKB sample locations for those samples collected prior to this study. Accurate locations for samples within the Stokes Mountain region shown on Plate 2.

Sample #	Latitude (N)	Longitude (E)	Sample #	Latitude (N)	Longitude (E)
WKB1	36°11'35 "	119°00'40"	WKB39	36°42'21"	119°21'54"
WKB2	36°18'03"	119°05'35"	WKB40	36°42'13"	119°21'44"
WKB3	Plate 2	Plate 2	WKB41	36°42'25"	119°20'19"
WKB4	Plate 2	Plate 2	WKB42	36°43'03"	119°18'47"
WKB5	Plate 2	Plate 2	WKB43	36°43'11"	119°17'57"
WKB6	Plate 2	Plate 2	WKB44	36°42'55"	119°17'01"
WKB7	Plate 2	Plate 2	WKB45	36°42'39"	119°17'27"
WKB8	36°51'36 "	119°21'14"	WKB46	36°41'36"	119°18'37"
WKB9	36°51'44 "	119°32'52"	WKB47	36°40'55"	119°19'23"
WKB10	36°52'22 "	119°32'11"	WKB48	36°42'32"	119°15'35"
WKB11	36°53'23 "	119°31'41"	WKB49	Plate 2	Plate 2
WKB12	36°53'48"	119°30'40"	WKB50	Plate 2	Plate 2
WKB13	36°53'40"	119°29'25"	WKB51	Plate 2	Plate 2
WKB14	36°53'14"	119°27'59"	WKB52	Plate 2	Plate 2
WKB15	36°53'02"	119°27'54"	WKB53	Plate 2	Plate 2
WKB16	36°52'46"	119°26'30"	WKB54	Plate 2	Plate 2
WKB17	36°51'08"	119°27'57"	WKB55	Plate 2	Plate 2
WKB18	36°20'52"	119°03'30"	WKB56	Plate 2	Plate 2
WKB19	36°25'05"	118°59'50"	WKB57	36°12'32"	119°00'20"
WKB20	36°23'52"	118°56'20"	WKB58	36°13'05"	119°00'00"
WKB21	36°25'22"	118°56'10"	WKB59	36°12'16"	119°00'40"
WKB22	36°27'41"	119°01'30"	WKB60	36°05'10"	118°58'00"
WKB23	36°28'42"	119°01'10"	WKB61	36°05'02"	118°58'00"
WKB24	36°25'05"	119°01'10"	WKB62	36°04'46"	118°58'10"
WKB25	Plate 2	Plate 2	WKB63	36°07'05"	118°57'10"
WKB26	Plate 2	Plate 2	WKB64	36°09'16"	118°57'20"
WKB27	36°37'05"	119°04'05"	WKB65	35°56'56"	118°52'50"
WKB28	36°38'19"	119°06'50"	WKB66	35°57'00"	118°53'20"
WKB29	Plate 2	Plate 2	WKB67	35°57'32"	118°53'30"
WKB30	36°39'08"	119°07'40"	WKB68	35°56'27"	118°56'10"
WKB31	Plate 2	Plate 2	WKB69	36°17'23"	119°04'55"
WKB32	Plate 2	Plate 2	WKB70	36°17'47"	119°05'15"
WKB33	Plate 2	Plate 2	WKB71	36°17'07"	118°58'10"
WKB34	Plate 2	Plate 2			
WKB35	Plate 2	Plate 2			
WKB36	36°42'14"	119°23'56"			
WKB37	36°42'22"	119°24'00"			
WKB38	36°42'31"	119°23'36"			

Chapter 4: Introduction to The Ivrea and Strona-Ceneri Zones

Direct study of the lower continental crust requires extremely unusual geologic circumstances. The difficulty of moving a sufficiently large mass of lower crustal material tens of kilometers vertically through the crust without completely destroying its original character makes the exposure of a useful crustal cross section seem highly unlikely. Fortunately, an auspicious combination of geologic events appears to have produced a small number of possible sections. The best exposed, best studied and most accepted example of such a crustal cross section is the Italian Ivrea-Verbano Zone. This reputation motivated our selection of the Ivrea Zone for the study of the oxygen isotope systematics of lower continental crust.

The Ivrea Zone presents a prime opportunity for the in situ study of igneous activity in the lower continental crust environment as it contains a large volume of igneous material, not the least of which is an extensive, layered ultramafic-mafic body known as the Mafic Complex. The focus of this investigation is the characterization of the oxygen isotope systematics of the Mafic Complex and the associated igneous rocks. The data will be interpreted in Chapter 5 with the goal of identifying the magmatic processes responsible for the growth of lower crust through additions of mantle-derived magma. The interpretations will be extended to possible implications for the oxygen isotope systematics of Hercynian igneous rocks found at higher crustal levels, both in the Strona-Ceneri Zone and in the northern European Alps.

The present chapter consists of a review of the pertinent geophysical, structural, and petrological data concerning the Ivrea and Strona-Ceneri Zones necessary for the interpretation of the oxygen isotopic data. Important questions which must be addressed prior to interpreting the isotopic systematics include the following: what rocks constitute this example of lower crust?; what is the nature of igneous activity in the lower crust?; is there a possible relationship to igneous rocks in higher parts of the section?; are the geological circumstances favorable to the preservation of the igneous isotopic signatures?

4.1. The Ivrea Zone as a Lower Crustal Cross Section

The Ivrea-Verbano Zone, or Ivrea Zone, is located in the northwest corner of Italy in the Southern Alps (Figs. 4.1 and 4.2). The Ivrea Zone consists of a near vertically dipping section of ultramafic-mafic igneous rocks and high grade metamorphic rocks (Fig. 4.2). A major fault, the Periadriatic Line, known locally as the Insubric Line (Gansser, 1968), bounds the northwest margin of the Ivrea Zone separating it from the Alpine orogen which formed during collision of the European and Adriatic plates. Another fault complex, the Pogallo Line (Fig. 4.3) (Handy, 1986), separates the Ivrea Zone from the Strona-Ceneri Zone to the southeast; this zone is composed of intermediate grade paraschists and orthogneisses. Lastly the Cremosina Line juxtaposes a Permo-Mesozoic volcano-sedimentary sequence against the Strona-Ceneri Zone at its southern margin.

Although the tectonometamorphic histories of these structural units are not completely understood, there is a general consensus that these zones once occupied various depth levels in a single continental plate (the Adriatic?): the Ivrea Zone in the lowermost crust in contact with upper mantle peridotites; the Strona-Ceneri Zone at mid-crustal levels; the volcanosedimentary suite at the surface. Subsequent early Mesozoic ductile extension attenuated the original crustal section (Brodie and Rutter, 1987; Handy and Zingg, 1991), but did not obliterate the predeformational lithologic characteristics and structural relationships.

Final rotation, obduction and emplacement of the Ivrea-Strona-Ceneri crustal section into the upper crust occurred during the Cenozoic Alpine orogeny (Schmid et al., 1987). The effects of this orogeny within the Ivrea Zone are surprisingly minor. Early Alpine effects are limited to mylonitization along the bounding faults and anticlinal folding adjacent to the Insubric Line (Schmid, 1967; Brodie and Rutter, 1987). Subsequently, during the Neogene, additional uplift associated with backthrusting of the Central Alps over the Southern Alps truncated a hypothesized antiform along the Insubric

Line (Fig. 4.2) (Schmid et al., 1987; Schmid et al., 1989; Zingg et al., 1990). The subvertically oriented Ivrea and Strona-Ceneri Zones are exposed in the dismembered southern limb of this antiform. Deformation during the Neogene stage of the Alpine orogeny was limited to faulting along the Insubric Line during dextral transpressive motion (Handy and Zingg, 1991).

Each of the structural units contains Hercynian igneous rocks: a compound, ultramafic-intermediate, layered igneous complex (285-270 Ma) in the Ivrea Zone (Pin, 1986; Voshage et al., 1988); a dominantly granitic suite containing lesser gabbroic material (295-275 Ma) in the Strona-Ceneri Zone (Koppel and Grunenfelder, 1978/79; Hunziker and Zingg, 1980; Pinarelli et al., 1988); and a dominantly acidic, volcanic suite (262 ± 1 Ma) in the overlying Permo-Mesozoic M. Nudo and Generoso basins (Stille and Buletti, 1987). Note that the igneous rocks are approximately contemporaneous and demonstrate a decrease in age upwards through the proposed crustal section. Based on chemical and isotopic evidence many researchers have suggested that these igneous suites are comagmatic (Fountain, 1986; Pin, 1986; Stille and Buletti, 1987). If this hypothesis is true then the Ivrea-Strona-Ceneri-M. Nudo section may expose different structural levels within a single Hercynian magmatic suite (Handy and Zingg, 1991).

The geophysical and petrologic data discussed below support the interpretation that the Ivrea and the neighboring Strona-Ceneri Zones expose an attenuated cross section through pre-Alpine, lowermost to middle continental crust (Mehnert, 1975; Fountain, 1976). The overlying Permo-Mesozoic volcanosedimentary section was not part of the present isotopic investigation and will be excluded from all but the summary discussion.

4.1.1. Geophysical Characteristics

The arcuate Ivrea geophysical body is defined by the presence of marked positive gravity and magnetic anomalies as well as a seismological signature indicating the presence of mantle material in the upper crust (Giese, 1968; Berckhemer, 1969; Zingg,

1990). The geophysical anomaly is modeled as an fan-shaped wedge of mantle material which slopes upwards northwesterly from a depth of 30 km reaching approximately 3 km beneath the Ivrea Zone (Berckhemer, 1969; Mehnert, 1975; Capedri et al., 1976; Zingg and Hunziker, 1982; Frei et al., 1989; Zingg et al., 1990). Recent seismic studies indicate the presence of multiple peridotitic slivers in the Alpine continental collision zone (Bayer et al., 1987; Nicolas et al., 1990).

The Ivrea and neighboring Strona-Ceneri Zones appear to comprise a relatively coherent section through attenuated lower and middle continental crust which rests upon this uplifted upper mantle slice (Fig. 4.3). The contact between the noncumulate peridotites exposed along the Insubric Line and the surrounding layered igneous complex may in places be magmatic in origin although it is generally tectonized. This contact is often referred to as the paleoMoho; the peridotite bodies may, however, represent diapirs of upper mantle-derived material emplaced a few kilometers upwards into the lowermost crust (Vielzeuf and Kornprobst, 1982). High pressure experimental seismic velocity and density studies on schists and gneisses from the Ivrea and Strona-Ceneri Zones yield properties similar to other in situ estimates of lower and middle crustal rocks (Christensen and Fountain, 1975; Fountain, 1976; Burke and Fountain, 1990). This correlation supports the genesis of the Ivrea and Strona-Ceneri Zones in the lower and middle crustal environments, respectively.

4.1.2. Metamorphic Facies and Thermobarometry

The distribution of metamorphic facies generally supports the interpretation of the Ivrea and Strona-Ceneri Zones as a vertically tilted cross section through middle to lower continental crust. The grade of metamorphism increases from the southeast to the northwest towards the Insubric Line from lower to middle amphibolite facies in the Strona-Ceneri Zone and from middle amphibolite to lower granulite facies in the Ivrea Zone (Peyronel-Pagliani and Boriani, 1967; Schmid, 1967; Zingg, 1980). Increasing

metamorphic grade within the Ivrea Zone is demonstrated by the appearance of first clinopyroxene then orthopyroxene in mafic lithologies, the stability range of calcite + quartz + actinolite in impure marbles, and the location of the second sillimanite isograd (reaction of muscovite and quartz to form K-feldspar and sillimanite) in the metapelites (Fig. 4.4) (Zingg, 1980). Following the disappearance of muscovite in the metapelites, biotite gradually reacts with sillimanite to form garnet and K-feldspar. The net effect is the formation of acidic granulites from muscovite-bearing sillimanite biotite plagioclase gneisses. In addition, mineral proportions and compositions vary regularly with increasing grade to the northwest: the variable g = garnet/garnet + biotite increases; the Mg contents of both garnet and biotite increase; the Ti content of biotite increases (Schmid and Wood, 1976).

Interpretation of the thermobarometric data is far from unambiguous (Zingg, 1983; Zingg, 1990). Thermobarometric estimates for metamorphic rocks of the Ivrea Zone indicate conditions ranging from 4.7 to 11 kbar and from 550 to 940 ¡C (Schmid and Wood, 1976; Hunziker and Zingg, 1980; Zingg and Hunziker, 1981; Bohlen and Liotta, 1984; Schmid et al., 1988) with pressures of 8-9 kbar and temperatures of 700-800°C being preferred for the granulite facies metamorphism (Sills, 1984; Zingg et al., 1990). The granulite facies conditions are comparable to estimates for recrystallization of the base of the Mafic Complex at pressures of 8-8.5 kbar and temperatures of 750-950°C (Shervais, 1979; Rivalenti et al., 1980; Sills, 1984).

While the age of the magmatic event is fairly well constrained, the age of peak regional metamorphism is a subject of great debate with estimates ranging from 478 Ma to the late Permian (290-270 Ma). The date of 478 Ma is based on a whole rock metapelite Rb-Sr isochron (Hunziker and Zingg, 1980) which is interpreted as dating peak metamorphism resulting in strontium isotopic homogenization and possibly anatexis. Similar interpretations have been made of strontium isotope systematics during regional

metamorphism (Bickle et al., 1988); however, in this example the oxygen isotopes were also homogenized yet this did not occur in the Ivrea Zone (Chapter 5). The 478 Ma date is consistent with cross cutting relationships between the Permian plutonic rocks and metamorphic foliations (Zingg et al., 1990) indicating that the peak metamorphic conditions were pre-plutonic. A late Permian synmagmatic age is supported by the following: similar pressures and different temperatures recorded for amphibolite and granulite facies support the hypothesis that the granulite facies metamorphism resulted from intrusion of magma into or through a section already experiencing amphibolite facies metamorphism and not by burial to lower crustal depths (Schmid and Wood, 1976); the metamorphic isograds (particularly the second sillimanite isograd) are generally parallel to both the apparent igneous and metamorphic layering but are apparently deflected parallel to the margin of the intrusive complex in Val Strona di Omegna (Zingg, 1980) suggesting a contact metamorphic effect at peak conditions.

Regardless of the geochronologic debate, the general parallelism of the metamorphic isograds, the metamorphic foliation and the igneous cumulate layering suggests that intrusion and crystallization of the igneous complex occurred within horizontally foliated host rocks and that intrusion occurred prior to rotation of the section (Schmid and Wood, 1976; Hunziker and Zingg, 1980). The thermobarometric history is further discussed in section 4.6.3.

4.1.3. Structural Relationship to the Strona-Ceneri Zone

The complex structure separating the Ivrea and Strona-Ceneri Zones has been given various names, including the Cossato-Mergozzo-Brissago Line (CMB), the Pogallo Ductile Shear Zone (PDSZ), and the Pogallo Line, reflecting the multiplicity of tectonic events which have occurred along this boundary. The structure is marked by faults and, in places, high temperature mylonite zones of various ages (Boriani and Sacchi, 1974; Handy, 1986; Handy, 1987; Zingg et al., 1990). Furthermore, it separates slight lithologic

and structural differences and is associated with an increased concentration of small gabbroic, dioritic and lamproitic intrusions. The older CMB structure may separate two unrelated metamorphic sections possessing different metamorphic histories that were juxtaposed prior to Mesozoic crustal extension (Boriani et al., 1990; Handy and Zingg, 1991). In contrast, the younger PDSZ has been interpreted as an early Mesozoic, low angle normal fault which accommodated extension during oblique sinistral uplift of the Ivrea Zone relative to the Strona-Ceneri Zone. This differential uplift may account for 8 km (Handy, 1986; Handy, 1987) to 15 km (Hodges and Fountain, 1984) of missing section within the previously continuous Ivrea-Strona-Ceneri crustal column.

4.2. Petrologic Overview of the Ivrea Zone

The isotopic interpretation of the Mafic Complex which is presented in the following chapter is highly dependent upon details of the petrology of all Ivrean lithologies. In this section the major Ivrean lithologic units are defined and described; this is not, however, an attempt at a comprehensive review of petrologic investigations in the Ivrea Zone. Instead emphasis is placed on those petrologic characteristics which are significant to the interpretation of the isotopic data, while the references cited provide an in depth analysis. See Figures 4.2 and 4.4 for geologic relations and place names.

4.2.1. Metamorphic Petrology

Understanding the metamorphic rocks of the Ivrea Zone is necessary for studying the petrogenesis of the igneous Mafic Complex for two reasons: (1) the metamorphic rocks represent possible contaminants of the magmas; (2) the protolith assemblages and metamorphic mineralogies provide constraints concerning the tectonic and thermal environment of metamorphism and possibly magma emplacement.

The Ivrea Zone consists of an approximately 11 km thick sequence of banded amphibolite and granulite-facies schists and gneisses (Fig. 4). Although the terms "kinzigite" and "stronalite" originally were used to describe specific mineral assemblages

and textures, these terms now are used as facies specific names in order to minimize confusion. "Kinzigite" refers to rocks of varying lithologies of the amphibolite facies while "stronalite" refers to the granulite facies rocks. In general these are biotite-rich and -poor, respectively.

The metamorphic section experienced a complex history of plastic deformation prior to emplacement of the Mafic Complex (Capedri and Rivalenti, 1973; Handy and Zingg, 1991). The predominance of equilibrium textures and assemblages suggests, however, preservation of peak metamorphic conditions. Limited retrogression of garnet, biotite and orthopyroxene occurred at 50°C and 1.5 kbar beneath the peak metamorphic conditions. For rocks in which the metamorphic peak occurred at relatively low PT conditions, the extent of retrograde reaction was greater possibly due to the less complete removal of water during peak conditions (Schmid and Wood, 1976). While rare relict andalusite, and possibly kyanite, has been found in amphibolite facies rocks, reequilibration at peak conditions appears to have been complete (Zingg, 1980).

The existence of graphite-bearing marble and calc-silicate pods in this lithogically diverse section along with other mineralogical and chemical data suggests a dominantly sedimentary protolith for this suite (Capedri, 1972). The protoliths consisted of shales and psammitic argillites with minor amounts of sandstones, graywackes and carbonates. The widespread presence of graphite (Capedri, 1972) in the metasediments, together with high mercury contents, suggests that reducing conditions dominated the depositional basin as would be consistent with the accumulation of organic matter. The interlayered amphibolites are chemically intermediate between mid-ocean ridge and oceanic basalts (normal and enriched types respectively) (Sills and Tarney, 1984). These basalts were deposited with or injected into the sedimentary pile which may have accumulated in an accretionary wedge formed at a Paleozoic subduction zone.

4.2.1.1. Metapelites

The pelitic gneisses contain biotite and/or garnet together with quartz, perthitic orthoclase, plagioclase and sillimanite. Typical mineral assemblages in the granulite facies are: quartz + plagioclase + perthite + garnet + orthopyroxene; quartz + plagioclase + perthite + garnet + sillimanite; orthopyroxene + clinopyroxene + plagioclase $\pm$ quartz (Sills, 1984). Accessory minerals include graphite, rutile, ilmenite, pyrrohtite and pyrite. In low grade rocks fibrolite predominates while the abundance of coarse-grained sillimanite increases with increasing grade.

The presence of orthopyroxene defines the transition from upper amphibolite to lower granulite facies conditions. The abrupt appearance of orthopyroxene suggests the possibility of there being an obscured tectonic boundary within the section (Schmid and Wood, 1976). The presence of ultramylonites at the facies boundary as well as the textural change from mainly granoblastic amphibolites to mylonitic granulites strengthens this latter hypothesis. Mylonitic extension of the section is discussed below in section 4.3.2.

4.2.1.2. Migmatites

Migmatites are common in the metamorphic section and often contain pegmatoidal veins and lenses. The migmatites are generally subconcordant with the foliation of the host rocks although pegmatitic dikes crosscut the amphibolites. The non-minimum melt composition of the granulite grade leucosomes (plagioclase; quartz + plagioclase; quartz + K-feldspar) may be evidence for either melt extraction from previously depleted, amphibolite grade metapelites (Schmid and Wood, 1976), or for leucosome production by metamorphic differentiation without melt production.

The migmatites may be the product of 50-70% degranitisation of the kinzigites, the degree of degranitization increasing with increasing metamorphic grade (Schmid, 1978; Zingg and Schmid, 1979). These calculations are based on melting either an average

pelitic or intermediate grade metapelitic (i.e., Strona-Ceneri type) composition. Melting produces a melt of granodioritic composition containing 3-8 weight % water and a restite similar to the Ivrean metapelites. The degranitization model would explain the increase of Mg, Fe and Ca contents with metamorphic grade found within the section as well as the decrease of K and H contents. Rb appears to be lost preferentially to K producing an increasing K/Rb ratio with increasing grade as is found in many high grade terranes (Sighinolfi, 1969). Additional supporting evidence for this degranitization model includes the calculated P, T and fO_2 conditions of metamorphism being conducive to melt production, and the association of some leucosomes with schlieren structures which may represent restitic selvages. Extraction of water by granitic melt may have, in fact, aided the development of granulite facies mineralogies within the metapelites.

4.2.1.3. Metacarbonates

Bands of carbonate-bearing rocks range in thickness from 0.5 to 100 m and comprise less than 2% of the Ivrea Zone. There are three main types of carbonate lithologies: dolomite-bearing calcsilicate marbles, dolomite-free calcsilicate marbles, and calcsilicate gneisses containing less than 5 % calcite (Zingg, 1980). Calcsilicate marbles contain olivine, clinopyroxene, amphibole, garnet, plagioclase, spinel (Baker, 1990) and scapolite in addition to calcite and display three types of mineralizations (Bigioggero et al., 1978/79; Mazzucchelli and Siena, 1986). The mineral assemblages indicate the presence of relatively water-rich fluids (Baker, 1990). Most granulite facies calcsilicates are tectonized with the calcite matrix strongly deformed or mylonitically recrystallized (Handy, 1986); there is, furthermore, evidence suggesting that the marbles were partially molten during peak metamorphic conditions (Brodie and Rutter, 1987).

4.2.1.4. Amphibolites

The amphibolites are medium- to fine-grained, well foliated with mafic/felsic compositional banding, and occur in 1 cm to 100 m thick layers (Sills and Tarney, 1984).

These rocks lack chilled margins or contact metamorphic signatures. Increasing metamorphic grade first produced clinopyroxene from amphibole and followed by the production of orthopyroxene ± garnet from amphibole. The amphibolites, therefore, become pyroxene granulites with increasing grade. Mineral compositions of clinopyroxene, amphibole and plagioclase (An 30-65) also change at the amphibolite-granulite transition, while hornblende changes color from green to brown (Mg-hornblende to ferroan-pargasite). Cumming et al. (1987) note a lack of Pb isotopic homogenization between amphibolites and metapelites. This may indicate a lack of pervasive fluid flow and isotopic exchange during or after metamorphism.

Most of the amphibolites are tholeiitic (N-type depleted) in composition; the petrogenesis may be modeled as dominated by the fractionation of olivine, clinopyroxene and plagioclase from a tholeiitic magma (Mazzucchelli and Siena, 1986). Stratigraphically higher amphibolites have enriched, transitional to alkalic compositions similar to oceanic basalts or continental tholeiites (Sills and Tarney, 1984; Mazzucchelli and Siena, 1986; Burghi, 1987; Cumming et al., 1987). The amphibolite chemistries suggest a mid-ocean ridge or back-arc origin for the majority of the amphibolites, while the enriched rocks could have formed at oceanic seamounts, fracture zones or transform faults. If both types of amphibolite protoliths were oceanic, the amphibolites may have been tectonically interleaved with the sedimentary rocks in an accretionary wedge environment (Sills and Tarney, 1984).

A second possibility is that the alkalic amphibolites have a continental genesis. This suggestion is based upon the regular association of the different amphibolite sub-types with specific carbonate mineralizations (Mazzucchelli and Siena, 1986). Amphibolites having a tholeiitic affinity occur in the central Ivrea Zone with carbonates bearing pre-metamorphic, stratiform Fe-Cu-Zn mineralizations (Bigioggero et al., 1978/79; Cumming et al., 1987) and in the northwest Ivrea Zone with carbonates having

Mn-mineralizations. These mineralization-lithologic associations are consistent with an oceanic environment of formation. In contrast, amphibolites of alkalic affinity occur stratigraphically higher in the southeast Ivrea Zone where they are associated with siliceous carbonates having Fe-Ba mineralizations. These deposits may suggest deposition in a shallow basin having a supply of continental detritus. If the mineralizations indeed reflect a change in depositional environment upwards through the metamorphic section, then the protoliths of the Ivrea Zone record an oceanic transgression during which crustal thickening, concomitant with sedimentation, would explain the tholeiitic to alkalic transition of the erupted magmas (Mazzucchelli and Siena, 1986).

A final possibility, noted by Voshage et al, (1987), is that some of the fine-grained mafic rocks located near the Mafic Complex may be sills of the Hercynian magmatic suite instead of meta-amphibolites.

4.2.2. Petrology of the Noncumulate Peridotites

A number of spinel peridotite bodies are located adjacent to the Insubric Line at the base of the Mafic Complex. Due to collaborative agreements, these upper mantle peridotites and the accompanying dikes were not extensively analyzed in this study. The important aspects of the peridotite petrology in regards to the interpretation of the Mafic Complex isotope systematics are the following: the peridotites are bodies of variably depleted mantle material which are chemically and texturally distinct from the cumulate peridotites in the layered series (Garuti and Friolo, 1978/79; Rivalenti et al., 1980); the chemistry of the dikes and gabbro pods may be interpreted as fractionated melts of a variably partially melted mantle; (Sinigoi et al., 1980); these melts, presumably generated from a larger unexposed mantle mass, may represent the parental magma(s) of the Mafic Complex (Rivalenti et al., 1975; Shervais, 1978/79; Sinigoi et al., 1980; Sinigoi et al., 1983); there is chemical evidence for local mantle heterogeneities (Garuti et al., 1984), some relationships possibly resulting from reaction with an alkali-rich fluid(s) of unknown

isotopic composition (Exley et al., 1982). Two of the largest peridotite bodies are described in detail below: Balmuccia and Finero. The large, but unsampled, Baldissero peridotite (Sinigoi et al., 1980) and many smaller, unnamed peridotites, such as those sampled in the Premosello area, are also present (Fig. 4.4).

4.2.2.1. The Balmuccia Peridotite

The Balmuccia peridotite is composed of clinopyroxene-poor spinel lherzolite, harzburgite (with 4-5% clinopyroxene) gradational with the lherzolite, and 10-15% dunite (Shervais, 1978/79). The olivine is of mantle affinity having a composition of Fo_{89-91} and a Ni concentration of 0.34 ppm. The orthopyroxene composition lies close to the enstatite-bronzite boundary; the clinopyroxene is diopsidic. These minerals are more Mg- and Ni-rich and more Fe- and Mn-poor relative to the corresponding phases in the cumulate layered series described below (Rivalenti et al., 1980). There is no ilmenite or magnetite; the spinel is Cr-hercynite to chromite. Estimates of crystallization conditions range from temperatures of 1100 to 1200°C (Capedri et al., 1976; Garuti et al., 1978/79; Rivalenti et al., 1978/79; Shervais, 1978/79; Shervais, 1979) and pressures of 12 to 20 kbar.

The peridotite is antiformal in structure and is 4.5 x 0.7 x 1.1 km in outcrop dimension (Shervais, 1979). Commonly the texture is foliated equigranular, occasionally with a relict protogranular texture (Skrotzki et al., 1990). A magmatic contact with the overlying layered series is preserved in some places along the western edge of the peridotite (Sinigoi et al., 1983); elsewhere, however, the contact is mylonitic, particularly near the Insubric Line. Two mineral foliations are found within the peridotite (Shervais, 1978/79). The first foliation trends NNE, is concordant with the peridotite mineralogical layering and may be a relict of the mantle regime. Where the peridotite is strongly recrystallized the foliation trends NNW concordant with the foliation found in the surrounding granulites. This overprinting of the mantle foliation is presumably related to

the diapiric emplacement of the peridotite into the crust; as might be predicted, the second foliation becomes pronounced towards the margins of the peridotite. Reequilibration after emplacement in the lower crust appears to have occurred at 850 to 950°C and 10 to 13 kbar (Ernst, 1978; Shervais, 1979).

Two major suites of dikes, which are dominantly concordant or sub-concordant with the main foliation, are found within the Balmuccia peridotite (Shervais, 1978/79). The Cr-diopside dike suite (Shervais, 1978/79) is characterized by an emerald green diopside similar in composition to the clinopyroxene in the host peridotite. The similar pyroxene composition indicates that these dikes are in equilibrium with the peridotite and may represent the first solid fractionate deposited by the liquids produced by peridotite partial melting (Sinigoi et al., 1983). Peridotite phase relationships are consistent with melt generation at pressures between 10 and 20 kbar (Shervais, 1978/79), and the generation of discordant dikes is consistent with hydraulic fracturing due to pressure related to magma generation (Nicolas and Jackson, 1982).

The Cr-diopside suite contains two sub-types. The dominant sub-type is composed of olivine-free websterites and clinopyroxenites and is usually found within the lherzolite. When found in dunite, this sub-type consists only of thin trains of Cr-rich spinel, flattened parallel to foliation. These spinel bands may represent either a residue after partial melting of websterite bands in a previously lherzolitic host (Shervais, 1978/79; Sinigoi et al., 1983) or be the products of reaction of websterite with a clinopyroxene-undersaturated, volatile-saturated melt (Quick, 1981). The second sub-type of the Cr-diopside suite is composed of bronzitites. These form discontinuous layers which pinch and swell and may change to websterite along strike. This sub-type may be derived from removing clinopyroxene from the websterites (Shervais, 1978/79) or may represent the first solid fractionated from liquids produced by partial fusion of a previously depleted source such as harzburgite (Sinigoi et al., 1983).

This second Cr-diopside sub-type forms a compositionally continuous series with the Al-augite dike suite (Sinigoi et al., 1983). The Al-augite suite is characterized by a modal average of 10% medium-grained, Al-rich hercynite surrounded by a grayish-tan, Al-augite matrix (Shervais, 1978/79). This type contains Al-rich and Cr-poor clinopyroxene with kaersuitic amphibole as a ubiquitous accessory phase but little to no olivine. These dikes have sharp margins and are less deformed than coexisting Cr-diopside dikes which they crosscut, and are, therefore, interpreted as being younger in age (Sinigoi et al., 1983). The older Cr-diopside dikes are concentrated in the interior of the massif while the Al-augite dikes are concentrated in the outer edges. Composite dikes having Cr-diopside margins and Al-augite interiors as well as compositionally intermediate dikes are also present. Rare Al-augite dikes with plagioclase-rich interiors and compositions are suggestive of highly fractionated magmatic fluids (Shervais, 1978/79).

The Cr-diopside dikes are believed to represent the first solid fraction formed from the first mantle melt while the Al-augite dikes represent a subsequent solid fraction of the evolved, mobilized parental liquid of the first generation dikes (Sinigoi et al., 1980). Compositionally the dikes display a slight iron enrichment trend similar to that in Lower Zone of the Mafic Complex, while fractionation trends of dike pyroxenes are similar to those in the cumulate peridotites of the Mafic Complex. These relationships are suggestive of a comagmatic relationship between the dikes and the overlying Mafic Complex (Shervais, 1978/79).

For similar suite of dikes in the Baldissero peridotite Sinigoi et al. (1980) suggest that removal of 10-20% melt from a pyrolitic mantle would produce a residue having a composition similar to Baldissero peridotite. The liquid would have a composition similar to picritic basalts, and would not vary significantly in composition up to 25% melting regardless of the modal composition of the primary lherzolite. The picritic basalt

produced by the previous depletion of these noncumulate peridotite bodies, or similar, unexposed mantle material, may be the parental melt of the Mafic Complex.

The roughly flat to LREE-depleted REE patterns of the Balmuccia peridotite are consistent with a depleted upper mantle character. The dikes are strongly LREE depleted with the Al-augite dikes having approximately twice the REE concentrations as the Cr-diopside dikes (Voshage et al., 1988) supportive of the model that the two dike suites represent fractionates of the evolving partial melts of the surrounding peridotite.

Scatter in the isotopic systematics of the Al-augite dikes suggests the possible introduction of a metasomatic fluid which initiated mantle melting (Voshage et al., 1988). This proposed metasomatic overprint is otherwise detectable only in the most chemically refractory assemblage being expressed as the slightly LREE-enriched signature of a Balmuccia dunite. The presence of a pervasive metasomatic fluid in the mantle may also be witnessed by the disturbance of Pb isotopes towards a higher, continental μ in both the phlogopite-bearing and phlogopite-free peridotites (discussed below) as well as in sulfides and silicates of the Mafic Complex (Cumming et al., 1987).

In the Balmuccia peridotite there are rare pods of undeformed gabbro (Sinigoi et al., 1983) which are olivine tholeiite in composition and which often have pyroxenite rims. These pods may represent trapped, unfractionated melts of the peridotite (Capedri et al., 1977), but the possibility cannot be ruled out that these represent pods of unrelated layered series gabbro which have been injected into the peridotite. Finally, there are rare amphibole and Ti-phlogopite-rich dikes (Garuti and Sinigoi, 1978; Sinigoi et al., 1983; Voshage et al., 1987) which possibly reflect a spatially restricted, alkali-rich metasomatizing agent of crustal isotopic character similar to that proposed for the Finero peridotite.

4.2.2.2. The Finero Peridotite

The Finero Complex (Fig. 4.5) is exposed as an antiformal structure adjacent to the Insubric Line in the northeastern Ivrea Zone (Steck and Tieche, 1976; Krull and Voll, 1978). This complex has experienced multiple deformational episodes involving shearing and isoclinal folding under granulite to greenschist facies conditions (Steck and Tieche, 1976; Krull and Voll, 1978; Zingg and Schmid, 1979; Brodie, 1980). Fluid flow in localized shear zones was aided by recrystallization and promoted retrogression under amphibolite facies conditions (Brodie, 1980).

The Finero Complex is unique in its extreme abundance of the hydrous phases, phlogopite and amphibole, which define a foliation. Phlogopite spinel peridotite forms the core of the antiform which is surrounded by a sheath of cumulate peridotites and gabbros. The phlogopite dunites and harzbugites contain 60-90% olivine, 5-20% orthopyroxene, 0-5% amphibole, and 10-15% coarse-grained, relatively undeformed phlogopite. Mineral compositions of the central peridotite define narrow ranges and compare to the surrounding cumulate peridotite as follows: olivine (Fo_{90-92}) in the central peridotite is Ni-rich; pyroxenes are Mg-rich and Al-poor; the amphibole (pargasitic hornblende) is Mg-rich, Cr-rich and Al-poor; the spinels are Cr-rich and Al-poor. Al-augite dikes are present in the central peridotite while dikes of Cr-diopside + hornblende + spinel are less common.

The igneous sheath surrounding the Finero phlogopite peridotite has been divided into three units: the lower gabbro, the amphibole peridotite and the upper gabbro (Coltorti and Siena, 1984). The locally garnet-rich lower gabbro is in sharp contact with the underlying phlogopite peridotite and is composed of interlayered hornblende peridotite, pyroxenite, anorthosite, hornblenditite and gabbro. The amphibole peridotite is 200 m thick and is lithologically diverse including dunites, harzburgites, lherzolites, websterites and bands, dikes and pods of pegmatoidal hornblenditite. The modal composition of the

amphibole peridotite is 60-80% olivine, 10-50% orthopyroxene, 5-40% clinopyroxene, 0-5% spinel and 10-80% pargasitic amphibole. Equilibrium 120° grain boundaries are more common than in the phlogopite peridotite although some cumulate textures are recognizable. Phlogopite is rare and always surrounds the amphibole. The banded upper gabbro is dominated by hornblende-rich pyroxene gabbros which may be garnet-bearing especially where located near metapelitic septa.

The central and amphibole peridotites are easily distinguished on chemical variation diagrams (Coltorti and Siena, 1984) and trends suggestive of fractional crystallization can be identified only within the amphibole peridotite field (Capedri et al., 1977). Isotopic compositions (Sr_{270}= 0.7025-0.7035; εNd_{270} = +7.5 $\pm$ 1.8; Voshage et al., 1987) and chemical trends defined by the amphibole peridotite suggest that the parent liquid may have been derived from a mantle melting event similar to, but post-dating, that event which left the pre-phlogopite, central peridotite as a residue (Hunziker et al., 1982; Coltorti and Siena, 1984).

The chemical, mineralogical and isotopic systematics of the complex is compatible with the model that the phlogopite peridotite represents a highly depleted mantle tectonite which suffered hydration by a crustally derived fluid prior to formation of the surrounding complex (Rivalenti et al., 1978/79; Hunziker et al., 1982; Coltorti and Siena, 1984; Voshage et al., 1987). Mineralogical and isotopic characteristics require a Ti-, Rb-, Sr- and Ba-rich hydrous fluid inequally distributed in the upper mantle (Exley et al., 1982; Voshage et al., 1987) to account for both the continental isotopic signature of the phlogopite (Sr_{305}= 0.7062 $\pm$ 5) (Hunziker et al., 1982) as well as the scarcity of phlogopite found in the other Ivrea mantle peridotites (Zingg, 1983). Work by Voshage et al. (1987) gives an Sr_{293} of 0.7063 $\pm$ 6 for phlogopite-bearing rocks from both Finero and Balmuccia indicating that the apparent phlogopite metasomatism was contemporaneous (at 266 $\pm$ 41 Ma from Sm-Nd systematics) and cogenetic at both locations.

4.2.2.3. The Premosello Area

Small, 10^1 - 10^2 m long bodies of phlogopite-bearing peridotite are located in the Premosello area adjacent to the Insubric Line (Fig. 4.4). These peridotites are grossly similar to the Finero Complex in that they are composed of a phlogopite peridotite core surrounded by a thin hornblende-rich pyroxenite and gabbro sheath. Apparently no petrologic data from these rocks is published in English; they were sampled in this study due to the presence of phlogopite and will be compared to the Finero data in the following chapter.

4.2.3. Petrology of the Mafic Complex

The focus of the present isotopic investigation is the layered Mafic Complex, or Basischer Hauptzug, which attains a maximum thickness of 8 km in the central Ivrea Zone (Rivalenti et al., 1980; Mazzucchelli, 1983). An igneous contact between the mantle peridotites and the base of this ultramafic-mafic intrusion is present but seldom preserved. The Mafic Complex is intruded into the banded granulites and amphibolites, and it is hypothesized that the stratiform intrusion may have provided the heat required for the granulite facies metamorphism (Schmid and Wood, 1976). The complex itself does not appear to have been metamorphosed, although reequilibration to granulite facies conditions (800-950°C and 8-9 kbar) occurred during protracted cooling in the lower crust from the conditions of crystallization (1000-1200°C and 6-8 kbar) (Rivalenti et al., 1980).

The Mafic Complex is composed of three units: a lowermost Layered Series (2 km thick), the middle, homogenous Main Gabbro (4 km thick), and an upper, banded "diorite" complex (2.5 km thick) (Fig. 4.6). The Layered Series may be divided into three zones (Basal, Intermediate, Upper) based upon the appearance or disappearance of certain mineral phases (olivine, pyroxenes, oxides) and their relative proportions (Rivalenti et al., 1975; Mazzucchelli, 1983; Rivalenti et al., 1984). The Monte Capio Sill is presented as a possible analog to an early stage of intrusion and crystallization of the Layered Series.

Neither of the two upper units of the Mafic Complex has been extensively studied. Cumulate textures are absent in the lithologically homogenous Main Gabbro, but noncumulate igneous textures are sometimes preserved. The uppermost "diorites" are actually monzodioritic to granodioritic in composition; the name diorite is maintained, however, for continuity in the literature. The diorite unit contains abundant metamorphic septa and commonly grades into a migmatite zone along the outer contact of the intrusion. In the southern exposures of the Mafic Complex a mineralogically distict lithology often occupies a position analogous to that of the more abundant diorites. These charnockites will be discussed separately.

A brief petrologic description of each of these Mafic Complex subdivisions is presented below. Themes addressed which are important to the following isotopic analysis include the following: the evidence for fractional crystallization of a mantle-derived melt at lower crustal conditions; the data suggestive of the possibility of multiple intrusions of variably evolved magmas; the relationships demonstrative of magma contamination through assimilation; the overall chemical character of the igneous suite and the resultant implications for the tectonic environment of magma emplacement.

4.2.3.1. The Layered Series

Cumulate and other igneous textures are recognizable in the Layered Series but, more frequently, the textures are granoblastic or equigranular polygonal (Garuti and Friolo, 1978/79; Rivalenti et al., 1984). This subsolidus recrystallization is believed to result from autometamorphism during cooling from igneous temperatures (Rivalenti et al., 1980; Sinigoi et al., 1991) to conditions of the pyroxene-garnet granulite facies, this being the most stable configuration for mafic rocks in the lower crust environment (Wood, 1983). The partial replacement of orthopyroxene by hornblende suggests limited retrograde metamorphism to the amphibolite facies. In addition to the textural reequilibration, autometamorphism permitted the formation of corona textures in some

gabbros (Mazzucchelli, 1983; Sills, 1984) and the sub-solidus unmixing of pyroxenes producing lamelli of pyroxene, a Ti-rich phase or rarely garnet in garnet-bearing gabbros which are found near metapelitic septa (Capedri et al., 1976; Sills et al., 1983; Rivalenti et al., 1984). Alternatively, the general lack of cumulate textures may be due to extensive adcumulus growth or in situ nucleation (McBirney and Noyes, 1979).

The olivine composition ranges from Fo_{83} to Fo_{35} with an average Ni content of roughly 0.20 % in the ultramafic lithologies, that being substantially lower than the mantle olivines (Capedri et al., 1977; Garuti et al., 1978/79; Rivalenti et al., 1984). Orthopyroxene is bronzite to hypersthene (En_{79-56}) while clinopyroxene varies in composition from diopside to low-iron salite. Pargasitic and ferroan pargasitic amphibole is a minor primary, intercumulus, and sometimes cumulus, phase throughout the Layered Series, becoming modally enriched in the Upper Zone. Ore deposits are relatively limited, being composed of Fe-Ni-(Cu)-(PGM)-bearing sulfides in the peridotites of the BZ and iron oxides in the UZ (Garuti et al., 1980; Cumming et al., 1987).

The apparent fractionation sequence in the Layered Series was olivine + spinel, (olivine) + clinopyroxene + orthopyroxene + spinel, spinel + plagioclase + orthopyroxene + clinopyroxene (Rivalenti et al., 1975; Rivalenti et al., 1980). This sequence of mineral assemblages can be modeled in the Fo-An-Di-SiO_2 system by the fractionation of olivine, orthopyroxene, clinopyroxene at high pressure (>8 kbar) (Rivalenti et al., 1975) followed by plagioclase higher in the series. In the IZ, the abundance of plagioclase and the coexistence of cumulate plagioclase and olivine may indicate a change in phase relationships reflecting a lower pressure of crystallization relative to the BZ in which pyroxene and spinel coprecipitate (Rivalenti et al., 1980). Alternatively, the change in phase relations may reflect shifts in the phase boundaries due to the generally more Fe-rich, evolved composition of the IZ and UZ parental magmas (Mazzucchelli, 1983).

Crystal fractionation modeling can simulate the production of the BZ, then the IZ and finally the UZ from a single parental liquid compositionally like a Balmuccia gabbro (Rivalenti et al., 1984). The stratigraphic variations in lithology and mineral compositions, however, only approximately support an upward fractionation model of a single melt. Such variations include an upwards decrease in olivine forsterite and Ni content (Rivalenti et al., 1980) and a decrease in the Al content of the orthopyroxene. A more plausible explanation is that multiple magma pulses, possibly primitive to variably evolved, were involved in the crystallization of the Layered Series.

Most Layered Series samples are characterized by positive Sr and Eu anomalies indicating the presence of cumulate plagioclase. The REE patterns range from LREE depleted and moderately enriched (X1-10) relative to chondritic abundances in the BZ to strongly LREE enriched in the UZ (Pin and Sills, 1986; Voshage et al., 1990). The BZ REE pattern is similar to that defined by Cr-diopside and Al-augite dikes. This correlation strengthens the hypothesis the parental magma(s) of the Mafic Complex is related to melts produced in the subjacent mantle peridotites.

4.2.3.1.1. The Basal Zone (BZ)

The BZ is composed of interlayered websterite and pyroxenite with minor peridotite and gabbro which display no clear pattern of cyclic variation (Rivalenti et al., 1984). Crystals are frequently deformed, especially near the Balmuccia peridotite where porphyroclastic textures occur (Rivalenti et al., 1984). Pegmatoidal clinopyroxenite layers displaying plastically deformed exsolution lamelli occur near the base of this zone. Olivine occurs in a reaction relationship with orthopyroxene. Plagioclase ranges in composition from An_{48} to An_{35} in the pyroxenites and from An_{80} to An_{60} in the gabbros (Rivalenti et al., 1984). Plagioclase in the pyroxenites is always intercumulus and never occurs with olivine. Spinel is cumulus in peridotites and websterites, but in the latter lithology it may occur also as an intercumulus product together with plagioclase.

Metapelitic septa and xenoliths are abundant and display textures suggestive of partial melting and mingling with the enclosing magmas. Massive sulfide ores are commonly associated with such inclusions (Ferrario et al., 1982).

In earlier literature the BZ and IZ were undifferentiated and together formed the Lower Layered Group (LLG) of Rivalenti et al. (1975). The present division recognizes the increased abundance of peridotite in the IZ as compared to the upper BZ as well as the switch from coexisting cumulate pyroxene and spinel in the BZ to coexisting cumulate olivine and plagioclase in the IZ.

4.2.3.1.2. The Intermediate Zone (IZ)

The Intermediate Zone (IZ) is composed of peridotite with minor interlayered orthopyroxenite and gabbro. The cumulus phases are olivine, orthopyroxene, spinel, and, in the gabbros, plagioclase. The olivine composition ranges between Fo_{60} to Fo_{35} (Rivalenti et al., 1980) with Ni contents of less than 0.15 wt. % in peridotites. The composition of intercumulus plagioclase is approximately An_{47} (Rivalenti et al., 1984), reaching a maximum of An_{78} in the gabbros interlayered with peridotites and falling to An_{43} in the upper gabbros where spinel is absent.

Kelyphitic intergrowths of Mg-Al spinel and pyroxene surround some olivine crystals. As in the Stokes Mountain suite (Chapter 2), these textures may represent the reaction of early crystallized olivine with an evolved interstitial melt. Further chemical disequilibrium in the IZ is demonstrated by thin layers of pyroxene which consistently separate peridotite and gabbro layers (Garuti et al., 1980). This disequilibrium may be the result of the coexistence of chemically distinct, variably evolved magmas which were produced by the fractionation of one or more parental magmas.

Peridotitic layers in the IZ vary extremely in thickness (1 cm to 50 m) along strike. Complex structures, such as synmagmatic isoclinal and sheath folding, are present in the layered cumulates found beneath such peridotite lenses. These structures may have been

formed by slumping of thick, peridotitic crystal mushes lubricated by underlying gabbroic liquids, and attest to a dynamic magma chamber during crystallization (Rivalenti et al., 1980). Such a dynamic chamber may reflect the tectonic environment and/or the violent injection of new magma pulses.

4.2.3.1.3. The Upper Zone (UZ)

The UZ is separated from the IZ by a 40-100 m thick septum of metapelites (Mazzucchelli, 1983; Rivalenti et al., 1984). A 6 m thick, fine-grained gabbro in which the plagioclase has a relatively calcic composition of An_{76} occurs along the contact with the basal metapelite (Rivalenti et al., 1984). The gabbro is overlain by a series of interlayered websterites and gabbros with rare, thin (< 2 cm thick) peridotites and olivine websterites at the base. Cyclic lithologic repetitions are common.

A crude iron enrichment trend is displayed in the UZ, especially when compared to the underlying zones. Within the UZ there is a stratigraphically controlled gap in olivine compositions and appearance between Fo_{76} and Fo_{66} (Garuti et al., 1980; Rivalenti et al., 1980; Mazzucchelli, 1983). Above this gap the olivine composition varies between Fo_{66} and Fo_{35}; at forsterite contents below Fo_{41} olivine does not coexist with pyroxene. Pyroxenes in the UZ olivine gabbros display the greatest iron enrichment found in the Mafic Complex (Rivalenti et al., 1980) while the amphibole is ferroan pargasite. The maximum anorthite content in the plagioclase is An_{78} while the most differentiated layers have compositions of An_{44} (Rivalenti et al., 1984). In the upper UZ is a gabbroic series which is melanocratic at the base and becomes increasingly leucocratic with stratigraphic height. Layers of ilmenomagnetite and apatite occur at the top of the unit.

The dominant texture of the Upper Zone (UZ) is polygonal equigranular indicating recrystallization consistent with autometamorphism in the granulite facies. Pyroxenes display well developed exsolution lamelli. Olivines are commonly surrounded by coronas of garnet or Mg-Al spinel + pyroxene which have been interpreted as forming by a

subsolidus reaction between plagioclase and olivine (Mazzucchelli, 1983; Sills, 1984). The Mg-Al spinel + pyroxene intergrowths may, however, indicate a near solidus reaction as described in the IZ. Unlike the IZ, pervasive deformation features are absent suggesting a relatively static crystallization environment. The spatial separation resulting from the continuous metapelitic septa in addition to the difference in deformation styles between the IZ and UZ further supports the model of multiple magma pulses in the Mafic Complex as mentioned above.

4.2.3.1.4. The Monte Capio Sill

The above description is based primarily upon the thickest and best developed section through the Mafic Complex, that being in the region of Valles Sesia and Mastellone. As can be seen on Figure 2, the Mafic Complex varies in form along strike, becoming thinner to the northeast and southwest. From these thinner sections, one particular area was chosen for isotopic study, the La Balma-Monte Capio Ultramafic-Mafic Sill which was previously recognized for its Fe-Ni-Cu ore deposits (Bigioggero et al., 1978/79; Ferrario et al., 1982).

This particular site was selected because the Monte Capio Sill is grossly similar to the lower Layered Series in mineralogy, structure and geologic setting. Our hypothesis is that this epiphysis may record of one stage of the formation of the lower Mafic Complex, specifically the multiple emplacement and internal fractionation of large sills 10^1 to 10^2 m in thickness within the lower crust. The comparison to the BZ and IZ, however, is not without problems. The Monte Capio Sill is believed to have formed by the intrusion and differentiation of a high-Mg (14-20 wt. %) magma; the melt was rich in sulfur and was fairly hydrous as all units contain primary hornblende (pargasite and pargasitic hornblende) (Ferrario et al., 1983). In contrast, the parental magma of Mafic Complex had a lower average Mg content and crystallized less amphibole (Rivalenti et al., 1975).

The Monte Capio Sill is 5 km x 400 m in maximum dimension and has been divided, from bottom to top, into four zones (Fig. 4.7) (Ferrario et al., 1983). The basal gabbro occasionally contains garnet while the adjacent kinzigite is black and mineralized. The central peridotite unit, which forms about 2/3 of the sill's width, is comprised of dunite and harzburgite with minor lherzolite. The dominantly equigranular texture with minor superimposed deformation may be cumulate in origin (Garuti and Friolo, 1978/79). The zone has low Al, Ca and Na contents resulting from a low modal content of pyroxene. Sporadic primary, intergranular phlogopite has been found in this zone, especially near the footwall metasediments, prompting the suggestion that crustal contamination has occurred (Ferrario et al., 1983). The central peridotite is usually bounded on either side by a thin pyroxenite unit which is in turn overlain by the layered gabbro unit. Compared to the basal gabbro, the layered gabbro has relatively low Na and K contents while it is rich in Cr and Ni. This unit is also distinguished by high Ti contents in contrast to the rest of the body; ilmenite is abundant while Fe-Ti oxides are otherwise rare.

The Monte Capio Sill, with its core of peridotite and sheath of gabbro, resembles feeder dikes, like that of the Muskox intrusion, for which the process of flow differentiation is invoked.

4.2.3.2. The Main Gabbro (MG)

While the Main Gabbro unit represents the thickest section (3.5 km) of the Mafic Complex, it has not been extensively studied because of its relative lithologic and isotopic homogeneity. The MG is composed of medium- to fine-grained gabbros, olivine gabbros, gabbro norites, norites and rare anorthosites. The unit is plagioclase-rich relative to the Layered Series. The general assemblage is plagioclase + orthopyroxene + clinopyroxene + spinel $\pm$ olivine $\pm$ biotite + opaques + hornblende. Neither olivine nor biotite exist at the base of the unit. At higher stratigraphic levels olivine has a composition of Fo_{66-50} and undetectable Ni contents. Plagioclase varies in composition between An_{85} and An_{50}. As

in the IZ and UZ, well developed coronas exist between olivine and plagioclase composed of a symplectic intergrowth of green spinel + clinopyroxene + orthopyroxene (Sills, 1984). Magmatic Fe-Ni-Cu-PGM ores are present in pyroxenite lenses (Cumming et al., 1987).

Igneous textures are preserved in the upper levels of the Main Gabbro while textures are polygonal recrystallized at lower stratigraphic levels. In some areas modal and textural variations occur within the bands, but the overall lithologic homogeneity of this unit promotes the common interpretation that this body crystallized from a large, convecting magma chamber in which both fractionated and unfractionated mantle melts mixed with crustal melts (Voshage et al., 1990). This unit is chemically intermediate to rocks from the BZ and UZ, and grades upwards into the diorite unit where the transition is marked by rapid increase in K_2O content.

4.2.3.3. Diorites

This unit forms the margin of the Mafic Complex, separating the Main Gabbro from the metamorphic wall rocks. Assemblages in the diorite unit include the following: plagioclase $\pm$ orthopyroxene $\pm$ clinopyroxene + hornblende + biotite; plagioclase $\pm$ orthopyroxene $\pm$ quartz + hornblende + biotite; plagioclase + hornblende + biotite $\pm$ quartz; plagioclase $\pm$ hornblende + biotite + quartz $\pm$ garnet $\pm$ K-feldspar (Sills, 1984). Plagioclase varies in composition between An_{70} and An_{35}. Pyroxene is usually enclosed by magmatic hornblende (Zingg, 1980). Medium- to coarse-grained, euhedral to anhedral, poikiolitic garnet is found near the metamorphic contact and adjacent to metapelitic septa as well as concentrated in bands within the unit. These garnet bands may indicate the previous existence of fully assimilated metapelitic septa.

These are not all true diorites, but the unit name is kept for continuity in the literature. Most rocks are monzodiorites, but some have silica contents similar to the adjacent gabbros, differing only in having elevated K_2O and H_2O contents (Bigioggero et al., 1978/79) and an greater abundance of biotite and hornblende (Sills, 1984). The

increase in K_2O content relative to the gabbros and the enhanced biotite and garnet stability near the diorite-metapelite transition suggests that some of the diorites may have been produced by the diffusion of potassium from the granitic migmatites into the adjacent gabbroic magma (S. Sinigoi, pers. comm.). Such diffusional exchange across gabbro-granite interfaces has been demonstrated experimentally at comparable pressures (Johnston and Wyllie, 1988). Coexistence of gabbroic and granitic magmas is documented by extensive mingling zones near the Main Gabbro to diorite transition.

Migmatization of the country rock along the contact is common and some diorites contain graphite suggestive of assimilation of metapelitic material (Capedri, 1972). Igneous textures are commonly preserved. Overall, the diorite unit may represent a differentiate of the Main Gabbro containing a significant contribution of country rocks assimilant and/or granitic melt. A slight variation of this hypothesis is that an evolved magma fractionated to form the UZ cumulates and the dioritic noncumulates. Gabbroic magma, represented by the Main Gabbro, was injected between these two zones and mingled with the base of the diorites (S. Sinigoi, personal communication). The isotope systematics demonstrate the presence of both mantle and crust components.

4.2.3.4. Charnockites

This lithology differs from the diorites in containing a greater abundance of K-feldspar megacrysts and orthopyroxene in the characterizing assemblage quartz + feldspar + garnet + biotite + orthopyroxene + clinopyroxene (Rivalenti et al., 1980; Burghi, 1987). Somewhat surprisingly the potassium content is significantly lower than diorites (Burghi and Klotzli, 1990). The charnockites are found in the southern part of the Ivrea Zone forming either the leucosomes in the migmatitic roof of Mafic Complex (Burghi, 1987) or interlayered with norites, amphibole gabbros and anorthosites. These rocks are dominantly leucocratic (leucocharnockites) and granodioritic in composition, while the association of mesoperthites and antiperthitic plagioclase with quartz and orthopyroxene

indicates an affinity with hypersolvus granites (Sinigoi et al., 1991). Relict igneous textures and structures include ophitic, hypidiomorphic granular and graphic textures, intrusive cross cutting contacts, and mingling relationships. In one study, associated quartz dioritic to tonalitic rocks lacking K-feldspar megacrysts and having a deformed, recrystallized fabric are labeled melacharnockites (Burghi, 1987).

Many features of the leucocharnockites are similar to S-type granites (high SiO_2 contents; presence of ilmenite, garnet, red biotite, white K-feldspar megacrysts, and metasedimentary xenoliths), but these rocks do not have a minimum melt composition (Burghi, 1987). The leucocharnockites are chemically distinct from the surrounding stronalites and instead plot on differentiation trends defined by the Main Gabbro (Rivalenti et al., 1975).

The leucocharnockites are considered to be younger than the foliation-forming deformation(s) that folded the underlying Mafic Complex (Burghi, 1987; Sinigoi et al., 1991). Four leucocharnockite define a whole rock Rb-Sr isochron yielding an age of 274 $\pm$ 17 Ma and a Sr_{274} of 0.71044; two melacharnockites yielded a rough Sr_i of 0.7089 (Burghi, 1987; Burghi and Klotzli, 1990). The leucocharnockite Sr_i value was confirmed by five additional samples (Sinigoi et al., 1991). While the strontium isotope systematics are not consistent with a simple two endmember mixing model (Burghi, 1987), the field, chemical and isotopic data suggest that the leucocharnockites represent complex mixtures between evolved mantle melts and melts of highly restitic metapelite (Sinigoi et al., 1991).

4.3. Structural Characteristics of the Mafic Complex

4.3.1. Syn-Magmatic Structures

Synmagmatic deformational structures have been previously discussed in section 4.2.1.3.2. Isoclinal and sheath folding of partially crystallized layered cumulates is beautifully displayed in the IZ. Dikes cross cutting the foliation are themselves folded (Quick et al., in press). Angular unconformities produced by the brecciation of solidified

layered cumulates subsequently enclosed, intruded by variably fractionated magmas, and draped by layered cumulates demonstrate a complex and dynamic intrusion-crystallization history.

Spherical to ovoid, aphanitic to fine-grained porphyritic, mafic enclaves are abundant in zones near the base of the diorite unit. As discussed extensively in Chapter 2, such swarms witness the mingling of mafic and felsic magmas. More complete, albeit small scale, mixing is suggested by textures adjacent to metamorphic septa in which diffuse threads of leucocratic mobilizate appear to be entrained and swirled into the surrounding monzodiorite. Further evidence for mixing is revealed by recent REE investigations which suggest that some garnets in the diorite unit have xenocrystic cores (Mazzucchelli et al., in press). The process of large scale mixing in the Mafic Complex will be addressed in Chapter 5 using combined radiogenic and stable isotope systematics.

4.3.2. Syn- to Post-Magmatic Shear Zones

Central to the interpretation of the Ivrea Zone as a representative cross section through pre-Alpine lower crust is the stipulation that there was little, localized internal deformation after the peak conditions of metamorphic and igneous activity. In their recent review, Zingg et al, (1990) define and examine three types of tectonometamorphic facies in Ivrea Zone. The first facies is characterized by deformation structures in the metamorphic section (Krull and Voll, 1978), such as isoclinal folds and boudinage, which have annealed microfabrics and presumably predate peak regional metamorphism.

The second facies consists of high temperature (>500°C) mylonites which accommodated horizontal extension subparallel to the metamorphic layering (Brodie and Rutter, 1987). The preservation of delicate intergrowths of compositionally high temperature plagioclase and pyroxene crystals (Brodie, 1981; Brodie and Rutter, 1985), the unusually small grain size of high temperature mylonitic quartz, and the lack of chemical equilibrium between the porphyroclasts and the porphyroblasts (Zingg et al.,

1990) suggest that mylonitization postdates the peak of metamorphism but may be synmagmatic (Handy and Zingg, 1991). These relationships further suggest that anhydrous conditions prevailed during and subsequent to mylonitization.

Thinning of the crustal section after peak conditions is suggested by estimates of the thermal gradient which are too low for normal continental crust. Pressure gradient estimates range between 0.29 kbar/km (Hunziker and Zingg, 1980) appropriate for an in tact crustal section, and 0.53 kbar/km (Sills, 1984), the latter consistent with subsequent crustal thinning. It should be noted that the age of high temperature mylonitization and extension is the subject of debate. For the purposes of this study the conflict resolves into whether or not extension in the lower crust accompanied or postdated emplacement of the Mafic Complex (Brodie and Rutter, 1987; Brodie et al., 1989; Zingg et al., 1990; Handy and Zingg, 1991). This subject and the implication for the tectonic environment of magmatism is addressed further below.

The third tectonometamorphic facies consists of low temperature (< 300°C) mylonites which are retrogressed to the greenschist facies and are associated with cataclasites and pseudotachylites (Handy, 1986). Such mylonites cross cut the high temperature mylonites (Brodie and Rutter, 1987) and are predominantly located along the Pogallo Line.

Two conclusions concerning fluids in the Ivrea Zone lower crust can be derived from the above discussion. First, the evidence for anhydrous conditions during and after high temperature mylonitization argues against any subsequent large scale, pervasive fluid circulation. Secondly, fluids accompanying retrogression appear to have been localized along spatially limited zones of brittle deformation as evidenced by the limited presence of greenschist facies hydrous mineralogies as well as partially reset biotite ages along the Insubric Line (Handy and Zingg, 1991). Both conclusions support the hypothesis that the

oxygen isotopic systematics record the signature of the Hercynian lower crust. This proposal is developed in the following chapter.

4.3.3. Post-Magmatic Faulting and Folding

Greenschist facies mylonitization and cataclasis related to the Alpine orogeny is concentrated along the Insubric Line (Handy and Zingg, 1991), although minor brittle deformation zones can be easily recognized inside the Ivrea Zone by the localization of low temperature mineral assemblages. Limited flow of meteoritic water in these zones is demonstrated in the following chapter.

The Proman antiform is a large, box-type antiform located adjacent to the Insubric Line. This structure folds the high temperature mylonites (Schmid, 1967) and therefore postdates crustal extension. As the foliation parallel flexural slip required that the lithologic foliation was in a near vertical orientation prior to folding, it is argued that the Ivrea Zone must have been rotated into its near vertical orientation prior to the late Alpine orogeny (Brodie and Rutter, 1987; Schmid et al., 1987). The Alpine age of deformation and tectonic interpretation of this structure were discussed in section 4.1.

4.4. Petrologic Overview of the Strona-Ceneri Zone

4.4.1. Metamorphic Serie dei Laghi

The rocks of the Strona-Ceneri Zone comprise the Serie dei Laghi and are broken into the Scisti dei Laghi and the Strona-Ceneri units (Boriani et al., 1977). The near vertical layering trends northeast roughly parallel to that in the Ivrea Zone. Metamorphic conditions reached the staurolite and kyanite zones of the amphibolite facies with only a slight increase in grade towards the northwest; retrogression to greenschist facies conditions occurred locally. The absence of pervasive retrograde metamorphism has been attributed to a lack of sufficient fluids (McDowell and Schmid, 1968).

The depositional and structural history of this zone is very complicated (Zingg, 1983). The protoliths assemblage has been interpreted as distal to proximal, terrigenous

sediments deposited along a continental margin with imbricated ophiolitic material that may preserve relict high pressure conditions (Boriani et al., 1990). Although it is commonly assumed that these rocks represent the intermediate crustal, less depleted cover of the Ivrea Zone metasediments (Handy, 1987), the Strona-Ceneri Zone may instead be allochthonous (Boriani et al., 1990).

The dominantly metapelitic Scisti dei Laghi unit is comprised of biotite muscovite garnet ± staurolite or kyanite schists with rare marbles. The zircon lower intercepts are 450-500 Ma; upper intercepts are 1900-2600 Ma (Koppel and Grunenfelder, 1971). Amphibolite bodies having variable abundance of plagioclase (An_{35}), hornblende ± quartz, biotite, microcline and garnet are also present. The metapsammitic Strona-Ceneri unit is composed of medium-grained, biotite-plagioclase gneisses (Ceneri gneiss) including K-feldspar augen gneisses, fine-grained (Gneiss minuti) gneisses and deformed flaser gneisses (Boriani et al., 1977). The mineralogy is dominantly plagioclase + quartz + biotite + muscovite + garnet with lesser K-feldspar, sillimanite and hornblende. A relatively continuous horizon of banded amphibolites separates this group from the underlying Scisti dei Laghi (Boriani et al., 1990).

Concordant bodies of granitic to tonalitic orthogneiss (Cumming et al., 1987) are concentrated near the boundary between the Strona-Ceneri unit and the Schisti dei Laghi. These calcalkaline, Ordovician (450-466 Ma) (Koppel, 1974; Boriani et al., 1982/83) rocks are dominantly composed of plagioclase (An_{25-32}) + biotite ± hornblende with variable K-feldspar, quartz and garnet. It has been suggested that these rocks may somehow be related to the proposed 450 Ma (Hunziker and Zingg, 1980) attainment of peak metamorphic conditions.

4.4.2. Igneous Graniti dei Laghi and Appinites

The metamorphic units are intruded by Permian (270-290 Ma) (Jager and Faul, 1959; Koppel and Grunenfelder, 1975; Hunziker and Zingg, 1980; Pinarelli et al., 1988)

granitic bodies called the Graniti dei Laghi. Most are granitic to grandioritic in composition, although diorite, tonalite (Boriani et al., 1987; Burlini and Caironi, 1988; Boriani et al., 1988b) and rare two mica granite are also found. Some facies contain numerous metasedimentary xenoliths. The granites have contact aureoles which are intensely hydrothermally altered, and examples such as the green granite of Mergozza (Pinarelli et al., 1988) demonstrate that alteration extended into the granitoids as well. The presence of contact aureoles and rare miarolitic cavities suggests an emplacement at relatively shallow crustal levels (Boriani et al., 1988b). A lack of pervasive foliation in the igneous rocks further indicates granitoid emplacement after the peak of regional metamorphism.

Late Carboniferous (Zingg and Schmid, 1979) microdiorites and gabbros are preferentially located near the CMB Line where they are called appinites in reference to similarities with a Scottish Caledonian igneous suite (Boriani and Sacchi, 1973). The appinites are texturally heterogeneous and generally define a calc-alkaline trend with the Graniti dei Laghi (Boriani et al., 1988b). Smaller bodies of lamprophyres, bearing pyroxene, biotite and rare olivine, are porphyritic to aphyric and also tend to cluster near the CMB Line (Boriani and Sacchi, 1973).

Cross cutting relationships were originally interpreted as indicating that the appinites are somewhat older than the granites, although documentation of intermingling structures (Burlini and Caironi, 1988) suggests a closer temporal and, perhaps, genetic relationship. The appinites have Sr_i values between 0.7051 and 0.7103 overlapping with both the more radiogenic granitoid Sr_i of 0.709 (Hunziker and Zingg, 1980) to 0.7100 (Pinarelli et al., 1988) and a gabbroic dike in the Montorfano intrusion which has an Sr_i of 0.7066.

As stated in the introduction, many researchers have suggested that the igneous suites in the Ivrea and Strona-Ceneri Zones are roughly comagmatic based upon chemical

and isotopic evidence (Fountain, 1986; Pin, 1986; Stille and Buletti, 1987; Voshage et al., 1990). Zingg et al. (1979) suggested that granitic magma produced by anatexis of the underlying Ivrean metapelites may have migrated into the overlying Strona-Ceneri Zone to form the Graniti dei Laghi. Voshage et al. (1990) note that modeled andesitic melts produced by AFC processes in the Mafic Complex are comparable to appinite compositions. In slight contrast, a similarity between the Sr_i of the leucocharnockites and the granitoids suggests that both may be hybrids of evolved gabbroic and crustal melts, while incompatible element differences between the two indicate a varying degree of depletion of chemically distinct metamorphic sources (Sinigoi et al., 1991). The relationship between magmatism in the two zones will be evaluated further in the following chapter.

4.5. Evaluation of the Proposed Compound Igneous Suite

As a comagmatic relationship will be difficult, if not impossible, to demonstrate definitively, we must instead investigate whether all available data is consistent with this proposal. As reviewed above, the geochronologic and structural data support the interpretation that the three structural units were distributed all various crustal heights during the Permian magmatic episode. Next we need to evaluate the geochemical and isotopic cohesiveness of the proposed suite and finally develop a model which accounts for the variation. At present, no detailed model for the compound suite is available although models for each of the structural units have been developed separately (Rivalenti et al., 1984; Stille and Buletti, 1987; Pinarelli et al., 1988; Voshage et al., 1990).

One advantage of attempting such modeling in the Ivrea-Strona-Ceneri crustal section is that there is no room in the lower crust to accommodate a "hidden" stage of magma modification prior to emplacement in the Mafic Complex. This requirement obviously results from the interpretation that the absolute base of the crust, or a close approximation thereof, is presently exposed. Therefore the data must be explained in

terms of in situ processes, although the degree of heterogeneity of the mantle source region is a poorly constrained parameter.

4.5.1. Geochemical Affinity of Compound Igneous Suite

The chemical character of various parts of the compound igneous suite has been addressed by many researchers (Rivalenti et al., 1975; Bigioggero et al., 1978/79; Rivalenti et al., 1980; Pin and Sills, 1986; Stille and Buletti, 1987). Most commonly the igneous suite is presumed to display a calcalkaline character, particularly when displayed on an AFM diagram. On such a plot, the calkalkaline assessment is dominated by the more siliceous lithologies, while rocks from the peridotite and mafic units display a tholeiitic Fe-enrichment (Rivalenti et al., 1975). When other parameters are considered, affinities to both suites can be demonstrated (Rivalenti et al., 1975; Bigioggero et al., 1978/79; Rivalenti et al., 1980; Pin and Sills, 1986; Stille and Buletti, 1987).

There are numerous potential difficulties in determining the chemical character of this suite from simple discrimination diagrams although coherent trends are at least consistent with a comagmatic interpretation. Possible difficulties for discriminating between calcalkaline and tholeiitic chemistries arise from the fact that this suite is definitely contaminated by large amounts of reduced metapelitic material of variable composition (as demonstrated in the following chapter), and that hydrothermal alteration of the high level siliceous lithologies may impose secondary trends indicative of alkali enrichment. At present, it appears prudent to apply caution in the interpretation of the geochemical data, although REE analyses have great potential for strengthening the comagmatic hypothesis.

4.5.2. Isotopic Models of Magmagenesis

Stille and Buletti (1987) were the first to present an isotopic model supporting the interpretation of a Permian-Mesozoic comagmatic suite. These authors plotted a simple mixing curve between depleted mantle and Ivrean paragneisses in ε_{Nd}-ε_{Sr} space and noted

that the field defined by Permian granitic and volcanic samples began on this curve and extended to significantly higher values of ε_{Sr}. They interpreted this trend as resulting from mixing between a mantle-derived melt and continental crust to produce the gabbro diorites of the Mafic Complex followed by further assimilation of siliceous crustal material to produce the higher level granites and volcanics. They supported the notion of increased crustal contamination in high crustal levels by describing inclusions of partially melted granophyres in the rhyolites and dacites. Pinarelli et al. (1988) demonstrated that the Rb-Sr systematics of appinite samples could be explained by AFC (assimilation, fractional crystallization) process involving a crustal contaminant.

Voshage et al. (1990) have proposed a similar but more refined model to explain the stratigraphic variation in radioisotopes in the Mafic Complex utilizing three magma chamber processes: AFC (DePaolo, 1981), MASH (melting, assimilation, storage, homogenization) (Hildreth and Moorbath, 1988), and RTF (refilled, tapped, fractionated) (O'Hara and Mathews, 1981). They seek to explain the following observations: irregular variations between mantle and crustal values of ε_{Nd} in the BZ and IZ; the relatively uniform ε_{Nd} found in higher parts of the section: the abundance of positive Eu and Sr anomalies; a stratigraphically upwards increase in LREE abundances.

The model involves two stages. In the first stage AFC and closed system crystallization dominate as sills of mantle-derived magma are injected into the base of the crust. Thick sills induce partial melting and become vulnerable to assimilation of crustally-derived granitic melt while thin sills lack the heat content to induce partial melting and therefore preserve mantle isotopic signatures. The BZ and part of the IZ were formed during this first stage while the UZ, MG and diorite units formed during the second MASH-RTF stage. In this stage a large, convecting magma chamber existed which was fed by mantle-derived melts. Fractional crystallization released energy which was balanced by the melting and assimilation of the surrounding metamorphic section.

Formation of plagioclase and pyroxene cumulates served to decouple the major from the minor elements producing an upwards LREE increase and cumulates with positive Eu and Sr anomalies. One ramification of this model is that the hybrid melts that supposedly were tapped and intruded to higher crustal levels, possibly represented by the Graniti dei Laghi and appinites, should have negative Eu anomalies.

Success of this model is judged by the fact that AFC and bulk mixing curves generate trajectories in Nd-Sr space which approximate the Mafic Complex data (Fig. 5.10) . This model will be evaluated in light of the oxygen isotope data in the following chapter.

4.6. Geologic History of the Ivrea Zone

In striking contrast to the Mesozoic continental margin of California discussed in earlier chapters, the geologic history of the Southern Alps is poorly understood. This lack is due both to the older age of the latter terrane as well as its location within a younger collisional orogen. Whereas a consensus has not been reached concerning all of the historical details, only three features of the following geologic history are important for the present study of the isotopic systematics of the Mafic Complex: intrusion of the Mafic Complex was not followed by a prograde metamorphic event; the geochronology indicates that the igneous rocks overlap in age despite a slight upward younging; and generation of the igneous suite occurred either in a continental margin arc (Stille and Buletti, 1987) or in a transtensional regime heralding continental rifting (Handy and Zingg, 1991). Following is a brief geological history of the Ivrea and Strona-Ceneri Zones, but recent, excellent reviews (Zingg et al., 1990; Handy and Zingg, 1991) of the data should be consulted for a more detailed discussion.

4.6.1. Tectonic Environment of Magmagenesis

There is little agreement in the literature concerning the tectonic reconstruction of central and northern Europe during the Hercynian orogeny. While most models invoke a

continental margin subduction zone environment, the location, polarity and number of subduction zones is highly variable and the absence of large granitic batholiths makes this scenario suspect. For example, based on the chemical and isotopic systematics of isolated Hercynian granitoids, one model invokes southward subduction from a northern European trench system beneath a southern continental mass (Liew and Hofmann, 1988) while another model invokes the northwestward subduction of a paleoTethys (Finger and Steyrer, 1990) beneath the Eurasian plate.

The tectonic reconstruction of the Southern Alps during the Hercynian orogeny is equally problematical. In past reconstructions, significant weight has been assigned to the purported calkalkaline character of the the Mafic Complex, the Grantiti dei Laghi and the Permo-Mesozoic compound igneous suite. Specifically, demonstration of a calcalkaline character has been presented as evidence supporting a convergent margin environment of magmagenesis. Recent detailed structural investigations in the Ivrea Zone (Handy and Zingg, 1991) suggest that this chemical and tectonic assignment may need to be reevaluated.

4.6.2. Tectonic Reconstructions

The metamorphic protoliths of the Ivrea Zone are generally considered to have been deposited on a stable margin preceding subduction and/or in an accretionary wedge (Sills and Tarney, 1984).

4.6.2.1. Convergent Margin

If the purported calcalkaline character of the igneous suite is indicative of the tectonic environment of magmagenesis then variations of the following continental margin arc scenario may be appropriate. The igneous suite was emplaced into different structural levels of a continental margin arc (Garuti et al., 1980; Rivalenti et al., 1980) overlying a southeastward facing subduction zone (Stille and Buletti, 1987). A variation on this subduction zone model suggests the unusual location of the Ivrea Zone (Southern Alps) on

the southern margin of the European continent (Mercolli and Oberhansli, 1988) instead of the more widely accepted position on the northern margin of the Adriatic plate. In this model the calcalkaline suite formed overlying a northerly facing subduction zone.

The radioisotopic systematics of the Permo-Mesozoic volcanics (Stille and Buletti, 1987) form pseudoisochrons which are consistent with mixing between mantle and crustal components of similar character as required for the Graniti dei Laghi. Hybridization is also believed to be important in the Mafic Complex (Voshage et al., 1990) and has been demonstrated in calcalkaline suites of known continental margin affinity (DePaolo, 1980).

4.6.2.2. Extensional Regime

An alternate group of hypotheses is that the parental magma of the igneous suite underplated the trailing edge of an incipiently rifted continent (Fountain, 1989; Quick et al., in press). In this family of models the lower crustal extension, magmatic underplating (Brodie and Rutter, 1987; Brodie et al., 1989) and graben formation occurred in a Late Paleozoic transtensional environment (Handy and Zingg, 1991). These events preceded the Late Triassic to Early Jurassic rift formation of the Neotethys basin (Trumpy, 1975; Lemoine, 1984) which is witnessed by the significantly younger (>50 Ma) extension along the Pogallo Ductile Shear Zone (Handy, 1986; Handy and Zingg, 1991).

The transtensional scenario is not dependent on the purported calcalkaline character of the igneous suite and reflects the growing amount of data supporting synmagmatic extension. The rift model is supported by pressure estimates (8-9 km) for the base of the Ivrean section which are surprisingly low for the base of a continental margin arc, thermobarometric estimates of geothermal gradients which are comparable to oceanic geotherms (Capedri et al., 1976), and synmagmatic deformation features in the Mafic Complex similar to structures found in ophiolites and having shear senses similar to those found in the younger extensional structures (Brodie and Rutter, 1987; Quick et al., in press). It should be noted that the mantle peridotites have been interpreted as being both

suboceanic (Capedri et al., 1976; Ernst, 1978) and subcontinental (Shervais, 1979) in character.

Based on a suite of lower crustal xenoliths from the Massif Central of France, Downes et al. (1991) hypothesizes that at the end of the Hercynian event crustal thinning promoted the intrusion of mafic melts and late-orogenic granulite facies metamorphism. A similar model was presented for the French Pyrenees in which intrusion of mafic melt into a thinned crust promoted Hercynian regional metamorphism in the overlying crust and extensive melting in the underlying crust; this melt would segregate at some latter time and be emplaced upwards after the metamorphic peak in the overlying rocks (Wickham and Oxburgh, 1987). These scenarios of crustal thinning and underplating of mafic magmas agree with observations from the Ivrea-Strona-Ceneri section.

A combination of subduction-related magmatism in an extensional environment may be possible in a successor basin formed by gravitational collapse of dense lower crust over a rolling-back subducting plate (Laubscher, 1990). This author also seeks to explain the nature of the Ivrean paleoMoho as a tectonic boundary formed by the removal of the original lower crust (the basement of the Ivrean protoliths) and replacement by mantle material in a convergent plate margin.

4.6.3. Geologic History of the Ivrea-Strona-Ceneri Crustal Cross Section

Numerous geochronologic studies have been combined with the geologic evidence discussed above to produce the following tentative history for the Ivrea Zone:

(1) Deposition of the sedimentary protoliths occurred between 700 and 450 Ma (Koppel, 1974; Hunziker and Zingg, 1980) on an unknown basement terrane. Detrital zircons in these sediments were derived from rocks of PreCambrian to Cambrian age (1900 to 2600 Ma) (Koppel and Grunenfelder, 1971).

(2) Basalts were interbedded with, intruded or emplaced into the sediments during burial of the volcanosedimentary pile to depths of approximately 30 km.

(3) Peak regional metamorphic conditions occurred at some time between 480 (Hunziker and Zingg, 1980) and 300 Ma (Schmid and Wood, 1976) due to burial and/or enhanced by the intrusion of large ultramafic and mafic bodies. Peak conditions were accompanied by intense deformation producing gneissic foliation and isoclinal folding (Handy and Zingg, 1991), and by large amounts of anatexis producing migmatites.

(4) A diverse igneous suite was emplaced in all crustal levels between 300 and 270 Ma. The geochronologic constraints for a Hercynian magmatic event and migmatization related to intrusion are listed below:

i) 6 zircon fractions from a diorite sample yielded a near concordant U-Pb date of 285 +7/-5 Ma (Pin, 1986);

ii) a date of 275 $\pm$ 2 Ma was obtained from concordant monazites separated from Ivrean paragneisses (Koppel, 1974);

iii) a whole rock Sm-Nd isochron indicating an approximate date of 270 Ma for the dikes in the Balmuccia Peridotite (Voshage et al., 1988);

iv) 295 $\pm$ 5 Ma for concordant monazites from Strona-Ceneri migmatite;

v) a concordant date of 285 $\pm$ 10 Ma from zircon fractions from three Ivrean paragneiss samples (Koppel, 1974);

vi) a concordant 295 $\pm$ 5 monazite date of the Mt. Orfano granite (Koppel, 1974);

vii) a Rb-Sr whole rock isochron yielded a date of 278 $\pm$ 3 Ma for the Baveno-Mt. Orfano Graniti dei Laghi suite (Hunziker and Zingg, 1980);

viii) 275-280 Ma from Rb-Sr whole rock $\pm$ biotite isochrons from three intrusions in the Graniti dei Laghi (Pinarelli et al., 1988);

ix) a Rb-Sr mineral isochron for a Lugano dacite yielded a date of 262$\pm$ 1 Ma (Stille and Buletti, 1987).

(4) The Ivrea-Strona-Ceneri section was extended and rotated during Mesozoic rifting (Handy and Zingg, 1991) related to opening of the Neotethys basin. Deposition of the base of Permo-Mesozoic volcanosedimentary sequence occurred unconformably on the southern margin of the Strona-Ceneri Zone. Limited subsequent rotation of the Permo-Mesozoic section indicates the presence of a poorly understood hinge structure in the southern Strona-Ceneri Zone (Handy and Zingg, 1991).

(5) Possibly the section was slightly reheated during an Alpine event (30-18 my) (Allegre et al., 1974; Koppel, 1974; Koppel and Grunenfelder, 1975; Zingg and Schmid, 1979; Hunziker and Zingg, 1980; Burghi and Klotzli, 1990).

(6) Mica K-Ar, 40Ar/39Ar and fission track ages reflect the subsequent rotational and uplift history, the details and ambiguities of which are summarized in Burghi and Klotzli (1990) and in Zingg et al. (1990).

(7) Final tilting of the Ivrea-Strona-Ceneri crustal cross section occurred prior to 12 Ma as little relative vertical offset has occurred across Insubric Line since 12.5 $\pm$ 2 Ma (Burghi and Klotzli, 1990).

4.7. Identification of Petrologic Significance

The justification for equating the Ivrea-Strona-Ceneri section with a mildly disrupted cross section through middle to lower continental crust should be evident from the preceding discussion. The petrologic descriptions are consistent with the emplacement of a large volume of mantle-derived magma into the base of the crust. Fractional crystallization combined with assimilation of the metamorphic wall rocks along the outer contact and around septa within a large, convecting magma chamber appear to have produced the gross upward evolution to more siliceous lithologies. There may be genetic relationship between the Permian magmatic suites in both zones, but the tectonic environment of magmagenesis is unclear. The absence of retrograde lithologies indicates

that little low temperature hydrothermal circulation occurred; the possible preservation of magmatic isotope systematics, however, must be demonstrated.

In the following chapter the feasibility of using oxygen isotopes to study magmatic processes in the lower continental crust will be evaluated. The coordinated use of radiogenic and stable isotopic studies to quantify the magmatic processes will be confirmed. Finally an attempt will be made to identify diagnostic patterns in the oxygen isotope systematics which can be applied to other Hercynian igneous suites in which the spatial and temporal relationships of the magmatism are less clear.

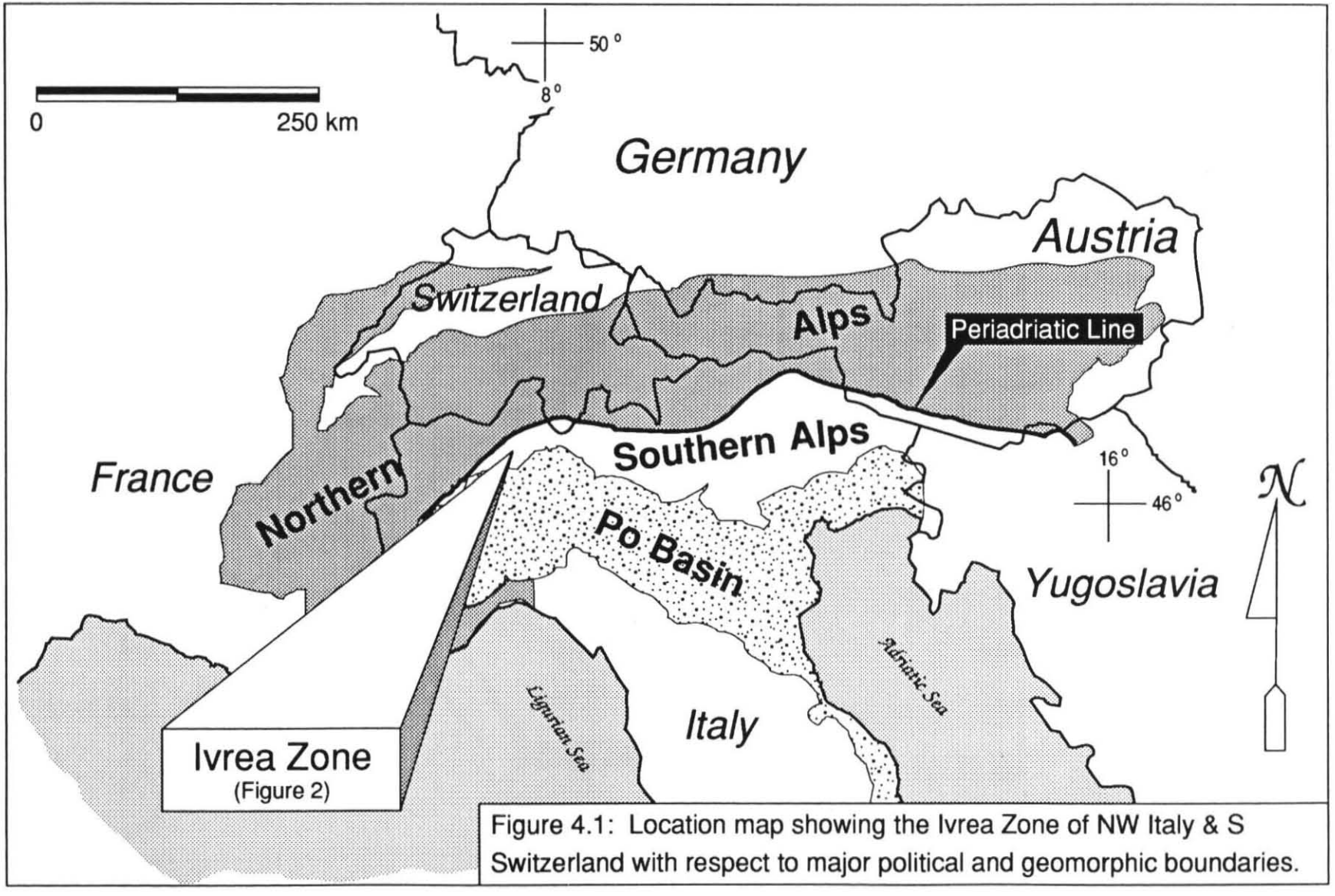

Figure 4.1: Location map showing the Ivrea Zone of NW Italy & S Switzerland with respect to major political and geomorphic boundaries.

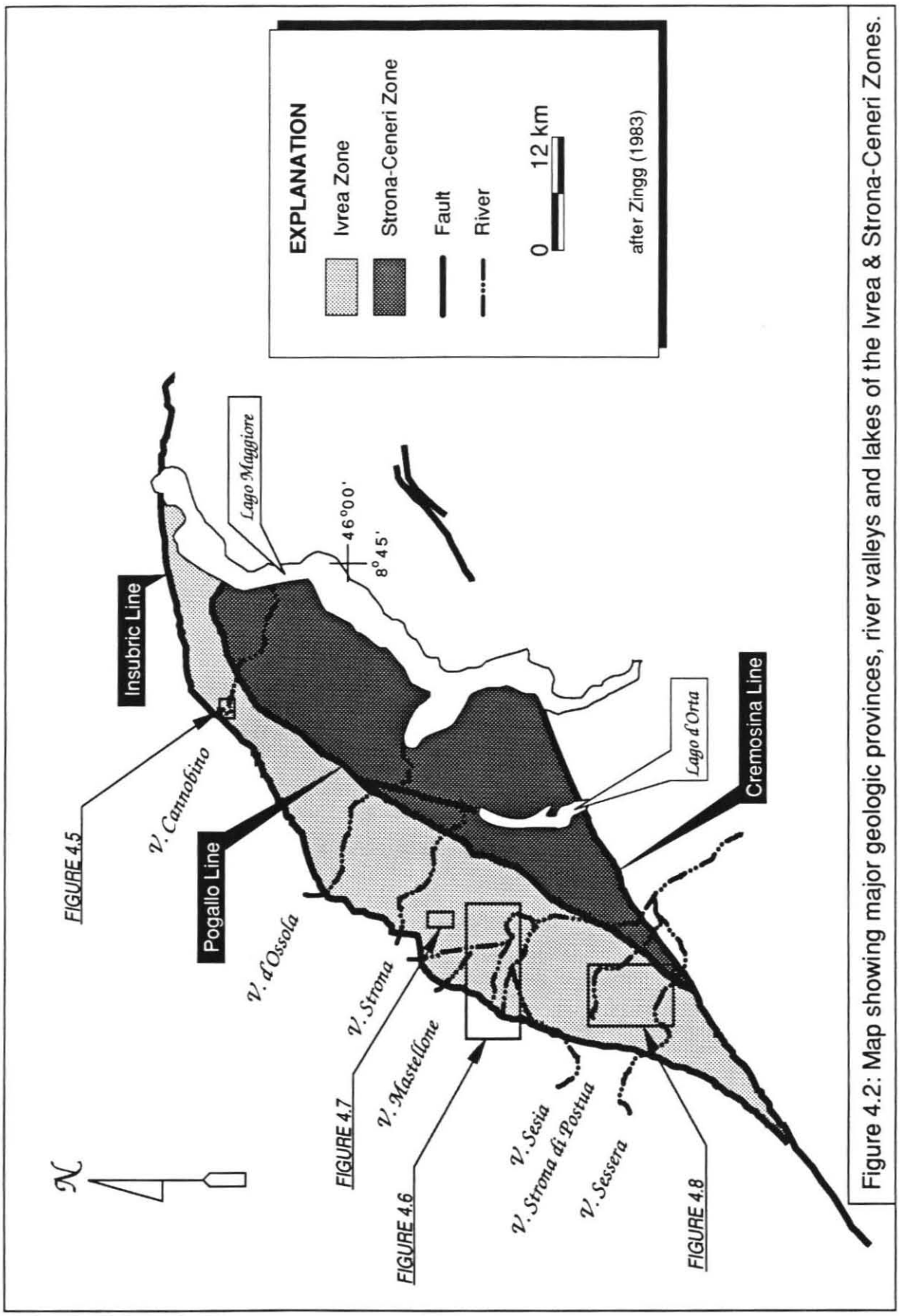

Figure 4.2: Map showing major geologic provinces, river valleys and lakes of the Ivrea & Strona-Ceneri Zones.

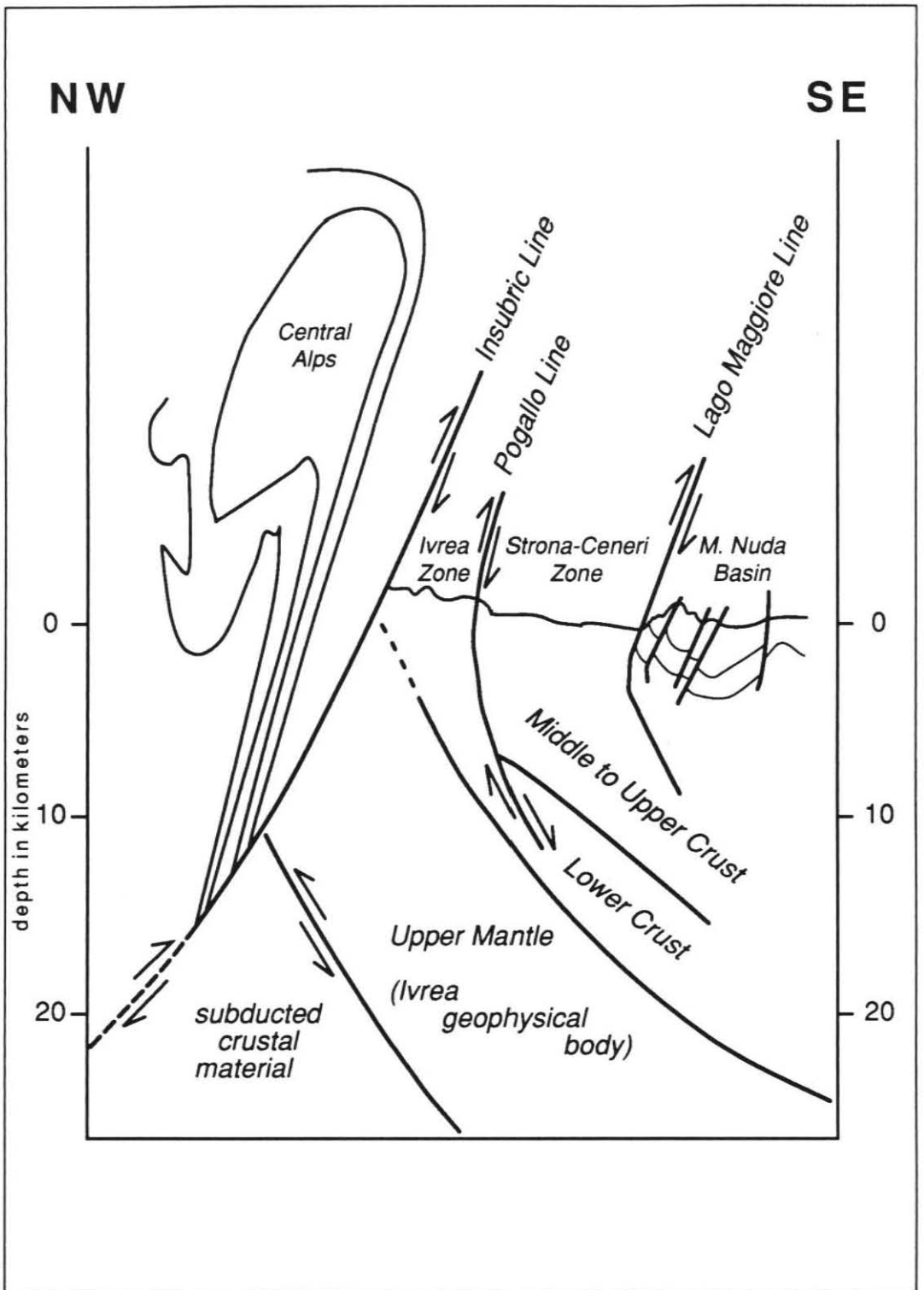

Figure 4.3: Schematic cross section through the northwestern Italian Alps in the vicinity of the Ivrea Zone, the Strona-Ceneri Zone and the M. Nudo basin (after Zingg et al., 1990).

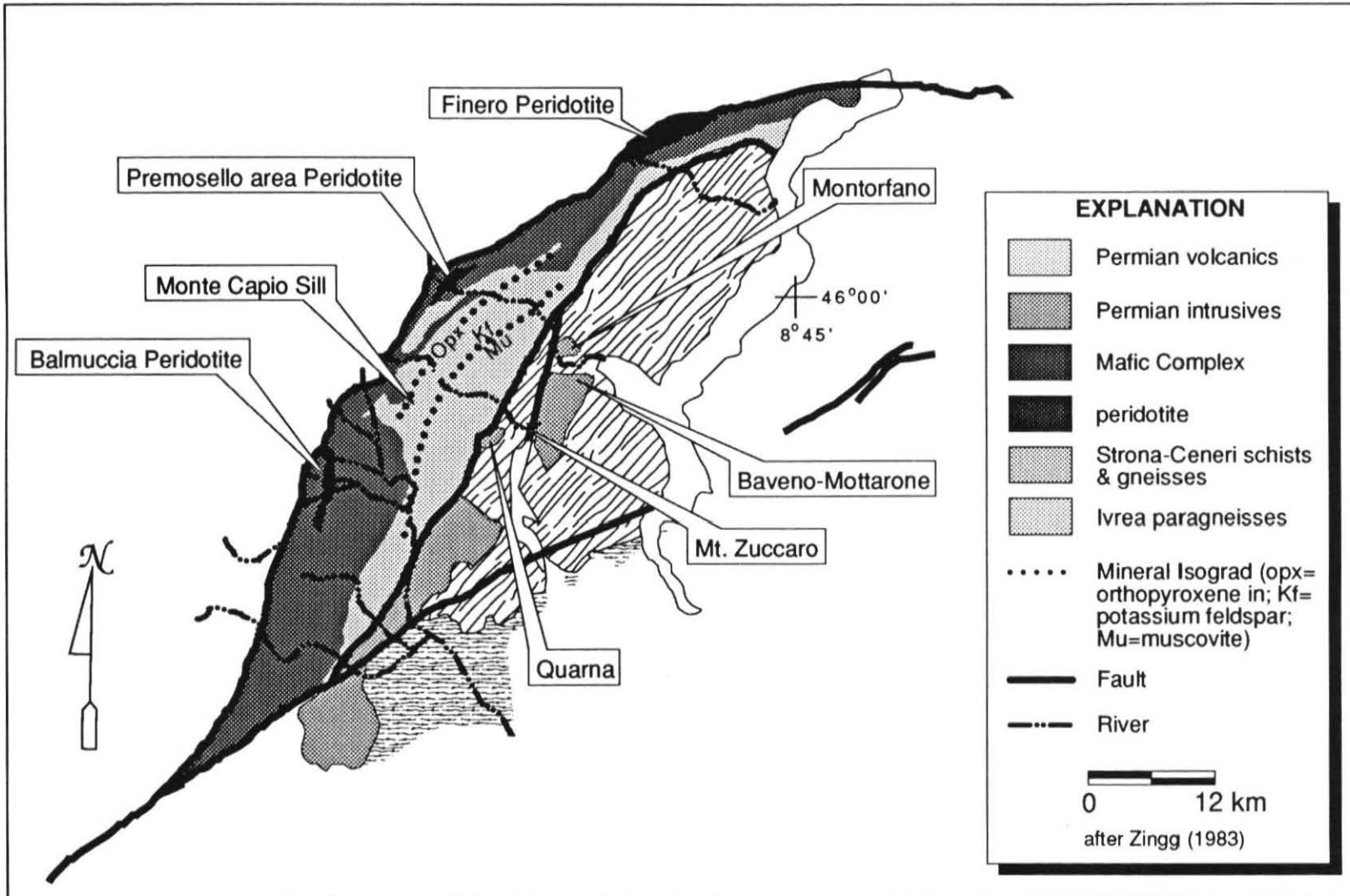

Figure 4.4: Map showing generalized geology, prominent igneous bodies and locations.

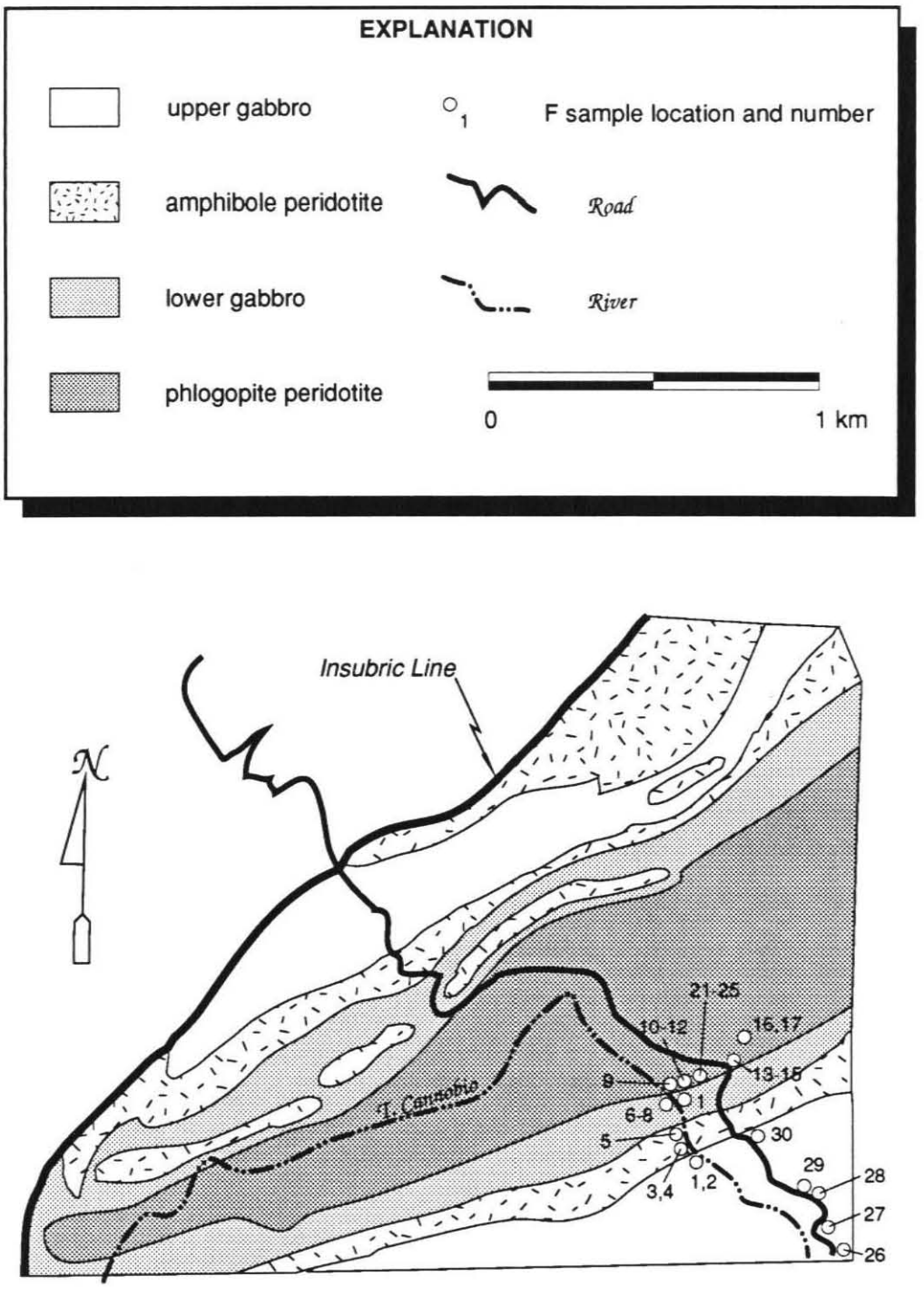

Figure 4.5: Sample locations and generalized geology of the Finero Peridotite Complex after A. Steck & J.-C. Tieche (1976).

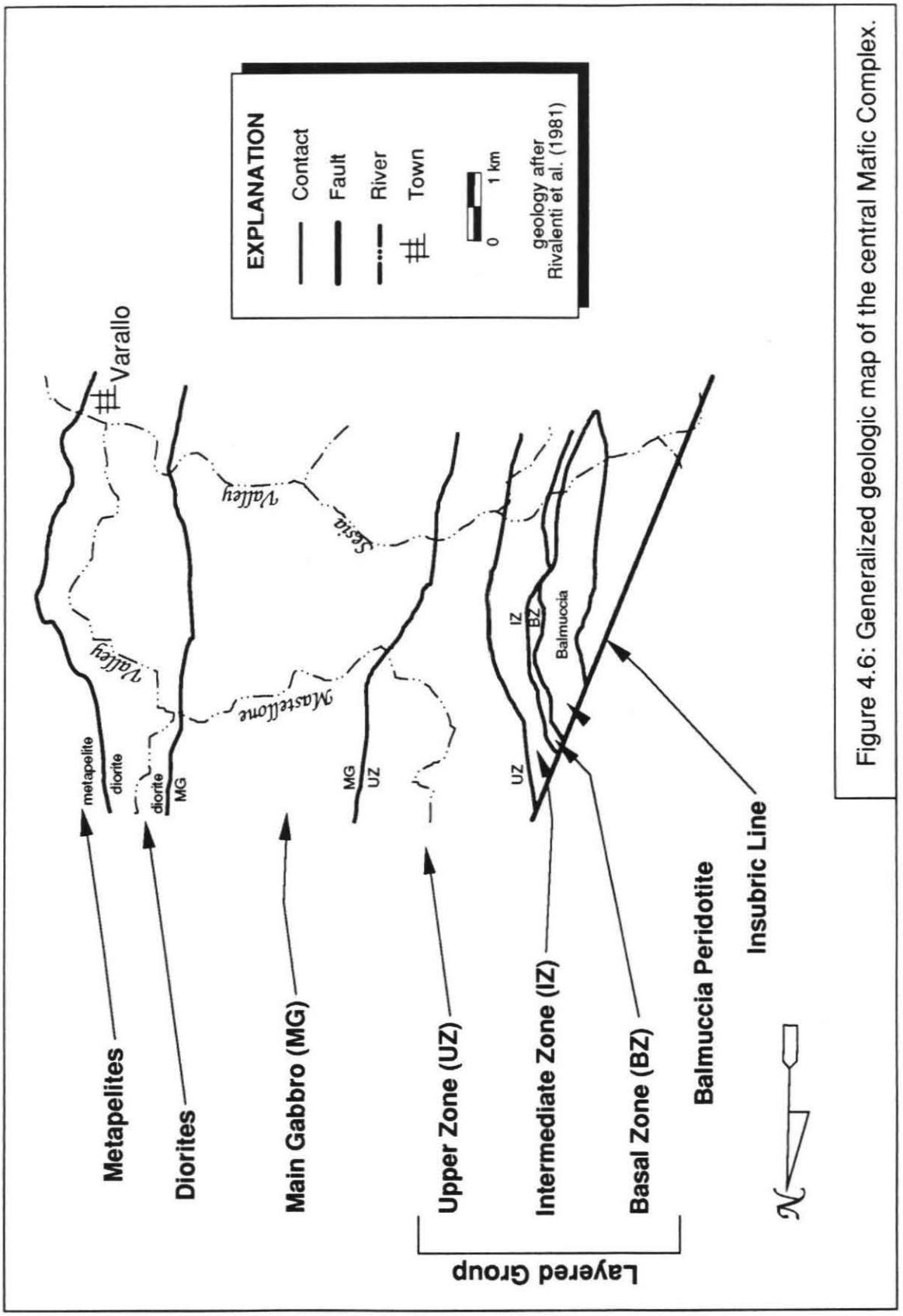

Figure 4.6: Generalized geologic map of the central Mafic Complex.

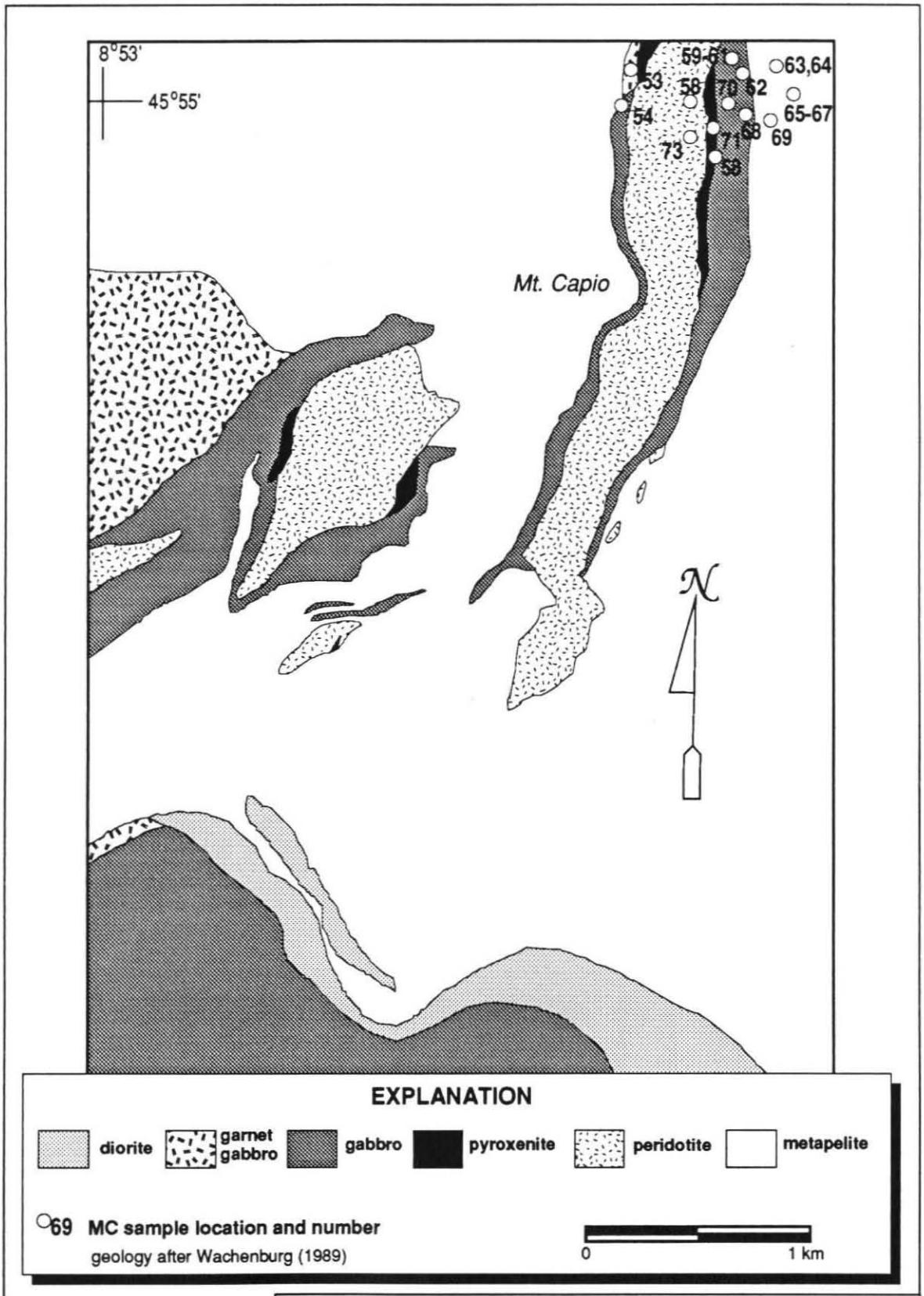

Figure 4.7: Map showing sample locations and generalized geology of the Monte Capio Region, Ivrea Zone

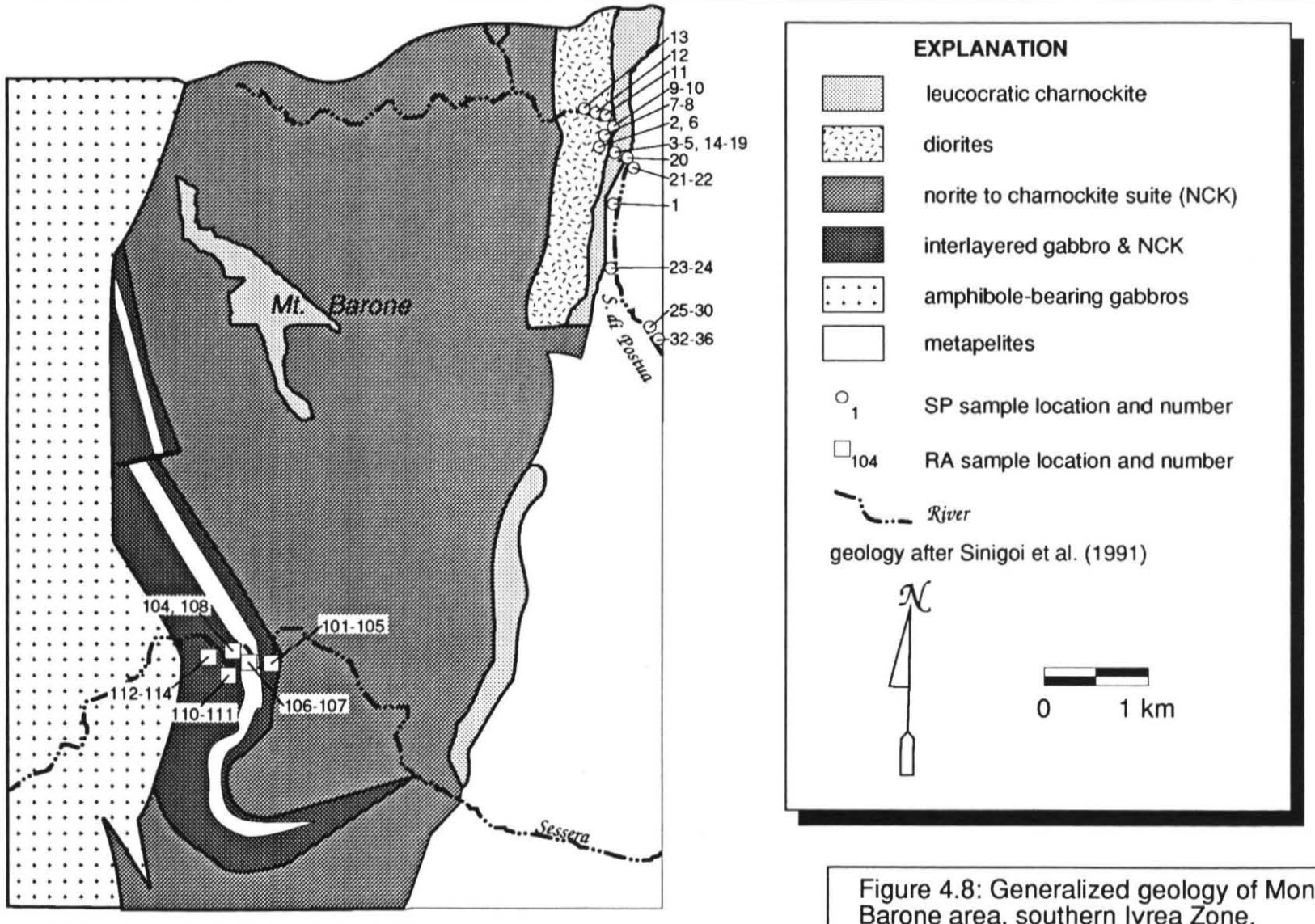

Figure 4.8: Generalized geology of Monte Barone area, southern Ivrea Zone.

Chapter 5: Oxygen Isotopic Investigation of the Mafic Complex and Associated Lithologies (Ivrea and Strona-Ceneri Zones, Southern Alps)

New oxygen isotope analyses of 237 whole rock and 26 mineral separates from the Mafic Complex of the Ivrea Zone and associated lithologies form an extensive data base with which to study igneous processes in a unique exposure of lower continental crust. The character of the parental magma(s) and contaminant(s) as well as constraints on the relative significance of processes such as crystal fractionation, assimilation and magma mixing will be addressed below.

The lithologic composition, structural evolution and geologic history of the Ivrea-Strona-Ceneri crustal cross section have been described in the preceding chapter. Chapter 4 should serve as a reference for the following discussion as stratigraphic divisions, foreign terms and other proper names used below were explained therein. Finally, the petrogenetic justification for a detailed study of the oxygen isotopes of this Hercynian igneous rock suite was presented and forms the necessary framework for the following interpretation of the isotopic data.

5.1. Review of Previous Oxygen Isotopic Work in the Ivrea Zone

Prior to the initiation of this study, no oxygen isotopic data were available from this region. In the past few years a significant number of analyses of the metamorphic section have been published, compared to only a limited number of analyses of the igneous lithologies. The present study serves to rectify this imbalance.

Oxygen isotope systematics confirm the sedimentary origin of the protoliths. Isotopically heavy values for quartz separates from metapelites ($\delta^{18}O_{SMOW}$ = +9-17‰) and calcite separates from marbles and calcsilicates ($\delta^{18}O_{SMOW}$ = +13-24‰) extend to premetamorphic values predicted for the appropriate protoliths: i.e. pelites ($\delta^{18}O_{SMOW}$ = +15‰) and limestones ($\delta^{18}O_{SMOW}$ = +28‰). The shift to isotopically lighter values has been partially attributed to the limited interaction with fluids derived from the

volcanosedimentary section during prograde metamorphism (Baker, 1988; Baker, 1990) possibly augmented by fluids released during crystallization of the Mafic Complex (Schnetger, 1988).

Baker (1990) found no evidence for correlation of $\delta^{18}O$ with increasing metamorphic grade. He argued for lithologically channelized fluid flow and low water-rock ratios in order to produce the cm scale isotopic gradients at found at pelite-carbonate interfaces. Schnetger (1988) perceived a slight lowering of $\delta^{18}O$ with increased metamorphic grade: amphibolite facies kinzigites (12.9 ± 1.0‰) and granulite facies stronalites (11.1 ± 1.7‰) with a total whole rock range of 10-14‰. He interpreted this minor distinction as resulting from the preferential depletion in heavy isotopes during progressive degranitization (Schnetger, 1988) which was proposed previously for the metamorphic section based on geochemical arguments (Schmid, 1978). Both investigators concluded that there had been no large scale isotopic homogenization resulting from pervasive fluid flow through these rocks.

Isolated analyses of the Mafic Complex are published. Analyses of five samples of the Balmuccia peridotite and associated dikes vary from +5.7 to 7.1‰ (Mayer, 1989; Baker, 1990) and are recognized as being similar to mantle values. Mayer also analyzed two mineral pairs from Al-augite suite dikes: (plag, cpx) equal to (5.9‰, 4.7‰) and (7.5‰, 5.8‰). These samples yield calculated temperatures of 500°C and 700°C similar to estimates for reequilibration of the base of the Mafic Complex at granulite facies conditions discussed previously. An unknown number of plagioclase separates from gabbros yielded $\delta^{18}O$ values of +8.5 to 8.9‰ with the exception of a diorite sample which had a $\delta^{18}O$ signature of +11‰ (Sills et al., 1986). The range is reasonable for igneous plagioclase, while the +11‰ undoubtedly reflects crustal contamination of the diorites.

Sixteen whole rock analyses from the southern Ivrea Zone yield a variation of +1.5‰ per 10% SiO_2 indicating that processes other than simple crystal fractionation were

important in their genesis (Sinigoi et al., 1991). These samples include amphibole gabbros ($\delta^{18}O$ = 6.6‰, 7.0‰) having Sr_i values comparable to the Main Gabbro (0.707) and leucocharnockites which have $\delta^{18}O$ signatures of +11.1 to 11.7‰ and Sr_i values comparable to the Graniti dei Laghi (0.710). The strontium and oxygen isotopic ranges are interpreted as reflecting the incorporation of both mantle and crustal components in these igneous rocks.

The main conclusions of these researchers - specifically the lack of isotopic homogenization, the preservation of igneous and/or metamorphic isotopic fractionations, and the reflection of both mantle and crustal resevoirs in the $\delta^{18}O$ values of the Mafic Complex - are corroborated and expanded by the following detailed investigation.

5.2. The Present Study

Most of the data presented in this study is the result of collaborative sampling with Professor Silvano Sinigoi and Doctoresse Gabriella Dimarchi, both of the Istituto di Mineralogia e Petrografia di Universita di Trieste, Italy, and their students. They identified a number of transects through the Mafic Complex which encompassed the variation in lithology and intrusion style which characterizes the body. Sampling was concentrated along these transects, particularly along the Sesia and Mastellone valleys where the Mafic Complex is well exposed and attains its maximum thickness. The samples were taken to Trieste where they were powdered in a tungsten carbide shatterbox and chemically analyzed by X-ray fluorescence. A split of the powder as well as a hand sample were then shipped for study at Caltech. Additional samples and chemical analyses from the Val Mastellone area were provided by Prof. Sinigoi. Oxygen isotope analyses were performed as described in Chapter 3. Additional sampling was performed by the author, and samples with previously published radioisotopic analyses were graciously provided by the following researchers (listed alphabetically): A. Burghi of Bern, Switzerland; A. del Moro and L. Pinarelli of Pisa, Italy; A. Hoffman and the late Hans Voshage of Mainz, Germany;

G. Rivalenti and M. Mazzucchelli of Modena, Italy. The new as well as the previously published isotopic and chemical data are compiled in Tables 5.1-5.7.

The Mafic Complex was picked for study because of its apparent location at the base of a crustal section. As such it was anticipated that the study may isolate the initial stages of modification of mantle material in the continental crust: specifically, no previous "hidden" stage of magma modification in a crustal environment could reasonably be invoked and the question of mantle source homogeneity versus heterogeneity might be addressed. The perceived goals were to isotopically characterize the material added to the continent as well as to identify the significant processes that subsequently modified the magma during formation of this large, layered ultramafic-mafic intrusion.

5.2.1. Mineral Separates

Before these goals could be addressed it was necessary to demonstrate that the isotope systematics reflected the magmatic event and not a subsequent modification. Such a modification might include high temperature hydrothermal alteration by a nonmagmatic fluid which could reset the oxygen isotope systematics without affecting the igneous mineralogy. This was particularly necessary as the collaborative study was designed around the analysis of whole rock samples which do not in themselves necessarily provide an internal check against subsequent isotopic modification. To address this problem twelve samples were chosen for the isotopic analysis of mineral separates. These samples were chosen after the analysis of numerous whole rock samples revealed no unusually low oxygen isotope signatures indicative of hydrothermal alteration, and included samples with normal magmatic as well as elevated whole rock $\delta^{18}O$ values. An additional concern was to chose samples from various stratigraphic positions within the igneous complex in order to investigate the possibility of stratigraphically limited fluid circulation.

The results are listed in Table 5.8 in their relative stratigraphic position within the central Mafic Complex. Two additional samples, VS128a and VS128b, are not true

mineral separates but instead come from adjacent, cm-thick anorthosite and pyroxenite layers; there is, therefore, no whole rock $\delta^{18}O$. Two samples from other localities, MC58 from the Monte Capio Sill and F26 from the Finero peridotite complex, have been inserted in their approximate stratigraphic positions.

5.2.1.1. Isotopic Reversals

Two important results are evident from the data. The first result is that there are no isotopic reversals (i.e., a negative value of $\Delta_{plag\text{-}mafic}$) between plagioclase and any coexisting mafic phase. Magmatic plagioclase is always isotopically heavier than coexisting mafic minerals but is much more sensitive to isotopic alteration. The existence of isotopically lighter plagioclase (resulting in a negative value of $\Delta_{plag\text{-}mafic}$) has been repeatedly demonstrated as recording the interaction of the rock with a low $\delta^{18}O$ fluid. Such interaction would produce a steep trajectory on a $\delta^{18}O_{mafic}$ vs. $\delta^{18}O_{plag}$ diagram; such a trajectory is not apparent in either Figure 5.1 or 5.2. Moreover, the whole rock $\delta^{18}O$ is consistently intermediate to the plagioclase and mafic phase $\delta^{18}O$ as would be expected if magmatic values have been preserved (Fig. 5.3), and it can be demonstrated that calculation of a whole rock $\delta^{18}O$ value using the sample mode and the mineral separate $\delta^{18}O$ values approximates the actual whole rock $\delta^{18}O$. In sum these observations strongly suggest that the magmatic values of $\delta^{18}O$ have been preserved throughout the Mafic Complex.

Using the modal data, trajectories (not shown) aimed at removing the subsolidus isotopic exchange between the two mineral phases can be drawn on Figures 5.1 and 5.2. The trajectory slopes are proportional to the relative modes of the two phases. By extrapolating these trajectories to an estimated magmatic value of $\Delta_{plag\text{-}mafic} = 0.5‰$ contour, the $\delta^{18}O_{magma}$ for the various stratigraphic levels can be estimated as follows: peridotite dike = 6.8‰; BZ = 7.5 - 9.2‰; IZ = 7.7 - 9.3‰; UZ = 7.5 - 8.6‰; diorite = 8.2‰. These estimates suggest an upwardly increasing and highly variable $\delta^{18}O_{magma}$

through the IZ unit with less extreme variation occurring at higher levels. Although based on few samples, these estimates approximate conclusions drawn from the extensive whole rock $\delta^{18}O$ data set and will be discussed in that context later.

5.2.1.2. Geothermometry

A second result from the study of mineral separates is that the temperatures calculated from the mineral pairs are generally consistent with the magmatic interpretation of the oxygen isotopic systematics. As the isotopic fractionation between a coexisting mineral and magma are temperature dependent, the values of $\Delta_{plag\text{-}mafic}$ (where "mafic" refers to either pyroxene or amphibole) are a function of temperature. Calibrations of plagioclase-pyroxene and plagioclase-amphibole fractionations (Bottinga and Javoy, 1975) have been used to calculate temperatures which are listed in Table 5.8 and displayed in Figure 5.4 . Before discussing the conclusions, two samples must be discussed. The temperature for sample VS114 is slightly higher than would be expected based upon other geothermometric estimates from the Mafic Complex (section 4.1.2). While this sample may record magmatic temperatures, this estimate is interpreted as being sensitive to rounding errors prior to temperature calculation and to the $\pm$ 0.15‰ analytical error. It must be noted that the temperature of 820°C calculated for sample VS132 is somewhat in question as the plagioclase-hornblende geothermometer is only calibrated to 800°C.

In Figure 5.4 an approximately bimodal temperature distribution is evident. This bimodality is not a function of the whole rock $\delta^{18}O$ as is shown on Figure 5.5. The higher temperature range between 764°C and 1066°C is interpreted as recording a possible range from an intrusion temperature of approximately 1000°C to temperatures of autometamorphic recrystallization of the Mafic Complex similar to those recorded by mineral pair geothermometers (750 - 950°C; section 4.1.2). The lower temperature range between 500°C and 608°C is interpreted as reflecting subsequent isotopic diffusion during subsolidus reequilibration. Such reequilibration is certainly possible given the textural

evidence discussed in Chapter 4 for autometamorphism of the Mafic Complex during slow cooling from magmatic temperatures in the lower crustal environment. The low temperature for sample VS107 (425°C), a diorite located within the migmatites along the roof of the Mafic Complex, may reflect either the lowest blocking temperature for diffusional isotopic exchange within the complex or a slight degree of subsolidus interaction with evolved magmatic fluids.

The above discussion demonstrates that a large scale hydrothermal system did not develop around and within the Mafic Complex as has been suggested for layered complexes in the upper crust (Norton and Taylor, 1979). A similar conclusion was reached by Baker (1988) based upon his analyses of the surrounding metapelites. Due to the limited number of mineral separates analyzed in the present study, however, the possibility that localized interaction with isotopically foreign fluids occurred cannot be ruled out. Indeed there is a possibility that limited amounts of layer parallel fluid flow and exchange occurred within the Mafic Complex as has been suggested for marble-metapelite interfaces (Baker, 1990). Investigating this possibility will entail detailed sampling and extensive mineral separate analysis, and will be the subject of a future study. Regardless, the approach taken by the present study, namely utilizing whole rock data to study igneous processes, appears to be justified. In particular, the elevated $\delta^{18}O$ values of ultramafic and mafic whole rock samples such as VS114 and VS138 does not appear to be correlated with the mineral pair temperature suggesting that these isotopically heavy samples reflect magmatic signatures and not subsequent alteration.

5.2.2. Stratigraphic Variations of Isotopic Systematics

The variation of isotopic systematics with stratigraphic, or vertical, position within layered intrusions has been considered petrogenetically significant in many studies. In the Bushveld Complex of South Africa, for example, abrupt variations of Sr_i values with height have been interpreted in terms of limited interaction between two isotopically and

chemically distinct parental magmas (Sharpe, 1985). Similar interpretations have been made for stratigraphic variations in mineralogy, metallogeny and $\delta^{18}O$ signature in the Stillwater Complex of Montana (Irvine et al., 1983; Dunn, 1986). Alternatively, stratigraphic variations of $\delta^{18}O$ in the Skaergaard intrusion of Greenland have been used to model the three dimensional hydrothermal fluid flow regime (Norton and Taylor, 1979).

In the Mafic Complex of the Ivrea Zone stratigraphic variations of $Sr_{(270)}$ from a limited number of samples were first attributed to the presence of isotopically distinct magmas (Pin and Sills, 1986). Recently, the upward variation of $\varepsilon_{Nd(270)}$ and $Sr_{(270)}$ in a significantly larger data set has been convincingly modeled in terms of in situ AFC and MASH processes involving a single parental magma (Voshage et al., 1990); this model has been described in section 4.5.2. and the calculations will be discussed in section 5.2.4.1.

A rapid and sporadic decrease of $\varepsilon_{Nd(270)}$ with increasing stratigraphic height complemented by a similarly sporadic increase in $Sr_{(270)}$ is displayed in Figure 5.6; the data is compiled in Tables 5.3 and 5.4. Much of the isotopic change occurs in the BZ with some extreme values present in the IZ. The rapid transition might be suggestive of an interface between two isotopically distinct magmas. This appearance, however, is deceptive and is most likely an artifact of limited sampling: it will be shown below that the rapid variation from BZ to IZ isotopic values occurs over a very limited range of magmatic fractionation in the AFC model. The wide isotopic scatter in the BZ and IZ is attributed to the sporadic operation of the AFC process with a crustal component during initial stages of sill emplacement. The relative lack of isotopic variation at higher levels, clearly shown by the $\varepsilon_{Nd(270)}$ data, is attributed to chemical and isotopic homogenization in a large, convecting magma chamber which developed above the metapelitic septa separating the IZ from the UZ (section 4.2.3.1.3.) (Voshage et al., 1990). Note, however, that there is

significant scatter of $Sr_{(270)}$ in the MG indicating that the purported homogenization was not complete for all systems.

The variation of $\delta^{18}O$ with stratigraphic position within the Mafic Complex is displayed in Figure 5.7; the analyses are listed in Table 5.1. Note that the vertical scale is based on a map view of the central Mafic Complex: the vertical position of each $\delta^{18}O$ sample has been projected horizontally across from the appropriate sample locality shown on the map. Also note that the data in Figure 5.7 is derived from a suite of samples distinct from those of Voshage et al. (1990); $\delta^{18}O$ values of both suites are displayed together on a histogram in Figure 5.8 (Tables 5.1 and 5.3).

The wide range of $\delta^{18}O$ values between +6.5‰ and 9.2‰ in the BZ and IZ indicates a highly variable degree of interaction at the base of the crust between mantle-derived magmas and high $\delta^{18}O$ crust. Rapidly crystallized magma, such as might have been emplaced as thin sills in cool crust, would retain the source signature, while thick sills, or intrusions emplaced into previously heated crust, would have great potential for assimilation. The variation in the thermal state of the wallrock may have been spatial, but was more likely temporal, the early intrusions interacting with a cooler crust which became progressively warmer promoting assimilation within the later pulses. Recall that evidence for extensive melting of the metamorphic lithologies was presented in section 4.2.1.2 and that the mineral separate data demonstrated that the heaviest $\delta^{18}O$ values (9.2‰ for sample VS 114) are magmatic. In some contrast to the Nd and Sr systems, partially resulting from the much larger $\delta^{18}O$ data base, the increase in $\delta^{18}O$ from BZ to IZ is relatively gradual. Numerous samples at the base of the IZ preserve light, mantle-like $\delta^{18}O$ values (Fig. 5.8) indicating that a substantial amount of magma reached this level of the chamber without isotopic modification.

A characteristic unique to the stable isotope data is the decrease in $\delta^{18}O$ from the UZ to MG with distance from the large septum reaching an approximately constant value of

8‰. Convection in a large chamber would account for the isotopic homogeneity (Voshage et al., 1990) while the isotopic decrease suggests that proportionally less crustal contaminant was involved in the MG than in the Layered Series. This is understandable as a large chamber has a smaller surface-to-volume ratio than a suite of sills and thus has a lesser interface area along which assimilation can occur. An alternate possibility is that the metamorphic rocks had been extensively depleted prior to the period of stabilization of the MG chamber. This restitic material would have a higher melting temperature than the original undepleted rocks and thus would require a proportionally greater energy input to produce a given amount of contamination. This latter possibility, however, conflicts with conclusions from the AFC modeling (section 5.2.4.5) which indicate that the UZ, MG and diorites units interacted with a contaminant of 12.5‰ or heavier and not a restitic material which would be predicted as having a slightly lighter $\delta^{18}O$.

Another trend that is not well displayed in the radiogenic isotope columns is the rapid increase in $\delta^{18}O$ which occurs in the diorites as the roof of the intrusion is approached; a similar, though less dramatic, increase is apparent in the $Sr_{(270)}$ column. As the upper contact is characterized by extensive migmatization and textures suggestive of mixing, these isotopic variations are best explained by extensive incorporation of crustal melt at these levels. This effect is best seen on Figure 5.8 in which roof diorites, those associated with the migmatite or large metapelitic septa, are distinguished from normal diorites, which lack these characteristics. The lack of variation in the Nd system in this level of proposed increased contamination results from mass balance considerations and is mimicked by the AFC modeling (section 5.2.4).

A final feature evident in Figure 5.8 is the presence of isotopically light aphanitic gabbroic enclaves and dikes in the diorite unit. A related feature may be recorded in the scatter to lower values of $Sr_{(270)}$ in the MG; the field relations of these samples, however, are unknown. The enclaves and dikes evidence the continued input of less contaminated

magma at the top of the MG, but suggest that the efficiency of homogenization at this stratigraphic level had decreased. These features will be discussed further with the chemical data in section 5.2.5.3.

In summary, the stratigraphic variations in the stable and radiogenic isotope systems are both marked and regular. The variations have been qualitatively interpreted based on field relations described in Chapter 4 and are consistent with the general model of Voshage et al. (1990; section 4.5.2): the BZ and IZ crystallized from variably contaminated sills while higher levels of the Mafic Complex formed in a large, convecting magma chamber. The UZ, representing in part the basal cumulates, was contaminated at the metapelitic floor of the chamber, while the diorites were extensively contaminated along the roof of the chamber. Additionally the traces of isotopically primitive magma have been identified in the upper chamber. Next, the potential will be evaluated for using the isotopic variations of the magmatic products to quantitatively characterize the reactants and processes in the lower continental crust.

5.2.3. Fractional Crystallization Modeling

Before examining the AFC model used by Voshage et al. (1990) the ineffectuality of a simple fractional crystallization model to describe the variations of $\delta^{18}O$ is readily apparent in Figure 5.9. This figure displays all data from igneous rocks of the Mafic Complex for which both chemical and $\delta^{18}O$ data is available. The triangular area encompasses the most generous increase in $\delta^{18}O$ attributable to simple fractional crystallization (0.5‰ per 10% SiO_2) (Blattner et al., 1983) of a parental magma having a $\delta^{18}O$ of +6.5‰. Obviously this process cannot account for the wide variation in $\delta^{18}O$ found at low values of SiO_2. Furthermore, a second unusually rapid increase in $\delta^{18}O$ between 65% and 70% SiO_2 must be explained. The variation of $\delta^{18}O$ with SiO_2 and the specific insight it lends into the evolution of the Mafic Complex will be discussed in much greater detail in section 5.2.5.

5.2.4. Assimilation-Fractional Crystallization Modeling

5.2.4.1. Extension of the Voshage et al. (1990) Model to Oxygen Isotopes

Recently Voshage et al. (1990) presented the most extensive isotopic model of the Mafic Complex petrogenesis to date. The model was based on 42 new or compiled Sr and Nd isotopic analyses and considered general trends in normalized REE patterns. Figure 5.10 is a duplicate of their $Sr_{(270)}$ vs. $\varepsilon_{Nd(270)}$ diagram in which samples are classified by lithology. The hyperbolic curves demonstrate that both simple mixing and AFC calculations involving appropriate endmembers roughly account for the spread in the existing data. The various parameters in their model are detailed in the figure caption. Figure 5.11 is a similar plot of a subset of their data (with an additional samples, KAW503 from Voshage et al., 1987 and TS4 from Voshage et al., 1988) for which $\delta^{18}O$ were obtained as a part of this investigation. This plot was included in order to demonstrate that the subset analyzed for $\delta^{18}O$ encompasses the equivalent variation displayed by the total radioisotopic data set of Voshage et al. (1990). In this figure samples are classified by stratigraphic position instead of lithology; the stratigraphic treatment will be used throughout the following isotope discussion. The three circled subsets will be discussed below in conjunction with Figures 5.17 and 5.18.

Two observations can be made concerning Figure 5.11. The first is that unit BZ spans nearly the complete range of radiogenic isotopes displayed by the Mafic Complex. This suggests that the processes responsible for producing and preserving isotopic heterogeneities were most active at the lowest, and presumably the earliest, levels of the intrusion. Additionally, there is an approximate progression along the hyperbolic trend of increasingly evolved isotopes from BZ to IZ to UZ levels with the UZ , MG and diorite samples clustering around similar isotopic ranges. When compared to Figure 5.10 this progression is grossly consistent with an upwardly increasing proportion of crustal contaminant.

Figures 5.12 and 5.13 display simple mixing and AFC curves in $\varepsilon_{Nd(270)}$ - $\delta^{18}O$ and $Sr_{(270)}$ - $\delta^{18}O$ space. The curves were generated using parameters identical to those used by Voshage et al. (1990) with the additional input of the $\delta^{18}O$ of the endmembers. The assimilant $\delta^{18}O$ signature was obtained in the manner identical to the method Voshage et al. used for estimating its radiogenic isotope composition, that being the calculation of the average value of ten stronalite and kinzigite samples. $\delta^{18}O$ values for these same samples are found in Schnetger (1988), and an average value of 12.5‰ was calculated for use in the present modeling. $\delta^{18}O$ of the parent magma was picked as the average value of the two most primitive samples from the subset of Voshage et al. (1990) data analyzed in this study. This value, 6.5‰, is greater than the best estimate of suboceanic mantle (5.7 ± 0.3‰) but is similar to estimates of parental magmas in other continental environments. Coincidentally, this value is identical to that used in modeling the isotopic evolution of the Stokes Mountain suite in the Sierra Nevada batholith (Chapter 3).

5.2.4.2. Evaluation of Model Parameters

The fit is fairly good on both figures although it is apparent that no single curve will account for all of the data. There is little distinction between simple mixing and AFC processes in $\varepsilon_{Nd(270)}$ - $\delta^{18}O$ space while the $Sr_{(270)}$ vs. $\delta^{18}O$ plot appears to require both granitic melt (curves A and C) and Sr-rich bulk crust (curves B and D) compositions for the assimilant in order to encompass the majority of the data.

The 12.5‰ model parameter is relatively light as worldwide estimates of metapelites converge on a $\delta^{18}O$ value of 15‰. This shift to lighter values might be the result of extensive degranitization as discussed in section 4.2.1.2. Use of an even lighter bulk crust contaminant with a $\delta^{18}O$ of +10‰ improve the model fit for the isotopically light Layered Series samples while shifting away from the high ^{18}O BZ samples. This calculation is plotted as curve E on Figures 5.12 and 5.13. Such a contaminant is

geologically reasonable only if extensive degranitization resulting in the preferential removal of ^{18}O had occurred prior to assimilation.

In order to investigate the nature of the contaminant, all whole rock $\delta^{18}O$ analyses available for the Ivrea and Strona-Ceneri Zones are plotted on Figure 5.14. It is apparent that the metapelites which are located near the Mafic Complex have a somewhat lighter average $\delta^{18}O$ signature (average of metapelitic septa = 10.2‰; average of adjacent wallrocks = 10.8‰) compared to either non-minimum melt mobilizates (11.4‰) or the average of Schnetger's (1990) 10 samples (12.5‰) which was used in the calculations. This relationship between melt extraction and lowering of the $\delta^{18}O$ of the product restite is also demonstrated by the Strona-Ceneri metamorphic rocks, albeit poorly sampled, which have a heavier average value (13.6‰) consistent with their presumably less depleted nature. If degranitization had preceded contamination then $\delta^{18}O$ values similar to depleted metamorphic septum, such as 10‰, may indeed be appropriate for the contaminant. It should be noted that the low abundance of marble (approximately 2%) within the metamorphic wallrock and the lack of isotopic homogeneity within the metamorphic section (Baker, 1988) preclude the possibility that there has been significant increase of the $\delta^{18}O_{metapelite}$ due to exchange with an isotopically heavy reservoir after magma intrusion but prior to sampling.

The spatial relationship between the presently low $\delta^{18}O$ (10.2 - 10.8‰) metamorphic rocks and the Mafic Complex indicates that the last episode of degranitization was simultaneous with the 290-270 Ma emplacement of the Mafic Complex (section 4.1.2). This episode may have been superimposed on a earlier degranitization event at 478 Ma which uniformly lowered the $\delta^{18}O$ of the whole section from an initial value of approximately 15‰ to 12.5‰. Alternatively, all degranitization was related to the Hercynian magmatism. Whichever scenario is correct, one implication of the isotopically light modeled assimilant is that degranitization must have produced relatively high $\delta^{18}O$, S-

type melts which were not incorporated by the Mafic Complex. This statement holds regardless of the age of degranitization. If degranitization was Hercynian then these melts may have traversed to higher levels of the crust and possibly were incorporated into the magma chambers which ultimately produced the Graniti dei Laghi. If degranitization occurred during the hypothesized 478 Ma event then there simply is no recognized trace of these S-type melts in the Ivrea-Strona-Ceneri crustal section.

An alternate possibility in the model is that the estimate of $\delta^{18}O_{magma}$ is too heavy. Starting with a magma of 5.7‰ similar to MORB would allow the lightest IZ samples to be successfully modeled but would present difficulties for the heavy BZ samples. This possibility is reasonable for the Ivrea Zone as suggested by an analyses of a lherzolite sample (TS9) having this value (Mayer, 1989). In addition, a single mafic enclave (VM117-8) interpreted below as relatively uncontaminated magma injected into the diorite unit has a comparably light value of 6.1‰ (Table 5.1). It is quite possible that the parental magma of the enclave had a slightly lighter value prior to traversing the Layered Series and Mafic Complex.

It is also geologically reasonable to postulate that the assimilant had a greater Sr content than the sampled wallrock as the Sr content might have been decreased by extraction of a high Sr melt prior to sampling. Maximum estimates of Sr content for post-Archean range to 450 ppm although more recent estimates approximate the model parameter of 220 ppm (Taylor and Mclennan, 1985). An Sr content of 450 ppm would account for the samples of the layered series that currently lie beneath the simple mixing curve B on Figure 5.13.

The model is less process sensitive in $\varepsilon_{Nd(270)}$ - $\delta^{18}O$ space in which there is little difference between the four curves. While all curves bracket the heaviest $\delta^{18}O$ of the data set and follow the general trend of the data set, the lighter samples are unaccounted for. Increasing the Nd content of the assimilant to 70 ppm would improve the fit but is not

geologically reasonable given that no estimates of post-Archaen shales have Nd contents greater than the model parameter of 40 ppm (Taylor and Mclennan, 1985). Lowering the $\delta^{18}O_{assimilant}$ would improve the fit for the light Layered Series samples (curve E), and the implications with this possibility have been discussed above.

5.2.4.3. Test of Mixing Models and Identification of Discrepancies of the Model

Hyperbolic mixing curves, such as those shown of figures 5.12 and 5.13, transform to straight lines on graphs of $\varepsilon_{Nd(270)}$ vs. 1/Nd and $Sr_{(270)}$ vs. 1/Sr. While such plots are useful tests of mixing in volcanic suites as rock compositions approximate magma compositions, they are not particularly appropriate for suites in which cumulate processes have operated. Despite this drawback, Figures 5.15 and 5.16 do demonstrate some characteristics of the suite and are included for completeness.

On Figure 5.15, known plagioclase-poor cumulates have been assigned open symbols. It is readily apparent that the mineralogy of these rocks has produced the scatter to greater values of 1/Sr. There is textural and REE evidence that many of the gabbros and diorites contain cumulate plagioclase, and these samples have correspondingly low values of 1/Sr (Voshage et al., 1990). In terms of confirming the AFC modeling, very little of a definitive value can be said. On Figure 5.16 only one curve (D) is plotted as there is little variation between the curves A through D on these axes. Again, the scatter towards greater values of 1/Nd is attributed to the operation of cumulate processes, but the interpretation is complicated as the 1/Nd parameter is a function of three phases (hornblende, pyroxene, olivine) instead of being dominated by the presence or absence of a single phase (i.e., plagioclase dominates 1/Sr). In this instance some of the greatest values of 1/Nd correspond to samples lacking appreciable hornblende. One sample (KAW1785) having a 1/Nd value of 26.37 ppm^{-1} has been excluded from this figure.

Upon detailed investigation of these figures further complications not attributable to cumulate processes become apparent which may aid in the interpretation of some of the

scatter in $Sr_{(270)}$ - $\varepsilon_{Nd(270)}$ space. On Figure 5.15, for example, if the $\varepsilon_{Nd(270)}$ values of samples having high Sr contents are compared to samples with comparable values of $Sr_{(270)}$ but having low Sr contents it is discovered that the $\varepsilon_{Nd(270)}$ values of the two groups differ significantly. In fact, when individual units of the Layered Series are considered it is found that samples with low Sr contents (i.e., pyroxenites) have more negative values of $\varepsilon_{Nd(270)}$ than samples with high Sr contents but having comparable values of $Sr_{(270)}$. If the scatter of 1/Sr was solely due to the degree of plagioclase accumulation, however, there should be no variation in $\varepsilon_{Nd(270)}$. A similar discrepancy exists on the 1/Nd vs. $\varepsilon_{Nd(270)}$ plot (Fig. 5.16), and suggests that another process other than cumulate formation was operative.

Although a detailed discussion is beyond the scope of this study it is possible that the subsolidus interaction with a percolating magmatic (i.e., isotopically mantle-like) aqueous fluid could account for some of the scatter. Based on what presently is understood about trace element solubilities in aqueous fluids, such a fluid presumably would have greater Sr contents and negligible Nd contents compared to the pyroxenites. Interaction might have decreased the $Sr_{(270)}$ signatures of the pyroxenites having low Sr concentrations without disturbing the $Sr_{(270)}$ values of the gabbros (high Sr content). Furthermore the $\varepsilon_{Nd(270)}$ (low Nd content of the fluid relative to any rock) and $\delta^{18}O$ (approximately similar isotopic value) signatures of any samples would be undisturbed. The mineral separate data requires that the fluid have a near-magmatic $\delta^{18}O$, but permits the possibility that such interaction might have occurred in the 500-600°C range of subsolidus reequilibration identified above. Alternatively, if low water-rock ratios are invoked then the $\delta^{18}O_{fluid}$ values are less constrained.

Other scenarios, such as interaction with a percolating melt or extremely localized variation in the chemical and isotopic properties of the assimilant have been considered and discarded due to the overwhelming complexity of the required assumptions. Further

discussion is not merited due to the large uncertainties involved in our understanding of trace element behavior, but the recognition that second-order affects might have complicated the isotopic systematics of the Mafic Complex is appropriate.

It should be recognized that Voshage et al. (1990) attributed the isotopic variation evident at higher levels of the complex to the operation of joint AFC-MASH (mixing-assimilation-storage-homogenization) processes. Additionally they attribute the upward increase of LREE abundances with little corresponding variation in the major element chemistry to the operation of an RTF (refilling-tapping-crystallization) process. There is a great likelihood that such processes occurred in this complex lower crustal environment, and an equally great chance that these processes may have produced much of the departure from a simple AFC trend in the three isotopic systems considered above. As these processes, however, are mathematically difficult to model as well as geologically highly unconstrained, further consideration at this time is not merited.

In conclusion, extension of the AFC model of Voshage et al. (1990) into $\delta^{18}O$ space is generally appropriate once reasonable assumptions concerning the $\delta^{18}O$ signatures of the endmembers are made. If the actual $\delta^{18}O_{assimilant}$ was roughly +10‰ then degranitization of the metamorphic section is required prior to assimilation, and the implications for the modeled Sr content of the contaminant used in the modeling may need adjusting towards higher values. The possibility of a variable $\delta^{18}O_{assimilant}$ within the Mafic Complex resulting from extraction and mobilization of high ^{18}O melt may account for much of the stratigraphic variation of $\delta^{18}O_{Mafic\ Complex}$. Furthermore, if the actual $\delta^{18}O_{magma}$ was +5.7‰ and not +6.5‰ as modeled, then the $Sr_{(270)}$ and $\varepsilon_{Nd(270)}$ of the parental magma used in the modeling may also be in need of adjustment towards less contaminated values.

5.2.4.4. Possibility of Isotopically Distinct Parental Magmas

A more detailed examination of this data in both $\varepsilon_{Nd(270)}$ - $\delta^{18}O$ and $Sr_{(270)}$ - $\delta^{18}O$ space in conjunction with consideration of the geochemical characteristics and stratigraphy reveals some interesting patterns. On Figures 5.17 and 5.18 groups with similar geochemical and stratigraphic characteristics have been delineated. Two exceptions have been made to the stratigraphic divisions: IZ sample FE41 is isotopically like BZ samples in all respects and as it most likely represents the upward intrusion of material from the BZ into the IZ horizon it has been grouped with BZ samples; BZ sample VS124 is more difficult to interpret but groups with the IZ suite on all plots despite its location at the top of the BZ. Whether this material was produced at the IZ horizon and emplaced into the uppermost reaches of unit BZ or whether it is truly BZ material highly evolved towards IZ characteristics is unclear. VS124 does not have the characteristics of either of the BZ trends discussed below, and the possibility that it is downwardly displaced IZ material is not absurd given the extensive evidence discussed in Chapter 4 (4.3.1) for a dynamic and deforming magma chamber at the time of IZ formation.

Of greatest interest is the clear isotopic division within the BZ between samples having SiO_2 contents greater than 46% and FeO* contents less than 13% from those having SiO_2 contents less than 45% and FeO* contents greater than 13%. The lower $\delta^{18}O$ signatures of the latter group may be due to the concentration of low $\delta^{18}O$ cumulus magnetite. Unfortunately, data concerning the modal abundance of magnetite is not available for these samples. Both trends are parallel and follow general AFC trends as shown above. The curious aspect is that these trends may also be distinguished on Figure 5.11, a plot of $Sr_{(270)}$ vs. $\varepsilon_{Nd(270)}$, on which cumulus processes should have no expression.

One possibility that should be explored is the existence of multiple parent magmas in the Mafic Complex. These magmas would have had only slightly different chemical and

isotopic properties which were relatively indiscernible in $Sr_{(270)}$ - $\varepsilon_{Nd(270)}$ space. These proposed phases do not replace the need to invoke AFC processes and do not have any clear relationship to stratigraphic position in the manner of Pin and Sills (1986). Certainly there is reason to believe that the sub-Ivrea mantle may have been isotopically heterogeneous as studies comparing the Finero peridotite to other Ivrean peridotites have suggested (section 4.2.2.2). Such heterogeneities have been interpreted as resulting from interaction with alkali-rich aqueous fluids possessing continental isotopic affinities (Exley et al., 1982).

The possibility of multiple parent magmas was explored in $Sr_{(270)}$ - $\varepsilon_{Nd(270)}$ - $\delta^{18}O$ space. The two magmas were defined as having the isotopic characteristics of sample Q1, a BZ gabbro with a REE pattern suggestive of no modification by cumulate processes (Voshage et al., 1990), and sample TS4, a pod of gabbro found within the Balmuccia peridotite adjacent to the magmatic contact with the base of the BZ (Voshage et al., 1988). These samples are identified on Figures 5.17 and 5.18. AFC curves (not shown) using these two mantle endmembers and a low ^{18}O assimilant (+10-11‰) approximate the two BZ chemical-isotopic trends distinguished on Figures 5.17 and 5.18. The divergent trends of these two chemical-isotopic subgroups in $Sr_{(270)}$ - $\varepsilon_{Nd(270)}$ space (Fig. 5.11) require that the Sr and Nd concentrations of the parental melts differ as well. More troubling, however, is why these two proposed isotopically distinct mantle melts would produce cumulates differing in their major element compositions when crystallization apparently occurred in identical PT conditions. These difficulties appear insurmountable at present given our current understanding of trace element behavior, and the hypothesis of multiple parental magmas cannot be adequately evaluated with the present data.

5.2.4.5. Nature of the Crustal Contaminant(s)

A few more features on Figures 5.11, 5.17 and 5.18 should be discussed. First, in Figures 5.17 and 5.18, the normal IZ samples form a cluster having a lighter $\delta^{18}O$ than the

UZ, MG and normal diorite samples which form a second cluster. A third cluster of roof samples, identified as samples collected adjacent to metapelites, have substantially heavier $\delta^{18}O$ values with only slightly greater $Sr_{(270)}$ values. The fact that there is no distinction between these groups in $Sr_{(270)}$ - $\varepsilon_{Nd(270)}$ space demonstrates that the $\delta^{18}O$ data is providing new insight into the petrogenesis of the Mafic Complex.

The trend defined by the IZ samples, which passes through the UZ and MG samples, is apparently the result of increasing interaction with the metapelites, but has a steeper slope than any of the AFC curves generated previously. A steep trend might be generated by using an assimilant having a heavier $\delta^{18}O$, such as 15‰, in the calculations. As discussed above, such an assimilant is geologically reasonable, but the justification for invoking an isotopically heavier assimilant at higher levels of the complex is not clear.

One possible scenario is as follows: dikes of BZ parental magma were emplaced into the base of the crust. The early dikes assimilated 12.5‰ material and heated the surrounding wall rock above its melting temperature. Degranitization shifted the $\delta^{18}O$ of the remaining wall rock towards values of 10‰; this restite was subsequently assimilated by later BZ dikes. Depletion through the removal of melt would not affect the radiogenic signatures of the assimilants over the relatively short period of emplacement of the Mafic Complex, so this change in character of the assimilant would not be recorded in $Sr_{(270)}$ - $\varepsilon_{Nd(270)}$ space. Meanwhile, the high ^{18}O mobilizate produced in the BZ level migrated upwards where it contaminated some of the IZ dikes producing the rapid increase in $\delta^{18}O$ displayed by this unit; other IZ dikes interacted with both normal and isotopically depleted wall rock. The $\delta^{18}O$ signature of the mobilizate would have varied as a function of the proportion of melt produced vs. restite. Finally, the UZ, MG and diorites units interacted with varying proportions of normal $\delta^{18}O$ wall rock (12.5‰). Some of the highest $\delta^{18}O$ roof diorites may have assimilated high ^{18}O mobilizate; such a process is easily envisioned as occurring along the migmatitic contact. This scenario implies that degranitization formed

three isotopically distinct assimilants which contaminated different structural levels of the compound magma chamber: restite (+10‰), mobilizate (> +12.5‰) and relatively undepleted bulk metapelite (+12.5‰).

The three lowermost UZ samples define a linear trend on Figures 5.11, 5.17 and 5.18. These samples would have formed immediately above the continuous metapelitic septum that divides the IZ from the UZ. Although not specifically modeled, the basal UZ trend has a slope similar to the BZ trends and is therefore suggestive of AFC processes involving a low $\delta^{18}O_{assimilant}$. As discussed above, it is possible that the underlying metapelitic septa had a low $\delta^{18}O$ (10‰) due to previous melt extraction resulting in a gently sloping AFC trend for the basal UZ. The stratigraphically higher UZ samples cluster with the single MG and diorite sample suggesting that subsequent interaction was with an assimilant having a heavier $\delta^{18}O$.

5.2.4.6. Summary of Variations in $Sr_{(270)}$ - $\varepsilon_{Nd(270)}$ - $\delta^{18}O$ Space

If the $\delta^{18}O$ data is considered in conjunction with $Sr_{(270)}$ and $\varepsilon_{Nd(270)}$ data, the general ability of simple mix and AFC modeling to describe the isotope systematics of the Mafic Complex is confirmed. The modeled parental magma has a $\delta^{18}O$ of 6.5‰ while the assimilant may have had a variable isotopic signature (10-12.5‰ and heavier) depending on how much granitic melt had been previously removed from the assimilant. While some degranitization appears to be related to emplacement of the Mafic Complex, the relatively light average $\delta^{18}O$ of the metapelites suggests that extensive degranitization occurred sometime prior to emplacement and contamination of the Mafic Complex. Details in the data set, such as superimposed chemical-isotopic trends and inexplicable relations between isotopic signatures and trace element abundances suggest that more complicated processes are involved. It is unconstrained as to whether or not the inclusion of MASH and RTF processes in the model, as proposed by Voshage et al. (1990), would explain these discrepancies or if additional, perhaps subsolidus, processes must be invoked.

Finally it should be noted that Stille and Buletti (1987) concluded that the radioisotopic systematics of samples from the Graniti dei Laghi and the Permian volcanic suite could be similarly modeled in terms of AFC processes between mantle and crustal materials.

5.2.5. Variations of $\delta^{18}O$ with SiO_2 Content

In the following section, the variation of $\delta^{18}O$ with SiO_2 will be examined at all stratigraphic levels of the Mafic Complex, proceeding upwards from the base of the section. The treatment will begin with samples from the central Mafic Complex (i.e., Valle Sesia and Valle Mastellone) subsequently turning to data from the outlying areas (i.e., Finero, Premosello, Monte Capio and Valle Sessera and Valle Strona di Postua). This treatment will demonstrate the utility of such analysis in identifying the operation or absence of specific magmatic processes at various stages in the evolution of the Mafic Complex. It should be noted that one advantage of using oxygen isotopic analyses in conjunction with radiogenic studies is the relative ease and speed of the stable isotope technique. These qualities allow a more extensive sampling than is reasonable with the radiogenic isotopes and thus has the potential to provide greater resolution concerning the details of the operative processes.

5.2.5.1. The Layered Series

All samples from the Layered Series are plotted on Figure 5.19. The first notable feature is that both units BZ and IZ encompass a 3‰ isotopic variation between 6.3‰ and 9.4‰ (also see Figure 5.7). The large range in SiO_2 is simply due to cumulate processes. The low $\delta^{18}O$ samples overlap with our best estimate of the $\delta^{18}O_{mantle\ source}$ while the isotopically heavy samples reflect the assimilation of high $\delta^{18}O$ metamorphic material as modeled in the previous section. This large isotopic range displayed by the cumulates validates the basic hypothesis of this study: specifically that lower crustal cumulates have

the potential for recording source characteristics as well as the initial stages of magma modification.

The preservation of such heterogeneity and its existence on a small spatial scale (up to 2‰ variation over 4 m) supports the hypothesized intrusion mechanism during the initial stages of development of the Mafic Complex. The feasibility of assimilation by thin dikes will be further explored with data from the Monte Capio Sill.

A third feature of this plot is that the UZ suite has a sharply defined base of 7.8‰. which indicates either the absence of isotopically primitive recharge and/or the efficiency of isotopic homogenization at the UZ level. Isotopically heavy samples are similar to those in the BZ and IZ; if contamination of the UZ occurred during dike emplacement then the absence of mantle $\delta^{18}O$ signatures could be attributed to a high temperature of the UZ wall rocks which would have prevented quenching of low ^{18}O magmas. Alternatively contamination of the UZ may have occurred along the floor of the MG chamber in which the UZ cumulates were not efficiently entrained in the convection of the MG magma. In this case the UZ formed a boundary layer along the base of the MG in which high ^{18}O rocks were produced through assimilation of the underlying metapelitic septum. Only the lowermost UZ samples (the basal UZ identified on Figs. 5.11, 5.17 and 5.18) would have assimilated previously depleted low ^{18}O restite. Alternatively the basal UZ samples represent isotopically primitive material which underplated the UZ cumulates and was unable to assimilate much of the underlying restitic septum. The boundary layer model is favored for the diorites and is discussed in more depth in section 5.2.5.3.

5.2.5.2. The Main Gabbro

Oxygen isotope data for the Main Gabbro is compared to that for the Layered Series in Figure 5.20; note that previous discussions were based on a single sample on which both stable and radiogenic isotopic analyses are available The restricted isotopic range of MG samples, between +7.7‰ and +8.3‰, might have been predicted from the limited

chemical and radiogenic isotope variations within this unit. The range of isotopic variation displayed by the MG falls within the UZ range with the exception of two samples having slightly lower $\delta^{18}O$ indicative of some recharge of less contaminated magma which escaped convective homogenization. Another noteworthy difference is the lack of isotopically heavy samples between 8.2 and 9.2‰ in the MG as found in the UZ. This suggests that the magma from which the UZ crystallized experienced more localized contamination by relatively fertile (12.5‰) crustal material than the homogenized MG magma.

5.2.5.3. The Diorites

For the purpose of this discussion, the diorite unit has been subdivided based upon sample location. Samples collected adjacent to the metamorphic roof, in migmatites or near metapelitic septa, have been designated "roof diorites" while samples intimately associated with textural zones of magma mingling but not including actual enclaves have been designated as "mingled diorites". Samples lacking either spatial association are referred to as "normal diorites".

Figure 5.21 displays the analyses from the UZ and MG units with normal diorite samples. The UZ and normal diorites occupy comparable fields suggestive of similar degrees of interaction with the isotopically heavy wall rocks as well as the absence of large-scale convective homogenization such as displayed by the MG. Both the UZ and diorite units include samples with high SiO_2 contents. The arrow on Figure 5.21 indicates the maximum possible increase in $\delta^{18}O$ attributable to fractional crystallization. As the arrow matches the trend for the most chemically evolved normal diorite samples, it is possible that fractional crystallization of a MG-type magma could produce the observed isotopic variation in the diorite unit. If these samples are compared to samples of roof diorites (Fig. 5.22), however, the clear evidence for assimilation attested to by the isotopically heavy roof diorites suggests that the normal diorites are also contaminated, albeit to a lesser degree. The increase in SiO_2 could be due to both fractional crystallization and assimilation

of siliceous crustal melt, although only the roof diorites which have the highest probability of being mixtures with siliceous melts, have SiO_2 contents greater than 55 wt. %. Note that the ordinant and abscissa on Figures 5.21 to 5.24 differ from those on Figures 5.19 to 5.21.

Within the diorite unit are 10^1 to 10^2 m wide zones of mingled silicic and mafic magma in which the mafic magma forms spheroidal to ellipsoidal, aphanitic to fine-grained porphyritic pillows. As discussed extensively in Chapter 2, such relations are strongly suggestive of a hotter mafic magma quenched in a cooler, silicic magma. In Figure 5.23, the oxygen isotope data for enclaves and the silicic host lithologies (i.e., mingled diorites) from the mingled zones are plotted relative to the normal diorite samples. Clearly the mingling process introduced isotopically primitive material ($\delta^{18}O$ = +6-7‰) and presumably heat to the upper levels of the Mafic Complex. Whether the mingled diorites represent true, mixed magmas or samples of normal diorite which experienced local, subsolidus reequilibration with the low $\delta^{18}O$ enclaves is unclear. Differentiation between these two possibilities would require mineral separate analyses, but this test was deemed inappropriate with the given samples. Testing of the mixing hypothesis using the chemical analyses is also inconclusive due to the large chemical variation characterizing the diorite unit, but may be possible using the trace element systematics of these samples (S. Sinigoi et al., in progress).

In Figure 5.24 the enclave samples, as well as samples of two, cm- to m- thick dikes from the diorite unit, are plotted with the MG samples. That the enclaves and dikes from the diorite unit are less contaminated than the MG samples probably reflects two factors. First, even if abundant primitive magma was injected into the MG as the stratigraphic variation of $\delta^{18}O$ suggests (Fig. 5.7), the process of convection would have erased most chemical and isotopic heterogeneities. Second, lesser amounts of isotopically primitive material may in fact be preserved in the MG (such as the two samples with $\delta^{18}O$

less than 8‰) but was not sampled due to the lack of visual contrast with the typical MG gabbros. What is clear is that the enclave and dike material is not typical MG magma which was injected into the overlying diorite unit, but instead records the presence of the primitive magma that fed the MG and was occasionally injected into the uppermost level of the chamber where it was quenched. Finally, since the mingled diorite field is distinct from either the MG or normal diorite fields, the possible production of mixed magmas of mafic-silicic proportions comparable to that recorded in the enclave swarms was either a local phenomenon or these mixtures were produced but subsequently obliterated through convective mixing in the MG chamber.

5.2.5.4. The Finero and Premosello Peridotites

The phlogopite-bearing peridotite body of Finero (section 4.2.2.2) has generated considerable interest regarding the cause and the timing of phlogopite formation. Such information is relevant to discussion of the chemical and isotopic character of the mantle-source of the Mafic Complex. While the significance of the phlogopite remains a subject of great debate, for the purposes of this discussion a few features should be reviewed. First, the distribution of phlogopite is strongly concentrated in the northeastern peridotites (Finero and Premosello). Second, the presence of phlogopite correlates with elevated $^{87}Rb/^{86}Sr$ ratios and Sr_i values but apparently undisturbed Nd systematics (Voshage et al., 1987) which could be explained in terms of the presence of variable amount of an alkali-rich metasomatic fluid. Finero and Balmuccia samples define a single Rb-Sr isochron suggesting that phlogopite stabilization occurred contemporaneously in both localities and was caused by a single agent. Finally, the Rb-Sr systematics of the gabbroic sheath in Finero are relatively nonradiogenic suggesting a paradox in that the depleted peridotite must have been metasomatized prior to sheath formation but could not have produced the parental magma of the surrounding sheath. The unmetasomatized mantle source of the sheath lithologies might have resided at a lower structural level during the metasomatic

event; subsequent mantle melting produced the parental basalt of the sheath which ponded around the previously metasomatized, and possibly impermeable, Finero peridotite.

$\delta^{18}O$ analyses of samples from the Finero Complex are displayed in Figure 5.25. The mantle peridotite samples, which consist of samples of Cr-diopside dikes, have light $\delta^{18}O$ values of mantle affinity (+6.4‰). That the $\delta^{18}O$ values do not show disturbance similar to that recorded in the Rb-Sr system is explicable by mass balance considerations. Interaction with small amounts of alkali-rich fluids could stabilize phlogopite in the mantle and disturb the Rb-Sr system without affecting the oxygen isotope systematics. Alternatively the metasomatic fluid could have had a mantle $\delta^{18}O$ signature. The surrounding ultramafic-mafic layered sheath has $\delta^{18}O$ values beginning at a similar level and extending to values enriched in ^{18}O by 1.2‰. There is no clear stratigraphic relationship with $\delta^{18}O$, but presumably the increase is a reflection of interaction with the isotopically heavy metapelitic septa found within the layered sheath.

Two gabbro samples (F27, F30; Table 5.2) from the sheath have anomalously light $\delta^{18}O$ values. An arrow connects these samples with the stratigraphically nearest unaltered, relatively undeformed gabbro (F26) indicating that $\delta^{18}O$ values may have been lowered by as much as 3‰. The low $\delta^{18}O$ samples contain textures indicative of plastic deformation, such as lenses of internally deformed plagioclase and pyroxene, followed by brittle deformation. This latter event produced fine, anatomizing fractures along which secondary epidote and micaeous minerals are concentrated. Brittle deformation and secondary alteration is relatively uncommon within the Mafic Complex, and perhaps it is of no surprise that the $\delta^{18}O$ systematics of these samples are disturbed. Metamorphic septa are present within the sheath, but the low ^{18}O fluid involved in the alteration appears to be meteoric. Although data are scarce, there is some suggestion from zircon fission track data that the Finero area may have been subjected to a thermal overprint (>220 ± 20°C) in the Tertiary related to its proximity to the tectonic boundary with the Central Alps (Burghi and

Klotzli, 1990). A slight thermal disturbance may have provided the necessary energy to drive a small meteoric hydrothermal circulation system in the Finero area. This circulation would have been limited to brittle fractures and involved low water rock ratios as pervasive disturbance of the oxygen systematics did not occur in the Finero area.

An even smaller data set is available for the phlogopite peridotites of Premosello in Val d'Ossola (Fig. 4.4; section 4.2.2.3). The oxygen data (Table 5.7) is compared to that from the Finero Complex in Figure 5.26. As in Finero, the single peridotite-enclosed pyroxenite sample has a normal, mantle-like signature (6.5‰) indicating that the stabilization of phlogopite did not disrupt the oxygen systematics of the mantle source. In contrast to Finero, the gabbros from the Premosello sheath record much greater interaction with high $\delta^{18}O$ metapelites (up to a 2.6‰ enrichment). This is most likely due to the relatively thinner width of the Premosello sheath which would have facilitated a greater degree of assimilation of the metapelitic wallrocks. In this manner the thin peridotite sheaths record crustal contamination as in bodies such as the Monte Capio Sill.

5.2.5.5. The Monte Capio Sill

The Monte Capio Sill was chosen for study because of the possibility that this body represents a large dike emplaced into a relatively cool lower crust. This process, and the possible assimilation that occurred during emplacement and crystallization, has been invoked to explain the heterogeneity in the radiogenic isotope systems within the BZ and IZ (Voshage et al., 1987) (section 4.2.3.1.4).

$\delta^{18}O$ and SiO_2 data for the Monte Capio Sill is displayed in Figure 5.27 and compiled in Table 5.2. The samples have been divided in terms of both lithology and position relative to the center of the sill: "internal" samples are part of the central peridotite while "external" samples come from the basal gabbro, pyroxenite or layered gabbro units. The lithologic division is made because the pyroxenites are cumulates while some of the gabbros may be noncumulate in origin. Pods of pyroxenite within the central peridotite

have the lowest $\delta^{18}O$ values, but it should be noted that these values are elevated relative to the presumed mantle source (6.5‰). The external gabbros and pyroxenites have a restricted and elevated isotopic range of 8.2 - 8.7‰ with no apparent correlation with distance from the outer contact. Included in this group is a single gabbro collected from the outer margin of the inner peridotite and interpreted, based solely on $\delta^{18}O$, as a gabbro from the sheath intruded towards the center of the sill. The dikes are thin (<1 m), aphanitic or fine-grained, generally cross cutting bodies found in the metapelitic wall rock. The heaviest sample was collected from within a migmatized metapelite.

The data demonstrate that elevated $\delta^{18}O$ values are produced in the outer gabbro of a large sill and possibly also within the interior peridotite. Further elevation occurs as small dikes shoot off of the main sill into the surrounding country rock, but as no mineral separations were attempted with these fine-grained samples it cannot be determined whether the isotopic enrichment occurred in the magmatic or subsolidus state. Regardless, it appears that elevated $\delta^{18}O$ values comparable to those in the BZ and IZ may be produced during an intrusion scenario similar to that for the Monte Capio Sill.

5.2.5.6. The Southern Ivrea Zone

The geologic relationships of the structurally and lithologically complicated southern Ivrea Zone have been recently described (Sinigoi et al., 1991) (Figure 4.8). Synmagmatic deformation, as evidenced by megascopic folding of laterally extensive metapelitic septa, is more extreme than in the central Mafic Complex (Rivalenti et al., 1980). The lithologic relationships are complicated by the presence of leucocharnockites and melacharnockites (section 4.2.3.5). The charnockites are best developed along the roof of the intrusion, occurring with or without the diorite unit, but also occur intermingled with the underlying amphibole-bearing gabbros and norites.

Oxygen isotope and SiO_2 data for igneous and metamorphic rocks from Valle Sessera and Valle Strona di Postua in the southern Ivrea Zone are presented in Figure 5.28.

On the silica-poor end of the spectrum, the gabbro and diorite samples are seen to overlap, with the gabbros including lighter $\delta^{18}O$ values and the diorites including heavier values. One gabbro sample yields the heaviest value, but as it was collected adjacent to a metapelitic septum its value presumably resulted from local interaction with the metapelite or its melt. This sample has been identified as a roof sample using the same logic as applied to the central Mafic Complex to samples collected adjacent to metapelitic septa.

The next heaviest group is composed of melacharnockites and mingled charnockites, the latter lithology collected from an enclave-rich and xenolith-bearing zone near the top of the intrusion in Valle Strona di Postua. This zone was previously identified as a migmatite zone in which the fine-grained mafic material was interpreted as being xenoliths of amphibolites from the wall rock suite (Burghi, 1987). While this interpretation cannot be definitively disproven, the present interpretation is that the aphanitic material is quenched mafic magma related to the Mafic Complex. A single analyzed enclave appears to be compositionally and isotopically similar to the diorite unit. Sharp angles on many of theses enclaves may have resulted from fragmentation of chilled dikes injected into the migmatite and do not necessarily argue against a comingling origin. Comparing these textures to the mingled zones in Val Mastellone (sections 4.3.1 and 5.2.5.3), it would appear that in the southern Ivrea Zone the host magma was more crystalline at the time the mafic magma was comingled. As a result, the mafic magma was emplaced as dikes instead of as pillows, and these dikes were subsequently disturbed and fractured by movements within the dynamic siliceous host. A circumstantial argument against the interpretation of these enclaves as amphibolitic xenoliths is the relative scarcity of the amphibolite lithology in the wall rock suite compared to the predominance of the enclaves over clearly metapelitic xenoliths within the mingled zone.

From the relationships shown in Figure 5.28 it appears that the mingled charnockites and melacharnockites represent mixtures between high $\delta^{18}O$

leucocharnockites and gabbroic or dioritic magma represented by the enclave sample. This would require, however, that in the Valle Sessera area the leucocharnockitic host had a low crystal content at the time of mingling in order for extensive mixing to occur. This statement is in contrast to the argument presented above for the thermal state of the Valle Strona di Postua mingling zone.

The exact origin of the leucocharnockites is presently unclear, although it it evident from their high $\delta^{18}O$ and Sr_i and the common metapelitic xenoliths that a relatively large component of crustal material is present in this lithology. In fact, the isotopically heaviest leucocharnockite sample plotted on Figure 5.29 was associated in outcrop with a metapelitic xenolith. On Figure 5.13, the leucocharnockites can be modeled as representing simple and AFC mixtures between mantle basalts ($\delta^{18}O$ =6.5‰) and granitic melt with a $\delta^{18}O$ of +12.5‰. Note, however, that the Main Gabbro and Layered Series samples fall significantly below these curves and thus cannot represent the preceding contaminated fractionates of a mantle melt as would be predicted from this simplistic model. Based upon field, geochemical and isotopic data, Sinigoi et al. (1991) have proposed that the leucocharnockites represent mixtures of evolved gabbros, such as the Main Gabbro, and crustal melts. In support of this hypothesis it is apparent that it would be possible to draw simple mix or AFC curves on Figure 5.13 (not shown) between the MG sample and the modeled granitic melt that would approximate the trend of the charnockitic samples. As discussed previously, it is possible that the actual assimilant was enriched in ^{18}O relative to the analyzed late stage mobilizates and restitic metapelites which are plotted on the abscissa of Figure 5.29. An isotopically heavier contaminant might account for the relatively steep trend displayed by the leucocharnockites (Fig. 5.13 and 5.29) and would result in a lower modeled proportion of assimilation to fractionation.

Analyses of three wall rock amphibolites are displayed as ranges on the abscissa of Figure 5.29 as no SiO_2 data is available. These amphibolite samples clearly have a heavier

$\delta^{18}O$ than the single enclave sample, in agreement with the above interpretation that the enclaves are not amphibolite xenoliths. It is possible, based only on the $\delta^{18}O$ data, that some of the amphibolites, particularly those adjacent to the contact, may be epiphyses of the Mafic Complex, but this hypothesis would need to be substantiated by other lines of evidence.

Two final groups of samples are plotted on Figure 5.29. The "mobilizates (?)" and the "fractionate(?)" were collected from pods of extremely siliceous lithologies located within gabbros and charnockites in Valle Sessera. The proximity to a large metapelitic septa prompted the field interpretation that these were metapelitic melts, similar to the roof mobilizates, which were emplaced into the surrounding igneous lithologies. For this interpretation to be correct would require that either the metapelitic host was more extensively depleted that the roof metapelites which are plotted along the abscissa or that the $\delta^{18}O$ values of the mobilizates had been decreased due to exchange with the surrounding gabbros. A last possibility is that the mobilizates are, in fact, fractionates, as suggested for a single sample (RA114) on Figure 5.29. This would require more extensive fractionation at the siliceous end of the suite than has been seen elsewhere in the Mafic Complex. Geochemical data would best evaluate this somewhat unlikely possibility which might have bearing on the proposed relationship between the leucocharnockites and the Graniti dei Laghi.

5.2.6. Variations of $\delta^{18}O$ with Sr_i in the Graniti dei Laghi, Strona-Ceneri Zone

Samples of Permian granitoids from the Graniti dei Laghi (section 4.4.2) of which Sr_i analyses were available were obtained in order to investigate the possibility of $\delta^{18}O$ - Sr_i correlations (Table 5.5). Unfortunately, chemical data is available for only a few of these samples (Table 5.6). On Figure 5.30 the position of the Graniti dei Laghi samples is intermediate to the Mafic Complex and the field of metamorphic rocks from the Ivrea and Strona-Ceneri Zones. A gabbro from the Montorfano granitic (GL6) complex is

isotopically quite similar to the Mafic Complex and indicates the input of MG-type magma at intermediate crustal levels. The more granitic lithologies appear to contain a greater metapelitic component as might have occurred if the AFC processes, such as those modeled in the Mafic Complex (section 5.2.4), were allowed to continue. The slight isotopic overlap with the Mafic Complex as well as the dominantly intermediate character of the Graniti dei Laghi are at least consistent with the hypothesis that the structurally higher granites are somehow related to the Mafic Complex.

Also shown in this figure is another example of the effect of hydrothermal alteration. In this instance the mineralogy of the green granite phase of Mergozza as well as its Sr_i value intermediate between unaltered granites and the surrounding metapelites (Pinarelli et al., 1988) is highly suggestive of hydrothermal alteration. The $\delta^{18}O$ data demonstrate that the fluid involved was lower in ^{18}O than any fluid that would have been evolved from the metamorphic lithologies and was instead probably meteoric in origin. Future mineral separate studies will be directed at evaluating this problem.

Isotopic data from the appinite lithology is plotted in Figure 5.31 (Table 5.5). An appinite sample collected along the Pogallo Line near Monte Zuccaro is plotted on the abscissa as it has no Sr_i analysis. The low $\delta^{18}O$ of this sample (DK29; Table 5.7) is comparable to the Mafic Complex range and again indicates the input of somewhat isotopically primitive mafic magma at this higher structural level. Other than those samples from Monte Zuccaro, the appinites fall intermediate to the Mafic Complex and the metapelite fields in a comparable position to the Graniti dei Laghi (Figure 5.30) suggesting a similar origin.

The two Monte Zuccaro appinite samples with Sr_i analyses have elevated $\delta^{18}O$ values compared to appinite DK29 (also from M. Zuccaro), the Val Sesia appinites or the Graniti dei Laghi. The cause of this isotopic elevation is not clear. The Sr analyses of these samples (GL9, GL10) have been arbitrarily corrected to an initial age of 255 Ma in

order to give a positive slope similar to the other appinites and all lithologic units. The justification for doing this exercise is that the Rb/Sr ratio of the high $\delta^{18}O$ sample (GL9) is unusually low making the elemental abundances suspect in terms of being magmatic in origin as well as the Sr_i being extremely sensitive to the age correction. The ^{18}O-enrichment of GL9 as well as its low Rb/Sr ratio may both be related to subsolidus exchange with a Sr-poor, ^{18}O-rich fluid derived from the metapelites. A similar process may account for the high-$\delta^{18}O$ mafic dikes associated with the Monte Capio Sill (section 5.2.6.2). Application of this hypothesized fluid interaction is not totally satisfactory as it is not clear why sample DK29, from roughly the same area, escaped this modification. Assimilation of high $\delta^{18}O$ metamorphic material is also not a satisfactory explanation of the high $\delta^{18}O$ M. Zuccaro appinites as no such high $\delta^{18}O$, low Sr_i metamorphic material has been identified.

Finally, in Figure 5.32 isotopic data from the Graniti dei Laghi, the Val Sesia appinites and the Ivrea Zone charnockites are compared. Although the overlap between these units is not complete and does not prove a genetic relationship, the similarity is intriguing. As discussed in section 5.2.6.3, Sinigoi et al. (1991) have suggested that the leucocharnockites represent mixtures between MG-type magma and lower crustal melt. Based on isotopic and trace element similarities, these authors and others (see section 4.4.2 for review) suggest a similar genesis for the Graniti dei Laghi although trace element systematics indicate that the crustal source was less depleted prior to melting than the source of the leucocharnockite contaminant.

In Sri - $\delta^{18}O$ space samples of appinites and granitoids from the Strona-Ceneri Zone overlap with the field defined by samples from the Mafic Complex of the Ivrea Zone. This similarity is consistent with either a comagmatic relationship between these suites or a similar magmagenesis of unrelated suites. Future work, including the analysis of mineral separates, on the Strona-Ceneri plutonics will be directed at distinguishing between these

two possibilities. Specifically, the extent of hydrothermal alteration must be investigated before proceeding with further whole rock analysis.

5.3. Summary and Interpretation of $\delta^{18}O$ Variations

The large isotopic variation displayed in the BZ and IZ units has been discussed previously and interpreted in terms of variable contamination of mantle-derived magma (6.5‰) emplaced as sills into a relatively cool, lower continental crust. A heterogeneous mantle source might explain some of the irregularities in the major and trace element systematics; this possibility was examined but could not be supported with the present data. The isotopic variations can be crudely modeled by AFC processes involving an assimilant with a $\delta^{18}O$ of +10‰ to 12.5‰ and possibly greater. Similar contamination is displayed by the relatively thin sheaths surrounding the Finero and Premosello peridotites and the Monte Capio Sill. The emplacement of large surface-to-volume ratio bodies into the lower crust appears to be an efficient mechanism for producing high $\delta^{18}O$ ultramafic and mafic material as well as lowering the $\delta^{18}O$ of the restitic metamorphic material.

Assimilation of the underlying, restitic metamorphic septum ($\delta^{18}O = 10‰$) is preserved only in the lowest UZ samples. The UZ cumulates may record the isotopic heterogeneity present during the early stages of the growth of the MG chamber by dike emplacement into fertile metapelite ($\delta^{18}O = 12.5‰$) in a manner similar to the scenario for the BZ and IZ, the absence of chilled primitive magma in the UZ resulting from the higher temperature of the wall rock. Alternatively the UZ may be viewed as a poorly developed boundary layer of the convecting magma chamber in which high ^{18}O magmas were produced prior to mixing with the MG chamber.

Development of the MG chamber may reflect an increased rate of intrusion of mantle-derived magma into the warmed lower crust. Development of a large, convecting magma chamber is documented by the homogeneity displayed by radiogenic and stable

isotopic systematics. The continued input of relatively primitive magma is documented by rare, low ^{18}O samples and a lower average $\delta^{18}O$ than the Layered Series.

Surrounding the MG, the diorite unit contains three subtypes distinguished on $\delta^{18}O$ and field occurrence. The roof diorites contain the largest proportion of high $\delta^{18}O$ metapelite or isotopically enriched granitic melt while the mingled diorites appear to have mixed with injections of isotopically light, relatively primitive magma. The normal diorite was probably produced by a combination of crustal assimilation and mixing with basaltic and granitic magmas while fractional crystallization, producing occasional cumulate textures and some of the increase in SiO_2 shown on Figure 5.21, also occurred.

The diorite unit may be viewed as a boundary layer in which isotopically heavy magmas were produced through the assimilation of country rock. In this scenario the high $\delta^{18}O$, contaminated magma was periodically stripped off by the convecting inner MG body, where it efficiently mixed with isotopically primitive magma. The resultant juxtaposition of the hotter MG magma against the outer metapelitic contact promoted melting and further assimilation of siliceous material which renewed the diorite boundary layer. Between periods of removal and mixing, intrusion of hot gabbroic magma, such as that which formed the enclaves, would conduct heat into the boundary layer and promote assimilation; crystallization in the diorite unit would have produced additional energy for assimilation. The upward and outward growth of the magma chamber could have continued in this fashion as long as the influx rate of hot primitive magma was maintained. Note that the general absence of xenoliths in the MG unit suggests that wholesale stoping of the roof was not the dominant process of chamber growth. The high ^{18}O UZ samples may also have formed in a boundary layer in a similar manner to the diorites. Because this layer was gravitationally stable at the base of the MG chamber, the high ^{18}O magma produced in the UZ level was probably not often mixed into the overlying convecting magma unless a fraction with high bouyancy was able to separate and rise into the MG.

The leucocharnockites have the heaviest magmatic $\delta^{18}O$ values found in the Ivrea Zone. Their signature is best interpreted as a mixture of a MG-type magma with a low Sr, high $\delta^{18}O$, S-type crustal melt. The similarity between the $\delta^{18}O$ of the leucocharnockites and the voluminous Graniti dei Laghi found in the middle crust Strona-Ceneri Zone is suggestive of a similar origin. This possibility would require that a large volume of MG-type magma was produced in the lower crust in an Ivrea-type chamber and subsequently mixed with a larger volume of crustal melt than recorded by the diorites. This suggests that the MG was emplaced to slightly higher crustal levels where the wall rocks were more hydrous and fertile. Such an environment would permit a larger volume of S-type melt to be produced and assimilated than possible in the previously depleted lower crust. The granites produced in this second tier of magma chambers were then emplaced into even higher crustal levels represented by the Strona-Ceneri Zone. A small amount of MG material may have also been emplaced into the Strona-Ceneri Zone forming the appinite suite.

This hypothesized second tier of magma chambers in which increased AFC produced voluminous granitic magmas is, conveniently, not exposed. As structural reconstructions of the Ivrea-Strona-Ceneri crustal column indicate that 8 - 15 km of crust have been removed along the Pogallo Ductile Shear Zone (section 4.3.2) the extension could account for the absence of the mid-crust magma chambers. Although not entirely satisfactory, there is some legitimacy in this model. Presumably a ductilely extending crust would tend to prohibit the upward migration of the MG-type magma. This melt might thus be forced to pond at some intermediate level: subsequent heating would not only melt the country rocks but might also facilitate extension in the thermally weakened crust. Ponding is required to keep the modeled ratio of assimilation to fractionation high. Further upward migration of the subsequently evolved granitic magma might have only become possible after a critical mass of bouyant, siliceous magma was produced in the MG-fed chambers.

Further extension of the crustal column would obliterate these transient second tier magma chambers.

In this interpretation, the leucocharnockites represent an aborted attempt at the production of granitic material in the lower crust. Granite production was enhanced in more fertile intermediate crustal levels where a lower total heat content was required to drive the AFC and/or MASH processes towards completion.

The absence of hydrothermal circulation in the Ivrea Zone appears to be the result of the low water content of the upper amphibolite to granulite facies metamorphic section and the inability of surface fluids to circulate to lower crustal levels. Such downward circulation would have been inhibited by ductile extension of the middle and lower crust. Hydrothermal circulation of low $\delta^{18}O$, presumably meteoric, water in the Strona-Ceneri Zone was possible due to the high structural level of emplacement of the Graniti dei Laghi. Additional limited hydrothermal circulation may have accompanied brittle deformation during the Alpine orogeny as evidenced by samples from the Finero Complex.

5.4. Discussion of Other Hercynian Localities

The Mafic Complex provides a rare opportunity to study a lower crustal, compound layered intrusion in great detail. The interpretations detailed above utilizing isotopic and geochemical parameters have been strongly dependent upon the field relationships that are, in general, well exposed in the Ivrea Zone. Moreover, without the field context, none of the stratigraphy-based conclusions concerning the evolution of the intrusion could have been reached. Given this rare opportunity, it is requisite that the conclusions derived from this study be applied to related suites which lack field context. Two types of suites need to be examined: middle and upper crustal Hercynian gabbroic to granitic suites which presumably have lower crustal igneous counterparts, and lower crustal igneous xenoliths which lack all field context relating to their environment of formation.

Hercynian plutonic rocks form three lithologic groups: calcalkaline granodiorites with lesser gabbro, diorite, tonalite and leucogranite with $\delta^{18}O$ = +7.4 - 10.4‰; subalkaline monzonites with lesser gabbro, diorite and granite with $\delta^{18}O$ = 8.1 - 9.5‰; aluminopotassic cordierite two-mica granodiorites, granites and leucogranites with $\delta^{18}O$ = 9.0 - 13.5‰ (Sheppard, 1986). Most are exposed in regionally metamorphosed, middle to upper crust terranes. All groups are characterized by limited basaltic material, such as lamprophyres, and relatively high $\delta^{18}O$, the latter quality indicating that the exposed rocks contain a large proportion of reworked continental material (Hoefs and Emmermann, 1983). Of these groups, the calcalkaline and aluminopotassic suites are found in the Ivrea-Strona-Ceneri section.

At present, three studies of appropriate Hercynian suites combine geochemical and $\delta^{18}O$ data. The first involves a detailed radiogenic and stable isotopic study of granulite facies xenoliths from the Massif Central of France (Downes et al., 1990; Downes et al., 1991). The xenoliths were collected from Tertiary alkaline volcanic rocks, and are believed to be Hercynian in age. The age assignment is based upon lower zircon intercepts and the presence of well-correlated ε_{Nd} - ε_{Sr} trend when an initial age of 300 Ma is used for the correction. The second study is of the Maladeta Igneous Complex - a gabbroic to intermediate suite located in the Central Pyrenees of Spain (Michard-Vitrac et al., 1980). A whole rock Rb-Sr isochron of three Maladeta granitoids yields a late Hercynian age of 277 ± 7 Ma. The third study is of assorted Hercynian granitoids from the Massif Central, also dated using whole rock Rb-Sr isochrons (Downes and Duthou, 1988; Downes et al., 1990).

The SiO_2 and $\delta^{18}O$ data for all sets are plotted on Figure 5.33. The high degree of overlap of the Mafic Complex data with the xenolith and granitoid data suggests that the conclusions concerning igneous processes in the Ivrean lower crust may be characteristic of the lower crust beneath the Massif Central during the Hercynian. The mafic xenoliths

reflect the highly variable degree of assimilation of high-^{18}O crustal material possible in the lower crust. The thermal control on the extent of quenching seems to be a common factor: i.e., cool crust enables preservation of mantle signatures while assimilation is enhanced in warm crust. The Maladeta gabbros and the felsic xenoliths define a horizontal trend comparable to the diorite, roof diorite and charnockite units of the Ivrea Zone. Mixing between lower crustal melts and evolved MG-type gabbros accounts for much of the horizontal trend while fractional crystallization may be of variable importance. The input of low-^{18}O magma at this level is either limited or obscured by homogenization processes. The gap between 55 and 60% SiO_2 in the xenolith suite may be a bias from the xenolith sampling or may indicate that the production of mixed second tier magmas was not universally efficient. The upswing to higher $\delta^{18}O$ recorded by the charnockites in the Ivrea Zone and the granitoids in the Massif Central indicates an increased degree of assimilation of more fertile middle crust or granitic melt and/or possibly an increase in the $\delta^{18}O$ of the assimilant.

The pattern supports the model for the Ivrea-Strona-Ceneri section that large amounts of mantle-derived magma underplated the crust during the late Hercynian. Lower crustal Ivrea-type magma chambers efficiently produced large volumes of isotopically evolved MG-type material. Ponding of such magma beneath lower and mid-crust high temperature mylonite zones produced mixed magmas while initiating melting in higher levels of the crust. The evolved mafic and silicic melts mixed to various degrees in the second tier chambers and rose to higher levels only after the peak of metamorphism had passed in the overlying crust. Magma that had the potential to reach the upper crust would be dominantly mixed MG-middle crust melt and S-type, two-mica granites with lesser MG-affinity basalt. Water-rich basalt might be more readily intruded to high crustal levels to form the lamprophyres as a result of high buoyancy.

The model prediction matches observed upper crustal Hercynian plutonic associations for which $\delta^{18}O$ is available. For example, the Maladeta complex is dominated by biotite granodiorite and two-mica cordierite granite with lesser gabbronorite and quartz diorite while the Ploumanac'h ring complex, France, is composed primarily of biotite granite with lesser two-mica cordierite granite and olivine gabbronorite to tonalite (Albarede et al., 1980; Michard-Vitrac et al., 1980). Biotite granodiorites and leucogranites predominate in the Trois Seigneurs Massif, French Pyrenees, while traces of mafic material form enclaves in a heterogeneous biotite granite (Wickham and Taylor, 1985). In these examples, the affinity of the high-^{18}O mafic lithologies to rocks from the Mafic Complex is clear. Moreover, similar high-^{18}O, S-type granites are found in the Graniti dei Laghi. The biotite granodiorites in all examples are similar to the diorites of the Mafic Complex and the bulk of the Graniti dei Laghi and as such would have formed in the hypothesized second tier magma chambers in which MG-type magmas mixed with mid-crustal melts and possibly underwent further crystal fractionation.

In each of the examples noted above, the various lithologies were interpreted by the authors as originating from intracrustal melting of a compositionally and isotopically stratified crust: the S-type leucogranites represent upper crustal melt of water-rich pelites; the biotite granitoids represent melting of lower crust graywackes and amphibolites of possible mantle origin. An alkaline mantle component is invoked for the mafic lithologies at Ploumanac'h while the mafic xenoliths of Trois Seigneurs are identified as lower crust or mantle material. While recognized as a viable heat source to promote crustal melting, the possibility of a significant mantle-derived magmatic component in the biotite granitoids is not favored due to the lack of exposed cumulates that would have been produced during AFC processes and the inability to predict actual rock compositions with simple mixing calculations between mantle and crust melts using major elements. The first objection is easily explained by the presence of appropriate cumulates in the lower crust. The second

objection is resolved by the recognition of the second tier of magma chambers in which the isotopic systematics of the MG-type mafic component have been substantially modified previously in the lower crust with little increase in SiO_2 content prior to mixing with crustal melt in the mid-crust.

Many of the rounded mafic enclaves in Hercynian plutonic and volcanic rocks have been recognized as representing quenched mafic magma (Cantagrel et al., 1984; Didier, 1987). Rb-Sr and Nd-Sm systematics of enclaves demonstrates that the mafic magma was not in isotopic equilibrium with its granitic host and was instead substantially less radiogenic and of probable mantle origin (Holden et al., 1987; Pin et al., 1990). These enclaves demonstrate that small amounts of relatively uncontaminated mafic magma reached upper crustal levels and suggest that both the mass and heat of larger amounts of such magma were important in the granitoid genesis. These observations are consistent with the proposed second tier of magma chambers in which most of the mafic magma reaching the middle crust mixed with crustal melts prior to emplacement at higher crustal levels.

As has been discussed earlier, the preservation of peak metamorphic assemblages as well as the oxygen isotope systematics presented in the following chapter indicate the lack of pervasive fluid infiltration in the lower crust. Pervasive infiltration and isotopic homogenization has been demonstrated as having occurred at high crustal levels in other extensional regimes in which crustal anatexis accompanied regional metamorphism (Wickham and Taylor, 1985; Wickham and Taylor, 1987; Bickle et al., 1988). In such environments isotopic exchange is facilitated as faults provide abundant conduits for fluids into the crust and the magmatism provides the energy required to drive fluid circulation and mineral reactions. Moreover, devolatilization reactions increase permeability of the metamorphic section. Perhaps the near horizontal, ductile mylonitic zones of the Ivrea Zone inhibited fluid infiltration to deep crustal levels. A lack of hydrostatically pressured fluid infiltration has been hypothesized for deep crust (Zone 3 - (Wickham and Taylor,

1987)) which is characterized by igneous activity, ductile extension, and heterogeneous metasedimentary and igneous $\delta^{18}O$ values. If the analogy is appropriate, then the middle crustal Strona-Ceneri Zone would be equivalent to Zone 2 in which extensive hydrothermal alteration is predicted. Hydrothermal alteration of the green granite of Mergozza from the Graniti dei Laghi has been demonstrated in this study; future work will be aimed at investigating the isotopic systematics of the Strona-Ceneri metamorphic rocks.

In conclusion, the similarities between plutonic rocks from the Ivrea-Strona-Ceneri crustal section and Hercynian lower crustal xenoliths and upper crustal plutonic rocks suggest that the model constructed in this study is of general relevance to Hercynian magmatism in the Massif Central and perhaps throughout the orogenic belt. This study of the Mafic Complex confirms what other researchers have deduced from limited data or indirect reasoning: specifically that mantle-derived magma was a volumetrically significant component of Hercynian magmatism.

Ivrea Zone Bibliography

Albarede, F., C. Dupuis and H. P. Taylor, Jr., 1980, 18O/16O Evidence for non-cogenetic magmas associated in a 300 Ma Old concentric pluton at Ploumanac'h (Brittany, France): Journal of the Geological Society of London, v. 137, n. 5, p. 641-647.

Allegre, C. J., F. Albarede, M. Grunenfelder and V. Koppel, 1974, U/ Pb- U/ Pb- Th/ Pb zircon geochronology in Alpine and non-Alpine environment: Contributions to Mineralogy and Petrology, v. 43, p. 163-194.

Baker, A. J., 1988, Stable isotope evidence for limited fluid infiltration of deep crustal rocks from the Ivrea Zone, Italy: Geology, v. 16, p. 492-495.

Baker, A. J., 1990, Stable isotopic evidence for fluid-rock interactions in the Ivrea Zone, Italy: Journal of Petrology, v. 31, n. 1, p. 243-260.

Bayer, R., M. Cazes, G. V. D. Piaz, B. Damotte, G. Elter, G. Gosso, A. Hirn, R. Lanza, B. Lombardo, J.-L. Mugnier, et al., 1987, Premiers resultats de la traversee des Alpes occidentales par sismique reflexion verticale (Programme ECORS-CROP): Comptes Rendus des Seances de l'Acadamie des Sciences, v. 305, p. 1461-1470.

Berckhemer, H., 1969, Direct evidence for the composition of the lower crust and the Moho: Tectonophysics, v. 8, n. 2, p. 97-105.

Bickle, M. J., S. M. Wickham, H. J. Chapman and H. P. Taylor, Jr., 1988, A strontium, neodymium and oxygen isotope study of hydrothermal metamorphism and crustal anatexis in the Trois Seigneurs Massif, Pyrenees, France: Contributions to Mineralogy and Petrology, v. 100, p. 399-417.

Bigioggero, B., A. Boriani, A. Colombo and A. Gregnanin, 1978/79, The "diorites" of the Ivrea Basic Complex (Central Alps, Italy). 2nd Symposium Ivrea-Verbano, Varallo Sesia (VC), Italy, Istituti di Geologia e Mineralogia dell'Universita di Padova.

Bigioggero, B., L. Brigo, A. Ferrario, A. Gregnanin, A. Montrasio and P. Zuffardi, 1978/79, Strona Valley (Fe-Ni-Cu) and (Fe-Ba) ore deposits: Excursion Book. 2nd Symposium Ivrea-Verbano, Varallo Sesia (VC), Italy, Instituti di Geologia e Mineralogia dell' Universita di Padova.

Blattner, P., V. Dietrich and A. Gansser, 1983, Contrasting 18O enrichment and origins of high Himalayan and Transhimalayan intrusives: Earth and Planetary Science Letters, v. 65, p. 276-286.

Bohlen, S. R. and J. J. Liotta, 1984, A new barometer and the P-T evolution of granulites: Geological Society of America Abstracts with Programs, p. 448.

Boriani, A., B. Bigioggero and E. O. Giobbi, 1977, Metamorphism, tectonic evolution and tentative stratigraphy of the "Serie dei Laghi"; Geologic map of the Verbania Area (Northern Italy): Memorie di Scienze Geologiche, v. 32.

Boriani, A., L. Burlini, M. Ferraris and A. Zappone, 1987, Carta geologica dei graniti dei Laghi, 1:50,000. Valsesia, Cusio e Verbano, Provincie di Vercelli e Novara, Dipartimento di Scienze della Terra, Universita degli Studi di Milano, Italia. 1:50,000,

Boriani, A., V. Caironi, M. Oddone and R. Vannucci, 1988b, Some petrological and geochemical constraints on the genesis of the Baveno-Mottarone and Montorfano plutonic bodies: Rendiconti della Societa Italiana di Mineralogia e Petrologia, v. 43, n. 2, p. 385-394.

Boriani, A., E. O. Giobbi and A. D. Moro, 1982/83, Composition, level of intrusion and age of the "Serie dei Laghi" orthogneisses (Northern Italy-Ticino, Switzerland): Rendiconti della Societa Italiana di Mineralogia e Petrologia, v. 38, n. 1, p. 191-205.

Boriani, A., E. G. Origoni, A. Borghi and V. Caironi, 1990, The evolution of the "Serie dei Laghi" (Strona-Ceneri and Scisti dei Laghi): the upper crust component of the Ivrea-Verbano crustal section; Southern Alps, North Italy and Ticino, Switzerland: Tectonophysics, v. 182, p. 103-118.

Boriani, A. and R. Sacchi, 1973, Geology of the junction between the Ivrea-Verbano and Strona-Ceneri Zones (Southern Alps). Memorie degli Instituti di Geologia e Mineralogia dell' Universita di Padova.

Boriani, A. and R. Sacchi, 1974, The "Insubric" and other tectonic lines in the Southern Alps (NW Italy): Memorie della Societa Geologica Italiana, v. 13, n. 1, p. 327-337.

Bottinga, Y. and M. Javoy, 1975, Oxygen isotope partitioning among the minerals in igneous and metamorphic rocks: Reviews of Geophysics and Space Physics, v. 13, p. 401-418.

Brodie, K. H., 1980, Variations in mineral chemistry across a shear zone in phlogopite peridotite: Journal of Structural Geology, v. 2, n. 1/2, p. 265-272.

Brodie, K. H., 1981, Variation in amphibole and plagioclase composition with deformation: Tectonophysics, v. 78, p. 385-402.

Brodie, K. H., D. Rex and E. H. Rutter, 1989, On the age of deep crustal extensional faulting in the Ivrea zone, northern Italy in Coward, M. P., D. Dietrich and R. G. Park, ed., Alpine Tectonics: Boulder, Colorado, Geological Society of America, p. 203-210.

Brodie, K. H. and E. H. Rutter, 1985, On the relationship between deformation and metamorphism, with special reference to the behavior of basic rocks in Thompson, A. B. and D. C. Rubie, ed., Metamorphic Reactions: kinetics, textures and deformation: Berlin, Springer, p. 138-179.

Brodie, K. H. and E. H. Rutter, 1987, Deep crustal extensional faulting in the Ivrea zone of northern Italy: Tectonophysics, v. 140, p. 193-212.

Burghi, A., 1987, Mineralogische und petrographische untersuchungen im Val Strona di Postua (Prov. Vercelli, Italien). Bern, Switzerland. doctorate,

Burghi, A. and U. Klotzli, 1990, New data on the evolutionary history of the Ivrea Zone (Northern Italy): Bulletin der Vereinigung Schweizerisches Petroleum -Geologen und - Ingenieur, v. 56, n. 130, p. 49-70.

Burke, M. M. and D. M. Fountain, 1990, Seismic properties of rocks from an exposure of extended continental crust - new laboratory measurements from the Ivrea Zone: Tectonophysics, v. 182, p. 119-146.

Burlini, L. and V. Caironi, 1988, Geological and petrographical data on the Quarna pluton (Serie dei Laghi, Northern Italy): Rendiconti della Societa Italiana di Mineralogia e Petrologia, v. 43, n. 2, p. 429-444.

Cantagrel, J.-M., J. Didier and A. Gourgaud, 1984, Magma mixing: Origin of intermediate rocks and "enclaves" from volcanism to plutonism: Physics of Planetary Interiors, v. 35, p. 63-76.

Capedri, S., 1972, On the presence of graphite and its bearing on the migmatic environmental conditions of the dioritic gneisses ("Diorites"), Basic formation Ivrea-Verbano, Italy: Atti della Societa Toscana di Scienze Naturali Residente in Pisa Memorie, Serie A: Processi Verbali, v. 79, p. 286-293.

Capedri, S., A. Coradini, O. Fanucci, G. Garuti, G. Rivalenti and A. Rossi, 1977, The origin of the Ivrea-Verbano basic formation (Italian Western Alps) statistical approach to the peridotite problem: Societa Italiano di Mineralogia e Petrologia, v. 33, n. 2, p. 583-592.

Capedri, S., C. B. Gomes, G. Rivalenti and E. Ruberti, 1976, Pyroxenes and olivines as indicators of the petrological evolution of the Ivrea-Verbano Basic Formation (Italian Western Alps): Tschermaks Mineralogishe und Petrographishe Mitteilungen, v. 23, p. 175-190.

Capedri, S. and G. Rivalenti, 1973, Metamorphic crystallizations in relation to plastic deformations in pelitic series (Valle Strona, Vercelli, Italy): Bollettino della Societa Geologica Italiana, v. 92, p. 649-668.

Christensen, N. I. and D. M. Fountain, 1975, Constitution of the lower continental crust based on experimental studies of seismic velocities in granulite: Geological Society of America Bulletin, v. 86, p. 227-236.

Coltorti, M. and F. Siena, 1984, Mantle tectonite and fractionate peridotite at Finero (Italian Western Alps): Neues Jahrbuch fur Mineralogie Monatshefte, v. 149, n. 3, p. 225-244.

Cumming, G. L., V. Koppel and A. Ferrario, 1987, A lead isotopic study of the northeastern Ivrea Zone and the adjoining Ceneri Zone (N-Italy): Evidence for a contaminated subcontinental mantle: Contributions to Mineralogy and Petrology, v. 97, p. 19-30.

DePaolo, D. J., 1980, Trace element and isotopic effects of combined wallrock assimilation and fractional crystallization: Earth and Planetary Science Letters, v. 53, p. 189-202.

DePaolo, D. J., 1981, A neodymium and strontium isotopic study of the Mesozoic calc-alkaline granitic batholiths of the Sierra Nevada and Peninsular Ranges, California: Journal of Geophysical Research, v. 86, n. B11, p. 10470-10488.

Didier, J., 1987, Contribution of enclave studies to the understanding of origin and evolution of granitic magmas: Geologische Rundschau, v. 76, n. 1, p. 41-50.

Downes, H., C. Dupuy and A. F. Leyreloup, 1990, Crustal evolution of the Hercynian Belt of Western Europe: Evidence from lower-crustal granulitic xenoliths (French Massif Central): Chemical Geology, v. 83, p. 209-231.

Downes, H. and J.-L. Duthou, 1988, Isotopic and trace-element arguments for the lower-crustal origin of Hercynian granitoids and pre-Hercynian orthogneisses, Massif Central (France): Chemical Geology, v. 68, p. 291-308.

Downes, H., P. D. Kempton, D. Briot, R. S. Harmon and A. F. Leyreloup, 1991, Pb and O isotope systematics in granulite facies xenoliths, French Massif Central: Implications for crustal processes: Earth and Planetary Science Letters, v. 102, p. 342-357.

Dunn, T., 1986, An investigation of the oxygen isotope geochemistry of the Stillwater Complex: Journal of Petrology, v. 27, n. 4, p. 987-997.

Ernst, W. G., 1978, Petrochemical study of lherzolitic rocks from the western Alps: Journal of Petrology, v. 19, part 3, p. 341-392.

Exley, R. A., J. D. Sills and J. V. Smith, 1982, Geochemistry of micas from the Finero spinel-lherzolite, Italian Alps: Contributions to Mineralogy and Petrology, v. 81, p. 59-63.

Ferrario, A., G. Garuti, A. Rossi and G. P. Sighinolfi, 1983, Petrographic and metallogenic outlines of the "La Balma-M. Capio" ultramafic-mafic body (Ivrea-Verbano Basic Complex, NW Italian Alps) in Schneider, H. J., ed., Mineral Deposits of the Alps and of the Alpine Epoch in Europe: Berlin, Springer-Verlag, p. 28-40.

Ferrario, A., G. Garuti and G. P. Sighinolfi, 1982, Platinum and palladium in the Ivrea-Verbano Basic Complex, Western Alps, Italy: Economic Geology, v. 77, p. 1548-1555.

Finger, F. and H. P. Steyrer, 1990, Granitoids as indicators of a late Paleozoic convergent continent margin along the southern flank of the central European Variscan orogen: Geology, v. 18, p. 1207-1210.

Fountain, D. M., 1976, The Ivrea-Verbano and Strona-Ceneri Zones, northern Italy: A cross-section of the continental crust - new evidence from seismic velocities of rock samples: Tectonophysics, v. 33, p. 145-165.

Fountain, D. M., 1986, Implications of deep crustal evolution for seismic reflection interpretation in Barazangi, M. and L. Brown, eds., Reflection Seismology: The Continental Crust. American Geophysical Union Geodynamics Series, v. 14, p. 1-7.

Fountain, D. M., 1989, Growth and modification of lower continental crust in extended terrains: the role of extension and magmatic underplating in Mereu, R. F., S. Mueller and D. M. Fountain, ed., Properties and processes of earth's lower crust: Washington, D.C., American Geophysical Union, p. 287-300.

Frei, W., P. Heitzmann, P. Lehner, S. Muller, R. Olivier, A. Pfiffner, A. Steck and P. Valasek, 1989, Geotraverse across the Swiss Alps: Nature, v. 340, p. 544-548.

Gansser, A., 1968, The Insubric Line, a major geotectonic problem: Schweizerishe Mineralogische und Petrographische Mitteilungen, v. 48, n. 1, p. 123-143.

Garuti, G. and R. Friolo, 1978/79, Textural features and olivine fabrics of peridotites from the Ivrea-Verbano Zone (Italian Western Alps). 2nd Symposium Ivrea-Verbano, Varallo Sesia (VC), Italy, Instituti di Geologia e Mineralogia dell' Universita di Padova.

Garuti, G., C. Gorgoni and G. P. Sighinolfi, 1984, Sulfide mineralogy and chalcophile and siderophile abundances in the Ivrea-Verbano mantle peridotites (Western Italian Alps): Earth and Planetary Science Letters, v. 70, p. 69-87.

Garuti, G., G. Rivalenti, A. Rossi, F. Siena and S. Sinigoi, 1980, The Ivrea-Verbano mafic-ultramafic complex of the Italian Western Alps: Discussion of some petrologic problems and a summary: Societa Italiana di Mineralogia e Petrologia, v. 36, p. 717-749.

Garuti, G., G. Rivalenti, A. Rossi and S. Sinigoi, 1978/79, Mineral equilibria as geotectonic indicators in the ultramafics and related rocks of the Ivrea-Verbano Basic Complex (Italian Western Alps): Pyroxenes and olivine. 2nd Symposium Ivrea-Verbano, Varallo Sesia (VC), Italy, Instituti di Geologia e Mineralogia dell' Universita di Padova.

Garuti, G. and S. Sinigoi, 1978, Occurrence of phlogopite in the peridotite of Balmuccia (Ivrea Verbano basic formation, Italian Western Alps): a preliminary note: Neues Jahrbuch fur Mineralogie Monatshefte, v. 12, p. 549-553.

Giese, P., 1968, Die struktur der Erdekruste im Bereich der Ivrea-Zone. Ein Vergleich verschiedener, seismischer Interpretationen und der Versuch einer petrographisch-geologischen Deutung: Schweizerishe Mineralogische und Petrographische Mitteilungen, v. 48, p. 255-260.

Handy, M. R., 1986, The Structure and rheological evolution of the Pogallo fault zone, A deep crustal dislocation in the Southern Alps of Northwestern Italy (Prov. Novara). Basel, Switzerland. (Ph.D. thesis)

Handy, M. R., 1987, The structure, age and kinematics of the Pogallo Fault Zone; Southern Alps, northwestern Italy: Eclogae Geologicae Helvetiae, v. 80, n. 3, p. 593-632.

Handy, M. R. and A. Zingg, 1991, The tectonic and rheological evolution of an attenuated cross section of the continental crust: Ivrea crustal section, southern Alps, northwestern Italy and southern Switzerland: Geological Society of America Bulletin, v. 103, p. 236-253.

Hildreth, W. and S. Moorbath, 1988, Crustal contributions to arc magmatism in the Andes of Central Chile: Contributions to Mineralogy and Petrology, v. 98, p. 455-489.

Hodges, K. V. and D. M. Fountain, 1984, Pogallo Line, south Alps, northern Italy: An intermediate crustal level, low-angle normal fault?: Geology, v. 12, p. 151-155.

Hoefs, J. and R. Emmermann, 1983, The oxygen isotope composition of Hercynian granites and pre-Hercynian gneisses from the Schwarzwald, SW Germany: Contributions to Mineralogy and Petrology, v. 83, p. 320-329.

Holden, P., A. N. Halliday and W. E. Stephens, 1987, Neodymium and strontium isotope content of microdiorite enclaves points to mantle input to granitoid production: Nature, v. 330, p. 53-56.

Hunziker, J. C., A. Steck, G. Rivalenti, I. Mercolli and A. Zingg, 1982, Emplacement and crustal contamination of the peridotites in the Ivrea-Zone: Terra Cognita, v. 2, n. 3, p. 237.

Hunziker, J. C. and A. Zingg, 1980, Lower paleozoic amphibolite to granulite facies metamorphism in the Ivrea Zone (Southern Alps, Northern Italy): Schweizerishe Mineralogische und Petrographische Mitteilungen, v. 60, p. 181-213.

Irvine, T. N., D. W. Keith and S. G. Todd, 1983, The J-M platinum-palladium reef of the Stillwater Complex, Montana: II. Origin by double-diffusive convective magma mixing and implications for the Bushveld Complex: Economic Geology, v. 78, n. 7, p. 1287-1334.

Jager, E. and H. Faul, 1959, Age measurements on some granites and gneisses from the Alps: Geological Society of America Bulletin, v. 70, p. 1553-1558.

Johnston, A. D. and P. J. Wyllie, 1988, Interaction of granitic and basic magmas: experimental observations on contamination processes at 10 kbar with H_2O: Contributions to Mineralogy and Petrology, v. 98, p. 352-362.

Koppel, V., 1974, Isotopic U-Pb ages of monazites and zircons from the crust-mantle transition and adjacent units of the Ivrea and Ceneri Zones (Southern Alps, Italy): Contributions to Mineralogy and Petrology, v. 43, p. 55-70.

Koppel, V. and M. Grunenfelder, 1971, A study of inherited and newly formed zircons from paragneissses and granitised sediments of the Strona-Ceneri-Zone (Southern Alps): Schweizerishe Mineralogische und Petrographische Mitteilungen, v. 51, p. 385-409.

Koppel, V. and M. Grunenfelder, 1975, Concordant U-Pb ages of monazite and xenotime from the central Alps and the timing of the high temperature Alpine metamorphism, a preliminary report: Schweizerishe Mineralogische und Petrographische Mitteilungen, v. 55, p. 129-132.

Koppel, V. and M. Grunenfelder, 1978/79, Monazite and zircon U-Pb ages from the Ivrea and Ceneri Zones: Memorie di Scienze Geologiche, v. 33, p. 257.

Krull, J. H. and G. Voll, 1978, Deformation and metamorphism of the western Finero complex. 2nd Symposium Ivrea-Verbano, Varallo Sesia (VC), Italy, Instituti di Geologia e Mineralogia dell' Universita di Padova.

Laubscher, H., 1990, The problem of the Moho in the Alps: Tectonophysics, v. 182, p. 9-20.

Lemoine, M., 1984, Mesozoic evolution of the Western Alps: Annales Geophysicae, v. 2, n. 2, p. 171-172.

Liew, T. C. and A. W. Hofmann, 1988, Precambrian crustal components, plutonic associations, plate environment of the Hercynian fold belt of central Europe: Indications from a Nd and Sr isotopic study: Contributions to Mineralogy and Petrology, v. 98, p. 129-138.

Mayer, A., 1989, Processi M.A.S.H. ed RTF in Zone Orogeniche Continentali: L'Esempio della Val Sesia. Treiste, Italy. tesi di Laurea,

Mazzucchelli, M., 1983, The upper zone of the Ivrea-Verbano layered complex (Italian Western Alps): Neues Jahrbuch fur Mineralogie Monatshefte, v. 146, n. 1, p. 101-116.

Mazzucchelli, M. and F. Siena, 1986, Geotectonic significance of the metabasites of the Kinzigitic Series, Ivrea-Verbano Zone (Western Italian Alps): Tschermaks Mineralogische und Petrographishe Mitteilungen, v. 35, p. 99-116.

Mazzucchelli, M., G. Rivalenti, R. Vannucci, P. Bottazzi, L. Ottolini, A. W. Hofmann, M. Parenti, in press, Primary positive Eu anomaly in clinopyroxenes of low-crust rocks: Geochimica and Cosmochemica Acta, v. 56.

McBirney, A. R. and R. M. Noyes, 1979, Crystallization and layering of the Skaergaard Intrusion: Journal of Petrology, v. 20, n. 3, p. 487-554.

McDowell, F. W. and R. Schmid, 1968, Potassium-argon ages from the Valle d'Ossola Section of the Ivrea-Verbano Zone (Northern Italy): Schweizerishe Mineralogische und Petrographische Mitteilungen, v. 48, n. 1, p. 205-210.

Mehnert, K. R., 1975, The Ivrea Zone - a model of the deep crust: Neues Jahrbuch fur Mineralogie Monatshefte, v. 125, n. 2, p. 156-199.

Mercolli, I. and R. Oberhansli, 1988, Variscan tectonic evolution in the Central Alps: A working hypothesis: Schweizerishe Mineralogische und Petrographische Mitteilungen, v. 68, p. 491-500.

Michard-Vitrac, A., F. Albarede, C. Dupuis and H. P. Taylor, Jr., 1980, The genesis of Variscan (Hercynian) plutonic rocks: Inferences From Sr, Pb, and O studies on the Maladeta Igneous Complex, Central Pyrenees (Spain): Contributions to Mineralogy and Petrology, v. 72, p. 57-72.

Nicolas, A., A. Hirn, R. Nicolich, R. Polino and E.-C. W. Group, 1990, Lithospheric wedging in the western Alps inferred from the ECORS-CROP traverse: Geology, v. 18, n. 7, p. 587-590.

Nicolas, A. and M. Jackson, 1982, High temperature dikes in mantle peridotites: Origin by hydraulic fracturing during plastic flow: Terra Cognita, v. 2, n. 3, p. 244.

Norton, D. and H. P. Taylor, Jr., 1979, Quantitative simulation of the transport theory and oxygen isotope data: An analysis of the Skaergaard intrusion: Journal of Petrology, v. 20, p. 421-486.

O'Hara, M. J. and R. E. Mathews, 1981, Geochemical evolution in an advancing, periodically replenished, periodically tapped, continuously fractionated magma chamber: Journal of the Geological Society of London, v. 138, p. 237-277.

Peyronel-Pagliani, G. and A. Boriani, 1967, Metamorfismo crescente nelle metamorfiti del "Massicio dei Laghi" nella zona bassa Val d'Ossola-Verbania: Rendiconti della Societa Italiana di Mineralogia e Petrologia, v. 23, p. 351-397.

Pin, C., 1986, Datation U-Pb sur zircons a 285 M.a. du complexe gabbro-dioritique du Val Sesia-Val Mastellone et age tardi-hercynien du metamorphisme granulitique de la zone Ivrea-Verbano (Italie): Comptes Rendus des Seances de l'Acadamie des Sciences des Paris, v. 303, p. 827-830.

Pin, C., M. Binon, J. M. Belin, B. Barbarin and J. D. Clemens, 1990, Origin of microgranular enclaves in granitoids: Equivocal Sr-Nd evidence from Hercynian rocks in the Massif Central (France): Journal of Geophysical Research, v. 95, n. B11, p. 17821-17828.

Pin, C. and J. D. Sills, 1986, Petrogenesis of layered gabbros and ultramafic rocks from Val Sesia, the Ivrea Zone, NW Italy: Trace element and isotope geochemistry in Dawson, J. B., D. A. Carswell, J. Hall and K. H. Wedepohl, ed., The Nature of the Lower Continental Crust: Geological Society Special Publication, p. 231-249.

Pinarelli, L., A. Boriani and A. D. Moro, 1988, Rb-Sr geochronology of the lower Permian plutonism in the Massiccio dei Laghi, Southern Alps (NW. Italy): Rendiconti della Societa Italiana di Mineralogia e Petrologia, v. 43, n. 2, p. 411-428.

Quick, J. E., 1981, Part 1: Petrology and petrogenesis of the Trinity Peridotite, northern California. California Institute of Technology (Ph.D. thesis).

Quick, J. E., S. Sinigoi, L. Negrini and G. Demarchi, *in review*, Synmagmatic deformation in the underplated igneous complex of the Ivrea-Verbano Zone: Evidence and implications.

Rivalenti, G., G. Garuti and A. Rossi, 1975, The Origin of the Ivrea-Verbano Basic Formation (Western Italian Alps) whole rock geochemistry: Bollettino della Societa Geologica Italiana, v. 94, p. 1149-1186.

Rivalenti, G., G. Garuti, A. Rossi, F. Siena and S. Sinigoi, 1980, Existence of different peridotite types and of a layered igneous complex in the Ivrea Zone of the western Alps: Journal of Petrology, v. 22, n. 1, p. 127-153.

Rivalenti, G., G. Garuti, A. Rossi and S. Sinigoi, 1978/79, Spinels as petrographic indicators in the Ivrea-Verbano Basic Complex (Italian Western Alps). 2nd Symposium Ivrea-Verbano, Varallo Sesia (VC), Italy, Instituti di Geologia e Mineralogia dell' Universita di Padova.

Rivalenti, G., A. Rossi, F. Siena and S. Sinigoi, 1984, The layered series of the Ivrea-Verbano Igneous Complex, western Alps, Italy: Tschermaks Mineralogishe und Petrographishe Mitteilungen, v. 33, p. 77-99.

Schmid, R., 1967, Zur petrographie und struktur der Zone Ivrea-Verbano zeischen Valle D'Ossola und Val Grand (Prov. Novara, Italien): Schweizerishe Mineralogische und Petrographische Mitteilungen, v. 47, n. 2, p. 936-1118.

Schmid, R., 1978, Are the metapelites of the Ivrea-Verbano Zone restites? 2nd Symposium Ivrea-Verbano, Varallo Sesia (VC), Italy, Instituti di Geologia e Mineralogia dell' Universita di Padova.

Schmid, R., V. Dietrich, M. Komatsu, R. C. Newton, R. Ragettli, T. Rushmer, M. Tuchschmid and R. Vogler, 1988, Metamorphic evolution and origin of the Ivrea zone. Italy-U.S. Workshop on the Nature of the Lower Continental Crust, Verbania, IT, Univ. Milano.

Schmid, R. and B. J. Wood, 1976, Phase relationships in granulitic metapelites from the Ivrea-Verbano Zone (Northern Italy): Contributions to Mineralogy and Petrology, v. 54, p. 255-279.

Schmid, S., A. Zingg and M. Handy, 1987, The kinematics of movements along the Insubric Line and the emplacement of the Ivrea Zone: Tectonophysics, v. 135, p. 47-66.

Schmid, S. M., H. R. Aebli, F. Heller and A. Zingg, 1989, The role of the Periadriatic Line in the tectonic evolution of the Alps in Coward, M. P., D. Dietrich and R. G. Park, ed., Alpine Tectonics: Boulder, Colorado, Geological Society of America, p. 153-171.

Schnetger, B., 1988, Geochemische untersuchungen an den kinzigiten und stronaliten der Ivrea-Zone, Norditalien. Gottingen, Germany. (Ph.D. thesis).

Sharpe, M. R., 1985, Strontium isotope evidence for preserved density stratification in the main zone of the Bushveld Complex, South Africa: Nature, v. 316, n. , p. 119-126.

Sheppard, S. M. F., 1986, Igneous Rocks: III. isotopic case studies of magmatism in Africa, Eurasia and oceanic islands in Valley, J. W., H. P. Taylor, Jr. and J. R. O'Neil, ed., Stable Isotopes in High Temperature Geological Processes: Wahington, D.C., Mineralogical Society of America, p. 319-372.

Shervais, J., 1978/79, Ultramafic and mafic layers in the Alpine-type lherzolite massif at Balmuccia, N. W. Italy. 2nd Symposium Ivrea-Verbano, Varallo Sesia (VC), Italy, Instituti di Geologia e Mineralogia dell'Universita di Padova.

Shervais, J. W., 1979, Thermal emplacement model for the Alpine Lherzolite Massif at Balmuccia, Italy: Journal of Petrology, v. 20, part 4, p. 795-820.

Sighinolfi, G. P., 1969, K-Rb ratio in high grade metamorphism: A confirmation of the hypothesis of a continental crustal evolution: Contributions to Mineralogy and Petrology, v. 21, p. 346-356.

Sills, J. D., 1984, Granulite facies metamorphism in the Ivrea Zone, N. W. Italy: Schweizerishe Mineralogische und Petrographische Mitteilungen, v. 64, p. 169-191.

Sills, J. D., D. Ackermand, R. K. Herd and B. F. Windley, 1983, Bulk composition and mineral paragenesis of sapphirine-bearing rocks along a gabbro-lherzolite contact at Finero, Ivrea Zone, N Italy: Journal of Metamorphic Geology, v. 1, p. 337-351.

Sills, J. D., C. Pin and P. B. Greenwood, 1986, Petrogenesis of meta-gabbros from Val Sesia, Ivrea Zone, NW Italy: trace element and isotope evidence: Terra Cognita, v. 6, n. 2, p. 184.

Sills, J. D. and J. Tarney, 1984, Petrogenesis and tectonic significance of amphibolites interlayered with metasedimentary gneisses in the Ivrea Zone, southern Alps, northwest Italy: Tectonophysics, v. 107, p. 187-206.

Sinigoi, S., P. Antonini, G. Demarchi, A. Longinelli, M. Mazzucchelli, L. Negrini and G. Rivalenti, 1991, Interactions of mantle and crustal magmas in the southern part of the Ivrea Zone (Italy): Contributions to Mineralogy and Petrology, v. 108, n. 4, p. 385-395.

Sinigoi, S., P. Comin-Chiaramonti and A. A. Alberti, 1980, Phase relations in the partial melting of the Baldissero spinel-lherzolite (Ivrea-Verbano Zone, Western Alps, Italy): Contributions to Mineralogy and Petrology, v. 75, p. 111-121.

Sinigoi, S., P. Comin-Chiaramonti, G. Demarchi and F. Siena, 1983, Differentiation of partial melts in the mantle: Evidence from the Balmuccia Peridotite, Italy: Contributions to Mineralogy and Petrology, v. 82, p. 351-359.

Skrotzki, W., A. Wedel, K. Weber and W. F. Muller, 1990, Microstructure and texture in lherzolites of the Balmuccia massif and their significance regarding the thermomechanical history: Tectonophysics, v. 179, p. 227-251.

Steck, A. and J.-C. Tieche, 1976, Carte geologique de l'antiforme peridotitique de Finero avec des observations sur les phases de deformation et de recrystallization: Schweizerishe Mineralogische und Petrographische Mitteilungen, v. 56, p. 501-512.

Stille, P. and M. Buletti, 1987, Nd-Sr isotopic characteristics of the Lugano volcanic rocks and constraints on the continental crust formation in the south Alpine domain (N-Italy-Switzerland): Contributions to Mineralogy and Petrology, v. 96, p. 140-150.

Taylor, S. R. and S. M. McLennan, 1985, The continental crust: its composition and evolution: Oxford, Blackwell Scientific Publications,.312 p.

Trumpy, R., 1975, Penninic-Austroalpine boundary in the Swiss Alps: a presumed former continental margin and its problems: American Journal of Science, v. 275-A, p. 209-238.

Vielzeuf, D. and J. Kornprobst, 1982, The ultramafic-granultic associations: An indication of paleo-Moho discontinuities: Terra Cognita, v. 2, n. 3, p. 241.

Voshage, H., A. W. Hofmann, M. Mazzucchelli, G. Rivalenti, S. Sinigoi, I. Raczik and G. Demarchi, 1990, Isotopic evidence from the Ivrea Zone for a hybrid lower crust formed by magmatic underplating: Nature, v. 347, p. 731-736.

Voshage, H., J. C. Hunziker, A. W. Hofmann and A. Zingg, 1987, A Nd and Sr isotopic study of the Ivrea Zone, Southern Alps, N-Italy: Contributions to Mineralogy and Petrology, v. 97, p. 31-42.

Voshage, H., S. Sinigoi, M. Mazzucchelli, G. Demarchi, G. Rivalenti and A. W. Hofmann, 1988, Isotopic constraints on the origin of ultramafic and mafic dikes in the Balmuccia Peridotite (Ivrea Zone): Contributions to Mineralogy and Petrology, v. 100, p. 261-267.

Wickham, S. M. and E. R. Oxburgh, 1987, Low-pressure regional metamorphism in the Pyrenees and its implications for the thermal evolution of rifted continental crust: Philosophical Transactions of the Royal Society of London, Series A, v. 321, p. 219-242.

Wickham, S. M. and H. P. Taylor, Jr., 1985, Stable isotopic evidence for large-scale seawater infiltration in a regional metamorphic terrane; The Trois Seigneurs Massif, Pyrenees, France: Contributions to Mineralogy and Petrology, v. 91, p. 122-137.

Wickham, S. M. and H. P. Taylor, Jr., 1987, Stable isotope constraints on the origin and depth of penetration of hydrothermal fluids associated with Hercynian regional metamorphism and crustal anatexis in the Pyrenees: Contributions to Mineralogy and Petrology, v. 95, p. 255-268.

Wood, B. J., 1983, Petrological constraints on the constitution of the lower crust: Geological Society of America Abstracts with Programs, v. 15, p. 722.

Zingg, A., 1980, Regional metamorphism in the Ivrea Zone (Southern Alps, N-Italy): Field and microscopic Investigations: Schweizerishe Mineralogische und Petrographische Mitteilungen, v. 60, p. 153-179.

Zingg, A., 1983, The Ivrea and Strona-Ceneri Zones (Southern Alps, Ticino and N-Italy) - A review: Schweizerishe Mineralogische und Petrographische Mitteilungen, v. 63, p. 361-392.

Zingg, A., 1990, The Ivrea crustal cross-section (northern Italy and southern Switzerland) in Salisbury, M. H. and D. M. Fountain, ed., Exposed Cross-Sections of the Continental Crust: Netherlands, Kluwer Academic Publishers, p. 1-20.

Zingg, A., M. R. Handy, J. C. Hunziker and S. M. Schmid, 1990, Tectonometamorphic history of the Ivrea Zone and its relationship to the crustal evolution of the Southern Alps: Tectonophysics, v. 182, p. 169-192.

Zingg, A. and J. C. Hunziker, 1981, Thermal evolution of the high-grade metamorphism in the Ivrea Zone: Terra Cognita spec. issue abs., v. 59, p. 91.

Zingg, A. and J. C. Hunziker, 1982, The Ivrea Zone, an example of the evolution of deep continental crust: Terra Cognita, v. 2, n. 3, p. 236-237.

Zingg, A. and R. Schmid, 1979, Multidisciplinary research on the Ivrea Zone: Schweizerishe Mineralogische und Petrographische Mitteilungen, v. 59, p. 189-197.

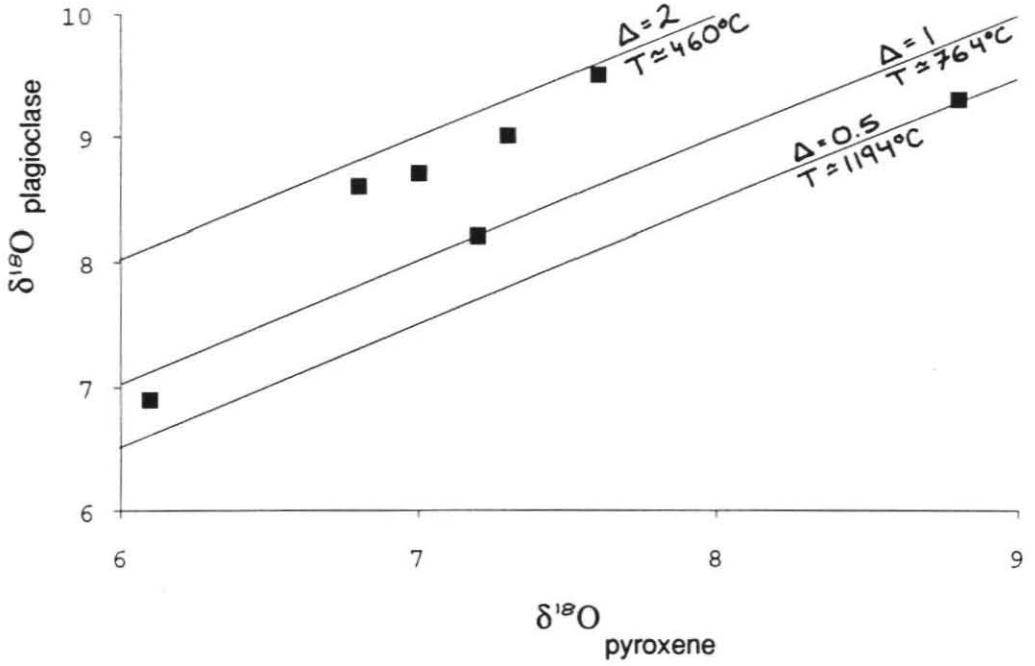

Figure 5.1: $\delta^{18}O$ for coexisting plagioclase and pyroxene.

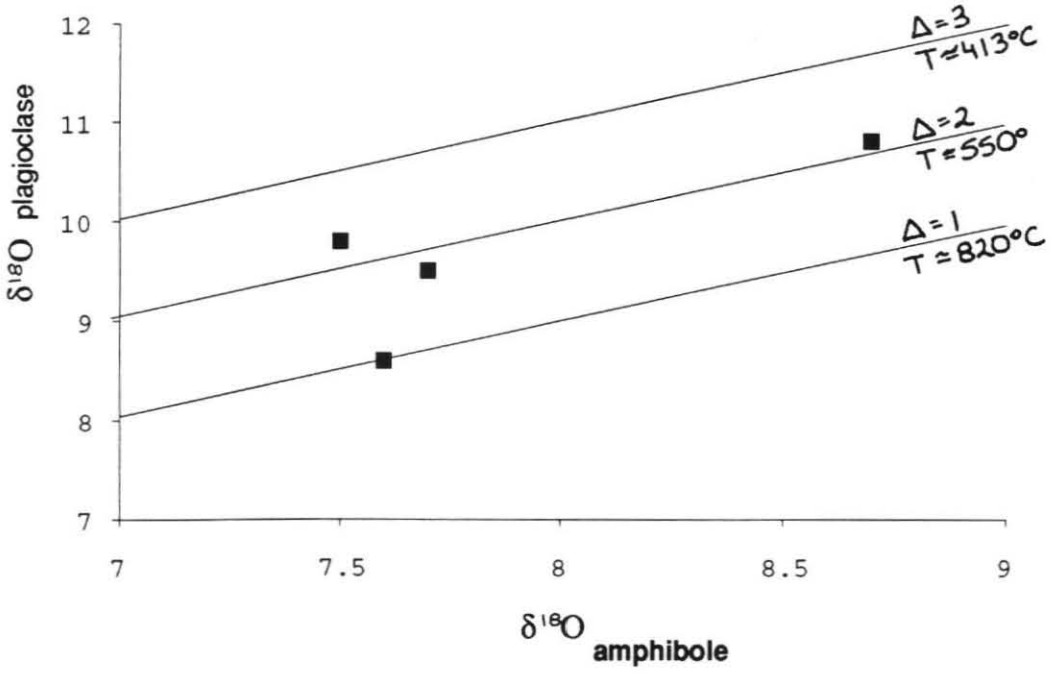

Figure 5.2: $\delta^{18}O$ for coexisting plagioclase and amphibole. Calibration for plagioclase-amphibole fractionation not accurate above 800°C.

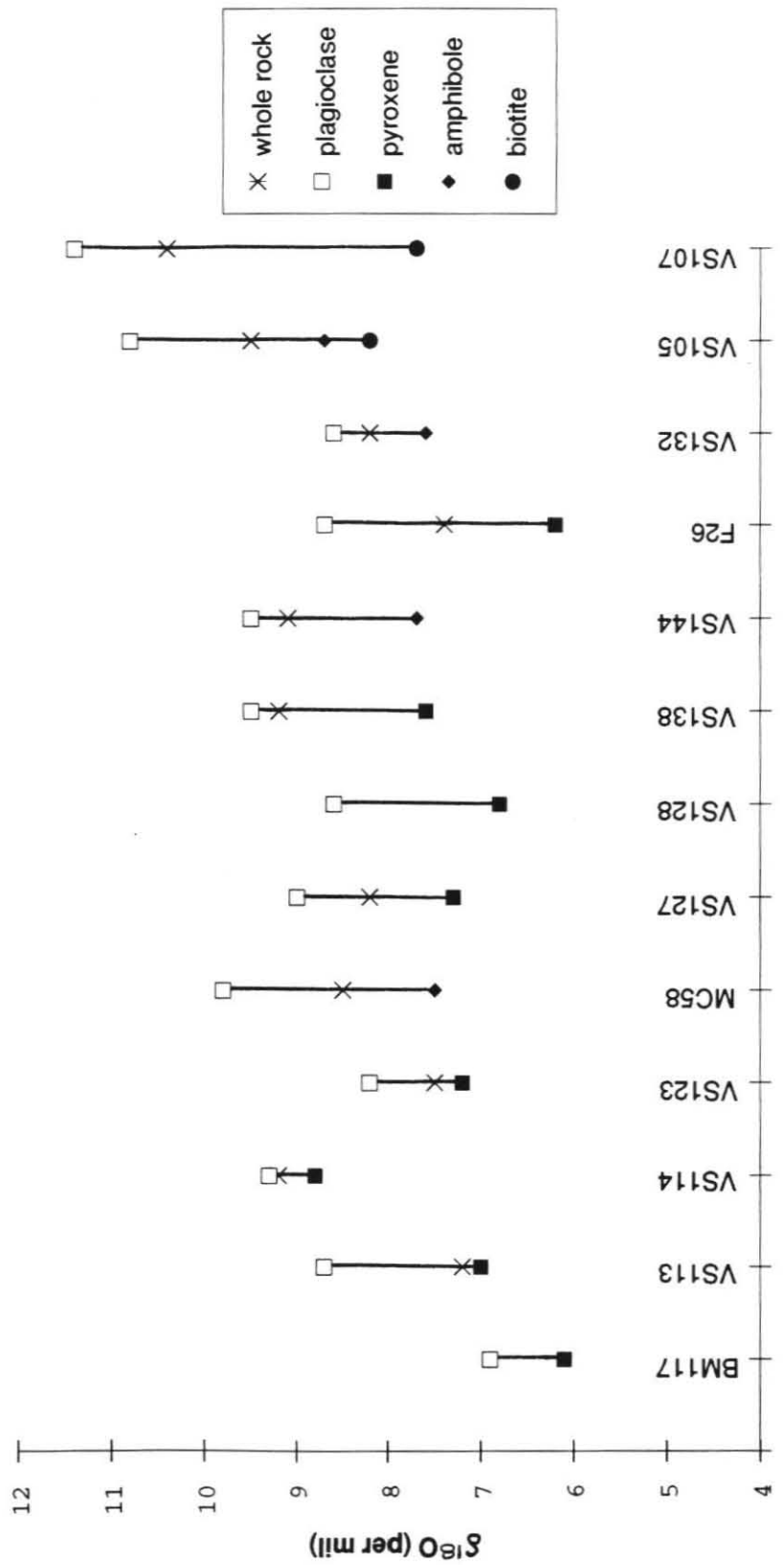

Figure 5.3: Variation of oxygen isotopic composition of mineral and whole rock samples with stratigraphic height within the Mafic Complex

Figure 5.4: Variation of mineral pair temperature with stratigraphic position within the Mafic Complex

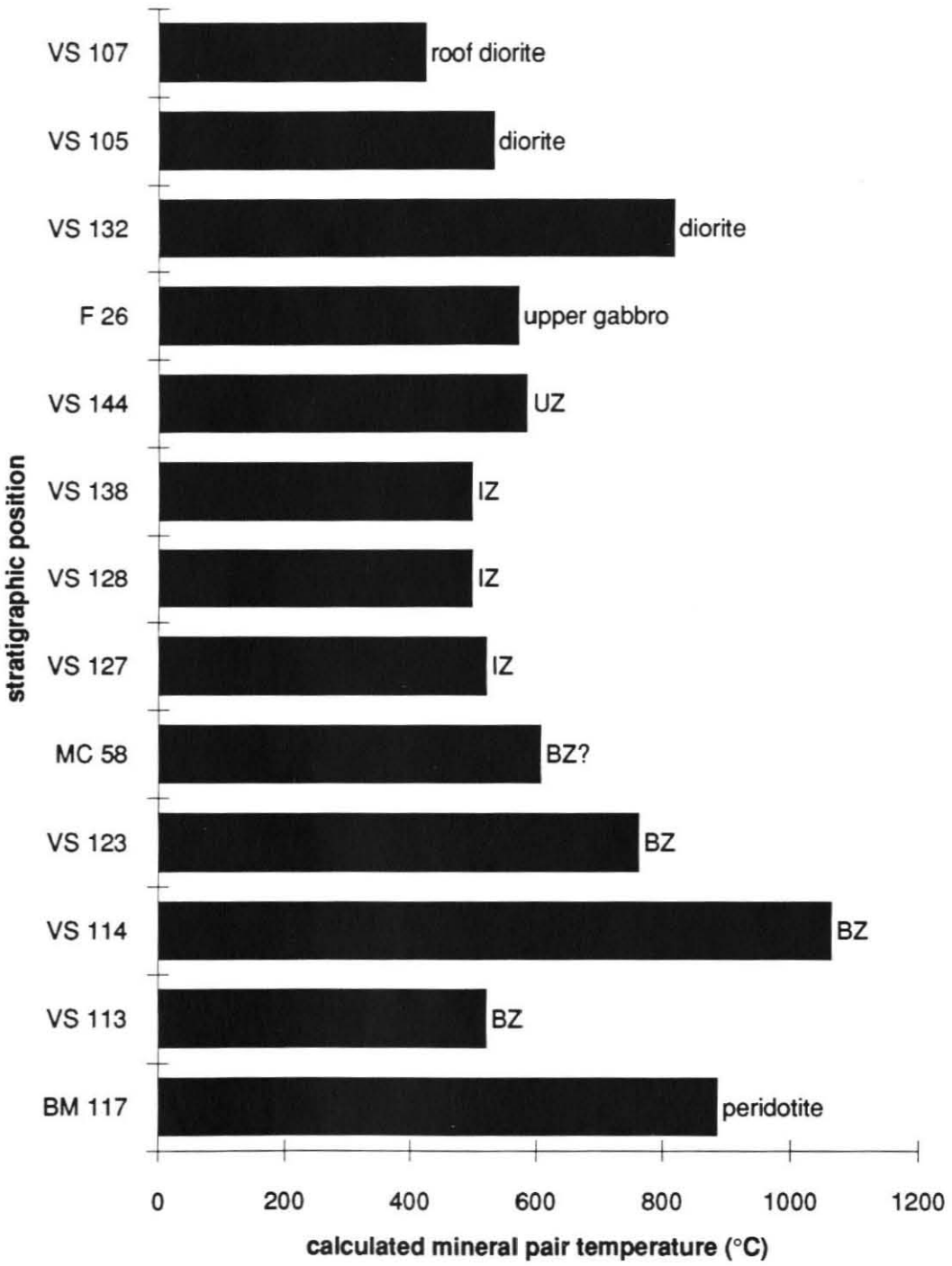

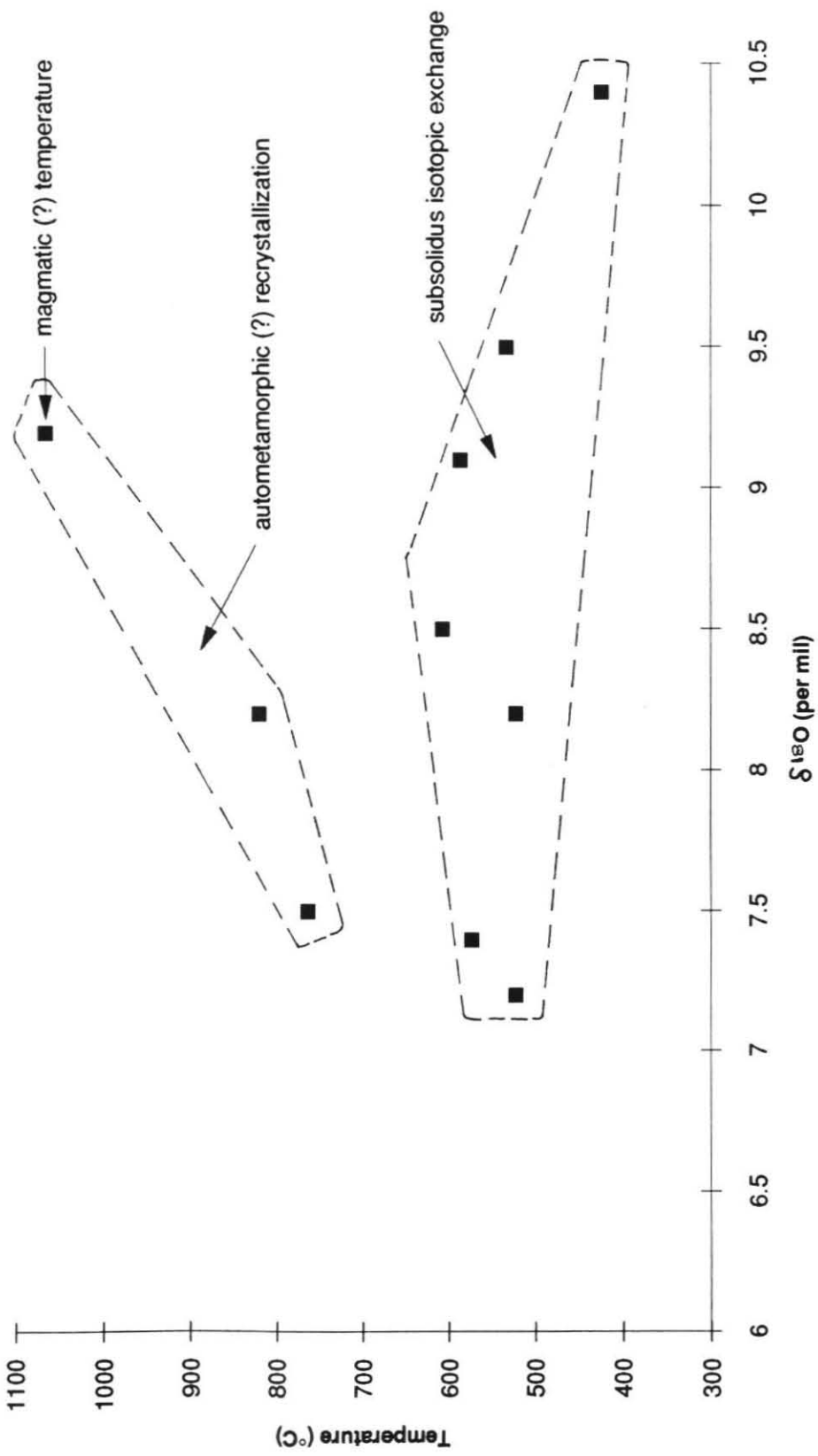

Figure 5.5: Whole rock $\delta^{18}O$ vs. calculated mineral pair temperature

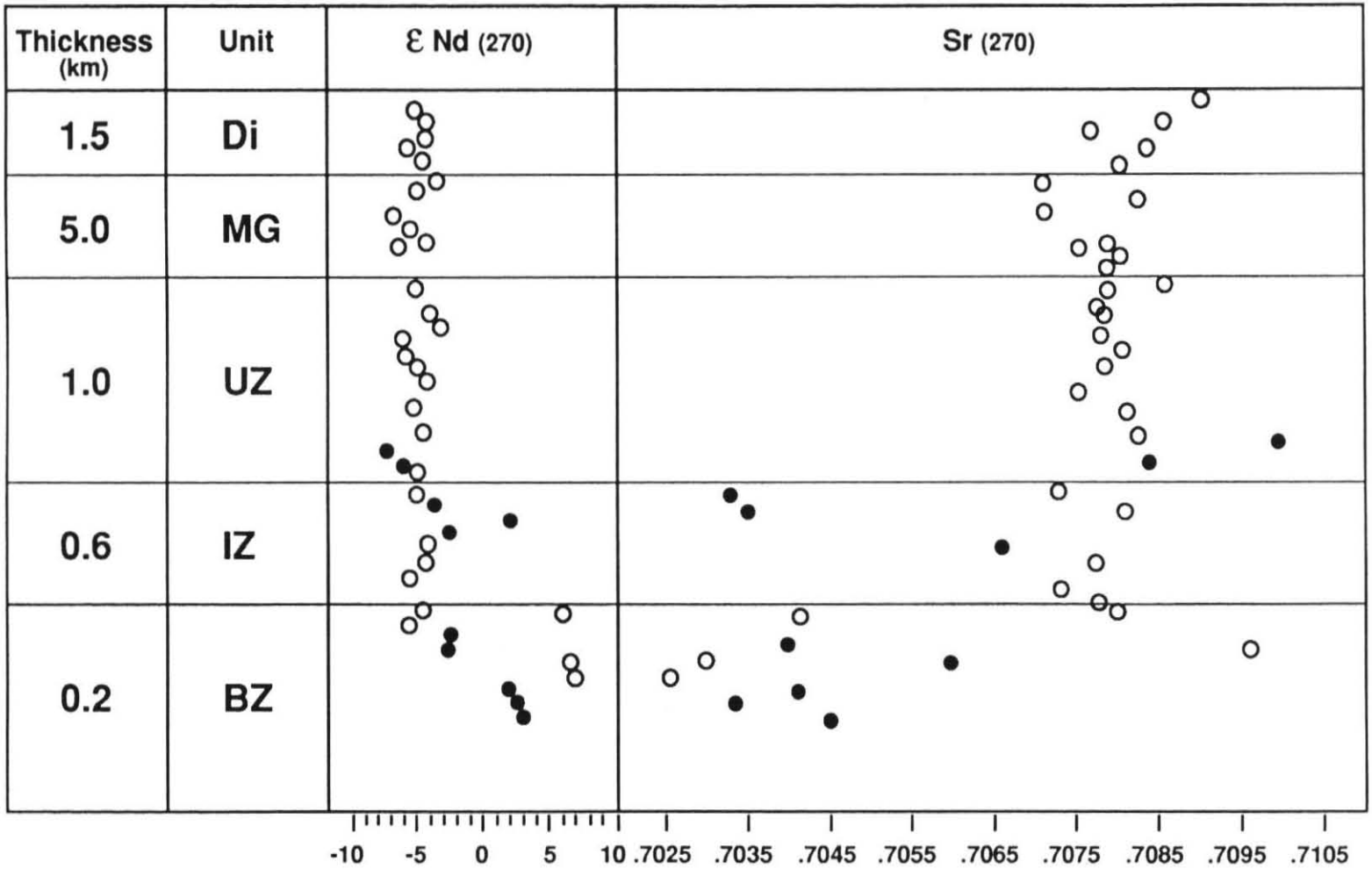

Figure 5.6: Stratigraphic variation of εNd (270) and Sr (270) within the Mafic Complex of the Ivrea Zone (after Voshage et al., 1990); o = peridotites and pyroxenites; ● = gabbros and diorites.

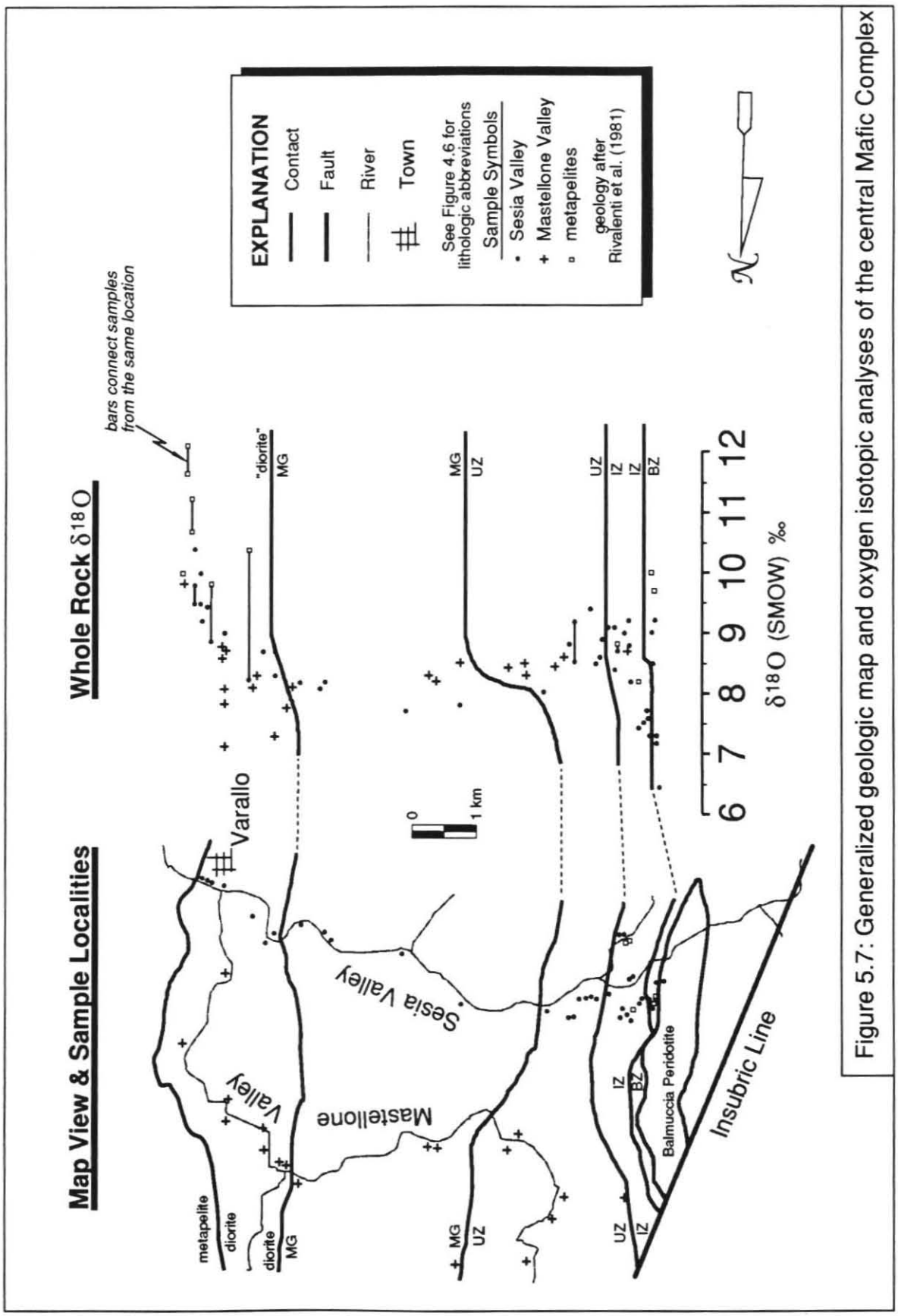

Figure 5.7: Generalized geologic map and oxygen isotopic analyses of the central Mafic Complex

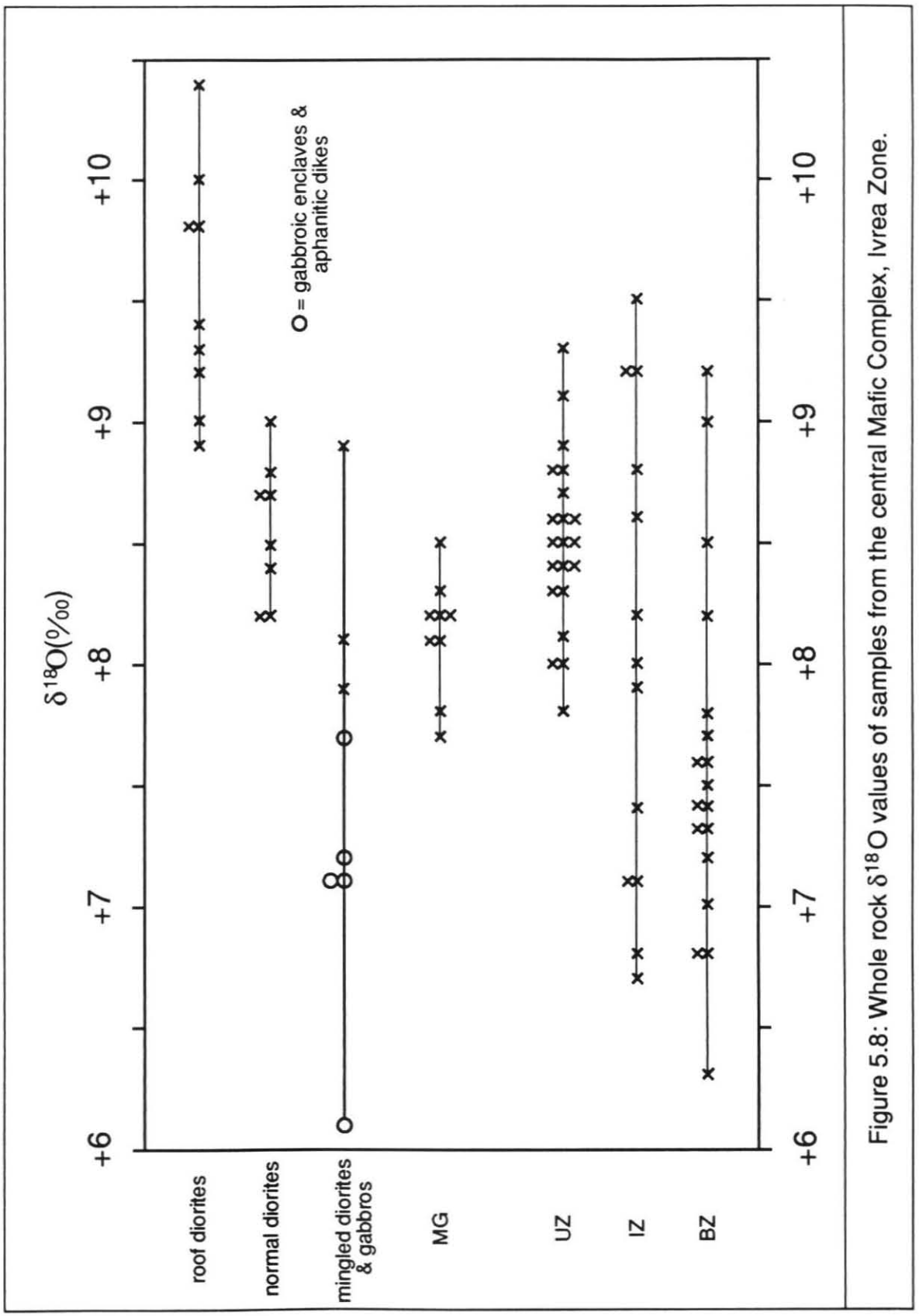

Figure 5.8: Whole rock $\delta^{18}O$ values of samples from the central Mafic Complex, Ivrea Zone.

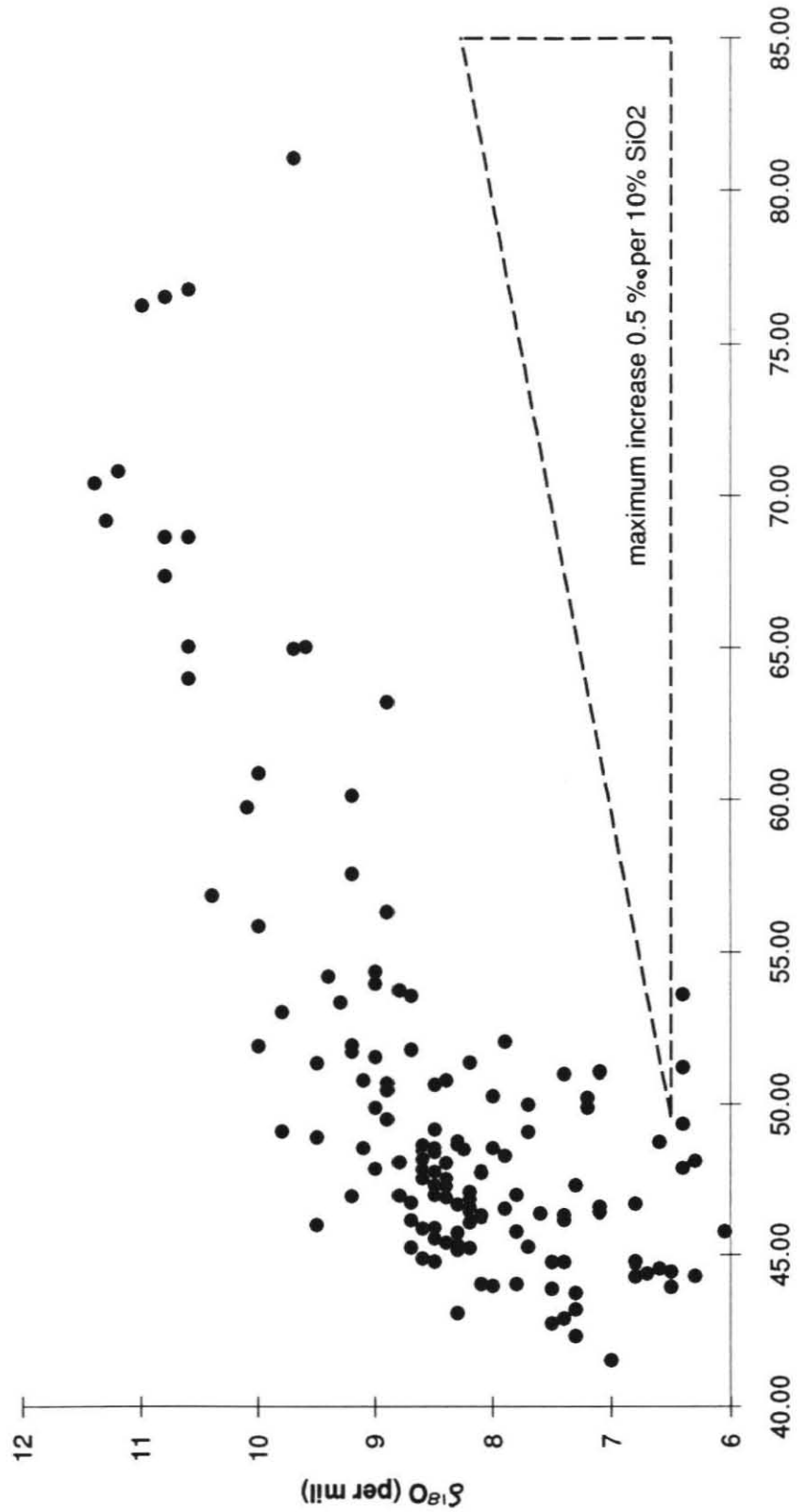

Figure 5.9: SiO2 vs.$\delta^{18}O$ for the Mafic Complex, Ivrea Zone. Triangular field encloses area attainable by simple fractional crystallization of a hypothetical parental magma having a $\delta^{18}O$ = +6.5‰.

Figure 5.10: Reproduction of Figure 4 from Voshage et al., 1990. "Initial (270 Ma) Nd and Sr isotopic compositions and mixing curves between mantle and crustal components. The rectangle represents the standard deviation of 10 representative metasediments from the Strona Valley .... The curves A to D represent mixing models between a primary basaltic melt (120 p.p.m. Sr, 8 p.p.m. Nd) and either an anatectic granitic melt (80 p.p.m. Sr, 35 p.p.m. Nd) as modelled by Schnetger (1988) or bulk metapelitic crust (220 p.p.m. Sr, 40 p.p.m. Nd). A, bulk-mixing basalt-granitic melt; B, bulk-mixing basalt-average metasediment; C, AFC-mixing basalt-granitic melt; D, AFC-mixing basalt-average metasediment. A ratio of assimilation to crystallization rates, r = 0.6, is used in both AFC calculations. The fractionating assemblage consists of 10% olivine, 30% orthopyroxene, 30% clinopyroxene and 30% plagioclase, resulting in bulk $K_d(Nd) = 0.087$ and $K_d(Sr) = 0.558$. An alternative fractionating assemblage (20% ol, 30% opx, 40% cpx, 10% plag) yields trajectories in the envelope of the curves shown. Even doubling Sr partitioning to $K_d = 1.1$ increases the $^{87}Sr/^{86}Sr$ ratios only slightly."

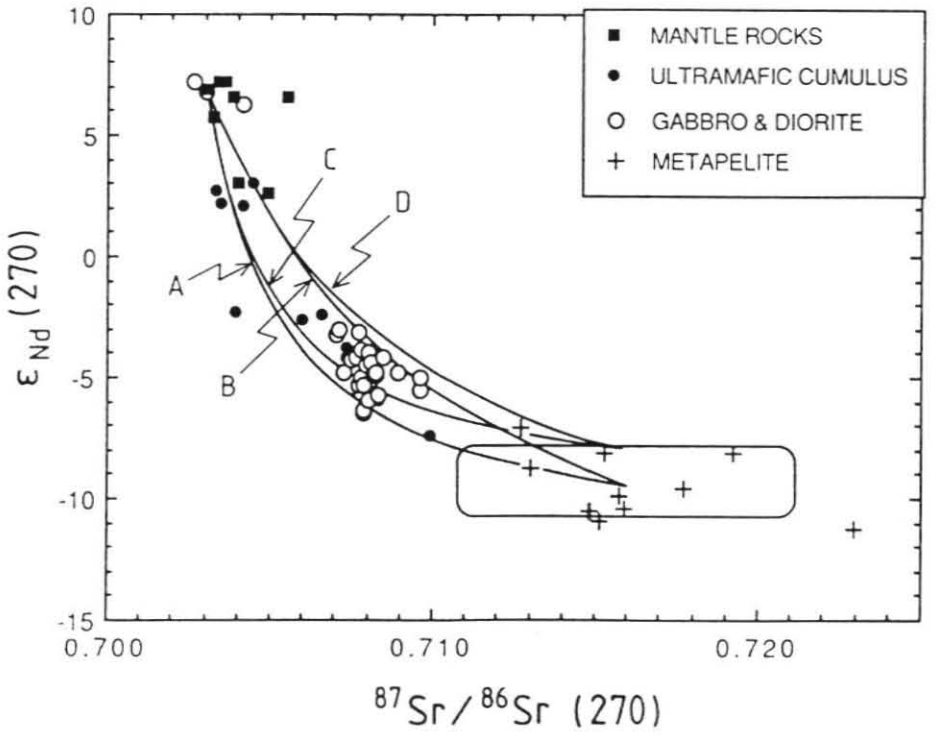

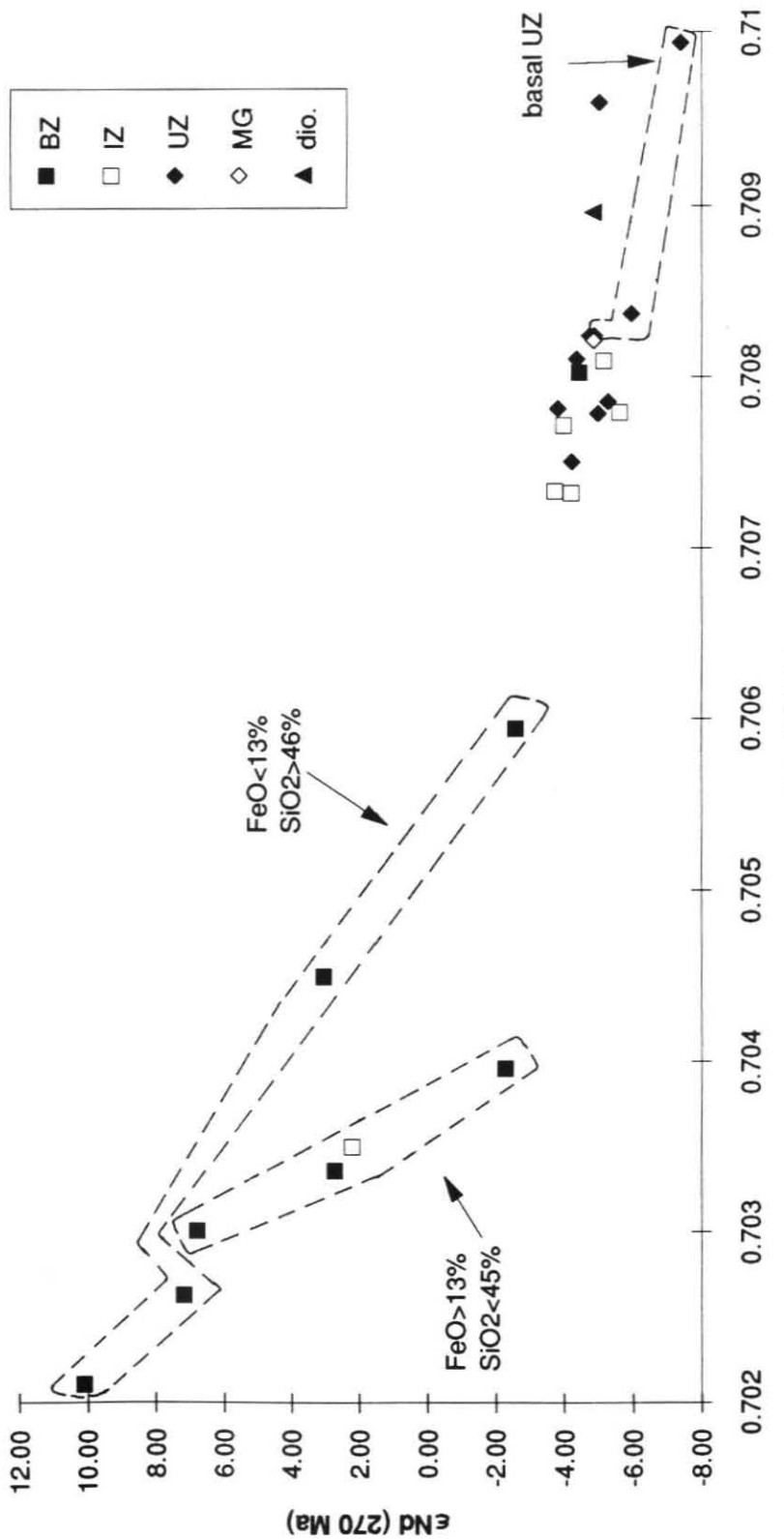

Figure 5.11: Sr_i(270) vs. εNd(270) for subset of Voshage et al. (1990) samples analyzed for $\delta^{18}O$. Dashed fields explained in text.

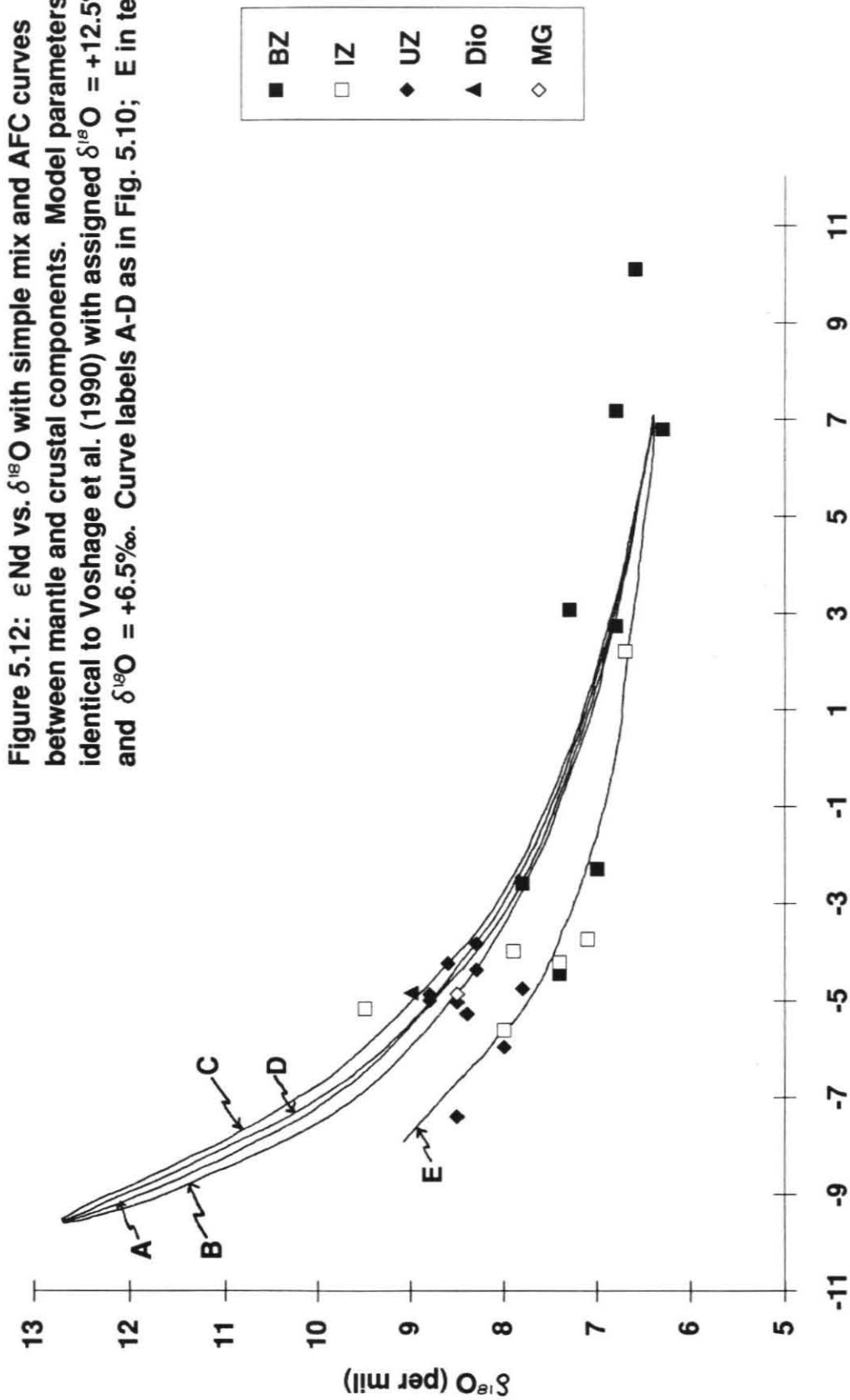

Figure 5.12: εNd vs. $\delta^{18}O$ with simple mix and AFC curves between mantle and crustal components. Model parameters identical to Voshage et al. (1990) with assigned $\delta^{18}O$ = +12.5‰ and $\delta^{18}O$ = +6.5‰. Curve labels A-D as in Fig. 5.10; E in text.

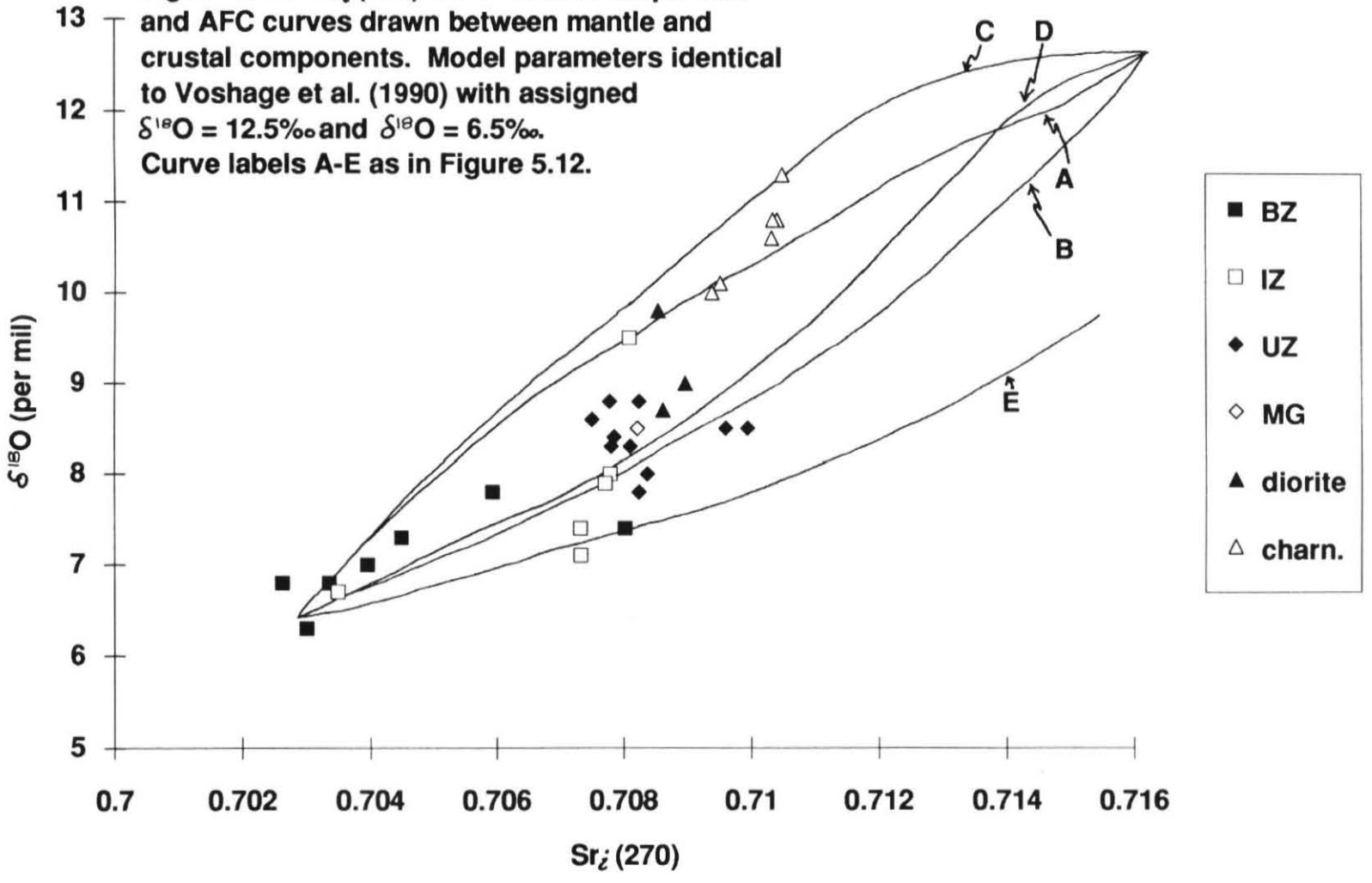
Figure 5.13: Sr_i (270) vs. $\delta^{18}O$ with simple mix and AFC curves drawn between mantle and crustal components. Model parameters identical to Voshage et al. (1990) with assigned $\delta^{18}O$ = 12.5‰ and $\delta^{18}O$ = 6.5‰. Curve labels A-E as in Figure 5.12.
13
12
11
10
9
8
7
6
5
$\delta^{18}O$ (per mil)
0.7
0.702
0.704
0.706
0.708
0.71
0.712
0.714
0.716
Sr_i (270)
A
B
C
D
E
BZ
IZ
UZ
MG
diorite
charn.

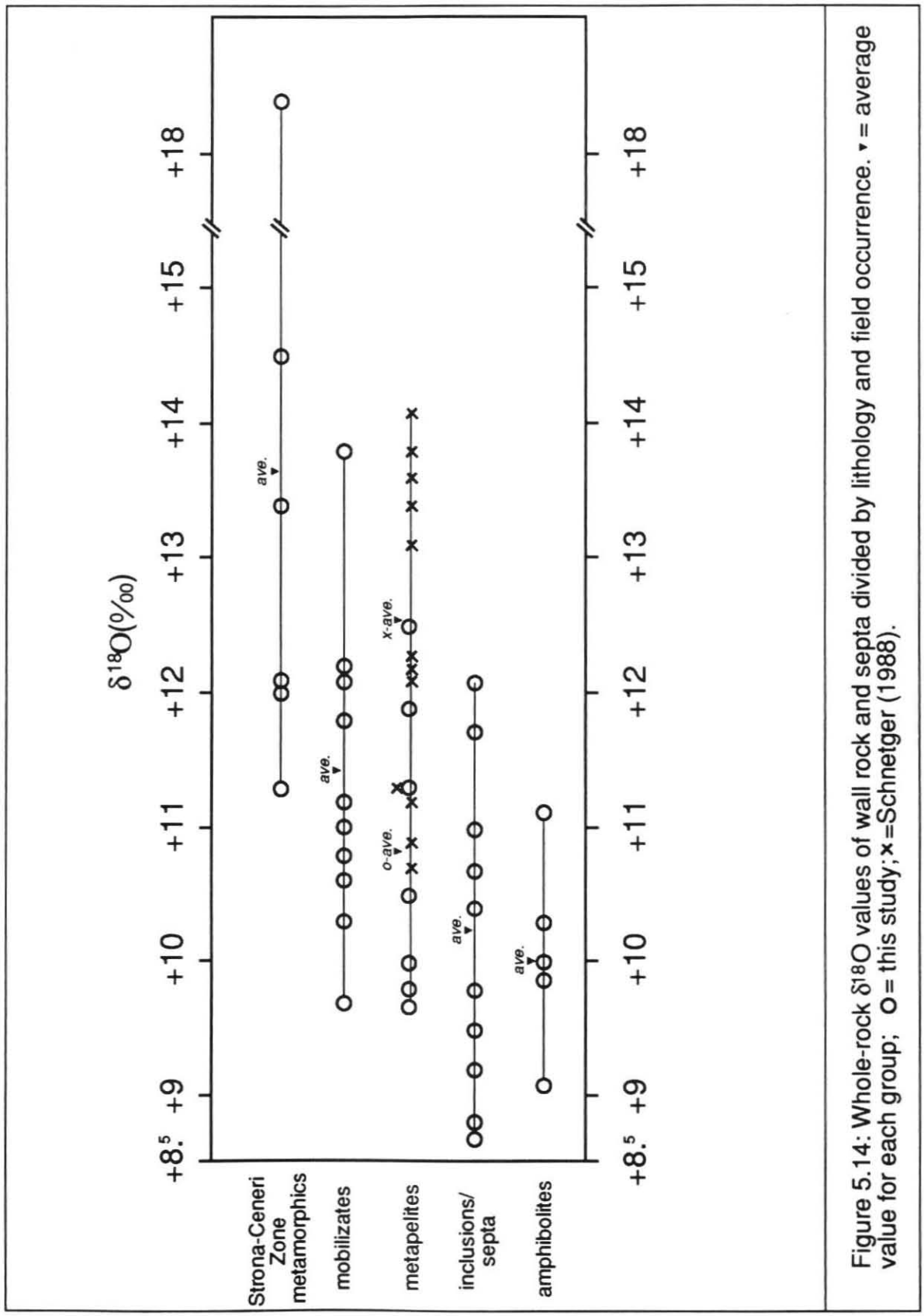

Figure 5.14: Whole-rock $\delta^{18}O$ values of wall rock and septa divided by lithology and field occurrence. ▾ = average value for each group; O = this study; × =Schnetger (1988).

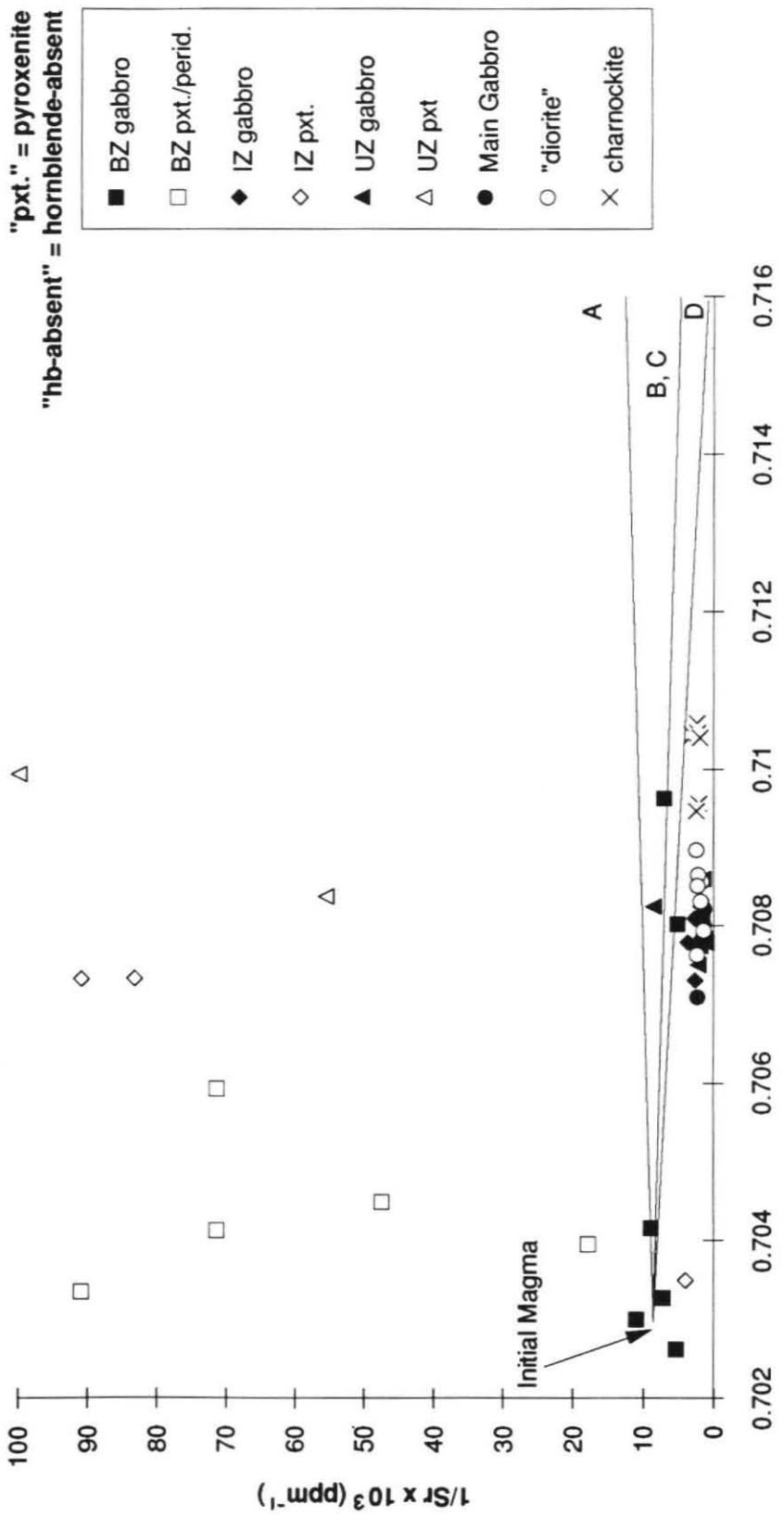

Figure 5.15: Sr_i vs. 1/Sr showing AFC and simple mixing curves. Units subdivided by lithology. Curves A-D explained in Figure 5.10.

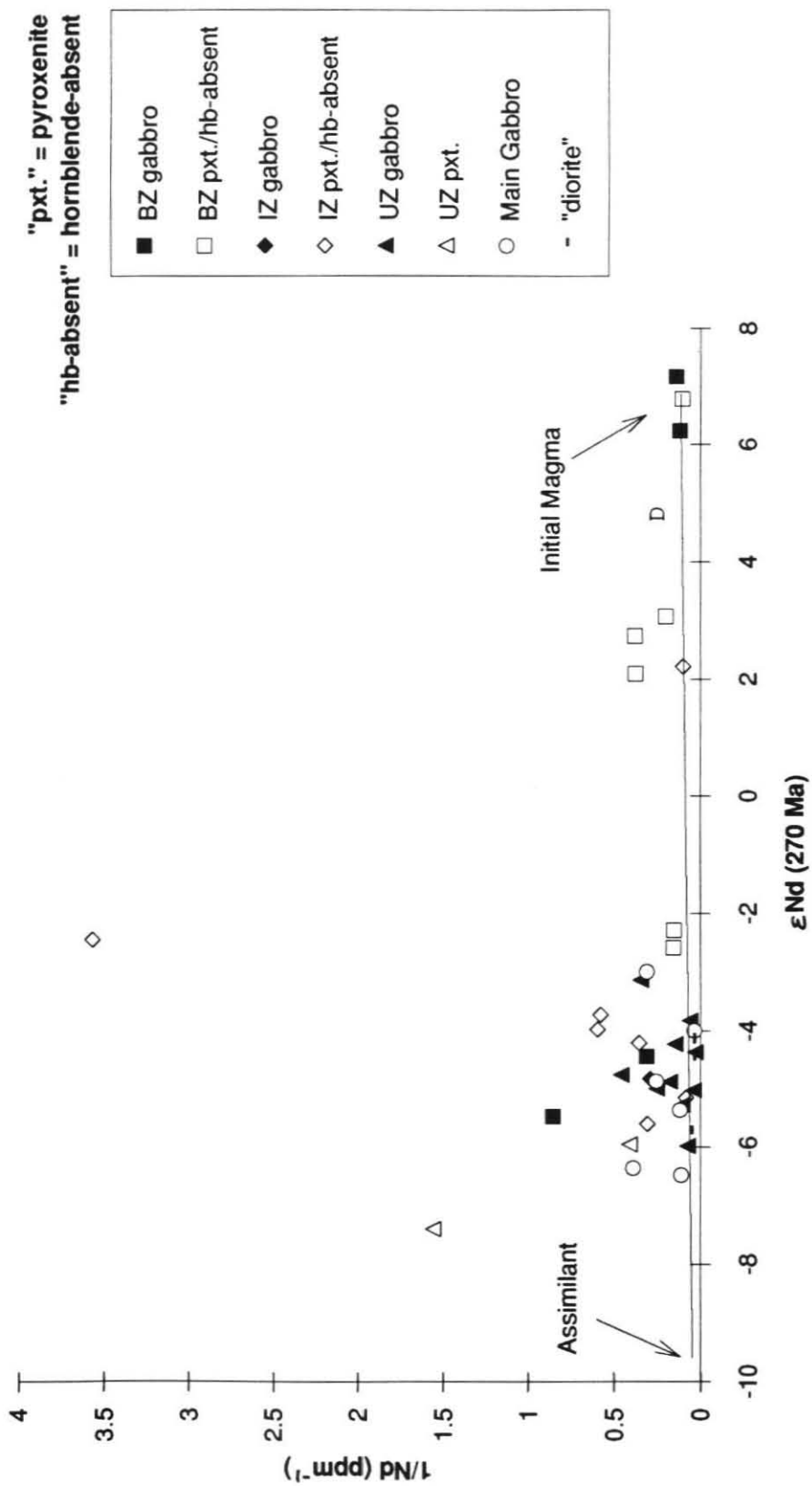

Figure 5.16: εNd vs. 1/Nd with mixing curve between mantle and crustal components. Units divided by lithology. Curve D explained in Figure 5.10.

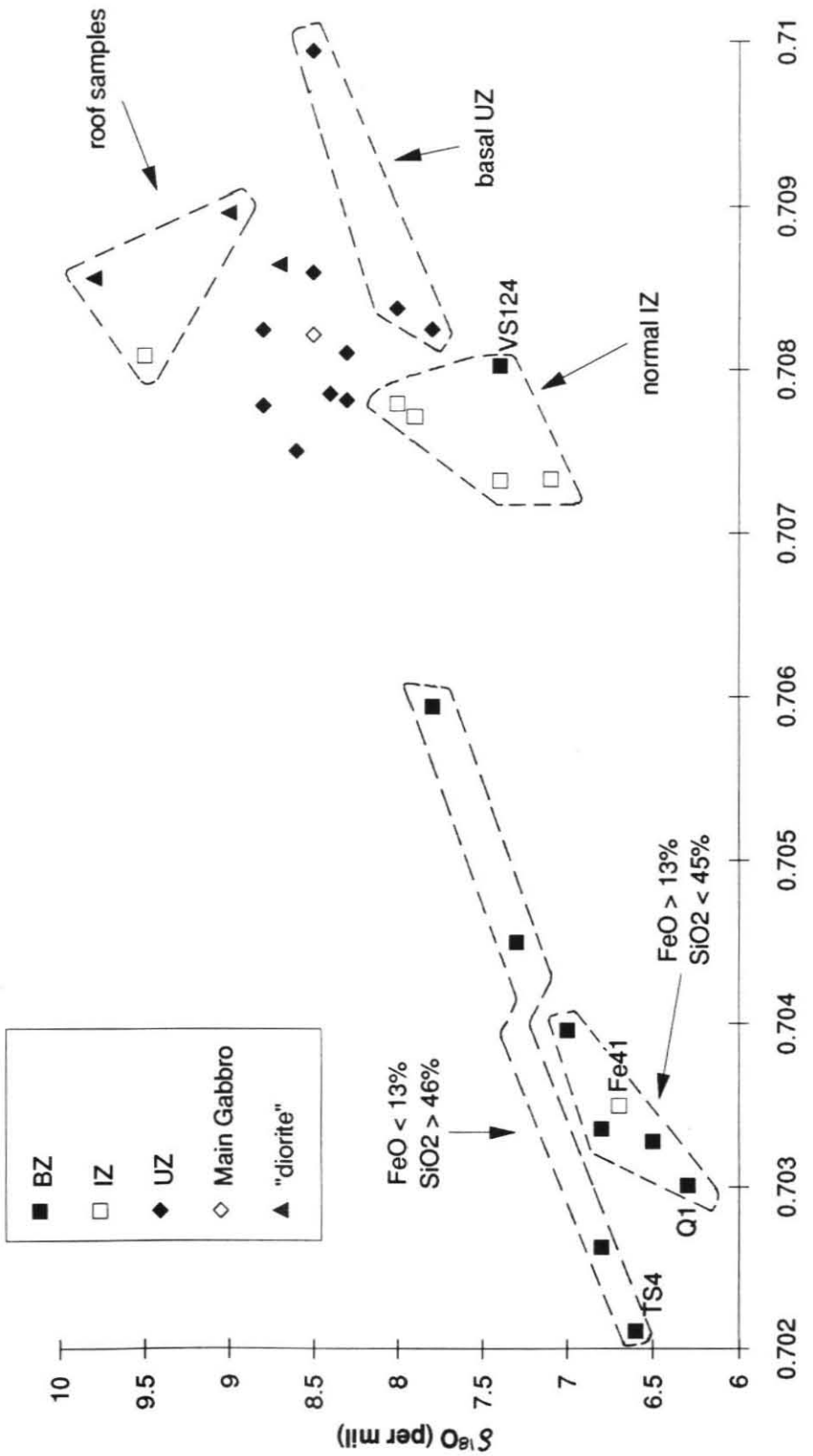

Figure 5.17: Sr_i vs. $\delta^{18}O$ for the central Mafic Complex, Ivrea Zone. Groupings and selected sample numbers explained in text.

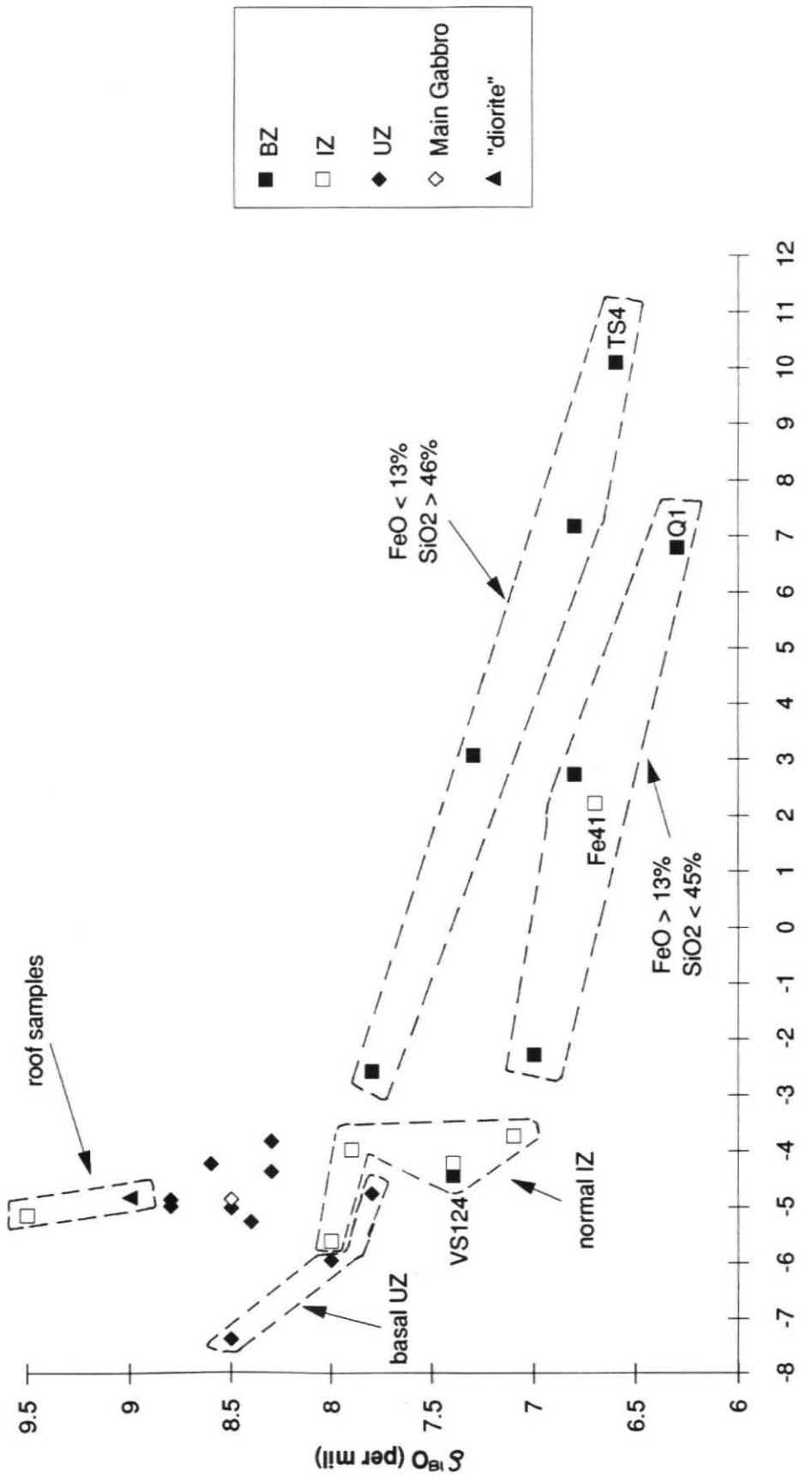

Figure 5.18: εNd vs. $\delta^{18}O$ for the central Mafic Complex, Ivrea Zone. Groupings and selected sample numbers explained in text.

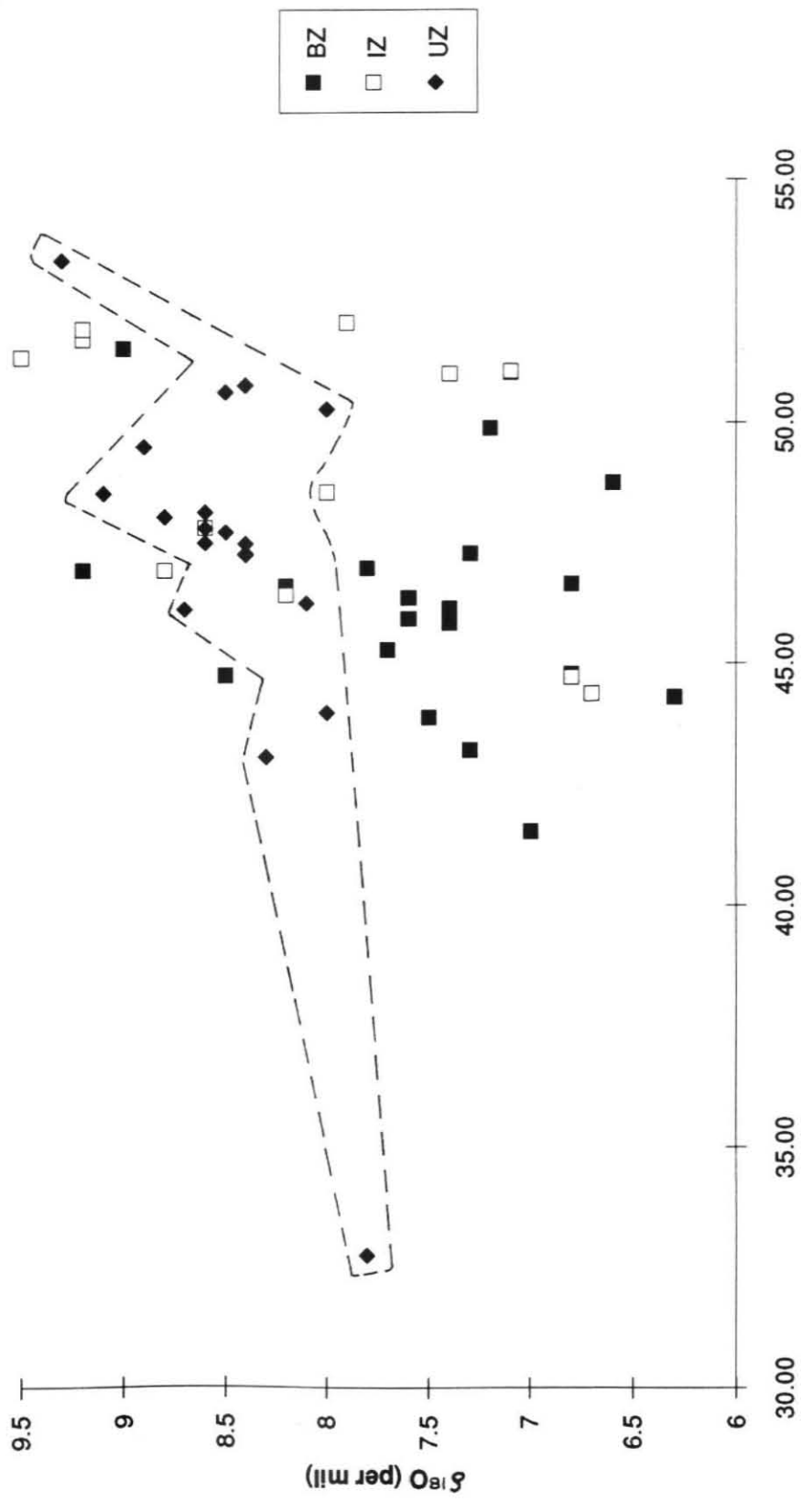

Figure 5.19: SiO2 vs.$\delta^{18}O$ for the Layered Series. Dashed field encloses the UZ samples.

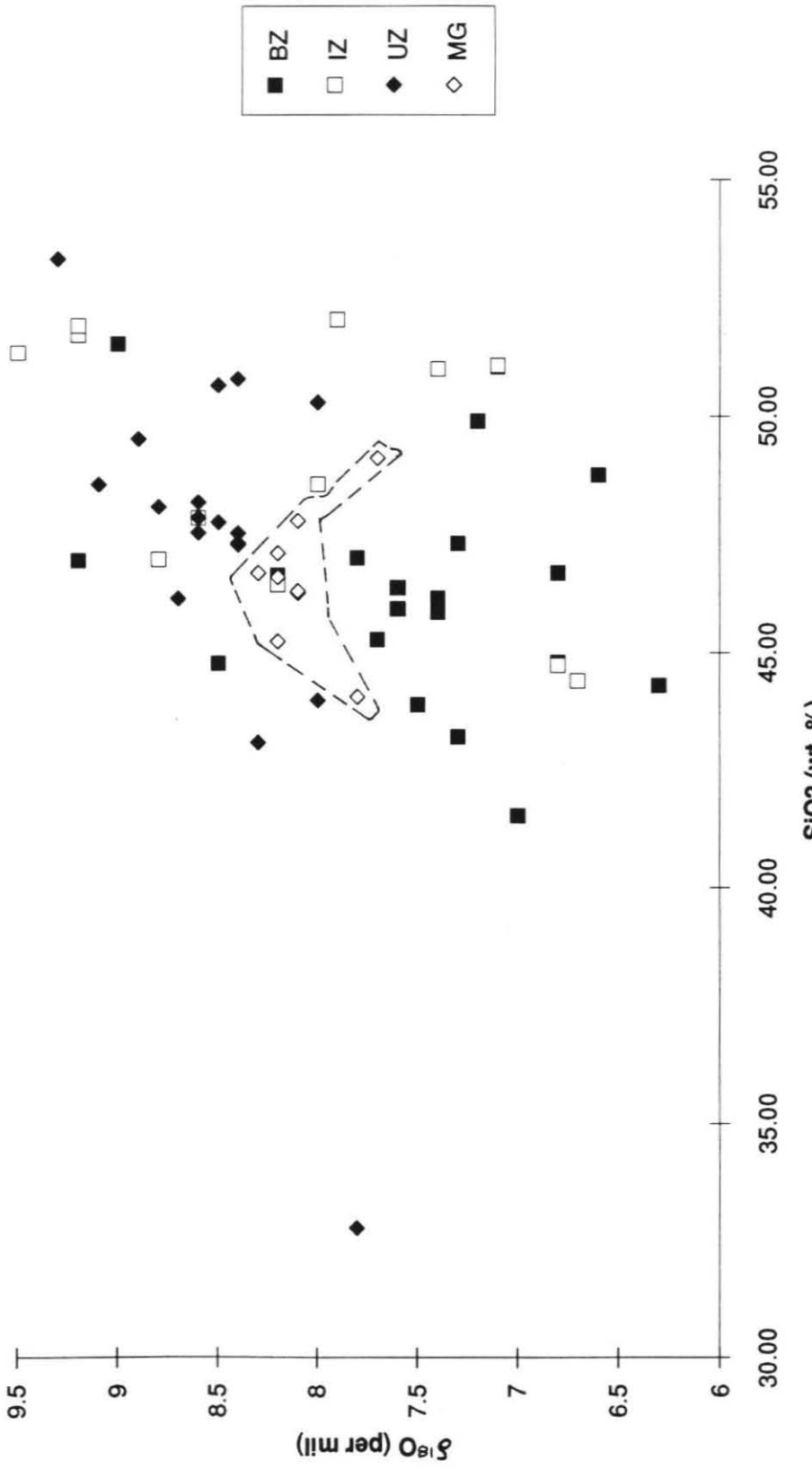

Figure 5.20: SiO2 vs. $\delta^{18}O$ for the BZ, IZ, UZ and MG. Dashed field encloses the MG samples.

Figure 5.21: SiO2 vs. $\delta^{18}O$ for UZ, MG and diorite samples with arrow showing maximum increase in ^{18}O attributable to fractional crystallization. Dashed field encloses normal diorites.

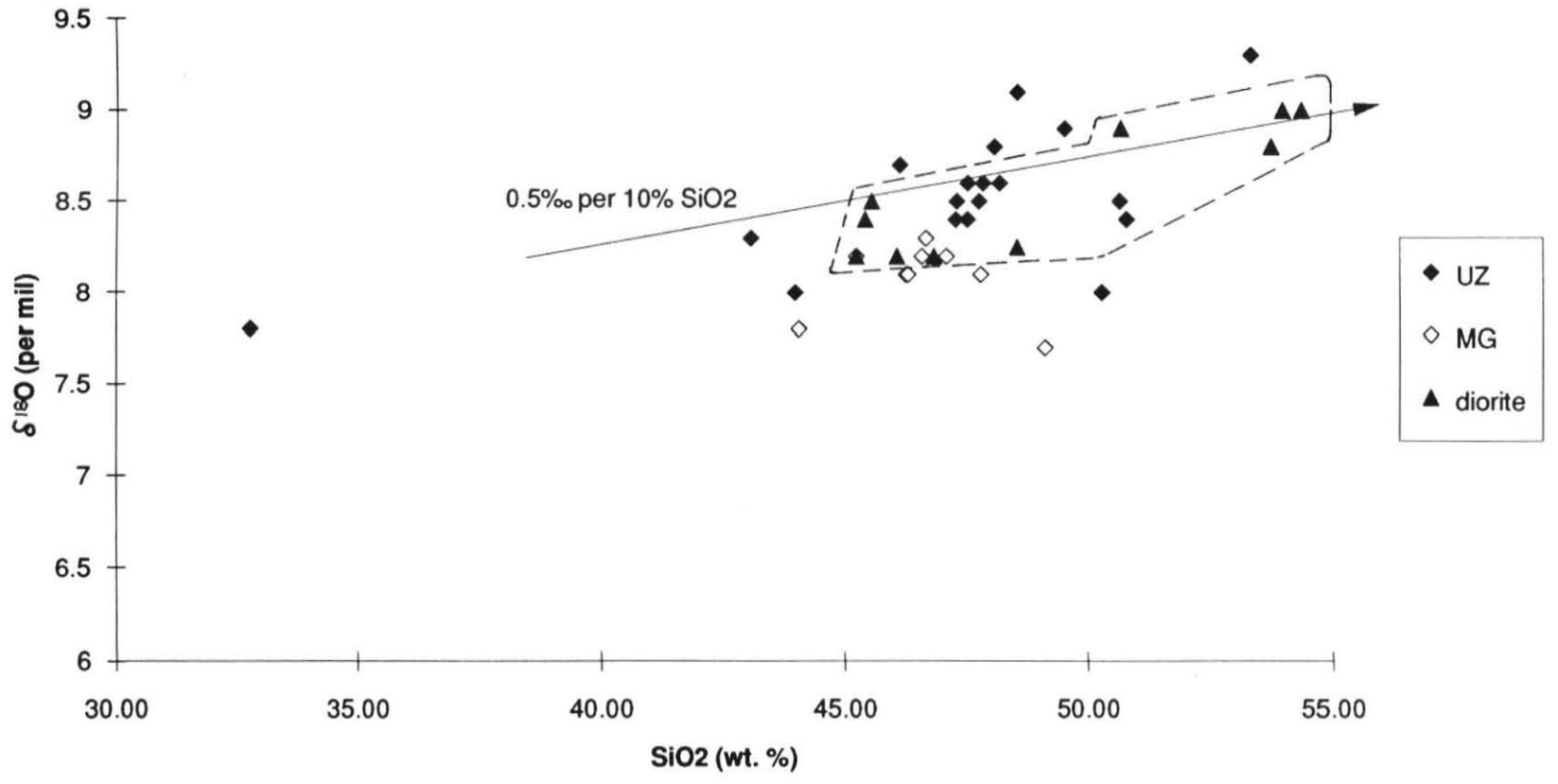

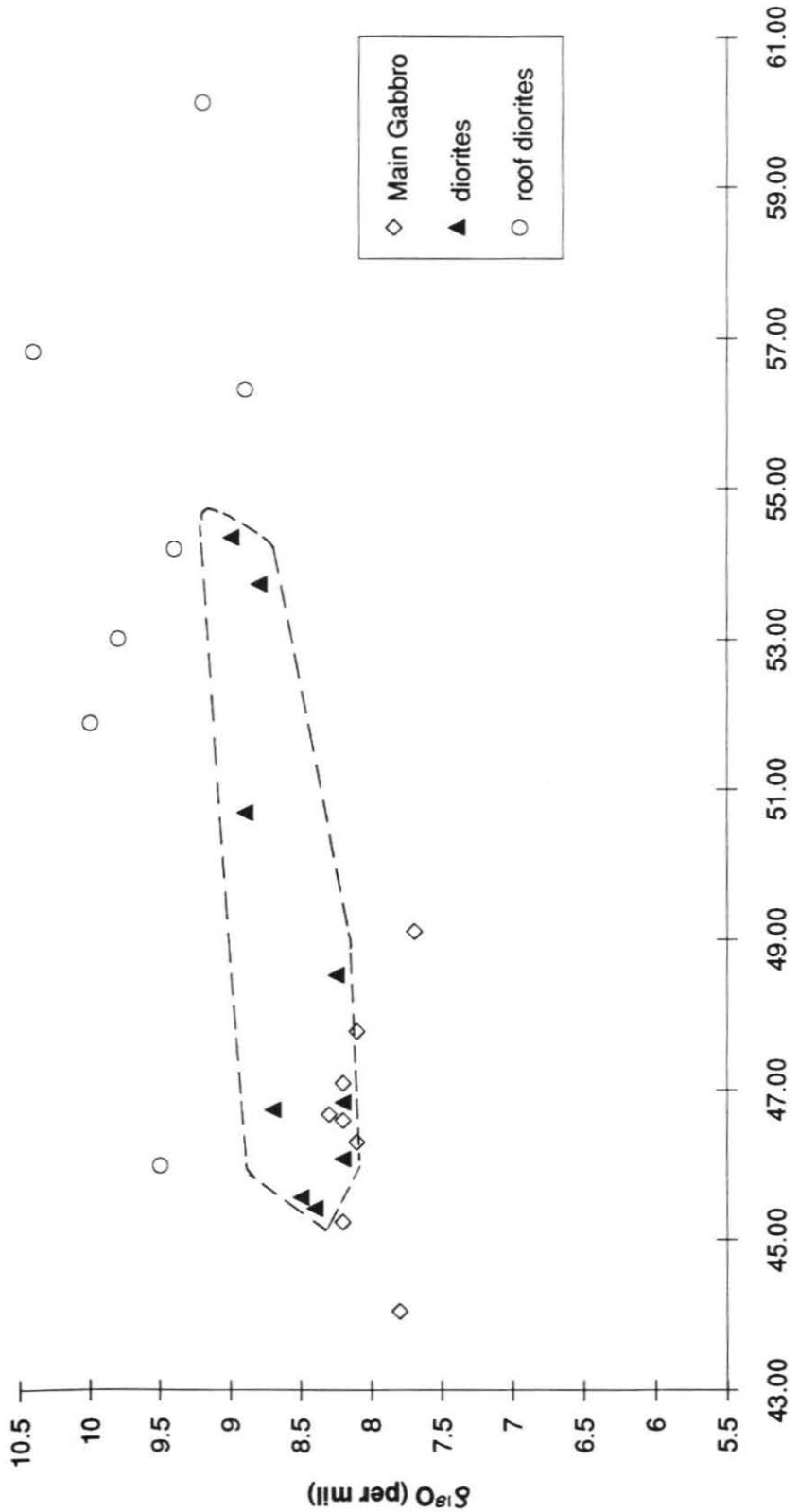

Figure 5.22: SiO2 vs. $\delta^{18}O$ contrasting normal diorites to roof diorites. Dashed field encloses normal diorites.

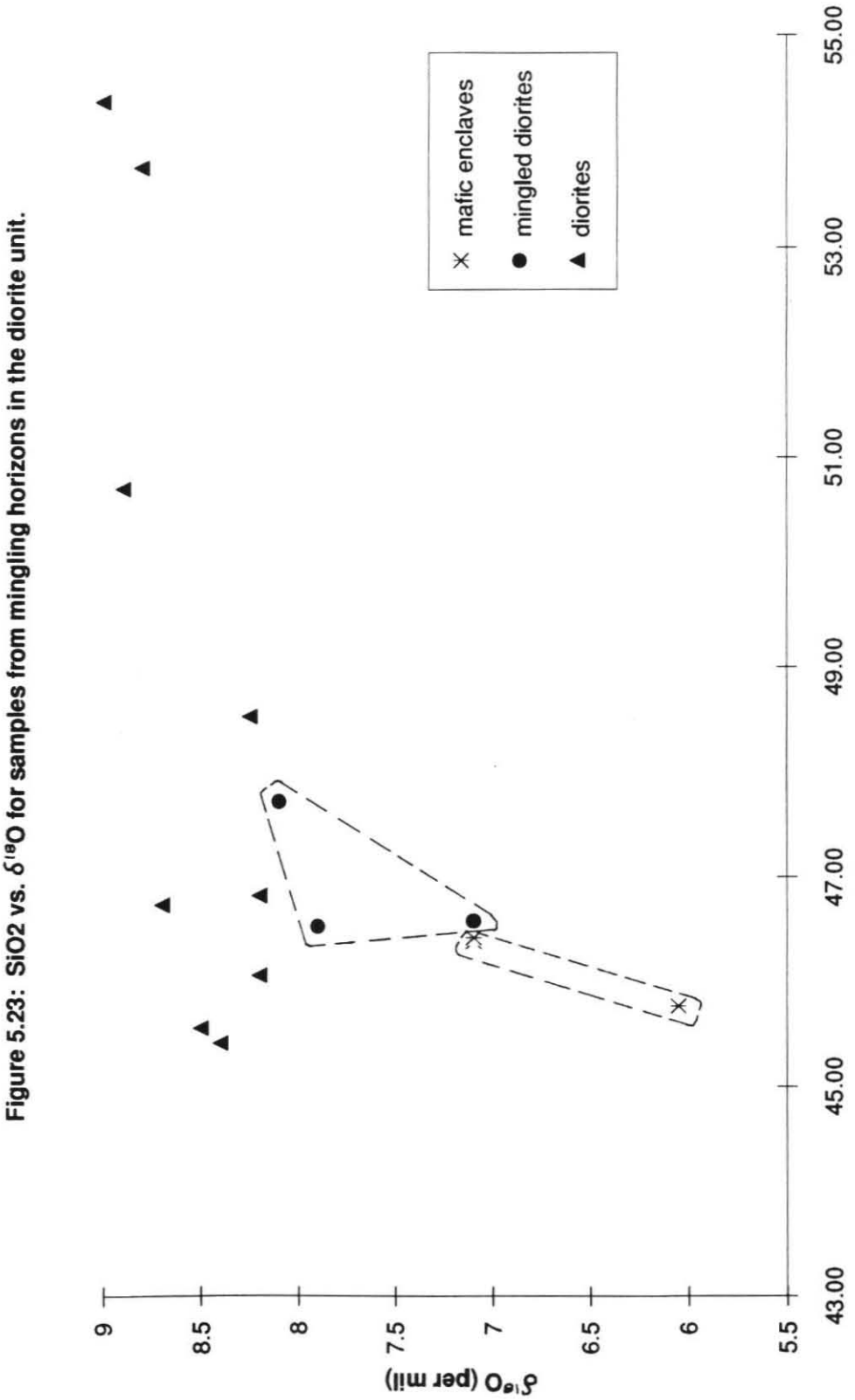

Figure 5.23: SiO2 vs. $\delta^{18}O$ for samples from mingling horizons in the diorite unit.

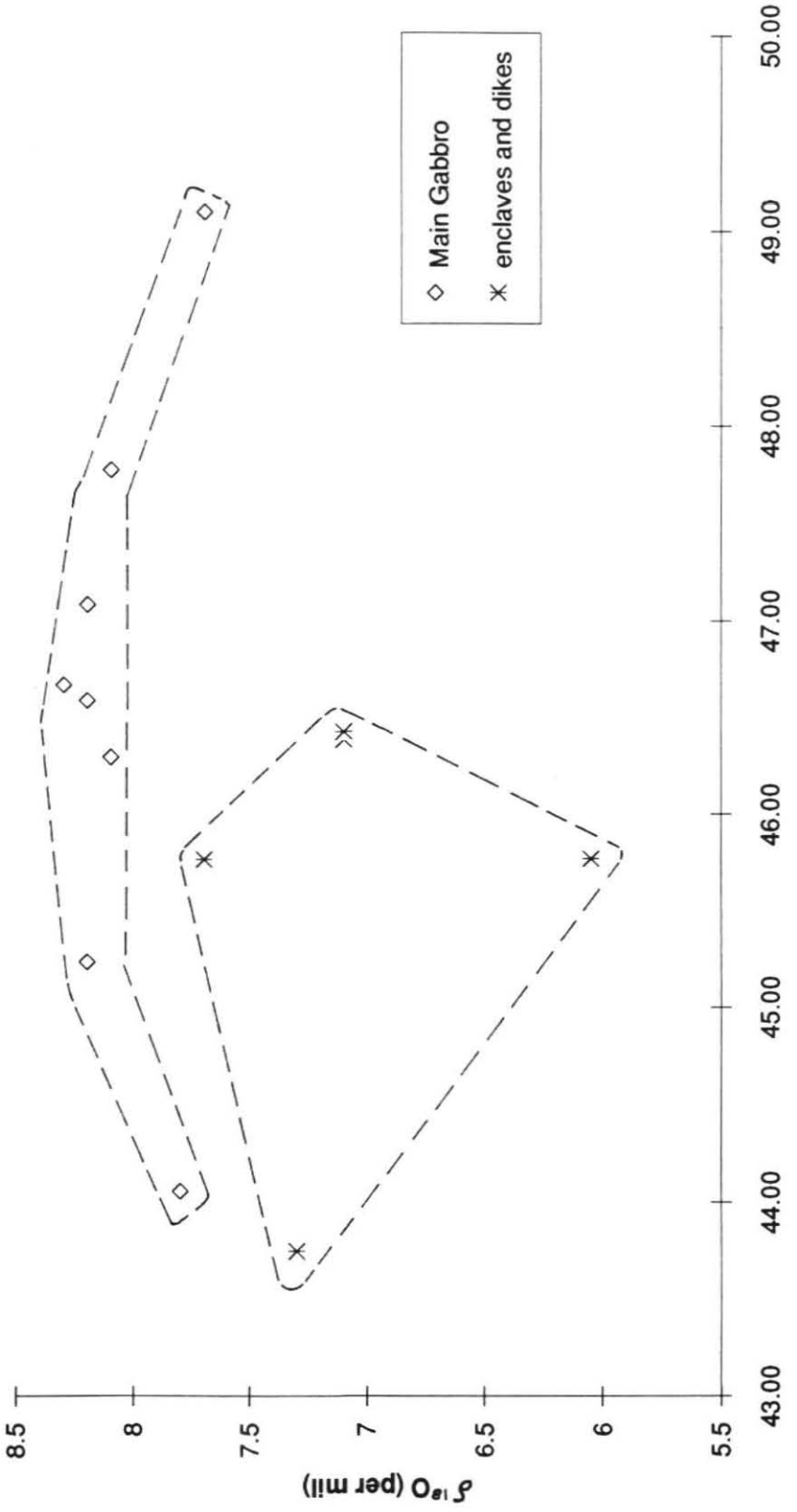

Figure 5.24: SiO2 vs. $\delta^{18}O$ for the MG compared to aphanitic dikes and enclaves found within the diorite unit.

Figure 5.25: SiO2 vs. $\delta^{18}O$ for samples from the Finero Complex, Ivrea Zone.

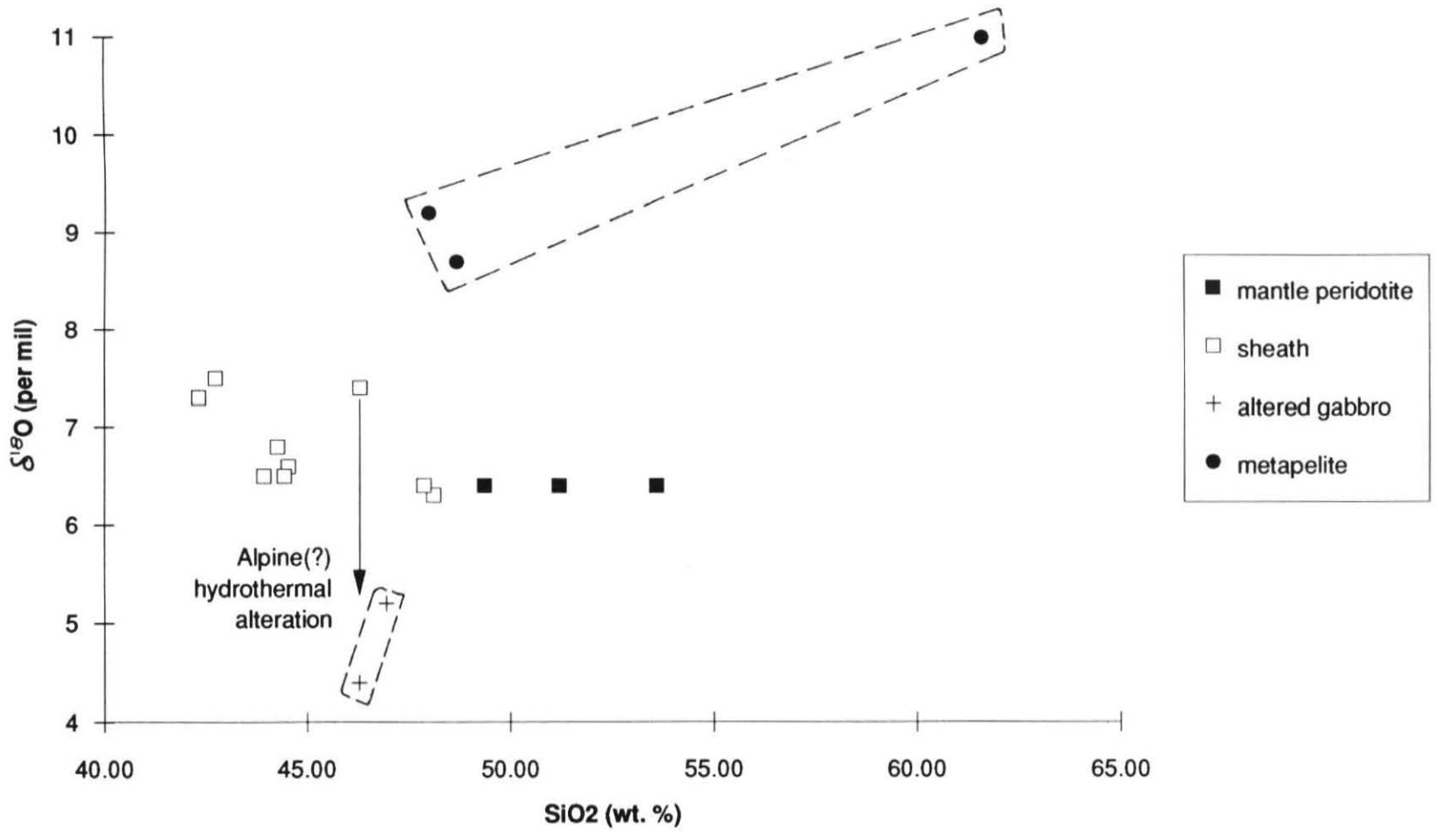

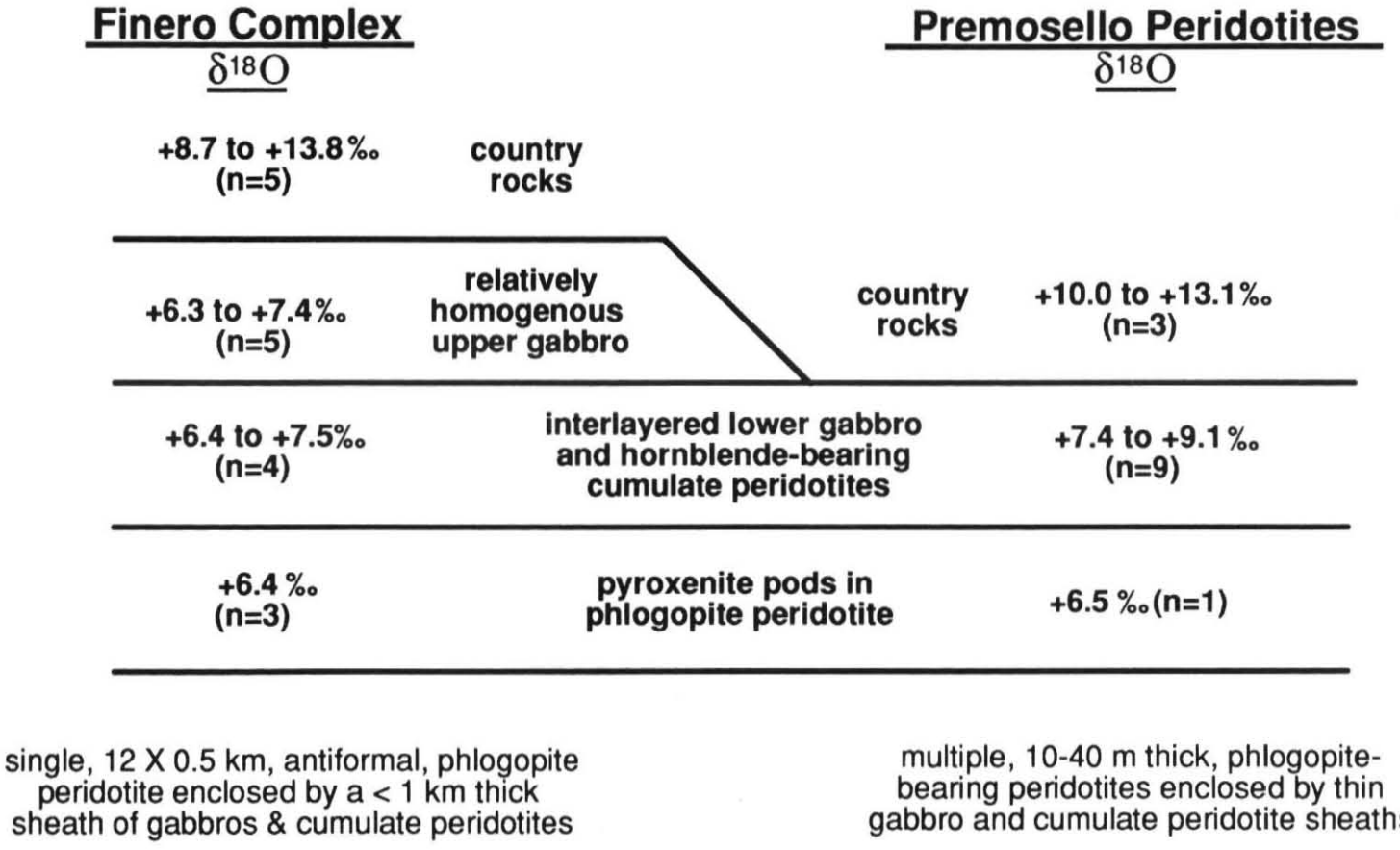

Figure 5.26: Stratigraphic comparison of $\delta^{18}O$ from the Finero and Premosello peridotite complexes; no vertical scale.

Figure 5.27: SiO2 vs. $\delta^{18}O$ for samples from the Monte Capio Sill. Samples differentiated by position relative to the central peridotite and lithology. See section 5.2.6.2 for further explanation.

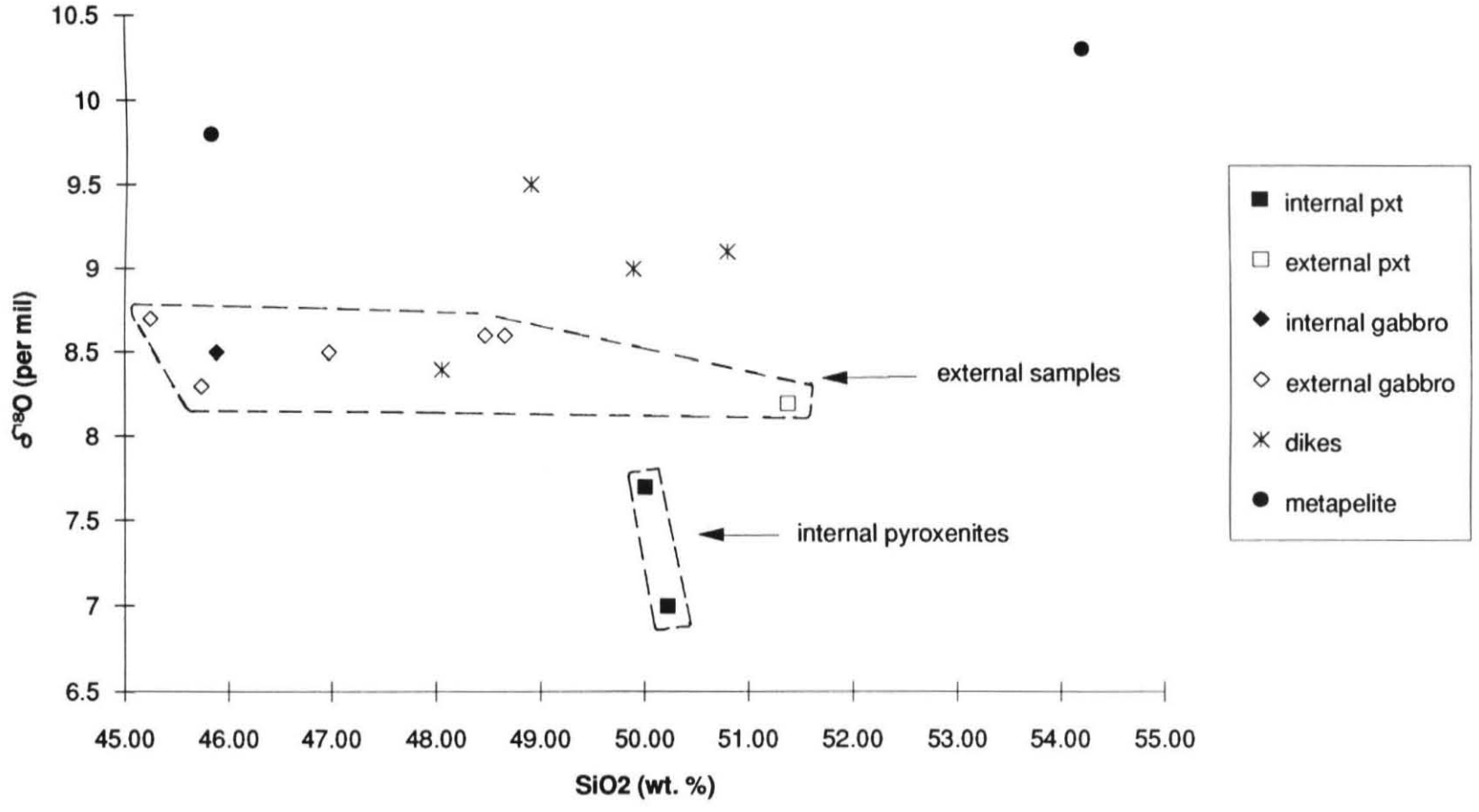

Figure 5.28: SiO2 vs. $\delta^{18}O$ for gabbros, diorites and charnockites from the southern Ivrea Zone. Arrow connects enclave to host charnockite.

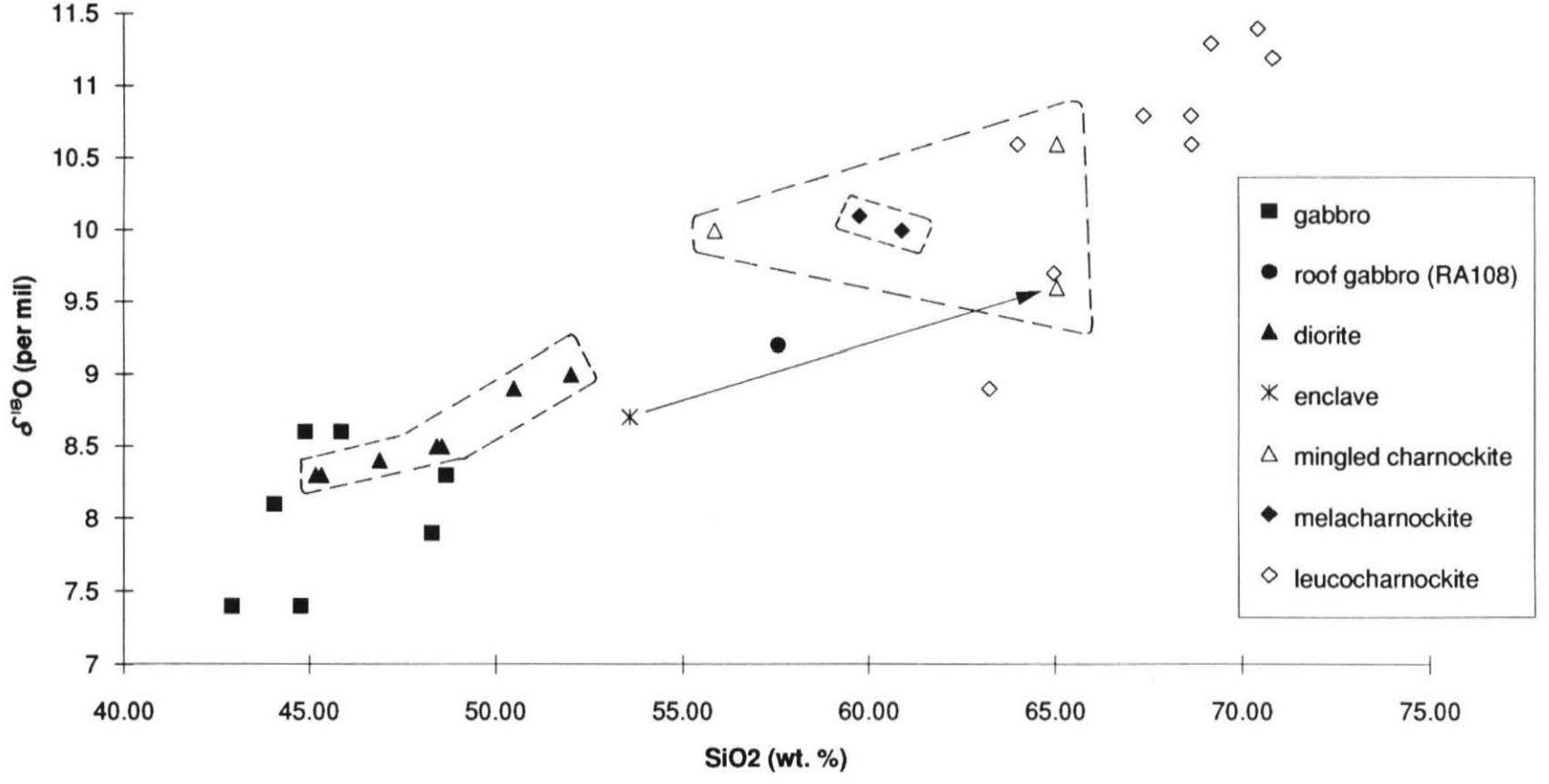

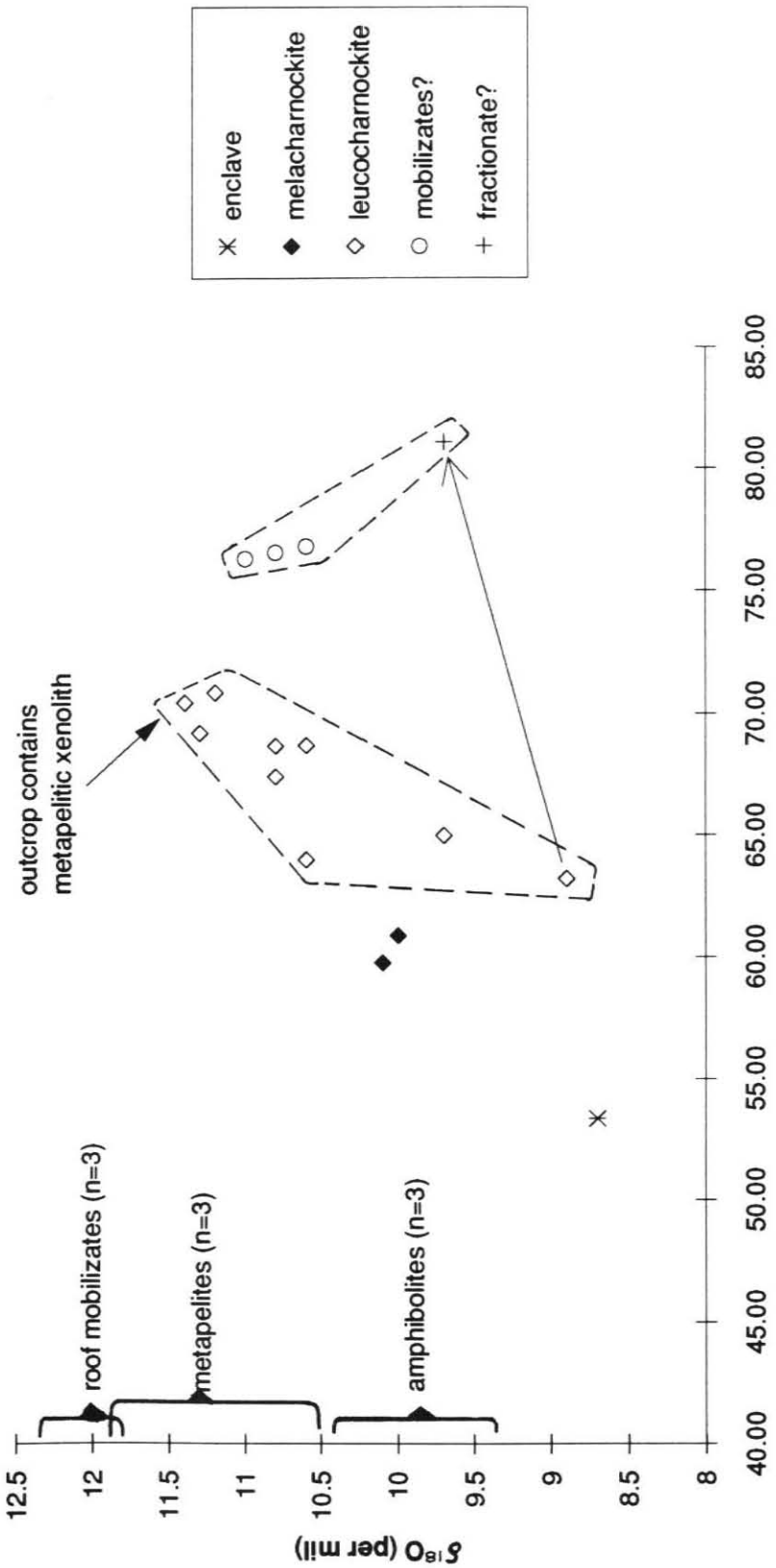

Figure 5.29: SiO2 vs. $\delta^{18}O$ for charnockites and wall rocks in the southern Ivrea Zone (Valle Sessera and Valle Strona di Postua). 9 samples lacking chemical data are plotted along the abscissa. Open arrow demonstrates possible fractionation trend.

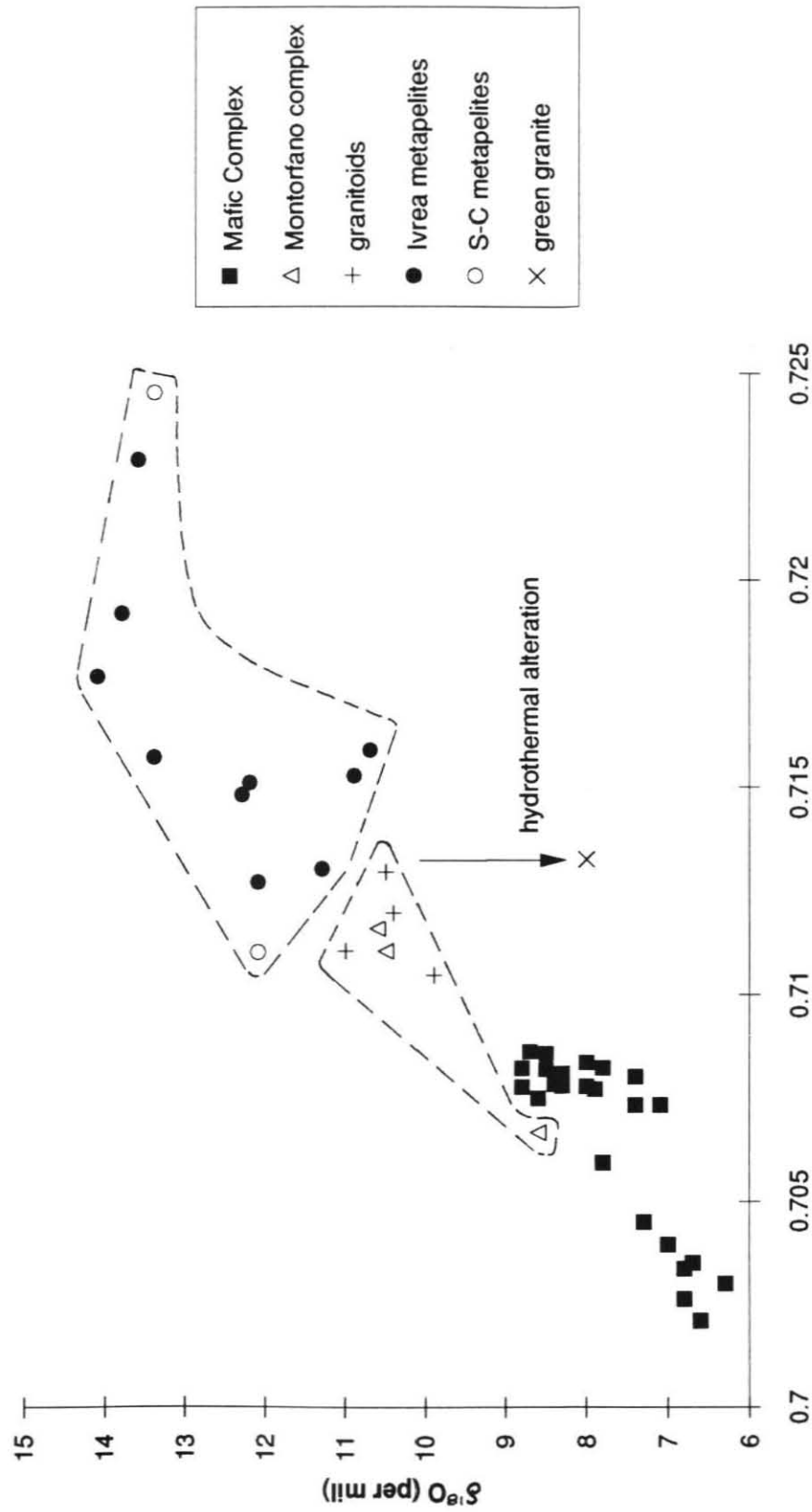

Figure 5.30: Sr_i vs. $\delta^{18}O$ comparing the Graniti dei Laghi to the Mafic Complex.

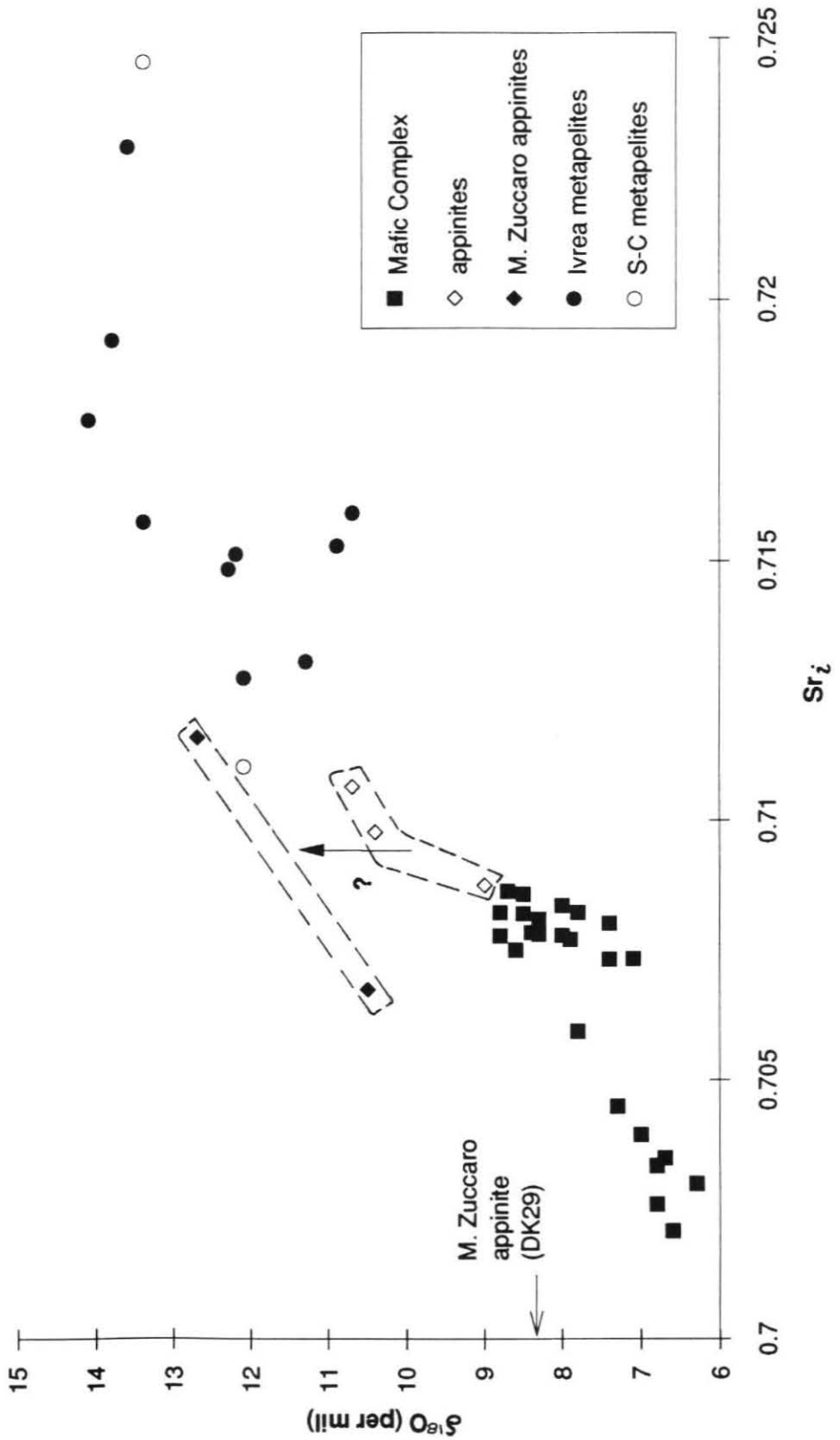

Figure 5.31: Sr_i vs. $\delta^{18}O$ comparing appinites from the Strona-Ceneri Zone to the Mafic Complex.

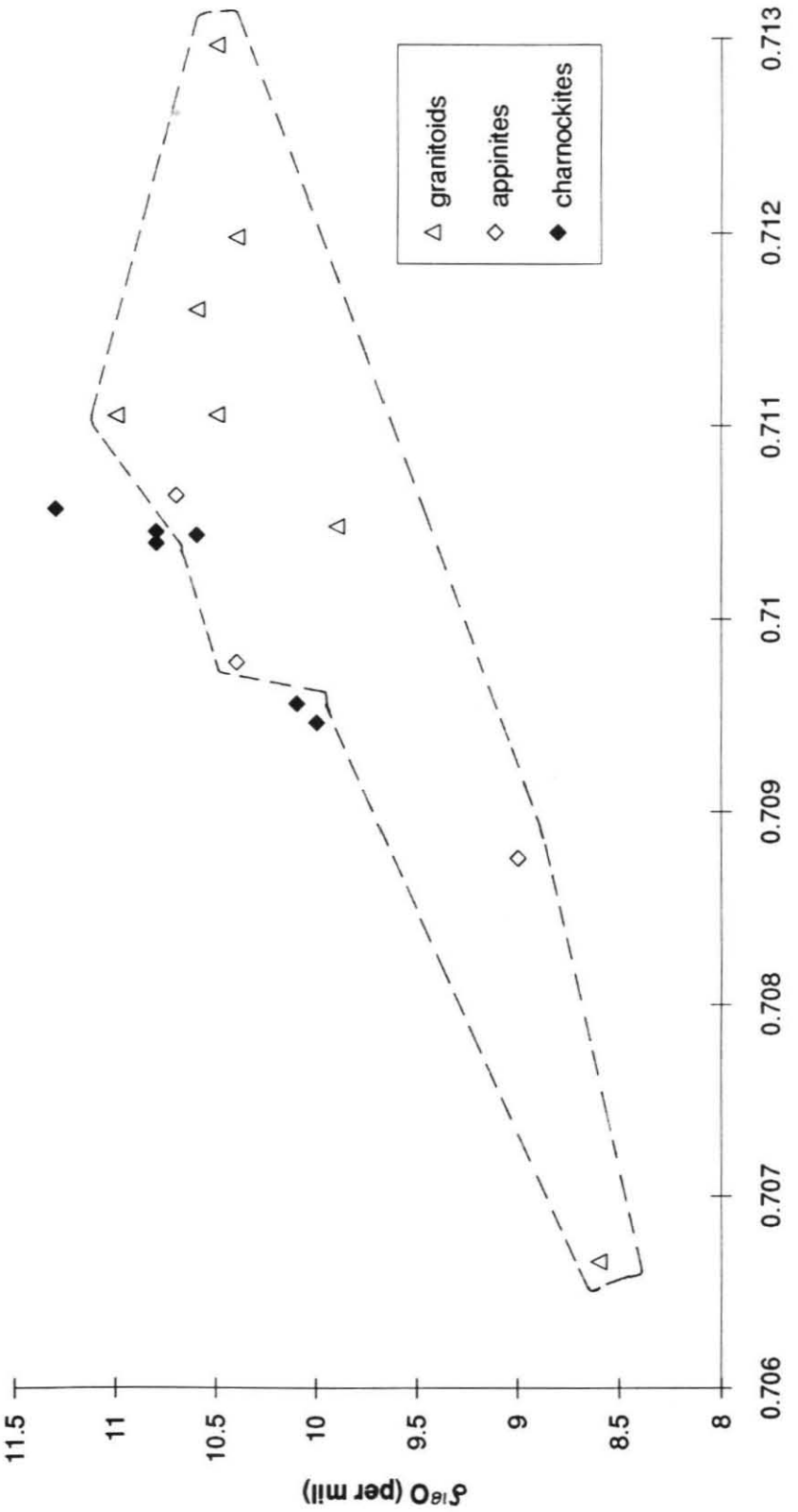

Figure 5.32: Sr_i vs.$\delta^{18}O$ comparing the appinites and granites of the Strona-Ceneri Zone to charnockites of the southern Ivrea Zone.

Figure 5.33: SiO2 vs.$\delta^{18}O$ for Massif Central xenoliths and Hercynian plutonics compared to the Mafic Complex, Ivrea Zone (dashed field; see Fig. 5.9).

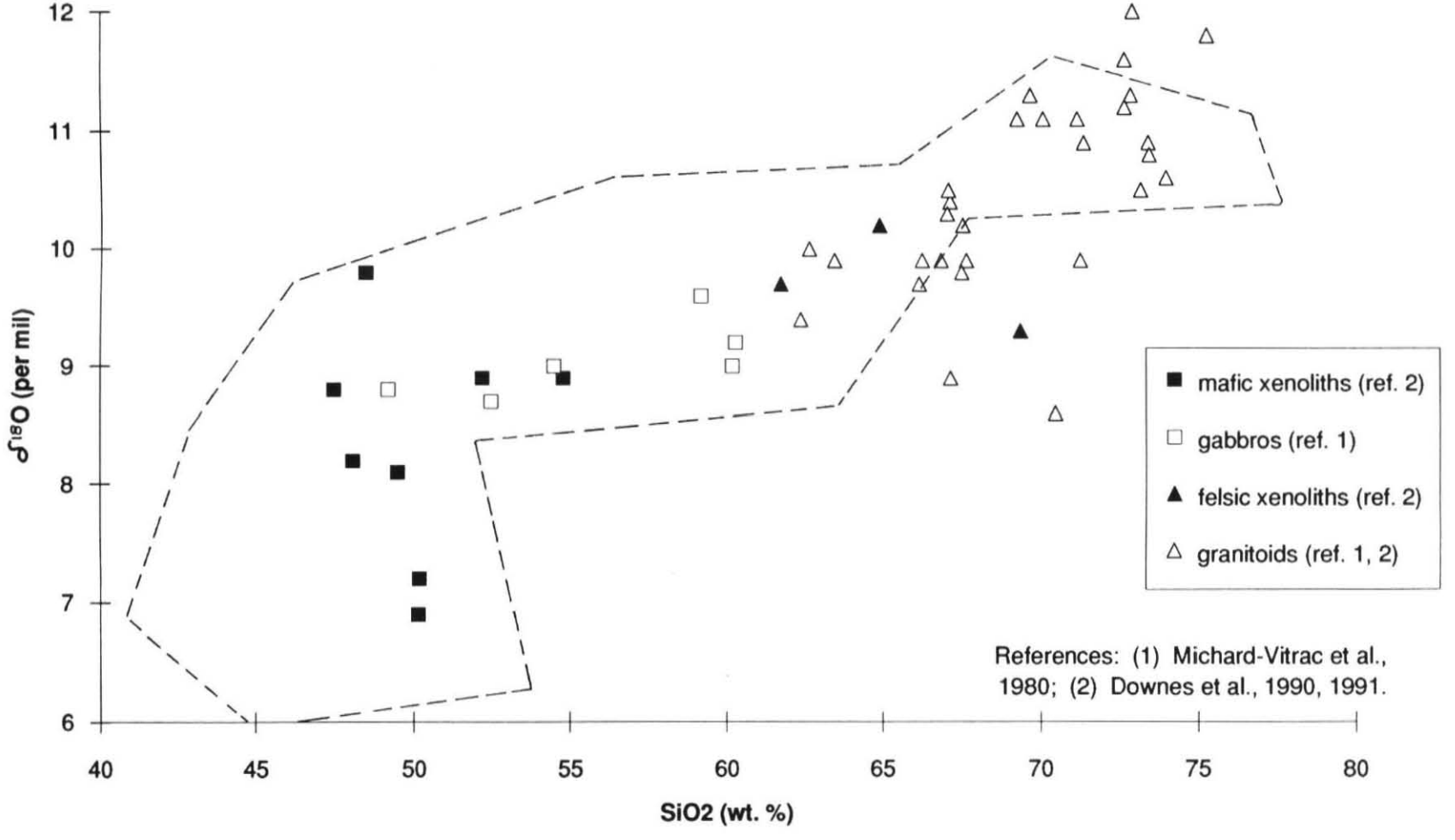

Table 5.1: Major element chemistry, location and oxygen isotope analysis of samples from the central Mafic Complex, Ivrea Zone, Italy

Sample #	VM2	VM3	VM12	VM13	VM14	VM15b	VM16	VM17	VM20
Lithology	hb gb dike	leucogabbro	diorite	diorite	leucogabbro	leucogabbro	hb gb dike	leucogabbro	norite
Unit	diorite	diorite	diorite	diorite	diorite	diorite	diorite	diorite	MG
Latitude (N)	45°49'14"	45°49'14"	45°50'31"	45°50'37"	45°50'46"	45°50'57"	45°51'10"	45°51'9"	45°51'12"
Longitude (E)	8°14'53"	8°14'53"	8°14'59"	8°14'54"	8°14'30"	8°14'25"	8°14'20"	8°14'17"	8°13'58"
SiO2	45.77	48.53	53.75	54.37	46.07	45.42	43.75	45.56	47.78
TiO2	1.57	1.92	1.12	1.12	1.71	2.28	2.00	1.79	0.90
Al2O3	14.00	19.08	20.26	20.36	22.51	21.63	17.18	24.12	18.98
FeO total	10.94	10.19	7.14	6.74	8.02	8.17	12.35	7.68	9.08
MnO	0.19	0.18	0.15	0.13	0.14	0.09	0.18	0.11	0.19
MgO	11.50	4.15	2.09	2.04	6.06	6.61	9.14	4.24	9.07
CaO	10.67	8.08	6.06	5.73	11.31	10.10	11.67	11.84	12.15
Na2O	1.52	3.17	3.42	3.48	1.81	1.90	1.63	2.14	1.42
K2O	1.82	2.93	4.95	5.07	1.86	2.40	0.60	1.37	0.19
P2O5	0.52	0.84	0.58	0.50	0.09	0.91	0.47	0.96	0.05
LOI	1.35	0.72	0.31	0.25	0.34	0.42	0.94	0.12	0.11
total	99.85	99.79	99.83	99.79	99.92	99.93	99.91	99.93	99.92
$\delta^{18}O$	7.7	8.3	8.8	9.0	8.2	8.4	7.3	8.5	8.1

Table 5.1: Major element chemistry, location and oxygen isotope analysis of samples from the central Mafic Complex, Ivrea Zone, Italy

Sample #	VM29	VM30	VM38	VM41	VM53	VM59	VM86	VM92	VM117-1
Lithology	norite	norite	norite	norite	norite	norite	norite	gabbro	enclave
Unit	MG	MG	UZ	UZ	UZ	UZ	UZ	UZ	mingled diorite
Latitude (N)	45°50'54"	45°50'54"	45°50'57"	45°50'59"	45°50'58"	45°51'38"	45°51'29"	45°51'20"	45°49'22"
Longitude (E)	8°12'34"	8°12'34"	8°11'31"	8°11'37"	8°11'20"	8°11'11"	8°10'9"	8°10'55"	8°14'52"
SiO2	46.67	47.09	46.26	47.52	50.80	47.31	46.15	47.54	46.39
TiO2	2.25	1.35	2.79	1.27	0.39	0.35	0.26	0.53	1.54
Al2O3	23.66	21.12	20.76	19.92	20.21	22.04	20.43	19.03	18.44
FeO total	7.34	10.17	9.82	9.26	6.84	7.92	10.11	9.62	11.04
MnO	0.12	0.17	0.16	0.18	0.13	0.17	0.16	0.20	0.21
MgO	3.23	5.92	4.63	6.21	7.16	6.96	10.48	7.09	8.13
CaO	12.08	11.37	10.91	12.26	11.24	12.65	10.72	13.13	11.13
Na2O	2.93	2.25	2.94	2.14	2.63	1.60	0.89	2.18	1.85
K2O	0.32	0.29	0.35	0.28	0.20	0.19	0.04	0.22	1.15
P2O5	1.35	0.10	1.29	0.12	0.04	0.04	0.03	0.05	0.03
LOI	0.00	0.11	0.00	0.78	0.28	0.71	0.64	0.36	0.00
total	99.95	99.94	99.91	99.94	99.92	99.94	99.91	99.95	99.91
$\delta^{18}O$	8.3	8.2	8.1	8.4	8.4	8.4	8.7	8.6	7.1

Table 5.1: Major element chemistry, location and oxygen isotope analysis of samples from the central Mafic Complex, Ivrea Zone, Italy

Sample #	VM117-2	VM117-6	VM117-8	VM117-9	VM117-10	VM118	VS101
Lithology	enclave	leucogabbro	enclave	leucogabbro	leucogabbro	leucogabbro	diorite
Unit	mingled diorite	mingled diorite	mingled diorite	mingled diorite	mingled diorite	diorite	roof diorite
Latitude (N)	45°49'22"	45°49'22"	45°49'22"	45°49'22"	45°49'22"	45°49'22"	45°48'38"
Longitude (E)	8°14'52"	8°14'52"	8°14'52"	8°14'52"	8°14'52"	8°14'52"	8°15'12"
SiO2	46.43	46.59	45.77	46.54	47.73	50.70	56.34
TiO2	1.57	1.94	1.75	2.24	2.00	1.00	1.12
Al2O3	18.43	15.23	18.73	18.94	18.16	18.45	19.46
FeO total	11.07	13.06	10.24	10.17	10.80	10.04	7.00
MnO	0.21	0.23	0.16	0.15	0.17	0.24	0.15
MgO	8.18	10.91	9.02	6.91	7.77	6.72	2.55
CaO	11.21	9.23	11.44	9.29	9.16	8.34	5.03
Na2O	1.78	1.46	1.54	2.03	1.65	2.33	3.14
K2O	1.00	1.15	1.05	2.56	2.35	1.91	4.76
P2O5	0.03	0.10	0.23	1.04	0.13	0.18	0.23
LOI	0.00	0.00	0.00	0.00	0.00	0.00	0.00
total	99.91	99.90	99.93	99.87	99.92	99.91	99.78
$\delta^{18}O$	7.1	7.1	6.1	7.9	8.1	8.9	8.9

Table 5.1: Major element chemistry, location and oxygen isotope analysis of samples from the central Mafic Complex, Ivrea Zone, Italy

Sample #	VS101b	VS102	VS103	VS104	VS105	VS106a	VS 106b	VS107
Lithology	inclusion	diorite	diorite	garnet diorite	garnet diorite	garnet diorite	inclusion	garnet diorite
Unit	roof diorite	roof diorite	roof diorite	roof diorite	roof diorite	roof diorite	roof diorite	roof diorite
Latitude (N)	45°48'38"	45°48'38"	45°48'38"	45°48'38"	45°48'38"	45°48'38"	45°48'38"	45°48'37"
Longitude (E)	8°15'12"	8°15'14"	8°15'16"	8°15'17"	8°15'18"	8°15'19"	8°15'19"	8°15'20"
SiO2	66.53	54.22	60.14	51.92	45.99	53.04	52.18	56.86
TiO2	1.05	1.32	1.11	1.76	2.08	1.60	1.68	1.66
Al2O3	17.70	19.67	18.49	22.92	20.71	23.29	22.66	18.84
FeO total	6.35	7.82	5.85	5.52	11.73	5.26	6.49	7.34
MnO	0.15	0.15	0.08	0.06	0.20	0.04	0.14	0.05
MgO	3.13	2.04	1.84	2.60	3.98	2.73	3.28	2.84
CaO	0.76	6.06	4.70	7.89	7.94	7.60	7.23	5.30
Na2O	2.29	3.59	3.27	4.40	2.18	4.25	3.92	3.38
K2O	1.92	3.97	3.92	1.90	3.25	1.90	2.11	2.92
P2O5	0.04	0.60	0.46	0.77	1.10	0.09	0.07	0.62
LOI	0.00	0.00	0.00	0.00	0.00	0.00	0.00	0.00
total	99.92	99.80	99.86	99.74	99.16	99.75	99.76	99.81
$\delta^{18}O$	9.8	9.4	9.2	10.0	9.5	9.8	9.5	10.4

Table 5.1: Major element chemistry, location and oxygen isotope analysis of samples from the central Mafic Complex, Ivrea Zone, Italy

Sample #	VS108a	VS108b	VS110a	VS110b	VS111	VS112a	VS112b	VS113	VS114
Lithology	mobilizate	metapelite	metapelite	metapelite	amphibolite	leucogabbro	metapelite	norite	gabbro
Unit	roof diorite	roof diorite	roof diorite	roof diorite	roof diorite	diorite	diorite	BZ	BZ
Latitude (N)	45°48'37"	45°48'37"	45°48'37"	45°48'37"	45°48'37"	45°49'3"	45°49'3"	45°49'46"	45°49'46"
Longitude (E)	8°15'21"	8°15'21"	8°15'22"	8°15'22"	8°15'23"	8°14'38"	8°14'38"	8°9'32"	8°9'34"
SiO2	72.70	64.58	54.45	59.65	47.58	46.83	66.53	49.90	46.95
TiO2	0.73	0.97	3.05	1.36	2.39	2.11	1.03	0.86	2.34
Al2O3	14.42	16.13	17.59	19.48	10.23	19.14	15.77	16.95	12.57
FeO total	2.06	6.14	9.22	18.05	11.88	10.48	6.28	7.64	10.92
MnO	0.03	0.13	0.03	0.11	0.17	0.17	0.14	0.16	0.17
MgO	1.16	3.10	4.97	3.54	15.88	6.96	3.88	8.17	10.91
CaO	4.71	4.03	3.63	2.48	9.73	9.87	2.52	14.71	14.61
Na2O	3.28	3.30	2.55	2.57	0.54	1.69	1.66	2.24	1.03
K2O	0.58	1.31	3.78	2.59	1.14	2.44	1.56	0.10	0.08
P2O5	0.25	0.21	0.60	0.05	0.27	0.21	0.06	0.01	0.05
LOI	0.00	0.00	0.00	0.00	0.00	0.00	0.00	0.00	0.00
total	99.92	99.90	99.87	99.88	99.81	99.90	99.93	100.74	99.83
$\delta^{18}O$	11.2	10.7	11.7	12.1	10.0	8.2	10.4	7.2	9.2

Table 5.1: Major element chemistry, location and oxygen isotope analysis of samples from the central Mafic Complex, Ivrea Zone, Italy

Sample #	VS115	VS116	VS117	VS118	VS119	VS120	VS121	VS122	VS123
Lithology	gabbro	norite	metapelite	metapelite	pyroxenite	gabbro	gabbro	norite	norite
Unit	BZ	BZ	BZ	BZ	BZ	BZ	BZ	BZ	BZ
Latitude (N)	45°49'48"	45°49'48"	45°49'48"	45°49'48"	45°49'47"	45°49'48"	45°49'47"	45°49'47"	45°49'46"
Longitude (E)	8°9'34"	8°9'34"	8°9'36"	8°9'38"	8°9'34"	8°9'39"	8°9'41"	8°9'40"	8°9'44"
SiO2	44.79	51.56	53.81	54.65	43.22	45.28	45.93	46.37	43.90
TiO2	2.07	0.70	1.59	1.36	3.10	1.43	0.67	0.21	1.38
Al2O3	17.10	17.10	20.08	20.97	9.21	17.12	21.42	24.48	21.74
FeO total	14.19	10.32	13.11	11.52	13.82	13.94	8.43	6.69	11.38
MnO	0.26	0.14	0.40	0.23	0.19	0.23	0.13	0.11	0.17
MgO	8.64	9.70	4.17	3.79	14.34	10.04	9.16	7.73	7.85
CaO	11.08	8.32	3.64	4.84	15.08	10.70	12.74	13.63	12.59
Na2O	1.69	1.67	2.62	2.77	0.84	1.12	1.07	0.70	0.90
K2O	0.06	0.39	0.42	0.24	0.05	0.06	0.10	0.03	0.04
P2O5	0.07	0.03	0.06	0.02	0.01	0.06	0.27	0.01	0.02
LOI	0.00	0.00	0.00	0.00	0.00	0.00	0.00	0.00	0.00
total	99.93	99.93	99.89	99.91	99.86	99.98	99.94	99.96	99.97
$\delta^{18}O$	8.5	9.0	9.7	10.0	7.3	7.7	7.6	7.6	7.5

Table 5.1: Major element chemistry, location and oxygen isotope analysis of samples from the central Mafic Complex, Ivrea Zone, Italy

Sample #	VS124	VS125	VS126	VS127	VS128a	VS128b	VS 129	VS130	VS131
Lithology	norite	gabbro	anorthosite	gabbro	anorthosite	pyroxenite	pyroxenite	leucogabbro	leucogabbro
Unit	BZ	BZ	IZ	IZ	IZ	IZ	IZ	diorite	diorite
Latitude (N)	45°49'46"	45°49'46"	45°49'49"	45°49'49"	45°49'49"	45°49'49"	45°49'49"	45°49'9"	45°49'12"
Longitude (E)	8°9'47"	8°9'48"	8°9'3"	8°9'3"	8°9'3"	8°9'3"	8°9'3"	8°14'25"	8°14'19"
SiO2	45.85	46.63	46.97	46.44	47.86	44.74	51.05	46.74	48.78
TiO2	0.38	1.46	0.26	0.91	0.08	0.23	0.31	2.18	1.76
Al2O3	21.40	19.63	30.31	27.05	32.27	8.20	3.63	19.80	18.80
FeO total	7.67	11.44	1.97	4.74	0.70	13.86	9.59	10.20	9.53
MnO	0.13	0.20	0.06	0.11	0.02	0.18	0.14	0.15	0.17
MgO	9.42	7.49	1.74	4.17	0.57	25.50	25.01	6.21	7.21
CaO	14.29	10.93	16.35	14.45	15.95	7.13	9.84	9.43	9.53
Na2O	0.75	2.03	2.14	1.97	2.45	0.18	0.13	2.88	2.30
K2O	0.04	0.09	0.10	0.08	0.05	0.02	0.01	1.91	1.59
P2O5	0.02	0.05	0.01	0.01	0.01	0.01	0.01	0.93	0.19
LOI	0.00	0.00	0.00	0.00	0.00	0.00	0.00	0.00	0.00
total	99.95	99.95	99.91	99.93	99.90	99.87	99.77	99.93	99.86
$\delta^{18}O$	7.4	8.2	8.8	8.2	8.6	6.8	7.1	8.7	8.3

Table 5.1: Major element chemistry, location and oxygen isotope analysis of samples from the central Mafic Complex, Ivrea Zone, Italy

Sample #	VS132	VS133	VS134	VS135	VS136	VS137	VS138	VS139	VS140
Lithology	leucogabbro	leucogabbro	leucogabbro	norite	norite	gabbro	norite	norite	gabbro
Unit	MG	MG	MG	MG	MG	UZ	IZ	IZ	UZ
Latitude (N)	45°49'8"	45°49'10"	45°49'13"	45°49'20"	45°49'55"	45°49'48"	45°49'37"	45°49'34"	45°49'44"
Longitude (E)	8°13'53"	8°13'47"	8°13'46"	8°13'00"	8°11'53"	8°11'6"	8°10'00"	8°9'55"	8°10'20"
SiO2	45.24	46.30	46.59	49.11	44.06	43.99	51.74	51.94	49.53
TiO2	1.89	1.63	1.90	1.30	0.58	3.12	0.55	0.69	1.35
Al2O3	19.91	19.46	17.00	17.28	19.33	16.57	20.48	20.14	23.62
FeO total	10.07	10.76	12.86	11.10	13.44	15.53	8.00	7.67	7.60
MnO	0.15	0.19	0.23	0.18	0.19	0.26	0.15	0.14	0.11
MgO	7.68	7.69	8.66	8.11	10.75	6.91	6.46	6.52	3.08
CaO	11.99	11.01	9.78	10.83	9.43	11.02	9.54	9.70	9.72
Na2O	1.78	1.39	1.47	1.63	1.69	2.19	2.90	2.93	4.00
K2O	0.57	1.46	1.15	0.19	0.15	0.23	0.14	0.21	0.29
P2O5	0.65	0.05	0.26	0.02	0.05	0.10	0.01	0.02	0.63
LOI	0.00	0.00	0.00	0.00	0.00	0.00	0.00	0.00	0.00
total	99.93	99.91	99.92	99.95	99.89	99.92	99.97	99.96	99.93
$\delta^{18}O$	8.2	8.1	8.2	7.7	7.8	8.0	9.2	9.2	8.9

Table 5.1: Major element chemistry, location and oxygen isotope analysis of samples from the central Mafic Complex, Ivrea Zone, Italy

Sample #	VS141	VS142	VS143a	VS144
Lithology	gabbro	gabbro	anorthosite	gabbro
Unit	UZ	UZ	UZ	UZ
Latitude (N)	45°49'46"	45°49'46"	45°49'48"	45°49'44"
Longitude (E)	8°10'25"	8°10'25"	8°10'35"	8°10'20"
SiO2	47.85	47.76	53.35	48.56
TiO2	2.02	2.02	0.15	1.73
Al2O3	21.20	20.66	27.88	22.45
FeO total	10.78	12.21	1.08	9.08
MnO	0.20	0.21	0.02	0.16
MgO	3.21	3.81	0.44	3.17
CaO	9.13	8.56	11.62	9.81
Na2O	3.99	3.82	4.61	3.93
K2O	0.35	0.33	0.53	0.29
P2O5	1.09	0.54	0.28	0.73
LOI	0.00	0.00	0.00	0.00
total	99.82	99.92	99.90	99.91
$\delta^{18}O$	8.6	8.5	9.3	9.1

Table 5.2: Major element chemistry and oxygen isotopes of samples from Finero (F), Monte Capio Sill (MC), Rocca d'Argimonia (RA) and Strona di Postua (SP), Ivrea Zone

Sample #	F1	F3	F5	F6A	F6B	F9	F13
Lithology	metapelite	pyroxenite	hornblendite	anorthosite	anorthosite	Cr-diopside dike	Cr-diopside dike
Unit	septum	upper gabbro	amphibole perid.	lower gabbro	lower gabbro	phlogopite perid.	phlogopite perid.
SiO2	48.69	48.12	44.55	42.34	42.76	49.37	51.23
TiO2	1.08	0.24	0.38	0.04	0.06	0.12	0.09
Al2O3	16.01	2.60	13.98	35.47	33.61	1.38	1.32
FeO total	9.81	7.39	8.28	1.67	2.31	4.80	4.32
MnO	0.19	0.14	0.12	0.02	0.03	0.10	0.11
MgO	9.41	29.06	18.45	1.77	2.64	28.68	27.44
CaO	11.74	11.76	11.91	17.32	16.92	15.09	14.78
Na2O	2.35	0.12	1.95	1.08	1.27	0.09	0.18
K2O	0.56	0.02	0.22	0.07	0.20	0.01	0.04
P2O5	0.08	0.01	0.02	0.03	0.02	0.01	0.01
LOI	0	0	0	0	0	0	0
total	99.92	99.46	99.86	99.81	99.82	99.65	99.52
$\delta^{18}O$	8.7	6.3	6.6	7.3	7.5	6.4	6.4

Appendix 5.2: Major element chemistry and oxygen isotopes of samples from Finero (F), Monte Capio Sill (MC), Rocca d'Argimonia (RA) and Strona di Postua (SP), Ivrea Zone

Sample #	F17	F20	F22	F23	F24	F26	F27
Lithology	Cr-diopside dike	pyroxenite	garnet gabbro	hornblendite	garnet gabbro	hb gabbro	hb gabbro
Unit	phlogopite perid.	lower gabbro	upper gabbro	upper gabbro	upper gabbro	upper gabbro	upper gabbro
SiO2	53.61	47.88	44.29	44.45	43.95	46.32	46.96
TiO2	0.08	0.08	0.48	0.48	0.55	2.47	3.06
Al2O3	1.52	7.08	16.00	15.48	15.49	14.64	13.35
FeO total	2.63	15.06	8.56	8.40	9.11	13.49	15.17
MnO	0.09	0.19	0.01	0.10	0.16	0.23	0.25
MgO	21.14	24.50	12.51	15.83	12.30	7.00	0.16
CaO	20.01	4.25	15.82	12.35	16.26	12.72	10.20
Na2O	0.27	0.79	1.97	2.54	1.94	2.63	2.06
K2O	0.02	0.09	0.13	0.19	0.12	0.17	0.05
P2O5	0.01	0.03	0.03	0.03	0.03	0.27	0.39
LOI	0	0	0	0	0	0	0
total	99.38	99.95	99.80	99.85	99.91	99.94	99.95
$\delta^{18}O$	6.4	6.4	6.8	6.5	6.5	7.4	5.2

Table 5.2: Major element chemistry and oxygen isotopes of samples from Finero (F), Monte Capio Sill (MC), Rocca d'Argimonia (RA) and Strona di Postua (SP), Ivrea Zone

Sample #	F29a	F29b	F30	MC54	MC58	MC59	MC60	MC61
Lithology	metapelite	metapelite	hb gabbro	gabbro	gabbro	aphanitic gabbro	garnet gabbro	mobilizate
Unit	septum	septum	upper gabbro	basal gabbro	peridotite	layered gabbro	layered gabbro	septum
SiO2	48.01	61.61	46.29	48.48	45.89	48.67	45.25	54.21
TiO2	1.54	0.83	3.05	1.64	1.71	0.50	1.89	0.56
Al2O3	21.63	17.51	12.36	18.36	17.68	20.13	18.06	25.26
FeO total	13.86	7.96	16.12	10.62	9.76	7.44	8.94	3.12
MnO	0.56	0.19	0.26	0.16	0.19	0.12	0.12	0.03
MgO	3.79	2.31	10.96	8.24	11.61	11.33	12.26	2.61
CaO	6.33	4.50	8.42	9.25	11.07	10.68	11.32	9.28
Na2O	3.55	3.09	1.83	2.13	1.73	0.95	1.78	4.63
K2O	0.58	1.68	0.04	0.69	0.26	0.10	0.27	0.12
P2O5	0.06	0.25	0.60	0.36	0.02	0.01	0.02	0.02
LOI	0	0	0	0	0	0	0	0
total	99.91	99.93	99.93	99.93	99.92	99.93	99.91	99.84
$\delta^{18}O$	9.2	11.0	4.4	8.6	8.5	8.6	8.7	10.3

Table 5.2: Major element chemistry and oxygen isotopes of samples from Finero (F), Monte Capio Sill (MC), Rocca d'Argimonia (RA) and Strona di Postua (SP), Ivrea Zone

Sample #	MC62	MC63	MC65	MC66	MC67	MC68	MC69
Lithology	aphanitic gabbro	metapelite	aphanitic gabbro	aphanitic gabbro	aphanitic gabbro	gabbro	aphanitic gabbro
Unit	layered gabbro	stronalite	stronalite	layered gabbro	stronalite	layered gabbro	metapelite
SiO2	46.98	45.82	48.06	49.90	50.81	45.74	48.92
TiO2	0.97	2.22	0.93	1.78	1.19	1.78	1.87
Al2O3	20.95	29.27	9.98	15.12	9.89	16.60	18.96
FeO total	8.33	6.47	10.95	11.07	9.83	10.09	11.28
MnO	0.12	0.11	0.18	0.16	0.14	0.14	0.15
MgO	9.85	1.40	20.29	11.50	19.07	12.86	8.52
CaO	11.30	12.28	8.62	8.62	7.75	11.04	8.91
Na2O	1.27	2.22	0.31	0.89	0.66	1.40	0.70
K2O	0.15	0.09	0.34	0.38	0.47	0.26	0.23
P2O5	0.01	0.02	0.13	0.42	0.04	0.02	0.37
LOI	0	0	0	0	0	0	0
total	99.93	99.90	99.79	99.91	99.85	99.93	99.91
$\delta^{18}O$	8.5	9.8	8.4	9.0	9.1	8.3	9.5

Table 5.2: Major element chemistry and oxygen isotopes of samples from Finero (F), Monte Capio Sill (MC), Rocca d'Argimonia (RA) and Strona di Postua (SP), Ivrea Zone

Sample #	MC70	MC71	MC73	RA101	RA102	RA103	RA104	RA105
Lithology	pyroxenite	pyroxenite	ol. websterite	diorite	gabbro	mobilizate	mobilizate	mobilizate
Unit	layered gabbro	pyroxenite	peridotite	diorite	gabbro	gabbro	gabbro	gabbro
SiO2	51.38	50.01	50.23	52.02	44.06	76.30	76.81	76.56
TiO2	0.42	0.68	0.49	2.18	4.33	0.13	0.15	0.03
Al2O3	4.89	6.42	5.33	18.89	16.64	12.84	12.70	12.94
FeO total	14.11	10.21	9.89	10.46	14.48	1.23	0.83	0.83
MnO	0.24	0.19	0.18	0.17	0.19	0.04	0.02	0.12
MgO	25.08	20.66	23.53	2.82	6.68	0.20	0.14	0.00
CaO	3.45	11.13	9.73	7.81	11.07	1.16	1.03	0.73
Na2O	0.17	0.37	0.31	4.29	1.81	3.37	2.76	3.00
K2O	0.03	0.05	0.05	0.55	0.19	4.65	5.48	5.72
P2O5	0.01	0.01	0.03	0.74	0.47	0.02	0.01	0.02
LOI	0	0	0	0	0	0	0	0
total	99.78	99.73	99.77	99.93	99.92	99.94	99.93	99.95
$\delta^{18}O$	8.2	7.7	7.0	9.0	8.1	11.0	10.6	10.8

Table 5.2: Major element chemistry and oxygen isotopes of samples from Finero (F), Monte Capio Sill (MC), Rocca d'Argimonia (RA) and Strona di Postua (SP), Ivrea Zone

Sample #	RA108	RA109	RA110a	RA110b	RA111	RA112	RA113	RA114	SP2
Lithology	roof gabbro	gabbro	aphanitic gabbro	gabbro	gabbro	leucocharn.	leucocharn.	leucosome	gabbro
Unit	gabbro	gabbro	gabbro	gabbro	charnockite	charnockite	charnockite	charnockite	gabbro
SiO2	57.57	44.77	42.92	48.68	49.18	64.97	63.22	81.05	45.87
TiO2	0.96	1.63	1.75	0.19	1.60	0.68	0.71	0.05	n/a
Al2O3	18.87	19.74	20.41	24.92	21.41	16.73	18.11	11.09	n/a
FeO total	7.98	12.77	13.54	7.46	10.28	5.15	5.24	0.68	n/a
MnO	0.14	0.18	0.19	0.13	0.17	0.07	0.09	0.01	n/a
MgO	3.06	6.81	7.30	4.92	3.84	1.77	1.26	0.16	n/a
CaO	6.52	11.39	11.71	11.68	9.02	4.59	5.55	3.07	n/a
Na2O	3.82	1.95	1.61	1.84	3.16	3.75	4.55	3.20	n/a
K2O	0.71	0.47	0.35	0.09	0.87	1.99	0.96	0.64	n/a
P2O5	0.30	0.20	0.16	0.03	0.38	0.22	0.24	0.01	n/a
LOI	0	0	0	0	0	0	0	0	n/a
total	99.93	99.91	99.94	99.94	99.91	99.92	99.93	99.96	
$\delta^{18}O$	9.2	7.4	7.4	8.3	8.5	9.7	8.9	9.7	8.6

Table 5.2: Major element chemistry and oxygen isotopes of samples from Finero (F), Monte Capio Sill (MC), Rocca d'Argimonia (RA) and Strona di Postua (SP), Ivrea Zone

Sample #	SP3a	SP3b	SP4	SP5	SP6	SP7	SP8	SP9	SP10
Lithology	charnockite	aphanitic gabbro	charnockite	charnockite	gabbro	leucogabbro	leucogabbro	leucogabbro	leucogabbro
Unit	migmatite	migmatite	migmatite	migmatite	gabbro	diorite	diorite	diorite	diorite
SiO2	65.37	53.38	55.71	65.00	44.89	48.57	48.43	46.91	50.49
TiO2	0.75	1.47	1.20	0.84	2.66	2.75	2.74	2.69	1.20
Al2O3	16.75	19.05	20.83	16.96	15.92	19.65	15.15	13.92	25.11
FeO total	4.48	8.99	7.71	5.01	17.93	11.25	12.70	18.06	5.82
MnO	0.04	0.15	0.15	0.08	0.27	0.17	0.15	0.31	0.08
MgO	2.93	6.42	1.85	1.66	6.67	4.48	7.60	8.47	3.06
CaO	4.45	6.47	6.99	4.90	7.11	8.98	9.41	6.55	10.48
Na2O	3.40	9.07	4.05	3.16	2.42	2.94	2.35	2.03	2.92
K2O	1.74	0.56	0.95	2.01	0.83	0.64	1.19	0.44	0.59
P2O5	0.06	0.84	0.48	0.28	1.22	0.56	0.18	0.55	0.17
LOI	0	0	0	0	0	0	0	0	0
total	99.94	99.90	99.92	99.92	99.94	99.93	99.90	99.95	99.92
$\delta^{18}O$	9.6	8.7	10.0	10.6	8.6	8.5	8.5	8.4	8.9

Table 5.2: Major element chemistry and oxygen isotopes of samples from Finero (F), Monte Capio Sill (MC), Rocca d'Argimonia (RA) and Strona di Postua (SP), Ivrea Zone

Sample #	SP11	SP12	SP13	SP16	SP17	SP18	SP19	SP21c	SP22
Lithology	gabbro	leucogabbro	leucogabbro	leucocharn.	leucocharn.	leucocharn.	leucocharn.	metapelite	mobilizate
Unit	diorite	diorite	diorite	charnockite	charnockite	charnockite	charnockite	stronalite	stronalite
SiO2	48.31	45.18	45.33	n/a	70.83	63.99	70.43	n/a	n/a
TiO2	2.12	3.85	3.60	n/a	0.33	0.67	0.28	n/a	n/a
Al2O3	20.17	18.70	17.74	n/a	15.79	17.74	16.69	n/a	n/a
FeO total	11.07	14.46	13.87	n/a	2.40	3.72	1.41	n/a	n/a
MnO	0.16	0.19	0.20	n/a	0.02	0.07	0.03	n/a	n/a
MgO	4.76	6.70	6.73	n/a	1.24	2.02	0.64	n/a	n/a
CaO	10.07	9.27	10.31	n/a	3.48	4.61	2.74	n/a	n/a
Na2O	2.44	2.07	1.38	n/a	3.10	3.66	3.03	n/a	n/a
K2O	0.40	0.29	0.23	n/a	2.64	1.40	4.63	n/a	n/a
P2O5	0.48	0.24	0.85	n/a	0.09	0.04	0.05	n/a	n/a
LOI	0	0	0	n/a	0	0	0	n/a	n/a
total	99.92	99.95	99.94		99.98	99.98	99.98		
$\delta^{18}O$	7.9	8.3	8.3	8.8	11.2	10.6	11.4	11.9	11.8

Table 5.2: Major element chemistry and oxygen isotopes of samples from Finero (F), Monte Capio Sill (MC), Rocca d'Argimonia (RA) and Strona di Postua (SP), Ivrea Zone

Sample #	SP23	SP25	SP27	SP30	SP33	SP34	SP36
Lithology	metapelite	amphibolite	mobilizate	mobilizate	metapelite	amphibolite	amphibolite
Unit	stronalite	stronalite	stronalite	stronalite	stronalite	stronalite	stronalite
SiO2	n/a	n/a	n/a	n/a	n/a	n/a	n/a
TiO2	n/a	n/a	n/a	n/a	n/a	n/a	n/a
Al2O3	n/a	n/a	n/a	n/a	n/a	n/a	n/a
FeO total	n/a	n/a	n/a	n/a	n/a	n/a	n/a
MnO	n/a	n/a	n/a	n/a	n/a	n/a	n/a
MgO	n/a	n/a	n/a	n/a	n/a	n/a	n/a
CaO	n/a	n/a	n/a	n/a	n/a	n/a	n/a
Na2O	n/a	n/a	n/a	n/a	n/a	n/a	n/a
K2O	n/a	n/a	n/a	n/a	n/a	n/a	n/a
P2O5	n/a	n/a	n/a	n/a	n/a	n/a	n/a
LOI	n/a	n/a	n/a	n/a	n/a	n/a	n/a
total							
$\delta^{18}O$	11.3	10.3	12.2	12.1	10.5	9.4	9.9

Table 5.3: Major element and isotopic data from the Ivrea Zone

Sample #	KAW503	TS4	GZ 7	GZ 8	MP 1	Q 1	Q 6	Q 10	VS 124	FE 19
Lithology	hornblendite	gabbro	pyroxenite	pyroxenite	gabbro	gabbro	pyroxenite	pyroxenite	gabbro	gabbro
Unit	Finero	BZ	BZ	BZ	BZ	BZ	BZ	BZ	BZ	IZ
SiO2	n/a	48.76	47.30	44.80	46.68	44.31	46.99	41.55	46.15	48.57
TiO2	n/a	n/a	0.93	0.61	1.51	2.75	0.86	1.48	0.37	1.42
Al2O3	n/a	n/a	6.14	7.30	13.97	15.66	6.00	14.56	21.31	17.55
FeO	n/a	n/a	12.04	13.24	10.98	14.06	12.69	14.36	7.65	11.07
Fe2O3	n/a	n/a	n/a	n/a	n/a	n/a	n/a	n/a	n/a	n/a
MnO	n/a	n/a	0.28	0.22	0.22	0.26	0.28	0.23	0.13	0.18
MgO	n/a	n/a	15.03	27.35	11.24	7.10	15.90	13.72	9.32	8.00
CaO	n/a	n/a	16.30	4.29	13.75	11.67	15.28	13.27	14.23	9.64
Na2O	n/a	n/a	0.64	0.23	1.50	2.42	0.51	0.73	0.73	2.06
K2O	n/a	n/a	0.00	0.00	0.06	0.04	0.00	0.02	0.04	0.17
P2O5	n/a	n/a	0.00	0.01	0.02	0.08	0.08	0.07	0.02	0.07
total				99.71	99.93	99.44	98.59	99.99	99.95	98.77
$\delta^{18}O$	6.5	6.6	7.3	6.8	6.8	6.3	7.8	7.0	7.4	8.0
reference	1	1	1	1	1	1	1	1	1	1
1/Sr x 10^3	7.19		47.6	90.9	5.32	11.0	71.4	17.9	5.1	3.68
Sr_i	0.70328	0.70211	0.70450	0.70336	0.70263	0.70301	0.70594	0.70396	0.70802	0.70779
1/Nd	n/a	.175	.202	.380	.141	.104	.156	.155	.311	.308
ε Nd	disturbed?	10.1	3.07	2.74	7.18	6.79	-2.58	-2.28	-4.43	-5.60
reference	3	5	2, 7, 9	2, 7, 9	7	7	7	7	7	7

Oxide data in weight %; all iron reported as "FeO total" unless nonzero value reported for Fe2O3; oxygen isotope values reported in (+) per mil; trace element data in ppm; Sr_i and ε Nd calculated for 270 Ma.

REFERENCES: (1) this study; (2) Pin and Sills, 1986; (3) Voshage et al., 1987; (4) Bürgi, 1987; (5) Voshage et al., 1988; (6) Schnetger, 1988; (7) Voshage et al., 1990; (8) Bürghi and Klotzli, 1990; (9) Sinigoi, unpublished data.

Table 5.3: Major element and isotopic data from the Ivrea Zone

Sample #	FE 21	FE 31	FE 41	FE 49	FE 51	GM 90	GM 24	MO 1127	MO 95	MZ 131
Lithology	pyroxenite	gabbro	pyroxenite	pyroxenite	roof gabbro	pyroxenite	pyroxenite	gabbro	gabbro	gabbro
Unit	IZ	IZ	IZ	IZ	IZ	UZ	UZ	UZ	UZ	UZ
SiO2	51.01	52.06	44.40	51.08	51.36	50.29	50.66	32.76	43.09	48.18
TiO2	0.39	0.65	2.22	0.27	1.04	n/a	0.25	5.20	2.93	0.81
Al2O3	4.28	21.93	10.01	3.80	20.64	n/a	4.17	7.49	20.46	21.75
FeO	11.20	7.38	9.95	10.54	9.00	n/a	13.17	29.48	10.10	8.31
Fe2O3	n/a	n/a	n/a	n/a	n/a	n/a	n/a	n/a	n/a	n/a
MnO	0.17	0.13	0.17	0.19	0.14	n/a	0.22	0.35	0.14	0.19
MgO	21.75	4.36	17.81	25.21	4.34	n/a	27.77	17.35	4.85	6.43
CaO	11.40	9.14	12.22	8.25	8.58	n/a	1.64	3.87	11.42	10.93
Na2O	0.22	2.98	1.26	0.19	3.14	n/a	0.02	0.00	3.06	2.07
K2O	0.01	0.47	0.10	0.01	0.62	n/a	0.01	0.14	0.38	0.32
P2O5	0.09	0.08	0.23	0.01	0.14	n/a	0.00	0.06	1.80	0.07
total	98.97	99.18		100.01	99.00		98.52	96.70	99.88	
$\delta^{18}O$	7.4	7.9	6.7	7.1	9.5	8.0	8.5	7.8	8.3	8.6
reference	1	1	1	1	1	1	1	1	1	1
1/Sr x 10^3	90.9	2.46	4.07	83.3	2.73	55.6	100.	8.62	1.74	2.18
Sr_i	0.70732	0.70771	0.70350	0.70733	0.70809	0.70837	0.70994	0.70824	0.70810	0.70750
1/Nd	.357	.599	.101	.581	.084	.412	1.56	.461	.029	.149
εNd	-4.20	-3.97	2.22	-3.72	-5.15	-5.95	-7.39	-4.75	-4.36	-4.22
reference	7	7	2, 7, 9	7	7	2, 7, 9	7	7	7	2, 7, 9

Oxide data in weight %; all iron reported as "FeO total" unless nonzero value reported for Fe2O3; oxygen isotope values reported in (+) per mil; trace element data in ppm; Sr_i and εNd calculated for 270 Ma.

REFERENCES: (1) this study; (2) Pin and Sills, 1986; (3) Voshage et al., 1987; (4) Bürgi, 1987; (5) Voshage et al., 1988; (6) Schnetger, 1988; (7) Voshage et al., 1990; (8) Bürghi and Klotzli, 1990; (9) Sinigoi, unpublished data.

Table 5.3: Major element and isotopic data from the Ivrea Zone

Sample #	MZ 132	MZ 145	GM/MP	KAW1680	KAW1681wr	KAW1681pl	KAW1778	KAW1779	KAW1781
Lithology	gabbro	gabbro	stronalite	anorthosite	gabbro	plag separate	gabbro	gabbro	roof diorite
Unit	UZ	UZ	IZ/UZ	UZ	UZ	UZ	MG	UZ	diorite
SiO2	48.08	47.28	n/a	n/a	n/a	n/a	n/a	n/a	49.12
TiO2	0.32	0.49	n/a	n/a	n/a	n/a	n/a	n/a	1.79
Al2O3	26.23	26.52	n/a	n/a	n/a	n/a	n/a	n/a	21.52
FeO	5.69	6.83	n/a	n/a	n/a	n/a	n/a	n/a	6.45
Fe2O3	n/a	n/a	n/a	n/a	n/a	n/a	n/a	n/a	1.14
MnO	0.20	0.10	n/a	n/a	n/a	n/a	n/a	n/a	0.14
MgO	4.32	3.81	n/a	n/a	n/a	n/a	n/a	n/a	4.16
CaO	12.17	11.11	n/a	n/a	n/a	n/a	n/a	n/a	9.14
Na2O	2.10	2.45	n/a	n/a	n/a	n/a	n/a	n/a	2.96
K2O	0.20	0.59	n/a	n/a	n/a	n/a	n/a	n/a	1.44
P2O5	0.06	0.06	n/a	n/a	n/a	n/a	n/a	n/a	0.30
total	99.37	99.24							99.24
$\delta^{18}O$	8.8	8.4	10.2	8.8	8.5	9.2	8.5	8.3	9.8
reference	1	1	1	1	1	1	1	1	1
1/Sr x 10^3	1.87	1.67	n/a	1.09	1.57	n/a	1.36	1.95	1.67
Sr_i	0.70824	0.70785	n/a	0.70778	0.70859	n/a	0.70821	0.70781	0.70856
1/Nd	.180	.107	.028	.253	.042	n/a	.258	.060	n/a
ε Nd	-4.87	-5.27	-9.48	-4.99	-5.02	n/a	-4.86	-3.82	n/a
reference	7	7	7	3, 5	3, 5	3	3, 5	3, 5	4, 8

Oxide data in weight %; all iron reported as "FeO total" unless nonzero value reported for Fe2O3; oxygen isotope values reported in (+) per mil; trace element data in ppm; Sr_i and ε Nd calculated for 270 Ma.

REFERENCES: (1) this study; (2) Pin and Sills, 1986; (3) Voshage et al., 1987; (4) Bürgi, 1987; (5) Voshage et al., 1988; (6) Schnetger, 1988; (7) Voshage et al., 1990; (8) Bürghi and Klotzli, 1990; (9) Sinigoi, unpublished data.

Table 5.3: Major element and isotopic data from the Ivrea Zone

Sample #	KAW1202	KAW1782	KAW1784	KAW1785	KAW2504	KAW2505	KAW2506
Lithology	diorite	leucocharnockite	melacharnockite	roof diorite	leucocharnockite	melacharnockite	leucocharnockite
Unit	diorite	charnockite	charnockite	diorite	charnockite	charnockite	charnockite
SiO2	51.79	69.20	59.76	53.98	68.67	60.89	67.39
TiO2	1.35	0.36	0.87	1.18	0.43	0.99	0.55
Al2O3	18.88	15.21	17.08	19.96	15.06	16.74	16.01
FeO	7.68	2.29	5.15	5.37	2.62	4.60	3.21
Fe2O3	1.37	0.43	0.85	1.51	0.62	1.52	0.41
MnO	0.21	0.04	0.10	0.13	0.06	0.11	0.07
MgO	2.61	1.22	3.20	1.89	1.00	2.54	1.84
CaO	5.69	2.82	5.33	5.83	2.90	5.21	3.61
Na2O	3.65	3.54	4.08	3.57	3.24	3.59	3.79
K2O	4.41	3.56	1.62	4.09	3.57	1.96	1.79
P2O5	0.58	0.07	0.28	0.45	0.11	0.29	0.07
total	98.52	99.12	99.55	98.55	98.68	99.23	99.14
$\delta^{18}O$	8.7	11.3	10.1	9.0	10.6	10.0	10.8
reference	1	1	1	1	1	1	1
1/Sr x 10^3	2.26	2.42	2.14	2.48	3.12	2.51	2.27
Sr_i	0.70864	0.71058	0.70956	0.70896	0.71044	0.70946	0.71046
1/Nd	n/a	n/a	n/a	.038	n/a	n/a	n/a
εNd	n/a	n/a	n/a	-4.83	n/a	n/a	n/a
reference	4, 8	8	8	3, 4, 7, 8	8	4	8

Oxide data in weight %; all iron reported as "FeO total" unless nonzero value reported for Fe2O3; oxygen isotope values reported in (+) per mil; trace element data in ppm; Sr_i and εNd calculated for 270 Ma.

REFERENCES: (1) this study; (2) Pin and Sills, 1986; (3) Voshage et al., 1987; (4) Bürgi, 1987; (5) Voshage et al., 1988; (6) Schnetger, 1988; (7) Voshage et al., 1990; (8) Bürghi and Klotzli, 1990; (9) Sinigoi, unpublished data.

Table 5.3: Major element and isotopic data from the Ivrea Zone

Sample #	KAW2507	VS 18	VS 14	VS 13	VS 23	VS 10	VS 9	VS 3	VS 5
Lithology	leucocharnockite	metapelite	metapelite	calcsilicate	metapelite	metapelite	metapelite	metapelite	metapelite
Unit	charnockite	kinzigite	kinzigite	calcsilicate	kinzigite	kinzigite	stronalite	stronalite	stronalite
SiO2	68.66	65.90	63.30	64.40	63.80	57.90	56.50	60.00	63.20
TiO2	0.37	0.80	0.87	0.80	0.80	1.00	1.18	1.44	1.00
Al2O3	15.69	15.50	19.10	14.60	15.90	19.20	21.10	19.70	16.40
FeO	2.05	4.70	5.10	4.00	5.20	6.80	8.10	7.40	5.70
Fe2O3	0.49	0.70	1.20	1.20	0.90	0.90	1.20	2.20	0.90
MnO	0.04	0.08	0.16	0.10	0.10	0.21	0.19	0.11	0.11
MgO	1.21	2.30	2.10	2.30	2.70	2.70	2.70	3.20	2.80
CaO	3.26	1.80	0.90	6.10	2.30	5.80	2.30	1.80	2.70
Na2O	3.18	2.30	1.20	0.70	4.20	2.40	1.10	1.20	4.10
K2O	3.51	3.10	4.00	4.10	2.60	1.60	2.60	0.90	1.20
P2O5	0.07	0.19	0.19	0.19	0.13	0.19	0.14	0.03	0.19
total	99.00	99.40	99.60	100.20	100.00	100.00	99.60	99.80	100.10
$\delta^{18}O$	10.8	10.9	12.3	13.8	12.2	14.1	13.4	11.3	12.1
reference	1	6	6	6	6	6	6	6	6
1/Sr x 10^3	1.93	4.83	4.72	6.80	3.91	5.59	4.83	3.38	3.57
Sr_i	0.71040	0.71530	0.71485	0.71924	0.71514	0.71771	0.71576	0.71306	0.71275
1/Nd	n/a	.030	.028	.032	.027	.022	.017	.023	.025
εNd	n/a	-8.17	-10.56	-8.12	-10.93	-9.62	-9.94	-8.80	-7.04
reference	8	5, 6	5, 6	5, 6	5, 6	5, 6	5, 6	5, 6	5, 6

Oxide data in weight %; all iron reported as "FeO total" unless nonzero value reported for Fe2O3; oxygen isotope values reported in (+) per mil; trace element data in ppm; Sr_i and εNd calculated for 270 Ma.

REFERENCES: (1) this study; (2) Pin and Sills, 1986; (3) Voshage et al., 1987; (4) Bürgi, 1987; (5) Voshage et al., 1988; (6) Schnetger, 1988; (7) Voshage et al., 1990; (8) Bürghi and Klotzli, 1990; (9) Sinigoi, unpublished data.

Table 5.3: Major element and isotopic data from the Ivrea Zone

Sample #	VS 19	VS 4
Lithology	metapelite	metapelite
Unit	stronalite	stronalite
SiO2	72.80	65.00
TiO2	0.99	1.06
Al2O3	13.40	16.60
FeO	5.40	6.60
Fe2O3	0.80	1.20
MnO	0.07	0.14
MgO	1.90	2.70
CaO	0.60	1.90
Na2O	0.60	2.00
K2O	2.40	1.70
P2O5	0.06	0.06
total	100.00	100.10
$\delta^{18}O$	13.6	10.7
reference	6	6
1/Sr x 10^3	7.30	3.58
Sr_i	0.72295	0.71592
1/Nd	.025	.031
εNd	-11.22	-10.42
reference	5, 6	5, 6

Oxide data in weight %; all iron reported as "FeO total" unless nonzero value reported for Fe2O3; oxygen isotope values reported in (+) per mil; trace element data in ppm; Sr_i and εNd calculated for 270 Ma.
REFERENCES: (1) this study; (2) Pin and Sills, 1986; (3) Voshage et al., 1987; (4) Bürgi, 1987; (5) Voshage et al., 1988; (6) Schnetger, 1988; (7) Voshage et al., 1990; (8) Bürghi and Klotzli, 1990; (9) Sinigoi, unpublished data.

Table 5.4: Major element and radiogenic isotope data from the Mafic Complex, Ivrea Zone

Sample #	GZ 10	IV 41	IV36	FE 37	IV 176	MAS 6	MAS 5	IV 146	IV 46	IV 144
Lithology	peridotite	gabbro	gabbro	peridotite	gabbro	gabbro	gabbro	anorthosite	gabbro	gabbro
Unit	BZ	BZ	BZ	IZ	IZ	UZ	UZ	MG	MG	MG
SiO2	43.94	49.4	43.5	43.51	n/a	47.3	50.9	52.1	40.6	n/a
TiO2	0.49	0.37	2.8	0.06	n/a	2.59	0.65	0.29	3.37	n/a
Al2O3	3.89	15.4	13.1	0.64	n/a	16.6	26	29	20.2	n/a
Fe2O3	13.52	10.94	17.42	11.39	n/a	12.78	4.73	1.07	14.27	n/a
MnO	0.21	0.18	0.3	0.21	n/a	0.2	0.07	0.02	0.16	n/a
MgO	33.54	15.95	8.11	41.45	n/a	7	3.08	0.23	6.1	n/a
CaO	4.13	8.25	13.25	2.54	n/a	11.44	11.84	11.65	10.44	n/a
Na2O	0.13	0.52	1.83	0.04	n/a	2.46	3.4	4.68	2.73	n/a
K2O	0	0.02	0.06	0	n/a	0.23	0.34	0.38	0.23	n/a
P2O5	0	0.02	0.02	0.04	n/a	0.38	0.03	0.06	1.56	n/a
LOI		0.43	0.36	0	n/a			0.52	0	n/a
total		101.05	100.39	100		100.98	101.04	100	99.66	
1/Sr x10^3	71.4	7.04	8.93	333	2.65	2.21	1.97	1.08	1.45	1.86
Sr_i	0.70413	0.70963	0.70416	0.7066	0.7073	0.70806	0.70774	0.70787	0.70801	0.70775
1/Nd	0.379	0.855	0.12	3.57	0.292	0.075	0.347	0.391	0.037	0.121
εNd	2.10	-5.47	6.24	-2.44	-4.82	-5.98	-3.13	-6.35	-3.99	-5.36
reference	1, 2, 3	1, 2	1, 2, 3	1, 2	2	1, 2	1, 2	1, 2	1, 2	1, 2

Oxide data in weight %; trace element data in ppm; Sr_i and εNd calculated for 270 Ma;
LOI = loss on ignition
REFERENCES: (1) Pin and Sills, 1986; (2) Voshage et al., 1990; (3) Sinigoi, unpublished data.

Table 5.4: Major element and radiogenic isotope data from the Mafic Complex, Ivrea Zone

Sample #	MAS 4	MAS 3	MAS 2	MAS 1b	MAS 1	MAS 0
Lithology	gabbro	gabbro	diorite	diorite	diorite	diorite
Unit	MG	MG	diorite	diorite	diorite	diorite
SiO2	48.5	45.5	45.2	47	45.8	n/a
TiO2	0.7	0.73	1.7	1.86	1.36	n/a
Al2O3	21.4	19.9	24.1	22.6	20.7	n/a
Fe2O3	8.87	11.24	8.49	8.77	9.81	n/a
MnO	0.14	0.18	0.09	0.11	0.15	n/a
MgO	5.85	9.81	4.32	4.2	6.21	n/a
CaO	12.08	11.66	12.14	9.76	11.92	n/a
Na2O	2.44	1.46	2.95	2.56	2.16	n/a
K2O	0.34	0.22	0.99	1.97	0.76	n/a
P2O5	0.06	0.03	0.7	0.5	0.17	n/a
LOI	0.09	0.55	0.2	1.29	1.12	n/a
total	100.38	100.7	100.29	99.72	99.04	
1/Sr x10^3	1.49	2.26	1.46	1.89	2.36	2.34
Sr_i	0.70786	0.70709	0.70794	0.70831	0.70763	0.70851
1/Nd	0.112	0.311	0.036	0.049	0.036	0.038
ε Nd	-6.47	-2.99	-4.50	-5.77	-4.17	-4.21
reference	1, 2	1, 2	1, 2	1, 2	1, 2	1, 2

Oxide data in weight %; trace element data in ppm; Sr_i and ε Nd calculated for 270 Ma;
LOI = loss on ignition
REFERENCES: (1) Pin and Sills, 1986; (2) Voshage et al., 1990; (3) Sinigoi, unpublished data.

Table 5.5: $\delta^{18}O$ and Sr_i data from the Strona-Ceneri Zone

Sample Number	Lithology	Location	Sr_i (270 Ma)	1/Sr x 10^3 (ppm)	ref.	$\delta^{18}O$	ref.
BB2	granite	Baveno-Mottarone	0.71198	39.4	2	10.4	1
BB3	pink granite	Baveno-Mottarone	0.71297	51.8	2	10.5	1
BB4	white granite	Baveno-Mottarone	0.71106	12.4	2	11.0	1
BB5	quartz diorite	Quarna	0.71048	5.16	2	9.9	1
BB11	appinite	Quarna	0.70978	3.86	2	10.4	1
GL1	granite	Montorfano	0.71106	10.2	2	10.5	1
GL5	acidic dike	Montorfano	0.71161	51.3	2	10.6	1
GL6	gabbroic dike	Mergozzo	0.70666	2.70	2	8.6	1
GL7	green granite	Mergozzo	0.71328	17.5	2	8.0	1
GL8	metapelite	metapelite	0.72457	2.82	2	13.4	1
GL9	appinite	M. Zuccaro*	0.71162	55.2	2	12.7	1
GL10	appinite	M. Zuccaro*	0.70674	3.18	2	10.5	1
GL15	leucosome	metapelite	0.71105	3.91	2	12.1	1
GL18	appinite	Val Sesia	0.71065	2.86	2	10.7	1
GL19	appinite	Val Sesia	0.70876	2.04	2	9.0	1

REFERENCES: (1) this study; (2) Pinarelli et al., 1988.
* = age correction made to 255 Ma (Pinarelli et al., 1988).

Table 5.6: Major element chemistry for samples in Table 5.5.

Sample #	**GL10**	**GL15**	**GL18**	**GL19**
Lithology	appinite	leucosome	appinite	appinite
Location	M. Zuccarro		Val Sesia	Val Sesia
SiO2	64.55	73.75	66.91	44.82
TiO2	0.66	0.13	0.65	1.51
Al2O3	15.87	15.01	15.91	20.6
FeO	3.42	1.1	4.55	10.42
Fe2O3	1.01			
MnO	0.06	0.01	0.06	0.18
MgO	0.99	0.67	1.69	6.31
CaO	2.96	3.78	3.7	11.45
Na2O	3.79	3.78	3.3	1.91
K2O	2.03	3.07	1.98	1.15
P2O5	0.2	0.09	0.21	0.29
LOI	1.08	0.68	0.53	0.2
total	96.62	102.07	99.49	98.84
reference	1	2	2	2

Oxide data in weight %; all iron reported as "FeO total" unless nonzero value reported for Fe2O3; LOI = loss on ignition.
REFERENCES: (1) Burlini and Caironi, 1988; (2) Pinarelli et al., 1988.

Table 5.7: Oxygen isotope values of samples from the Ivrea and Strona-Ceneri Zones which lack other isotopic or chemical data

Sample Number	Lithology	$\delta^{18}O$ (per mil)	Latitude (N)	Longitude (E)
PR 101	phlogopite peridotite	6.5	46°01'24"	8°21'07"
PR 102	gabbro	7.7	46°01'24"	8°21'07"
PR 103	gabbro	8.9	46°01'24"	8°21'07"
PR 105	pyroxenite	7.8	46°00'43"	8°20'51"
PR 106	pyroxenite	7.4	46°00'43"	8°20'51"
PR 109a	pyroxenite	9.1	46°00'39"	8°20'49"
PR 110	pyroxenite	7.7	46°00'39"	8°20'49"
PR 111	pyroxenite	7.7	46°00'41"	8°20'47"
PR 113	sheared garnet gabbro	5.5	46°00'48"	8°20'35"
PR 115	pyroxenite	8.4	46°00'26"	8°19'15"
PR 116	metapelite	11.2	46°00'27"	8°19'18"
PR 117	pyroxenite	8.0	46°00'24"	8°19'18"
PR 119	amphibolite	10.0	45°49'49"	8°23'47"
PR 121	metapelite	13.1	45°48'45"	8°25'07"
IS 1	pyroxenite	9.1	45°49'23"	8°10'16"
IS 2	pyroxenite	8.4	45°49'23"	8°10'16"
IS 5	metapelite septa	8.8	45°49'24"	8°10'15"
IS 6	gabbro	8.7	45°49'23"	8°10'15"
IV 305	hornblende gabbro	10.7	45°59'	8°13'
IV 306	mylonitic gabbro	10.2	45°59'	8°13'
IV 307	mylonitic metapelite	12.5	45°59'	8°13'
DK 3	amphibolite	11.2	46°05'44"	8°32'09"
DK 4b	mobilizate in metapelite	13.8	46°05'42"	8°32'14"
DK 22	Balmuccia pyroxenite	7.3	45°49'	8°9'
DK 27	Strona-Ceneri gneiss	14.5	45°48'07"	8°15'35"
DK 28	Strona-Ceneri metapelite	18.4	45°48'05"	8°15'38"
DK 29	M. Zuccaro appinite	8.2	45°54'49"	8°23'03"
DK 31	Strona-Ceneri metapelite	12.0	45°54'49"	8°23'03"
DK 32a	Strona-Ceneri amphibolite	7.3	45°54'49"	8°22'58"
DK 37	Strona-Ceneri metapelite	11.3	45°48'10"	8°10'00"
DK 38	Strona-Ceneri gabbro	9.4	45°48'10"	8°10'00"

Table 5.8: Oxygen isotope data and calculated mineral pair temperatures from the Mafic Complex, Ivrea Zone

sample number	lithology	mode (pl : px : hb : bi)	unit	$\delta^{18}O$ plagioclase (+‰)	$\delta^{18}O$ pyroxene (+‰)	$\delta^{18}O$ amphibole (+‰)	$\delta^{18}O$ biotite (+‰)	$\delta^{18}O$ whole rock (+‰)	T (ºC)
BM117	Al-augite dike	(85 : 15)	peridotite	6.9	6.1				887
VS113	norite	(35 : 65)	BZ	8.7	7.0			7.2	523
VS114	norite	(15 : 85)	BZ	9.3	8.8			9.2	1066
VS123	pyroxenite	(35 : 60 : 5)	BZ	8.2	7.2			7.5	764
MC58	gabbro	(60 : 25 : 15)	BZ?	9.8		7.5		8.5	608
VS127	gabbro	(65 : 35)	IZ	9.0	7.3			8.2	523
VS128a	anorthosite	(100 : 0)	IZ	8.6					500
VS128b	pyroxenite	(0 : 90)	IZ		6.8				
VS138	gabbro	(80 : 10)	IZ	9.5	7.6			9.2	500
VS144	leucogabbro	(65 : 35)	UZ	9.5		7.7		9.1	587
F26	gabbro	(50 : 35 : 15)	upper gabbro	8.7	6.2			7.4	574
VS132	diorite	(60 : 0 : 40)	diorite	8.6		7.6		8.2	820
VS105	diorite	(70 : 0 : 5 : 20)	diorite	10.8		8.7	8.2	9.5	534
VS107	diorite	(? : 0 : ? : 15)	diorite	11.4			7.7	10.4	425

Samples from the central Mafic Complex listed in relative stratigraphic position with two additional samples, MC58 and F26, inserted in the approximate relative positions. Sample VS128 has been divided into cm-thick anorthosite and pyroxenite layers. Abbreviations: pl = plagioclase; px = pyroxene; hb = hornblende; bi = biotite.